Development of Optoelectronic Sensor-Based Technologies Towards Small Molecule Detection

By

Sherlyn Chung Jing

submitted to the University of Hertfordshire in partial fulfilment of the requirements for the degree of MSc by Research,

July 2022.

Acknowledgements

First of all, I would like to express my utmost gratitude to my main supervisor, Dr. Jesus Calvo-Castro, for his guidance and support throughout this research master. It has been a great pleasure to work under your supervision. I have learned a lot from him – he has been a great mentor, always selfless and willing to share his experiences and knowledge with me as well as always making sure that I am on the right track throughout the research. I would also like to express my deepest appreciation to the incredible and supportive supervisory team, which were led by my main supervisor and two co-supervisors, Prof. Darragh Murnane and Dr. Michael Cook. Thank you for your patience and putting your trust on me. Without your support and encouragement, this would have never been possible.

Furthermore, a big thank you to Prof. Uwe Pischel of the University of Huelva (Spain), one of our collaborators, for providing the lifetimes and making this research more informative. Additionally, I appreciate the great facilities provided by the University of Hertfordshire, such as laboratories where I am able to work and study under a comfortable environment.

I would like to thank my family, for their unconditional love and support all these times. I thank everyone who has been there for me when I needed their support, especially Nelly, Kristy, Phoebe and See Yew. Lastly, I should thank myself for not giving up and managed to get this thesis done.

Abstract

The development of detection methods for nitroaromatics has always been at the forefront of research interests, both industrially and academically. A series of small molecule diketopyrrolopyrroles were studied in this work, and their ability towards nitroaromatic sensing by optical signal transduction evaluated. The main purpose of this project is to study structure-property relationships on these diketopyrrolopyrroles and the effect of these systematic substitutions on their application as fluorescent turn-off probes for the sensing of nitroaromatic compounds.

Firstly, the photophysical properties of the seven different diketopyrrolopyrroles were evaluated by UV-Visible absorption and fluorescence emission spectroscopies. In all cases, these systems exhibited large absorption factors and strong fluorescence quantum yields, in line with those reported for this class of materials. In all cases, we report larger absorption factors and bathochromic spectral shifts for furan- and thiophene-bearing systems when compared to their phenyl counterparts, which can be attributed to the greater planarity and enhanced conjugation of the former. As a result of this, smaller Stokes shifts and clear vibronic progression were observed for these highly planar systems. All exhibited emission spectral shapes which were irrespective of the excitation wavelength used and fluorescence lifetimes in line with those previously reported.

Next, their ability to act as sensing platforms for nitroaromatic materials was evaluated in solution. In the case of non-phenol based nitroaromatic materials, nitrobenzene and 2,4-dinitrotoluene, we report quenching rate constants in line with their reduction potentials and the predicted oxidation potentials of the diketopyrrolopyrroles. In turn, counterintuitive behaviour was observed in the case of the quenching of phenol-based nitroaromatic compounds, nitrophenol and 2,4-dinitrophenol. Despite their lower reduction potentials as a result of the hydroxyl instead of methyl substitution, these were observed to yield greater quenching rate constants. We attribute this to a different sensing mechanism, for which additional studies must be carried out. In all cases, we report quenching rate constants which approach diffusion controlled rates in the solvents used.

Table of Contents

1 Introduction 5

1.1 Organic materials for sensing applications 5

1.2 Diketopyrrolopyrroles 9

1.3 Photophysical processes 11

1.3.1 Absorption of light 11

1.3.2 Jablonski diagram and photophysical processes 15

1.3.3 Characteristics of fluorescence emission 18

1.4 Fluorescence Quenching 21

1.4.1 The Quenchers: Nitroaromatic Compounds 29

Materials and Methods 31

2.1 Materials 31

2.2 Methods 32

2.2.1 Absorption measurements 32

2.2.2 Fluorescence emission measurements 32

2.2.3 Fluorescence quenching measurements 33

3 Results and Discussions 35

3.1 Photophysical properties 35

3.2 Sensing of nitroaromatic compounds 46

3.2.1 Detection of non-phenol based nitroaromatic compounds 47

3.2.2 Detection of phenol-based nitroaromatic compounds 52

4 Conclusions and Future perspectives 59

5 References 61

Appendix A 80

Appendix B 97

1 Introduction

1.1 Organic materials for sensing applications

The development of a rapid, low-cost, high accuracy and sensitivity sensing techniques has always been an urgent societal need[1-4], as the inquiry of the detection and tracing of a wide range of chemicals and biological elements has become more common in the society.[5] Sensing applications have been widely used by different disciplines such as chemistry, biology and environmental analysis to monitor several types of analytes.[2,6] A large variety of organic and inorganic materials have been used in the development of sensing applications. Metal oxide nanostructures (MONs) such as tin oxide (SnO_2) is one of the most widely employed inorganic chemical sensing materials in detecting various types of gases.[7] It could detect the target gases within few seconds and highly sensitive (<1 ppm) as well as very selective to acetone.[8] Despite inorganic materials being an outstanding material for the development of sensing applications, the utilization of organic based materials for sensing applications has seen an increasingly large surge of interest in the last decades on account of their highly desirable photophysical properties, ability to yield highly pure compounds and ease of structural modification. In addition, when compared to their inorganic counterparts, organic materials are often characterized by their lower prices.[9]

Organic materials that have been extensively used for sensing could be divided into three major groups: macrocyclic compounds, polymeric compounds[10] and small molecules[11]. Phthalocyanine is a blue-green coloured organic macrocyclic molecule with an 18 π-electron system. Its excellent photophysical and electronic properties[12,13] have caught the attention of researchers in the field and made these materials important in the developments of material science. These have been used various fields such as optoelectronic and photoconduction as chemical sensors.[12,14-16] Phthalocyanine was reported as being ultrasensitive to nitrogen oxide (NO_2) in very low concentrations from 0.1 to 1 ppm at room temperature in a gas detection study.[17] Macromolecular organic field-electronic transistors (OFETs), that can be made by conjugated polymer have emerged as a reliable electrical sensor in the biomedical[18,19], vapour detection,[20] as well as environmental fields[21]. For example, a novel OFET-based sensor was proposed in 2013 to detect vapour.[20] The material applied on the sensor was an ion-

conducting organic dielectric material – static co-polymers that are selective to ammonia (NH_3). The materials were spin coated on the OFET and following by a non-ammonia selective homopolymer, dimethyl 5-norborrene-2,3-dicarboxylate. The OFET proposed was highly sensitive to ammonia (NH_3) at concentration as low as 100 ppm.[20]

Polymers and small molecule fluorescent organic materials have been introduced as sensors in the detection of explosives such as electron deficient nitroaromatic compounds by quenching method, especially for their exceptional sensitivity and ease of reproducibility. In the past decades, polymers have always been the better choice for researchers as polymeric sensors have higher detection efficacy in contrast to monomers or small molecules. Fluorescent polymers have raised interest for their physical and chemical properties such as large number of electron acceptor, high stability and tuneable elasticity of polymeric sensors has contributed the enhanced results, this response also known as amplification.[22-24] In addition to the inherent properties of the polymer materials, especially the conjugated polymeric materials, they further enhanced the fluorescence response signal and the sensitivity. These polymer materials required less energy to excite an electron to a higher energy level as conjugated polymers have more delocalized electronic structure that are ready for electron donation as well as more π-conjugated backbones that can transfer electron or energy quickly.[25] It is noteworthy that the optical and electrochemical properties of fluorescence polymer sensors have led to positive effects on the polymer-analyte interactions, therefore enhances the response time and sensing efficacy. The polymeric materials were often designed as thin film to detect probes in vapour or solution phase.[26] A study of novel diphenyl sulfone-functionalized water-soluble polymer (poly (NIPAM-AM-BMPS)) quenched by p-nitrophenol was done by Wang and co-workers. The tests were done in deionized water.[27] The fluorescence quenching of this polymer quencher has outstanding quenching efficiency as well as was highly sensitive – they claimed that their polymer sensor has higher quenching efficacy than other previously done studies in recent years.[28-33]

On the other hand, small molecule materials are important for their sensing application in a wide range of fields.[34-36] Especially, in the biomedical field they consist of various small molecules that could be used as diagnostic makers for peptides, steroids and thyroid hormones[37,38] as well as bacterial pathogens in food.[39] Furthermore, the detection of explosive molecules such as nitroaromatic compounds has been a concerned to the public.

Although having lower sensing result than polymer fluorophore, small molecule fluorophore still has its own advantages in the sensing of nitroaromatic compounds. Small molecule fluorescence sensors are easy to synthesise and reproduce as well as having high quantum yield.[40-44] Besides, small molecule-based fluorescence sensors are easier to modify and improve their properties and performance by substituting suitable functional groups.[45] Significant results were shown when these sensors are on contact with nitroaromatic compounds – static fluorescence quenching were shown in most of the detecting process.[46] In such cases, a complex is formed at the ground state due to the multiple intermolecular interactions between the monomers of the fluorescent polymer and the detected analyte. A small molecule fluorophore, pyrene was studied in detecting nitroaromatic compound nitrobenzene.[47] Besides, in 2018, Sriyab et al designed and studied three types of pyrene based nitroaromatic explosives fluorescent sensors – the pyrene derivatives were studied to detect nitroaromatic compounds like 2,4-dinitrotoluene in dichloromethane solvent.[48] As an exceptional sensing material for nitroaromatic compounds, pyrene has extraordinary fluorescence lifetime which average lies between ~50 to 90 ns [49,50] has made them useful in sensing nitroaromatic even though they have strong aggregation tendency[51,52], that could decrease the fluorescence intensity of the fluorophore at solid state.[53]

As mentioned above, optical sensors are important as a sensing tool in analytical science and clinical research.[54] Optical sensor method was used in this project for the study of small molecule detecting nitroaromatic explosives. Optical detection is a type of chemical transduction which includes the monitoring of various photophysical parameters such as intensity, wavelength, lifetime, polarisation and quantum yield.[54-57] Optical sensors can detect analytes at different spectral regions from infrared to ultraviolet regions. Transduction mechanisms can be chosen according to different electromagnetic spectrum regions, for example, absorbance, luminescence (fluorescence or phosphorescence), scattering, etc.[2] Optical sensing applications have been rapidly developing. To date, there are various of optical sensor platforms have been developed, such as fluorometric[2,58-60] and colorimetric sensors[2], fibre optic sensor[61-63], planar waveguide optical devices[64] and surface enhanced Raman scattering (SERS)[65-67]. Optical sensors have been the particularly preferred method to use in the biological or chemical analytical applications as they are very beneficial for remote use and multimodal sensing function.[54,68] The outstanding sensitivity of fluorescence is the

main advantage that this transduction method was commonly used,[2,6,11] it is especially sensitive enough to detect single molecules.[6]

Fluorescence sensing has been one of the most popular approaches in optical sensing applications. Fluorescence spectroscopy was first used to analyse the concentrations of ionic and non-ionic analytes.[2,11,69] Fluorescence sensing has extremely high sensitivity and outstanding selectivity, which are key aspects for researchers to choose it as sensing tool over other methodologies.[2,6,11,70] It is able to cover large range of analyte studies, from characterising macromolecules[71-73] to ions[74-77] to small molecules[71,74-76]. The sensitivity of spectrofluorometry can be up to 1000 times higher than spectrophotometry.[77] This highly sensitive method could be an effective method to detect nitroaromatic compounds as sensitivity have always been the largest concern in sensing these analytes.

The sensitivity and selectivity of a sensing material is always a concern for the efficiency of the detection. Sensitivity is important for obtaining the optimum quantitative analytical measurement with high precision and accuracy while keeping the minimal qualitative use for an analyte.[69,78] Sensitivity also indicated as the detection capability of a method – a sensing material with high sensitivity can detect the analyte even with minimal concentration. Meanwhile, selectivity refers to the capability of the material to determine particular analyte(s) in a complex environment such as an aqueous solution with interferent.[78,79] As one of the three major organic compounds being used for sensing, small molecules fluorescent probes have become a promising and important material in optical sensors, especially in fluorescence emission signal monitoring.[11] Optical sensors, specifically fluorescence sensing was the most common sensing method for small molecules because of its outstanding sensitivity. There has been significant fluorescence sensing work with organic small molecules. For example, rhodamine 6G, a common fluorescent probe for metal ion detection was reported to have high response to mercury ion (Hg^{2+}) in a fluorescence study.[69] The fluorescence sensor was made by adopting rhodamine 6G and 3-mercaptopropionic acid co-modified nanoporous gold as the plasmonic substrate. This fluorescence sensor has shown ultrasensitive to the analyte as it was able to detect Hg^{2+} and CH_3Hg^+ ions at very low concentration. Besides, diketopyrrolopyrrole, was used as a fluorescent probe to monitor small molecules. A small molecule diketopyrrolopyrrole fluorescent probe (DPP-DNBS) was reported to have established as a turn-on fluorescence optical sensor for the detection of

small molecule cysteine.[80] The fluorescent probe was very sensitive, it managed to detect the analyte at concentration as low as 5 μM. Besides, the optical biosensor also shown highly selective to cysteine – it was able to make a rapid sensing and 15-fold enhancement of red emission was observed at 615 nm upon the detection of cysteine in HEPES:DMSO = 3:7 solvent. Diketopyrrolopyrrole, a high performance pigment will be investigated in this work. The brief history and introduction of this material will be discussed in the next section.

1.2 Diketopyrrolopyrroles

Diketopyrrolopyrroles (DPPs) are high-performance organic pigments that were discovered in 1974[81-84] then developed and introduced to the market since 1986[82,85] as manufacturing materials for conventional pigment applications such as printings, paints, inks and plastics.[82,86-88]

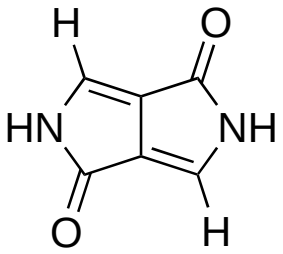


Figure 1.2.1: Chemical structure of 2,5-Dihydropyrrolo[3,4-c] pyrrole-1,4-dione, diketopyrrolopyrrole or DPP.

First diketopyrrolopyrrole derivative was reported by Farnum et.al[84] (Figure 1.2.2) as a minor product obtained from a synthesis of 2-azetinones that was proposed to produce β-lactam. A small quantity of DPPs were yielded from the reaction of benzonitrile with ethyl bromoacetate and zinc.

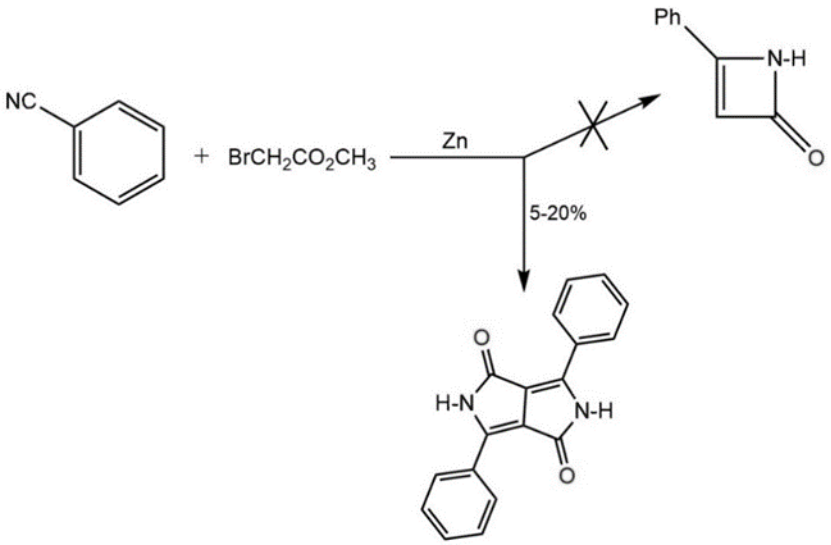


Figure 1.2.2: The first synthesis of diketopyrrolopyrrole as a by-product in the synthesis 2-azetinones.

Due to the simple synthetic protocols and their outstanding properties such as intense brightness, excellent stability and low solubility, DPP pigments have been dominating the pigment industry relatively fast.[81,82,86-90] Most DPP derivatives have very poor solubility in organic solvents as well as significant heat and chemicals resistant[91] which originate from their strong intermolecular hydrogen bonding and π-π stacking.[89,92] The strong intermolecular interaction in most of the pigments causes them to have solubility difficulties in most of the organic solvents,[92] at the same time also the main reasons that contributes the high photostability of the pigments.

Many studies have been reported trying to improve the solubility of DPPs. It was first revealed that disruption of these strong intermolecular interactions by substitutions on the lactam nitrogen atoms led to the generation of dyes, soluble in most organic solvents.[92,93] As a consequence, diketopyrrolopyrrole, a photostable and high quantum yield fluorescent dye that is highly soluble in organic solvents was discovered. This discovery soon resulted in high attention to the researchers, leading to work on DPP as functional dyes quickly being carried out in many areas such as organic optical sensing materials[94,95], organic field effect transistors (OFETs)[96,97] and solar cells[98,99]. DPPs can be synthesised as small molecules and polymers.

The efficiency of an organic material is highly dependent on the π-conjugated system for electron and charge transfer, a more π-conjugated system in a particular molecule would be more beneficial to the efficiency of a material.[101-103] Certainly, this system could be one of

the advantages for conjugated polymers as such materials would have more π-conjugated system than a small molecule monomer. For example, it has been reported that conjugated polymers have higher performance in sensing analyte compared to small molecules because π stacking in polymers are very closed[100] therefore, enhanced film crystallinity[104] and charge transfer.[100] Other than that, small molecules are of more definite chemical structure than polymers, they can have higher purity than polymers as they do not contain a mixture of different molecular weight chains hence are easier in reproducing them.[105,106] Besides, small molecules are much less flexible than the monomers constituting long chain polymers while having higher degree of crystallinity than polymers.[105] The advantages of small molecule – more convenient and cost-effective with high efficiency is the better option as an optical sensor. The next subsection will be discussing the photophysical processes.

1.3 Photophysical processes

1.3.1 Absorption of light

In general, it can be considered that the following processes can be observed when light interacts with matter: absorption, transmission, reflection or scattering.[107,108] In diluted solutions, it is assumed that light can only be absorbed or transmitted. Absorption of light occurs when the energy of a photon is absorbed by the molecule and promotes it to an excited state. Then, that energy can be released as heat energy or emission of light. Luminescence is a photophysical process occurs after the absorption of light. Instead, transmission of light occurs when radiation passes through the matter without it being absorbed whereas light scatters when the light is deflected away from the molecule, rather than passing through the sample in a straight line, the light goes off in a different angle.

Light is often defined as electromagnetic radiation and can be referred by a wave model. Electromagnetic radiation is a form of energy that can be defined by the wavelength (λ), frequency (ν), and speed of light (c). Their relationship can be explained with the Einstein-Planck relationship, where E denotes the energy of the photon.[109]

$$\mathrm{E} = \mathrm{h}\nu = \frac{\mathrm{hc}}{\lambda}, \text{which } \mathrm{c} = \nu\lambda \quad \text{Equation 1.3.1}$$

Equation 1.3.1 explains the energy carried by a photon at a particular radiation wavelength (λ) has an inversely proportional relationship to its frequency (ν); h is the Planck's constant while c is the speed of light in vacuum state, with a value of 2.998 x 10^8 m s^{-1}. The radiation can also be expressed as wavenumber, $\tilde{\nu}$ in cm^{-1}:

$$\tilde{\nu} = \frac{1}{\lambda} \quad \text{Equation 1.3.2}$$

There are various types of radiation in the electromagnetic spectrum where the energy is categorised by their wavelengths or frequency, ranging from low to high frequency (long to short wavelengths) from radio waves, microwaves, infrared, visible light, ultraviolet (UV), x-ray to gamma rays. Visible light spectrum (Figure 1.3.1) is the only electromagnetic spectrum that is visible to human eyes, with wavelength ranging from 400 nm to 700 nm, approximately.

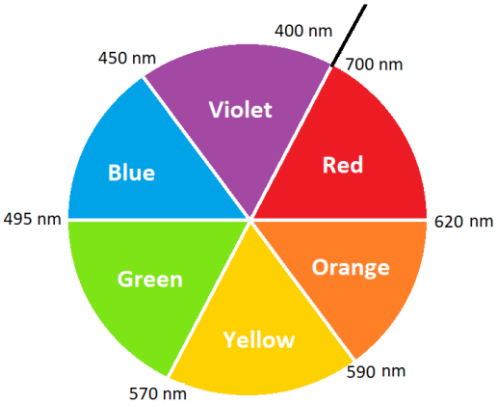


Figure 1.3.1: Visible region colour wheel shows the wavelength being absorbed and the colour transmitted.

The excitation of an electron requires energy to be promoted from the lowest energy state, also known as ground state, to a higher energy level – the process of light absorption. Light with appropriate excitation wavelength for a particular molecule will be the energy source to promote the molecule to an upper excited state. Absorption of light takes about 10^{-15} s. The absorption of light can be expressed as:

$$h\nu = E_x - E_0 \quad \text{Equation 1.3.3}$$

E_x and E_0 denote the energies of the excited and ground states, respectively.

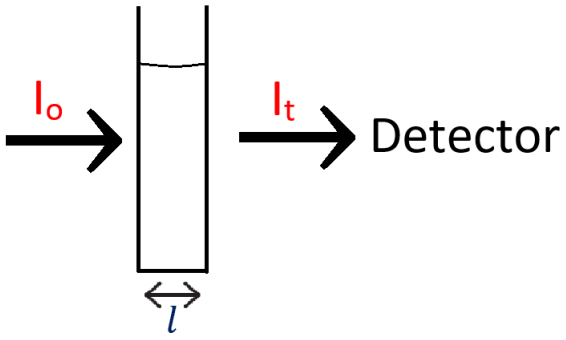


Figure 1.3.2: Illustration of light passing through a cuvette. I_o: incident radiation; I_t: transmitted radiation; I: path length. The radiation collected at the detector is the ratio of I_o/I_t, also known as transmittance.

The absorption properties of a chromophore are often measured by absorption spectroscopy, which measures the absorbance, as a function of the radiation wavelength.[110] Beer-Lambert law explains that absorbance, concentration, as well as thickness of the medium share a direct proportional relationship. The absorbance of light can be expressed as:

$$A = -\log(T) = -\log\left(\frac{I}{I_0}\right) = \varepsilon \cdot l \cdot c \quad \text{Equation 1.3.4}$$

-where the absorbance (A) can calculated from the light transmitted (I) from an incident light source (I_0), while T represents the fraction of transmitted incident light. Besides, absorbance can also be expressed as optical density (O.D.), it dictates the ratio of light absorbed by the sample to the light transmitted through the material. Equation 1.3.4 shows that the three factors, absorption factor (ε), concentration (c) and path length (l) are directly proportional to each other – as the concentration of the sample increases and longer path length is used during the measurement of absorbance, the numbers of species or samples involved will be increased therefore more radiation will be absorbed during the measurement.

An ideal concentration versus absorbance plot should be a linear plot – absorbance should increase when concentration is higher, where Beer-Lambert law is obeyed. However, when the sample is too concentrated, there is a higher chance the light will scattered away

from the sample and decreases in absorbance hence lead to a negative deviation from Beer-Lambert law.

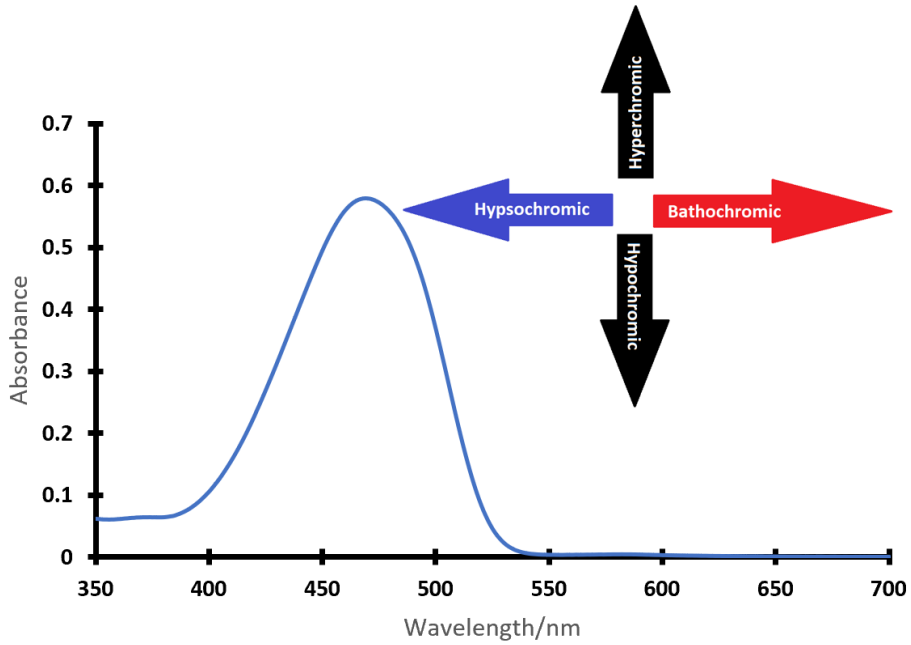


Figure 1.3.3: Illustration of main spectral shifts in absorption spectroscopy.

Four possible spectral shifts can be observed: hyperchromic, hypochromic, hypsochromic and bathochromic shifts. Changes in the absorption factor of a material could lead to hyperchromic or hypochromic shifts in the absorption band. Whereas hyperchromic shifts are associated to an increase in the absorption factor, a hypochromic shift can be ascribed to a diminish in it.[111] Hypsochromic shift happens when a compound shifts to a shorter wavelength, in accordance with the wavelengths of visible spectrum, blue colour has a lower wavelength thus it is often called as blueshift. Conversely, bathochromic shift is often referred to as a redshift as red colour has a higher wavelength.[111]

1.3.2 Jablonski diagram and photophysical processes

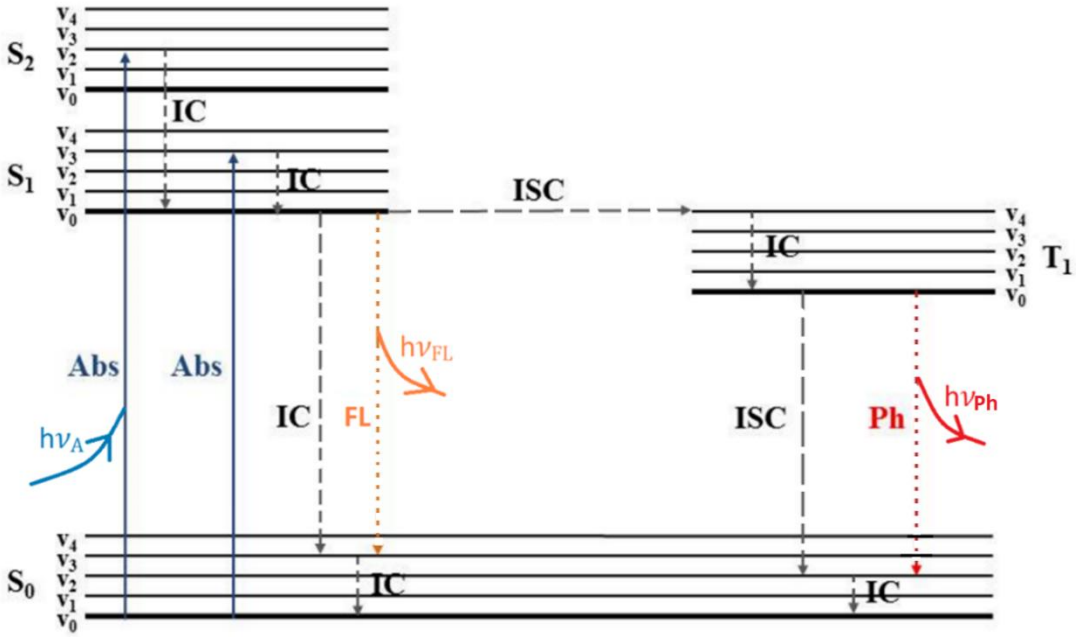


Figure 1.3.4: Illustration of the Jablonski diagram which summarises the most important electronic transitions in small organic molecules.

The Jablonski[112] diagram is often used to depict and explain the main photophysical processes occurring in organic conjugated compounds – both radiative and non-radiative.[113,114] Fluorescence (Fl) and phosphorescence (Ph) describes the phenomenon of light emission by a material. Before the emission, there must be absorption of light (Abs) so that the molecule can be promoted to an excited state. The thick horizontal lines in Figure 1.3.2.1 represent the electronic or main energy levels($S/T_{0,1,2,...}$), where S_x indicates the single electronic state and triplet electronic state for T_x, while the thin lines represent vibrational energy levels in the molecular orbital ($v_{0,1,2,...}$). The excited molecule will undergo de-excitation by radiative and/or non-radiative relaxation processes. The radiative de-excitation processes are known as photoluminescence, which were used in various field of science and technology such as chemistry, physics, material science and biomedical.[70,113,115] Meanwhile, the radiationless or non-radiative transition (indicated by dash lines in Figure 1.3.4) from a higher energy excited singlet and triplet state to a lower energy excited state or the ground state can eventually release as heat ($h\nu_{FL/Ph}$) to the surrounding molecules by collisions.[70] Two types

photoluminescence can be emitted during the de-excitation process – fluorescence and phosphorescence. Fluorescence normally occurs within nanoseconds (10^{-9} s) while phosphorescence takes longer to perform (10^{-3} to 10 s).[77,91115] Fluorescence emission usually occurs from the transition of lowest vibrational state of the singlet excited electronic state (S_1) to the ground state, apart from a few exceptions[77], such as the emission of azulene molecule from S_2. Also, in some cases, indole can have emission from S_1 and S_2 in some solvents. Since the phosphorescence is a de-excitation process that requires the transition from excited triplet state to ground state ($T_1 \rightarrow S_0$), the net spin in the molecule must change for the emission to occur and this is why the time phosphorescence takes for deexcitation is relatively longer than fluorescence.[70] However, this is a classically-forbidden transition as there is low probability for this transition to de-excite from $T_{(\pi,\pi^*)}$ to S_0 by emitting a photon or phosphorescence.[70,77,115,116] Due to spin-forbidden, the emission of phosphorescence usually has less intensity compared to fluorescence emission. The transition of a triplet from the ground state has lower possibility thus less absorption will take place which results in less intense phosphorescence than fluorescence.[77] Nonetheless, phosphorescence has been introduced in many important applications over the years such as bioimaging[117-119], chemosensors[120-122] and organic light emitting technologies.[123-128]

The solid arrows in Figure 1.3.4 represent the absorption of light where the molecule is promoted from the ground state(S_0) to higher energy excited state. The dashed lines represent non-radiative decay process, internal conversion (IC) and intersystem crossing (ISC). The dotted lines represent the luminescence emission from the lowest vibrational energy level (S_1/T_1, v_0) to the ground state (S_0). The ground state of a molecule, whether it is in the single or triplet electronic state is affected by the arrangement of electrons spin in a molecule, which is their spin multiplicity. For instance, electrons spin in different directions because of the vector quantities, although having the same magnitude of spinning. In electrons, there are only two orientations occur in the spinning, it is either parallel or anti parallel to the magnetic field.[129] A molecular orbital can accommodate a maximum of two electrons – they are either spinning at the same or opposite direction. The spin multiplicity is a term used to determine the orientation of the angular momentum corresponding to the net spin of the electronic state. The spin of electron in the molecular is expressed in either +1/2 if the

electron spins along the magnetic field or -1/2 if it goes parallel. The spin multiplicity can be defined as:

$$m_s = 2S + 1 \quad \text{Equation: } 1.3.5$$

S is denoted as the net spin of the molecule and m_s equals to spin multiplicity. For example, if S is equal to 0, the overall spin multiplicity can be cancelled out, then m_s= 1, which is the singlet state multiplicity. Alternatively, if S is equal to 1, then m_s = 3, which is a triple state spin multiplicity. As mentioned, there are singlet and triplet ground state – most of the molecule has singlet ground state and triplet oxygen molecule has triplet ground state. According the Hund's rule of maximum multiplicity, the molecules with highest spin multiplicity has the lowest energy because it is the least stable excited state.[129] Besides, triplet state is more stable compared to singlet state because there is less interelectronic repulsion between the unpaired electrons.[114] Non-radiative intersystem crossing (ISC) is a transition from a singlet lowest excited state to the highest excited state to a different electron transition ($S_1 \rightarrow T_1$); internal conversion (IC) explains the de-excitation of electron from a higher electronic transition to a lower electronic transition ($S_1 \rightarrow S_0$). Before any emission occurs, the electrons should decay to the lowest excited electron transition as well as the lowest vibrational state (v_0), this explains the Kasha's rule.

1.3.3 Characteristics of fluorescence emission

Whilst the terms chromophore and fluorophore can often be used indistinguishable in the literature, chromophores do not necessarily emit light, i.e., all fluorophores are chromophores but not all chromophores are fluorophores.[116] Fluorophores are chemical compounds that emit light as fluorescence. Similar to the use of parameters such as the absorption maximum and absorption factor to characterise a chromophore, there are a few fluorescence characteristics that are important parameters to determine a good fluorophore – Stokes shift, lifetime (τ_0) and fluorescence quantum yield (ϕ_f).

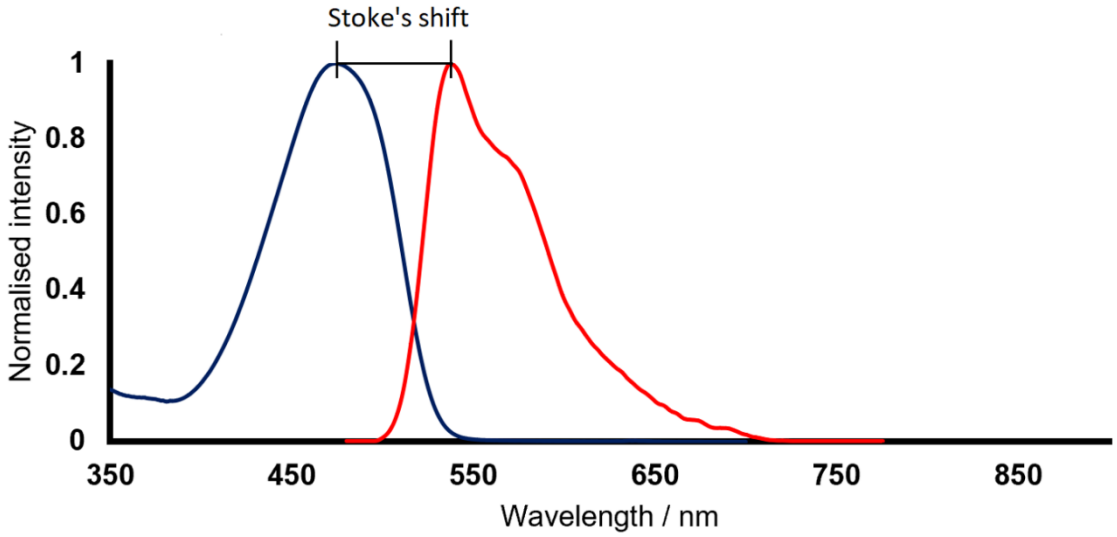


Figure 1.3.5: Normalised absorption (blue solid line) and fluorescence emission (red solid line) spectra of a material investigated in this work in acetonitrile.

The fluorescence emission spectrum is always bathochromically or red shifted with respect to the absorption spectrum as shown in Figure 1.3.5. The difference between these spectra is known as the Stokes shift. Stokes shift is the result of rapid electron relaxation where the energy losses from when the electron falls back to the ground state. [77,130,131] Stokes shift usually expressed in wavenumbers, $\tilde{\nu}$ with unit cm^{-1}:

$$\Delta\lambda = \lambda_{\mathrm{Em\ max}} - \lambda_{\mathrm{A\ max}}$$

$$\Delta\tilde{\nu} = \tilde{\nu}_{\mathrm{A\ max}} - \tilde{\nu}_{\mathrm{Em\ max}} = \frac{1}{\lambda_{\mathrm{A\ max}}} - \frac{1}{\lambda_{\mathrm{Em\ max}}} \qquad \text{Equation 1.3.6}$$

-Δλ denotes the Stokes shift in wavelength; $\lambda_{Em\ max}$ and $\lambda_{A\ max}$ as wavelength (in nm) of the maximum fluorescence emission and absorption respectively; Δṽ denotes the Stokes shift in wavenumber; $\tilde{\nu}_{A\ max}$ and $\tilde{\nu}_{Em\ max}$ as maximum wavenumber of absorption and fluorescence emission respectively. In the design of materials for bioimaging, it is better to have a larger Stokes shift than a smaller ones, as the overlapping in the absorption emission spectra will be smaller on larger Stokes shift band, thus decrease the probability of self-absorption and energy transfer during the absorption and the emission processes.[132] Self-absorption indicates the ground state molecular entities absorb the fluorescence emitted by the same excited species.[133]

The energy diagram below (Figure 1.3.6) illustrates the absorption and fluorescence emission band during Franck-Codon transitions. Since absorption and fluorescence emission occur in very short time, about 10^{-15} s, the internuclear distance remains the same as the time is too short for the nuclei to have a significant displacement. Hence, the vibrational transitions are depicted as vertical lines Franck-Condon principle plays an important role in vibronic transition theory. It explains that a molecule can have vibronic transitions occurring when there are simultaneous changes in the electronic and vibrational energy levels.

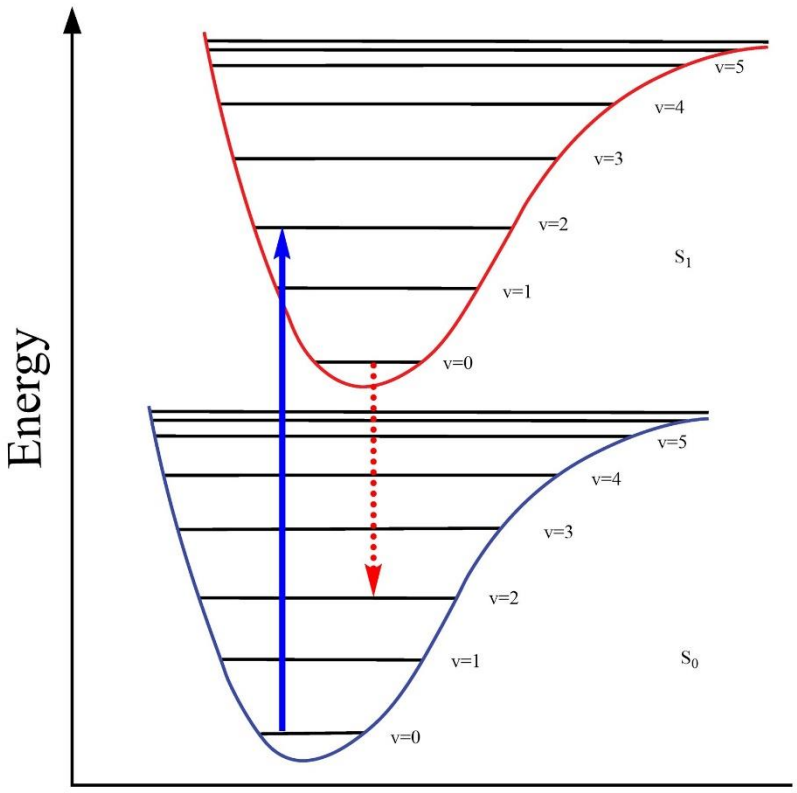


Figure 1.3.6: The Franck-Condon energy diagram. Blue arrow: absorption; red dotted arrow: emission of light.

The fluorescence lifetime (τ_0) and quantum yield (ϕ_f) are two of the important parameters alongside the emission maximum of a fluorophore. Fluorescence lifetime is a parameter that indicates the time that the fluorophore remains at the lowest vibrational energy level (v=0) of the first singlet excited state (S_1). Organic molecules have lifetime of singlet excited state (fluorescence) ranges from 10^{-10} to 10^{-7} s, whereas for the triplet excited state (phosphorescence) is from 10^{-6} to ~10 seconds.[77,130] The lifetimes of fluorophores at excitation state can be expressed as:

$$\tau_0 = \frac{1}{k_r + k_{nr}} \quad \text{Equation 1.3.7}$$

$$k_{nr} = k_{ic} + k_{isc} \quad \text{Equation 1.3.8}$$

τ_0 is the lifetime of fluorescence, k_r and k_{nr} denote the rate constants for radiative emission and non-radiative decays, respectively. With respect to the non-radiative deactivation rate, it

includes all contributions from all possible radiationless processes including the rate constant of internal conversion (k_{ic}) and rate constant of intersystem crossing (k_{isc}).

The fluorescence quantum yield (ϕ_f) is the ratio of the emitted fluorescence photons relative to the absorbed light this term is often used to describe the de-excitation processes following the absorption of light:

$$\phi_f = \frac{k_r}{k_r + k_{nr}} = k_r \cdot \tau_0 \quad \text{Equation 1.3.9}$$

Equation 1.3.8 also shows the relationship between the quantum yield and the fluorescence lifetime. Equation 1.3.8 shows that the quantum yield is directly proportional to the lifetime of chromophore. In this regard the quantum yield and lifetime, they can affect the efficiency of a fluorophore.

1.4 Fluorescence Quenching

The IUPAC defines the quenching of fluorescence as "the deactivation of an excited molecular entity intermolecularly by an external environmental influence (such as quencher) or intramolecularly by a substituent through a nonradiative process."[133] Quenching can be used as fluorescence sensing method by decreasing the intensity of fluorescence intensity upon interaction with the target analyte.[77,130] There are different types of mechanisms in electron transfer, including the non-radiative resonance energy transfer (RET, also known as Förster resonance *energy* transfer (FRET)) and Dexter energy transfer. Förster resonance energy transfer is a non-radiative energy transfer quenching mechanism through dipole-dipole system which is a quenching mechanism that is dependent on donor-acceptor distance. Then, Dexter energy transfer is an electronic exchange mechanism which is one of the very important mechanisms in the development of solar cells and optoelectronic materials.[134] Then, there is the photoinduced electron transfer (PET). More details of PET mechanism will be discussed in the following paragraphs. Quenching can happen in any of the electron transfer processes stated. Fluorescence quenching can be collisional (dynamic) or static. Molecules (or ions) that bind with the fluorophores and results in decrease in fluorescence intensity are known as the quenchers in fluorescence quenching.

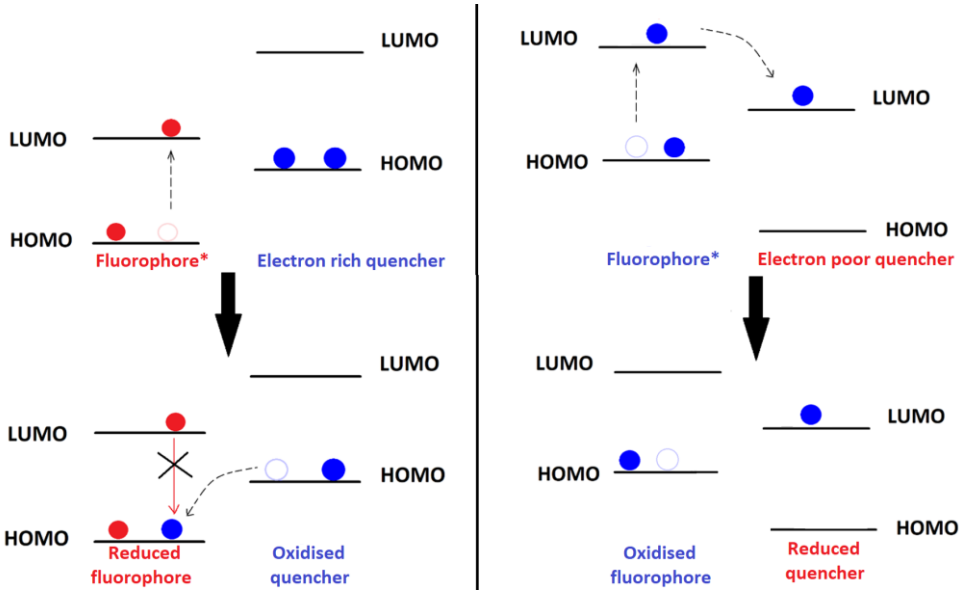


Figure 1.4.1: Reductive (left) and oxidative (right) electron transfer. HOMO: highest occupied molecular orbital (S_1); LUMO: lowest unoccupied molecular orbital (S_0). Red coloured wordings are for the electron acceptor and blue coloured wordings are for the electron donor.

The photoinduced electron transfer (PET) is a general mechanism in organic chemical reactions[77,130,135] and was especially responsible for fluorescence quenching in organic materials.[77,130] An illustration of PET quenching process is shown in Figure 1.4.1. The left side of the Figure showing a reductive quenching that the electron rich quencher donated one electron to the excited fluorophore to stop the de-excitation process in the fluorophore and hence reduced fluorophore. Meanwhile the right side of the figure showing an oxidative electron transfer quenching process. The lowest unoccupied and highest occupied molecular orbital (LUMO and HOMO) shown in the Figure take important role in the PET mechanism. Depends on the nature of the fluorophore i.e., redox potential, the quencher will act as electron donor or electron acceptor. In oxidative quenching, the fluorophore in the excited state donates one electron to the LUMO of the electron deficient quencher, generating therefore a reduced quencher and oxidised fluorophore. The oxidised fluorophore is thus unable to perform fluorescence emission as there is no electron for de-excitation to the ground state for the emission of fluorescence. The reductive and oxidative electron transfer processes shown in Figure 1.3.6 can be expressed as:

$$A^* + D \rightarrow A^- + D^+ \quad \text{Equation 1.4.1}$$

$$D^* + A \rightarrow D^+ + A^- \quad \text{Equation 1.4.2}$$

A^* and D^* are the fluorophore as electron acceptor or donor in excited state, respectively, A^- denotes the reduced acceptor while D^+ denotes the oxidised donor.

In PET quenching, the excited fluorophore can be either electron donor or acceptor – depends on the oxidation and reduction potential of the ground and excited state species, which is the excited fluorophore and the quencher.[130] There are many important parameters that can affect the electron transfer, such as distance or sizes of the fluorophore and quencher. Not to mention, the possibility of electron transfer in photoinduced electron transfer can be predicted from the redox potentials of the fluorophore and quencher hence calculate their quenching efficiency. Redox potential is a scientific way to measure the oxidation-reduction potential of a system, it is applied to calculate the efficiency of a chemical species to be reduced or oxidised. The reduction and oxidation (or redox) potentials are electrochemical as well as physicochemical property of materials, denoting their ability to accept (reduction) or donate (oxidation) electrons and undergo a transition onto their respective radical anion and cation species, respectively. In all cases, redox potentials are quoted against a reference and by convention, reduction potentials are given negative values and oxidation potentials positive ones. In short, the reduction potential increases (becomes more negative) as the ability of the molecule to accept electrons decreases. Similarly, the oxidation potential increases (becomes more positive) as the ability of the molecule to donate electrons decreases. These have clear consequences in the feasibility of the electron transfer processes discussed in this work.

Redox potentials can be studied with electrochemical measurements or by calculating the LUMO and HOMO energy levels. Furthermore, the redox potentials can also be expressed as ΔG in kcal/mol, they can be calculated with Rehm-Weller equation:

$$\Delta G = E(D^+/D) - E(A/A^-) - \Delta E_{0,0} - \frac{e^2}{\varepsilon d} \quad \text{Equation 1.4.3}$$

The redox properties of donor and acceptor can be measured with $E(D^+/D)$ or $E(A/A^-)$, the oxidative and reductive potential of the donors and acceptors in photoinduced electron transfer processes as shown in Equation 1.4.1 and 1.4.2. The oxidation and reduction potentials are needed to calculate the ability of the molecules as electron donor and acceptor. $\Delta E_{0,0}$ (also known as the crossing point energy) denotes the energy needed for the fluorophore to undergo the transition from ground state to excited state ($S_0 \rightarrow S_1$) in volts and $\frac{e^2}{\varepsilon d}$ is the coulombic energy of the ion pair formed following the PET reaction; where e is the electron charge, ε is the dielectric constant of the solvent used and d is the distance between two ions. The electron withdrawing/donating properties of fluorophore and analyte play important role in the photoinduced electron transfer quenching mechanism.[136,137]

Since fluorescence quenching is the process of diminishing of the fluorescence intensity, it involves radiative and non-radiative energy. In the following equations, k_r and k_{nr} denote the radiative and non-radiative rate constants. The lifetimes in the absence (τ_0) and the presence (τ) of quencher can be expressed as:

$$\tau_0 = \frac{1}{k_r + k_{nr}} \quad \text{Equation 1.4.4}$$

$$\tau = \frac{1}{k_r + k_{nr} + k_q[Q]} \quad \text{Equation 1.4.5}$$

Combination of Equation 1.4.4 and Equation 1.4.5:

$$\frac{\tau_0}{\tau} = \frac{k_r + k_{nr} + k_q[Q]}{k_r + k_{nr}} = 1 + \frac{k_q[Q]}{k_r + k_{nr}} = 1 + \frac{1}{k_r + k_{nr}} \cdot kq[Q] \quad \text{Equation 1.4.6}$$

Hence,

$$\frac{\tau_0}{\tau} = 1 + \tau_0 k_q[Q] \quad \text{Equation 1.4.7}$$

The quenching equations show that the bimolecular quenching rate constant (k_q) is assumed to be lifetime dependent. $[Q]$ is the concentration of quencher used. Equation 1.4.7 can be used to determine the type of photoinduced electron transfer quenching process happened in the system. If the lifetime of the fluorophore changes upon the increased quencher concentration, then the quenching can be considered as dynamic, where the quenching takes place at excited state. Conversely, if increasing the quencher concentration result in non-changed lifetime of the fluorophore, then this is a static quenching where the quenching process takes place at the ground state. Collisional or dynamic quenching occurs when the quenching of fluorophores happens in S_1 excited state – electron transfer will take place at the singlet lowest excited state. There would have lifetime changes in collisional quenching i.e. lifetime of the excited state decreases upon the interaction of quencher and the fluorophore then the decrease of fluorescence intensity.[77,130,118] The quenching performed in paramagnetic oxygen is an important collisional quenching mechanism, which the fluorophores have to undergo intersystem crossing in order to perform the quenching of phosphorescence at triplet state.[130] Other collisional quenchers included halogenated compounds such as bromobenzene and trichloroethanol.[130] Dynamic quenching can be expressed in:

$$\frac{I_0}{I} = \frac{\tau_0}{\tau} \quad \text{Equation 1.4.8}$$

The quenching mechanism can be determined as dynamic if the Stern-Volmer plot obtained from Equation 1.4.8 is equal to the straight line plotted from lifetime against concentration of quencher.

In contrast, static quenching occurs in the ground state and the excited state lifetime will remained the same throughout the quenching processes. A non-fluorescent complex will be formed in the ground state therefore the quenching of fluorescence will be diminished – as the fluorophore react with the quencher, the intensity of the fluorescence decreases. In static quenching, the fluorescence intensity was observed decreasing as the concentration of quencher increases, with no changes in the fluorescence lifetime. This phenomenon can be explained with an equation:

$$\frac{\tau_0}{\tau} = 1 \quad \text{Equation 1.4.9}$$

The lifetimes in the absence and presence of quencher will be presented as a horizontal straight line at 1 which appears to be different from the Stern-Volmer plot, which will be presented as a linear positive gradient.

Furthermore, the quantum yield of the fluorophore without (ϕ_0) and presence (ϕ_q) of quencher can be calculated with:

$$\phi_0 = \frac{k_r}{k_r + k_{nr}} \quad \text{Equation 1.4.10}$$

$$\phi_q = \frac{k_r}{k_r + k_{nr} + kq\,[Q]} \quad \text{Equation 1.4.11}$$

Combination of Equation 1.4.10 and Equation 1.4.11:

$$\frac{\phi_0}{\phi_q} = \frac{k_r + k_{nr} + kq\,[Q]}{k_r + k_{nr}} = 1 + \frac{k_q[Q]}{k_r + k_{nr}} = 1 + \frac{1}{k_r + k_{nr}} \cdot kq[Q] \quad \text{Equation 1.4.12}$$

Besides, the Stern-Volmer constant (Equation 1.4.13), K_{sv} is an important parameter in quenching mechanisms as it indicates the sensitivity and efficiency of the fluorophore to the quenchers.[130,139-143] The Stern-Volmer equation (Equation 1.4.14) was introduced for the evaluation of fluorescence quenching processes and can be expressed as a function of the lifetimes or the fluorescence intensity, as shown in Equation 1.4.15.

Stern Volmer constant, K_{sv}:

$$K_{sv} = \tau_0 \cdot k_q \quad \text{Equation 1.4.13}$$

Hence, Stern-Volmer equation:

$$\frac{\phi_0}{\phi_f} = \frac{I_0}{I} = 1 + \tau_0 k_q [Q] \quad \text{Equation 1.4.14}$$

Stern-Volmer equation expressed with fluorescence intensity:

$$\frac{I_0}{I} = 1 + K_{sv}[Q] \quad \text{Equation 1.4.15}$$

Besides, k_q is also a measurement to determine the quenching efficiency or the affinity of the fluorophores to quencher. Theoretical calculations of k_q can be obtained if the diffusion coefficients (D) and molecular radii (R) of the quencher are known.[130] The radii, can be obtained from the molecular weights and densities of the quencher as well as from molecular models, meanwhile diffusion coefficients can be calculated with Stokes-Einstein equation:

$$D = \frac{kT}{6\pi\ \eta R} \quad \text{Equation 1.4.16}$$

-k is the Boltzmann's constant, T is the absolute temperature, η is the solvent viscosity, and R denoted as the molecular radius. The k_0, diffusion-controlled bimolecular rate constant can be calculated from the Smoluchowski equation:

$$k_0 = 4\pi RDN/1000 = \frac{4\pi N}{1000}(R_f + R_q)(D_f + D_q) \quad \text{Equation 1.4.17}$$

-R and D are denoted as the same functions in Equation 1.4.16, R_f and R_q are the molecular radii of fluorophore and quencher, D_f and D_q are the diffusion coefficients of the fluorophore and quencher, N denoted as Avogadro's number. $4\pi N$ needs to be divided by 1000 to convert molarity to molecules/cm^3. Finally, the quenching efficiency, f_Q can be calculated as below:

$$k_q = f_Q k_0 \quad \text{Equation 1.4.18}$$

The highest value of f_Q can be predicted is 1.0, as the highest collisional frequency will be having 100% quenching rate. For instance, if the f_Q=0.5, then the effective quenching by collisional frequency will be 50%. The typical diffusion-controlled quenching rate, k_0 in liquid is around $1 \times 10^{10}\ M^{-1}s^{-1}$.[77,130] A quenching system that has larger quenching rate constant than the diffusion-controlled k_q value will have higher efficiency in quenching as $k_q > 1 \times 10^{10}\ M^{-1}s^{-1}$indicates that the diffusion of fluorophore and the quencher is higher. At the same time, if the $k_q < 1 \times 10^{10}\ M^{-1}s^{-1}$can result from a low quenching efficiency or steric shielding hence less effective in binding the fluorophores and quenchers.[130] As the benchmark for the diffusion-controlled quenching constant (k_q), the collisional frequency in oxygen with tryptophan is highly effective, having $f_Q = 1.0$ and $k_q \sim 1 \times 10^{10}\ M^{-1}s^{-1}$. As shown in Equation 1.4.16 and 1.4.17, the size of a quencher can also affect the diffusion rate and quenching rate of a system, therefore larger quenchers such as acrylamide has lower k_q values than the quenching rate of oxygen-tryptophan.[130] Motivated by these findings, a number of DPP-based materials are evaluated in relation to their use as fluorescence-based sensing platforms for nitroaromatic compounds such as non-phenolic and phenol-based nitroaromatics. The main objective of this project is to investigate the substitution of DPP and its impact on photophysical properties and the quenching effect on nitroaromatic compounds.

1.4.1 The Quenchers: Nitroaromatic Compounds

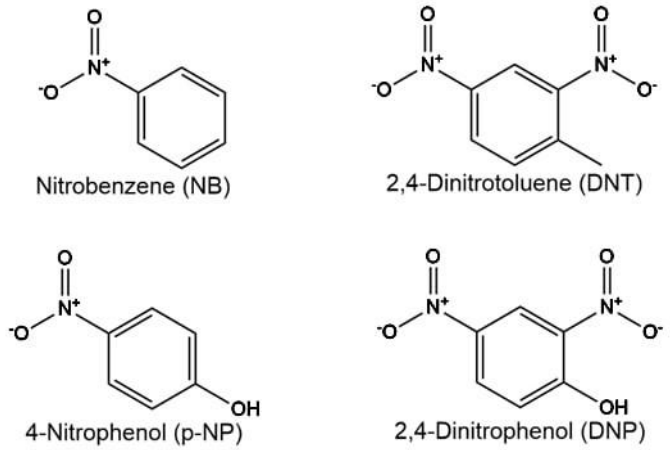


Figure 1.4.2: The nitroaromatic compounds studied in this project.

Nitroaromatic compounds are among the widely distributed and most important industrial chemistry groups. The demand of nitroaromatic compounds in the industrial for the use of pesticides[144-146] and explosives[144,147] have always been a major focus on the environmental contamination and security concern for public as these can directly harm the quality of life for human as well as this planet Earth. Two groups of NACs were studied in this project – non-phenol (NB and 2,4-DNT) and phenol-based (p-NP and 2,4-DNP) NACs. Nitroaromatic compounds are the combination of strong electronegativity nitro group attached to a benzene ring.

The nitro group are made up of a partially positive nitrogen atom and two electron-deficient oxygen atoms. The nitro group ($–NO_2$) is ready for the delocalization of π-electrons to the benzene core for balancing the charge deficiency, causes the benzene ring to decrease in electron density. As these nitroaromatic compounds are electron deficit, they can be detected by π-electron rich fluorophores by photoinduced electron transfer[148-155] – the study of nitroaromatic detection was performed through fluorescence quenching of DPPs. The nitro group would have a high tendency to pull electrons from another molecule – as the nitro group increases, the quenching efficiency of DPPs will increases too. Hence the hypothesis of this study is that fluorophores quenched by 2,4-DNT and 2,4-DNP will have higher K_{SV} and k_q than those quenched by nitrobenzene and p-NP.

It is of the highest priority to design a highly efficient nitroaromatic detection technique to solve the current issues that these chemical compounds have caused, namely the threat on human safety as well as pollution to the environment. To date, a range of methods such as ion mobility spectrometry[156,157], nuclear quadrupole resonance[158], gas chromatography[159,160], mass spectrometry[161,162], x-ray diffraction[163] and Surface Enhanced Raman Scattering (SERS) spectrometry[164,165] have reported for their sensitivity and selectivity. These methods have been widely utilised for the detection of NACs. Nonetheless, compared to fluorescence quenching method, these techniques suffer from several drawbacks such as bulky instrumentation, not time-and-cost-effective and inconvenient such as pre-treatment of samples prior the tests.[166] Besides, one of the challenges for these detection technologies is that they should be able to perform the tests at the forefront when detecting explosives or pollutants.[167,168] The drawbacks have deemed the methods abovementioned are not suitable for the detection of nitroaromatic components at the field. The most ideal detection tool should be highly selective, sensitive and working remotely – capable in identifying and distinguishing the nitroaromatic compounds chemically or structurally in a sample that are contaminated with different types of analyte by a remote instrument that are not too bulk and be able to bring to the field for analytical testing. A field portable of selective and sensitive NACs detection are indeed important for the defence industry and environmental concern – antiterrorism and to improve detection for pollution issues.[144,145]

Materials and Methods

2.1 Materials

ClNDPP, ClN6DPP, FNDPP and TNDPP were synthesised by our group and the remaining materials (ClBDPP, FBDPP and TBDPP) were provided by Dr Callum McHugh from the University of the West of Scotland.[169,170] Dichloromethane solvent (anhydrous ⩾99.8 %, contains 40-150ppm of amylene as stabilizer, CAS: 75-09-2, LOT #1990394) were purchased from Acros Organics and HPLC grade acetonitrile solvent (⩾ 99 %, CAS: 75-05-8, LOT #1946093 / LOT #1995992) were purchased from Fisher Chemical and Acros organics respectively and used without any further purification. Nitrobenzene (99%) was purchased from Thermo Fisher. 2,4-dinitrotulene (97%), 4-nitrophenol (⩽ 100%) and 2,4-dinitrophenol (with approx. 0.3ml H_2O/g) were purchased with Sigma-Aldrich and used as supplied. These nitroaromatic compounds were used as it is and not purified before use.

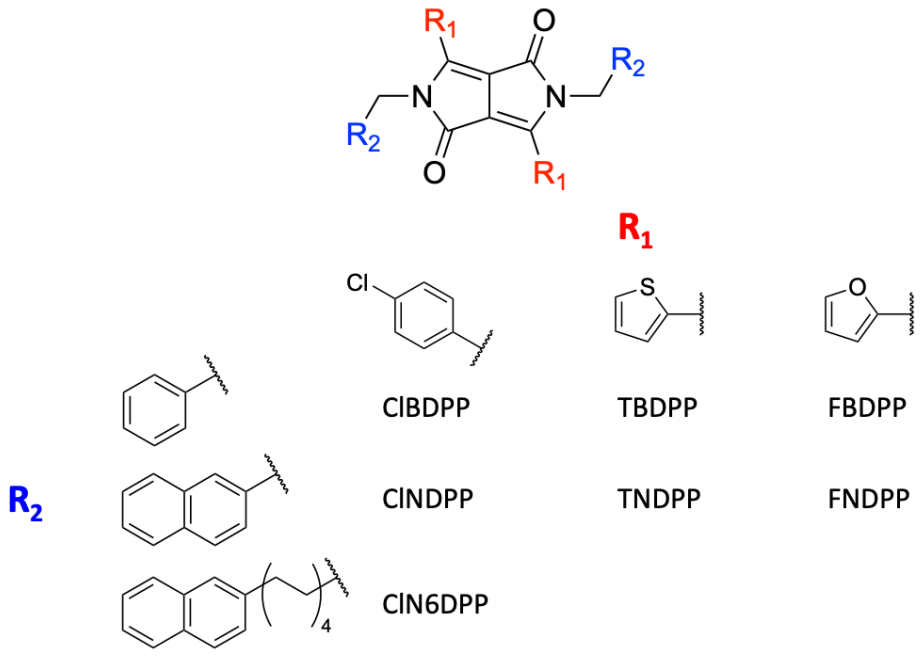


Figure 2.1.1: Illustration of the different DPP systems investigated in this work.

2.2 Methods

2.2.1 Absorption measurements

All absorption measurements were performed with a Perkin Elmer Lambda 25 UV/Vis spectrometer. All absorbance measurements in solution phase were conducted with a pair of 10 mm quartz cuvettes from Hellma® Analytics. The instrument was operated by Perkin Elmer UV Winlab software. The absorption coefficients of the diketopyrrolopyrroles were measured by means of the Beer-Lambert law.[130] The stock solution of each DPPs were made by dissolving 2 to 3 mg of dye in 10 mL of dichloromethane. The dyes were weighed out making use of a glass measuring boat and a high precision (5 decimal places) analytical balance from Sartorius™. The glass weighting boat was rinsed with dichloromethane several times and all sample were assumed to be transferred into the 10 mL volumetric flask. Five DPPs standard solution were made up for the calculation of the absorption coefficients from the stock solution prepared. 250 and 500 µL removable-needle glass syringes purchased from SGE Analytical Sciences were used to aliquot increasing volumes of stock solution into five 5 mL volumetric flasks and filled up to volume with dichloromethane.

2.2.2 Fluorescence emission measurements

The fluorescence emission measurements were performed with a Perkin Elmer LS 55 fluorescence spectrometer. All fluorescence emission measurements were conducted with a 10 mm quartz cuvette from Hellma® Analytics. The luminescence spectrometer was operated by FL Perkin Elmer Winlab Data Processor and Viewer Software. The photomultiplier tube voltage and emission filter were set differently according to each of the DPPs. For the simultaneous excitation-emission maps, the excitation wavelength was always set starting from 250 nm, scan speed set at 200 nm/min and excitation increment at 10 nm. Besides, the excitation and emission slit were set differently in different DPPs, but was advice to maintain at a maximum of 10.0 nm. Slit ranges from 8.5 nm to 10.0 nm was used in this study. The optical density of the samples for fluorescence emission study was always below 0.1 at the excitation wavelength.

Lifetime measurements were performed using a time-correlated single-photon-counting instrument (Edinburgh Instruments FLS 920). To excite the samples a picosecond-pulsed EPLED 485 (482.0 nm, pulse width FWHM: 100.6 ps). Deconvolution analysis of the decay kinetics yielded the fluorescence lifetimes. A light-scattering Ludox solution was used to obtain the instrument response function. The lifetimes were provided by our collaborator, Prof. Uwe Pischel of the University of Huelva (Spain) and unfortunately, quantum yield was not provided nor studied in this work. The lifetimes were presented in Table 3.1.1 at 'Results and Discussion'.

2.2.3 Fluorescence quenching measurements

The fluorescence quenching measurements were performed with Perkin Elmer LS 55 fluorescence spectrometer – fluorescence intensity of the DPPs with and without quenchers were measured. Besides, the absorbance of each standard solution prepared were measured before the fluorescence measurements to ensure consistency. The absorbance measurements were performed with Perkin Elmer Lambda 25 UV/Vis spectrometer. The instruments were operated with the same software used in absorbance and fluorescence emission measurements. The fluorescence quenching measurements were done in duplicate, and the results stated were the average of the two quenching results.

Stock solution of quenchers and fluorophores were made up before performing any measurements. The stock solution of the dyes was made as described in 2.2.1. On the other hand, the quenchers were weighted out with appropriate amount making use of a glass measuring boat and a high precision (5 decimal places) analytical balance from Sartorius™. The glass weighting boat was rinsed with dichloromethane or acetonitrile for several times and all samples were assumed to be transferred into the 25 mL volumetric flask. The stock of the quenchers was then filled up to volume with the solvent. Note that in the case of nitrobenzene, the liquid quencher was syringed into the 25 mL volumetric flask with a 500 µL of removable-needle glass syringes purchased from SGE Analytical Sciences. p-nitrophenol and 2,4-dinitrophenol were studied in acetonitrile only as they have very poor solubility in

dichloromethane as the quenchers contained water – dichloromethane is only slightly miscible with water.[150]

Seven quenching standard solution were made up to perform the Stern-Volmer experiments from the stock solution prepared. 50, 100 and 500 µL of removable-needle glass syringes purchased from SGE Analytical Sciences were used to syringe different amount with increasing volumes of quenchers and identical amount of DPPs in seven 5 mL volumetric flask. The samples were filled up to volume with dichloromethane or acetonitrile. The Stern-Volmer studies performed for 2,4-dinitrophenol were prepared in five standard solutions because of limited amount of the quencher. The fluorescence intensity of the DPPs with and without quenchers were recorded for the calculation of Stern-Volmer values of each DPP. The lifetime and quantum yield of DPPs with quencher were not studied.

3 Results and Discussions

3.1 Photophysical properties

The DPP systems studied (please refer to Figure 2.1.1 in section 2.1) in this work were substituted with different rings at the aryl carbon-3 and carbon-6 position of the DPP core, as well as the substitution at the nitrogen atoms. Parameters such as the absorption factor (ε) and maximum absorption wavelength (λ_{max}^{abs}) are important spectral features in defining the applicability of a chromophore,[172-174] hence it is important that a highly efficient optical sensor material exhibits optimum photophysical properties in relation to their absorption properties, for example, chromophores with higher absorption factors have superior ability to absorb light at a given wavelength.

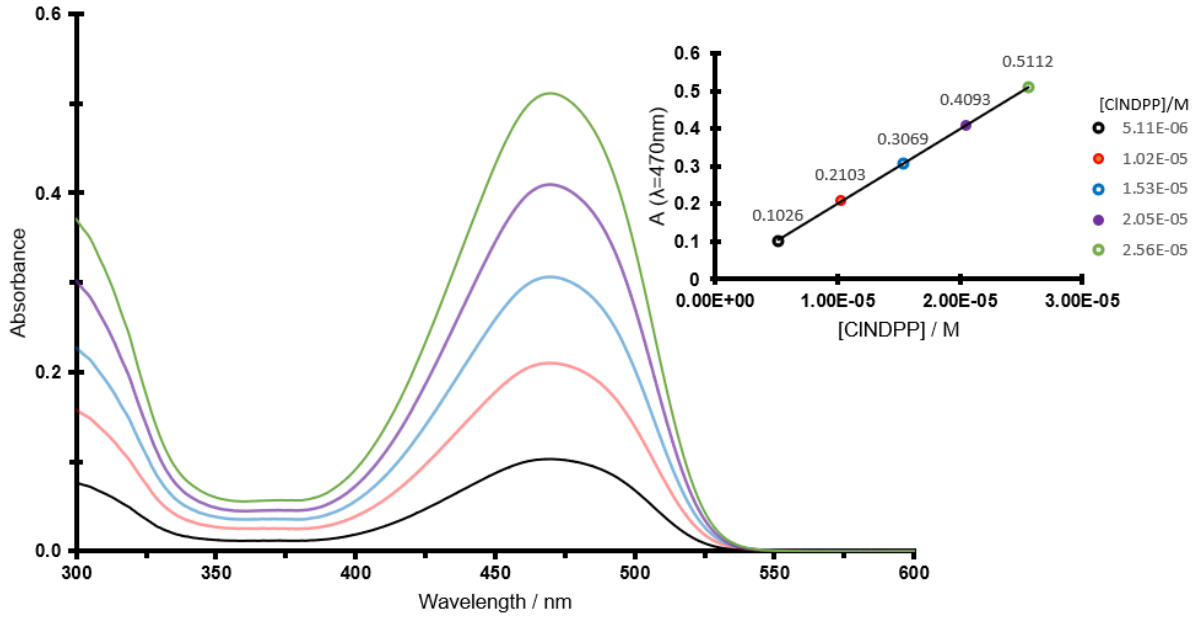


Figure 3.1.1: Absorption spectra of increasing concentration ClNDPP solutions in acetonitrile. Inset illustrates the linear Beer-Lambert plot for absorbance at λ_{max} = 470 nm.

Figure 3.1.1 illustrates the absorption spectra of ClNDPP in the solvent of acetonitrile and the resulting Beer-Lambert plot for the experimental determination of the absorption factor. In all cases, linear Beer-Lambert plots were obtained, with r^2 value ≥ 0.995. Failure to obey the Beer-Lambert law, which is the linear relationship of asorbance vs concentration

might resulting from the aggregation at high concentrations, or interfering of other absorbing species.[77]

Table 3.1.1: Molar absorptivity (ε), absorption maximum (λ_{max}^{abs});: emission maximum (λ_{max}^{em}) and Δṽ: Stokes shift for all investigated materials in the solvents of acetonitrile (ACN) and dichloromethane (DCM).

	ε_{max} / $\times 10^4$ M^{-1} cm^{-1}	λ_{max}^{abs} / nm	λ_{max}^{em} / nm	Δṽ / cm^{-1}	τ/ns
DPP			**ACN/DCM**		
ClBDPP	2.02 / 2.03	469 / 473	533 / 534	2560 / 2415	6.05/5.97
ClN6DPP	1.89 / 1.98	470 / 475	538 / 540	2689 / 2534	6.62/6.51
ClNDPP	1.99 / 2.09	470 / 474	535 / 537	2585 / 2475	6.04/5.89
FBDPP*	4.81 / 4.81	532 / 536	541 / 546	313 / 342	5.73 ≥ x ≥ 5.56 / 5.93 ≥ x ≥ 5.71
FNDPP	4.96 / 7.13	533 / 537	542 / 545	312 / 273	5.56/5.71
TBDPP	2.73 / 2.77	541 / 545	556 / 560	499 / 491	5.73/6.02
TNDPP	1.41 / 1.59	542 / 546	556 / 561	465 / 490	5.73/5.93

*The lifetime of FBDPP was not experimentally determined.

Having high absorption factor is one of the most important properties of a chromophore, as high absorption factor chromophores have higher possibility for excitation over a range of wavelengths.[77] This also can be explained that there are higher chances the chromophore can excite to a higher energy level and emit light. Absorption factors of ca $2.50 \times 10^4\ \mathrm{M^{-1}cm^{-1}}$, have been reported for DPPs.[175-177] Various small molecule DPPs studied in different solvents were reported having absorption factors, ranging from $1.26\times 10^4 - 1.29\times 10^5\ \mathrm{M^{-1}cm^{-1}}$.[176-187] In all cases, we observed absorption factors which are in line with those reported for DPPs, with particularly high values in the case of furan-containing materials, namely FBDPP and FNDPP.

The effect of substitutions on the absorption maximum was observed to be more significant when this takes place on the core rings and not on the lactam nitrogen atoms (Table 3.1.1) This can be attributed to the greater planarity and better conjugation in DPPs containing furan and thiophene core rings when compared to classical phenyl substituted ones. As the increasing of π-conjugated system resulting in narrower HOMO-LUMO gap, and in this case, furan/thiophene required less energy to promote a π → π* transition than a benzene ring. Besides, the results show that TNDPP has lower ε than TBDPP, even though it has more π-conjugated system, this is because of the low oscillator strength in TNDPP than

TBDPP. Low oscillator strength indicates low absorption rate of the chromophore during excitation electron transition.[188]

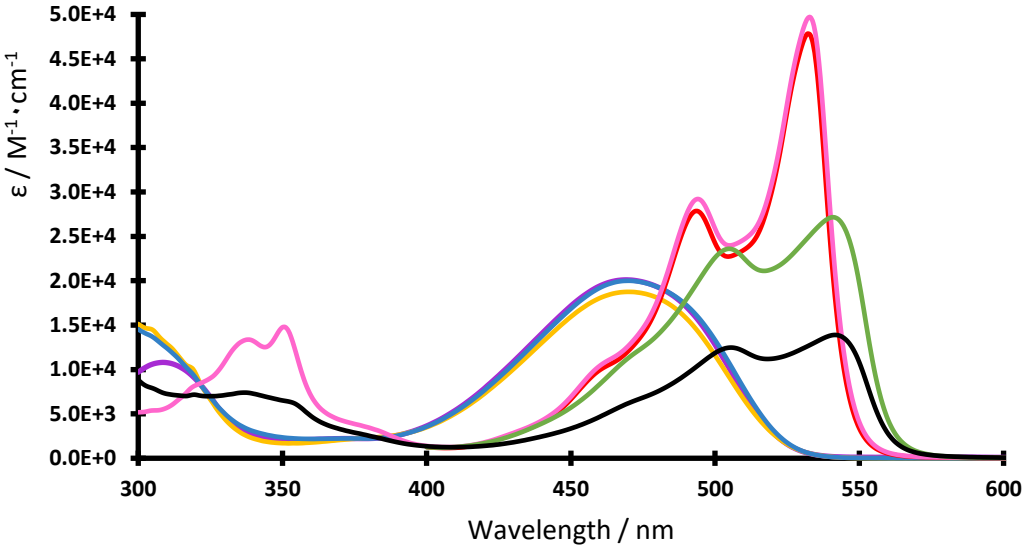


Figure 3.1.3: Molar absorptivity spectra of ClBDPP (purple), ClN6DPP (orange), ClNDPP (light blue), FBDPP (red), FNDPP (pink), TBDPP (green) and TNDPP (black) in acetonitrile from 300nm to 600 nm.

Figure 3.1.3 illustrates the absorption spectra normalized for the absorption factor for all investigated materials in the solvent of acetonitrile. The chlorinated DPPs show similar spectral shape and are hypsochromically shifted compared to other substituted DPPs. As chlorobenzene is a larger moiety and is more flexible, it has higher tendency for rotation during electronic transition,[81] hence the broad absorption spectral shape in chlorinated DPPs.[77,81] These broad absorption bands were made up by several vibrational progression bands during $S_0 \rightarrow S_1$ transitions.[77,189] The photophysical properties of a chromophore can be strongly affected by its planarity and π-extension.[81,176,177,190] Results have shown very small difference in the maximum absorption wavelengths between the N-benzyl DPPs and N-naphthyl DPPs. Considering that reduced π-extension does result in blue shift in the maximum absorption and fluorescence emission wavelength, which could possibly decrease the absorption factor and decreasing the electron donating nature of the substituents – though the elongated π-conjugation is not from the core, less conjugation in a molecule also

decreases the number of electrons that are readily available for donate to neighbouring moiety.

Vibronic peaks were found at the absorption spectra of furan- and thiophene-containg systems, FBDPP, FNDPP, TBDPP and TNDPP. These distinguishable vibronic progressions show that furan and thiophene are very planar and rigid – less flexibility for rotation or vibration. Although they are highly planar, furan has shown better planarity as furan is smaller than thiophene.[81,191] The furyl-substituted DPPs presented sharper absorption spectra – FNDPP and FBDPP have better π-conjugated system due to their higher planarity. The strong π-conjugation also results in higher absorption factor than TBDPP and TNDPP therefore were hyperchromic shifted compared to the phenyl-substituted absorption spectra. The higher absorption factor observed in FNDPP also indicates it has higher oscillator strength as well as higher electron donating ability than FBDPP. Previous studies also found vibronic shape absorption spectra in some furyl[176-178,192,193] and thienyl[194-196] substituted DPPs.

The size of a substituent should be taken into consideration as this can be a factor that affects the properties of a chromophore. For example, a larger molecule 2-cyanobenzofuran[176-178] substituted DPP was reported to have a ε_{max}= 4.31 x10^4 M^{-1}·cm^{-1}. To compare with the smaller furan, FBDPP (ε_{max}= 4.81 x10^4 M^{-1}·cm^{-1}) and FNDPP (ε_{max}= 7.41 x10^4 M^{-1}·cm^{-1}), show higher absorption factor. This can be associated to the rigidity and planarity of 2-cyanobenzofuran, it is less rigid and lower in planarity than FNDPP and FBDPP, which results in lower absorption factor. This also can be explained based on the strength of the oscillator for the transition as this parameter can affect the planarity of a chromophore. As mentioned above, FBDPP and FNDPP has higher oscillator strength than the reported DPP.

In another report, a carbon-2 and carbon-3 thiophene substituted DPP were reported[176,177] to have similar absorption factor ε_{max}= ~2.40 x10^4 M^{-1}·cm^{-1} in chloroform. The 2-thienyl substituted DPP had maxima absorption wavelength at 533 nm while the 3-thienyl had it at 493 nm. Here it shows that 2-thienyl substituted DPP, which was the same substituents in TNDPP and TBDPP, has higher oscillation strength than the carbon 3 thiophene substituted DPP. The report also pointed out that the carbon-2 thiophene substituent has less steric hindrance, higher in planarization and rigidity than carbon-3 thiophene.

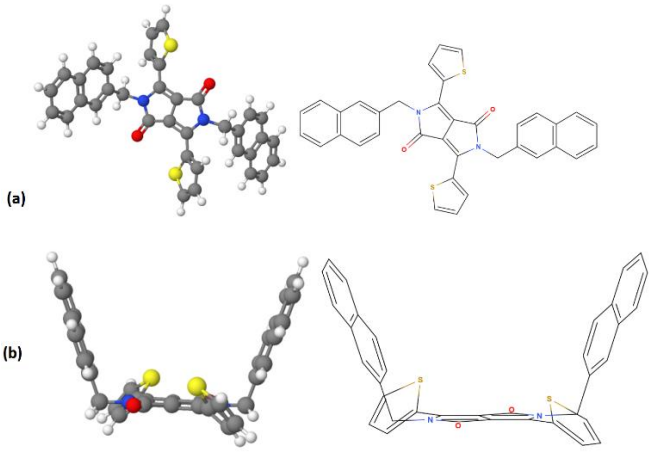


Figure 3.1.4: 3D and 2D illustration of (a) planar as well as (b) eclipsed conformation steric hindrance of TNDPP.

As mentioned above, rigidity and planarity of are very important as they are responsible for the photophysical properties of a DPP.[81,197] As expected, N-substitution also could modify the optical properties of DPPs. First of all, N-substitution can affect the electron density on the DPP core through the nitrogen atoms. Moreover, it can increase the steric hindrance (Figure 3.1.4) of the side chain on the aromatic substituents – steric hindrance can lead to rotation in the backbone[81,198-202] and decreases the planarity of the DPP, and consequently, reducing the π-conjugation between the carbon 3 and 6 substituents.[81,198]

Previous studies have compared N-substitutions of methyl, hexyl, allyl and 2,4-dinitrophenyl, which react differently at their dihedral angles with contact of the DPP core, from 30.5°, 34.2°, 36.3° to 44.3°respectively.[93,179,203] Normally, the benzene rings of para-substituted phenyl groups carbon-3 and carbon-6 are 30-40° twisted from the DPP core[93,179,180,204-209]. Interestingly, there was one noteworthy exception for chlorobenzene substituted DPP. The torsion angles of the DPP were reported between 45-48° [180,181] when the methyl and benzyl N-substituted DPPs were aryl-substituted with p-chlorophenyl. The angle was studied with X-ray crystallographic methods.

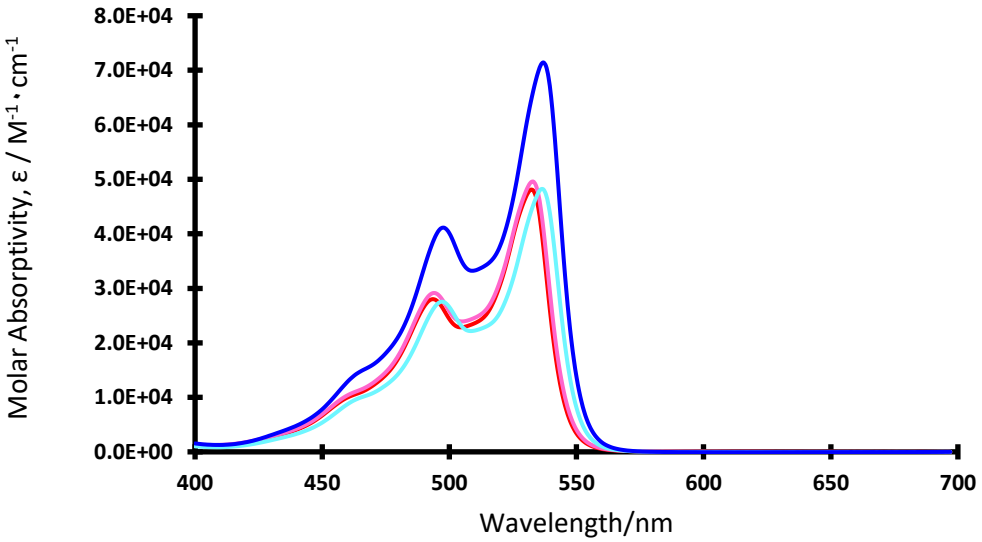


Figure 3.1.5: The molar absorptivity plot of FNDPP in acetonitrile (pink) and DCM (blue); absorption spectrum of FBDPP in acetonitrile (red) and DCM (turquoise).

Solvatochromism has been reported previously in DPP materials.[210-212] Compounds that shift their absorption and emission spectrum dependant on solvent polarity are called solvatochromic. Bathochromic (red) and hypsochromic (blue) shift to the increase in polarity are known as positive and negative solvatochromism, respectively.[77,213-217] Results show that the λ_{max}^{abs} of the studied DPPs in acetonitrile is shorter than in dichloromethane, where the spectral shifted to the shorter wavelength. However, these are arguably small changes. For example, as shown in Figure 3.1.5, FBDPP has λ_{max}^{abs} of 532 nm in acetonitrile and 536 nm in DCM. FNDPP has 1 nm longer of λ_{max}^{abs} than FBDPP in both solvents. This phenomenon hereby shows negative solvatochromism in the DPP compounds in this project – spectra were blue shifted with increasing solvent polarity. The blue colour absorption band shows FNDPP has a strong $\pi \rightarrow \pi^*$ transition in DCM compared to in acetonitrile, thus red shifted band and higher absorption factor. The blue shifts with increasing solvent polarity also shows that the furan-substituted DPPs were less polar during excited state ($S_0 \rightarrow S_1$) than in ground state – more energy is needed to promote the electron to excited state therefore increase in energy gap between the ground and excited state and result in hypsochromic shift.[218,219] Previous studies also show the same spectral shift under same conditions.[193,220-222] Substitution wise, FBDPP and FNDPP are having the similar maximum absorption wavelength with 1 nm difference.

However, as for the FNDPP in DCM, it has the highest absorption factor with the narrowest Stokes shift among these DPPs. This can be explained that FNDPP may have the highest planarity, which this is why FNDPP is slightly bathochromically shifted compared to FBDPP, also positively affecting the oscillator strength for the transition where it enhances the dipole moment during the π-π* transition, hence increased molar absorptivity.

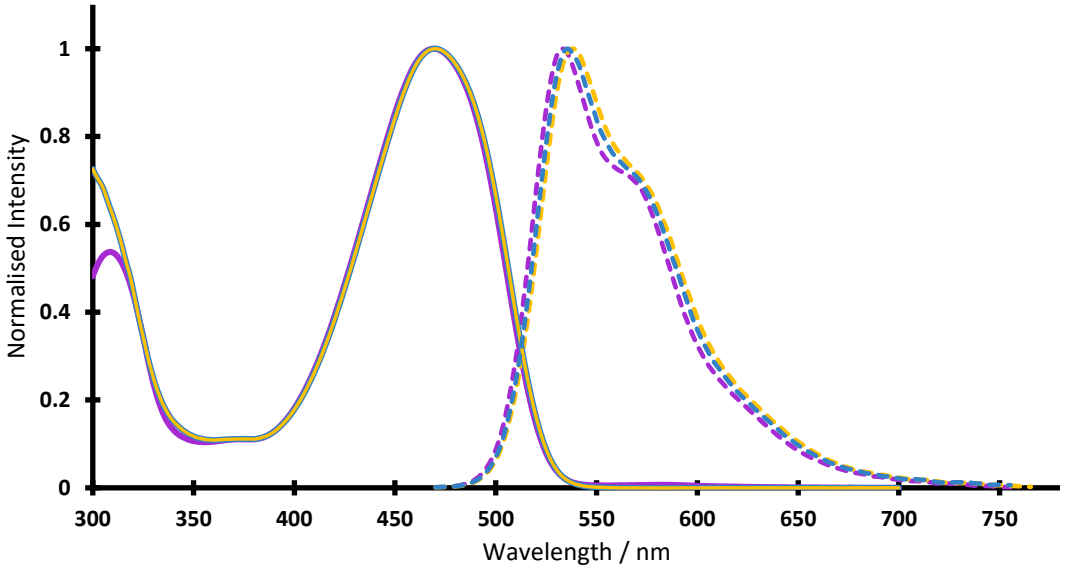


Figure 3.1.7: Normalised absorption (solid line) emission (dashed) spectra of ClBDPP (purple), ClN6DPP (orange) and ClNDPP (blue) in acetonitrile.

ClBDPP, ClN6DPP and ClNDPP have the largest Stokes shift among the DPPs studied. The fluorescence emission spectra of ClBDPP, ClNDPP and ClN6DPP were broad and have less distinguishable vibronic peaks. This is because chlorobenzene is less rigid and less planar with respect to the DPP core when compared to furan- and thiophene-containing systems. The chlorinated DPPs have shorter maximum absorption and emission wavelength compared to the other DPPs and among them, ClBDPP has the shortest maximum emission wavelength, because it is less π-conjugated. The emission spectra were consistent with that expected for a single fluorescence emission species. From the results obtained it shows that the chlorobenzyl substituted DPPs have the largest Stokes shift also indicates that this group DPPs

would have less chances to undergo self-absorption or inner filter effect, which can represent a problem in the application of these materials as optical sensors.[223,224]

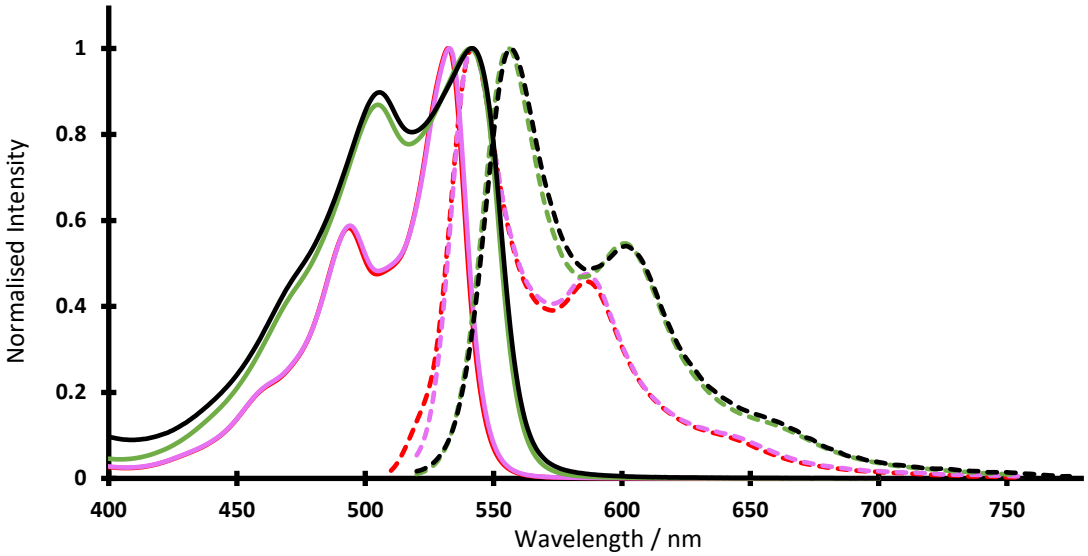
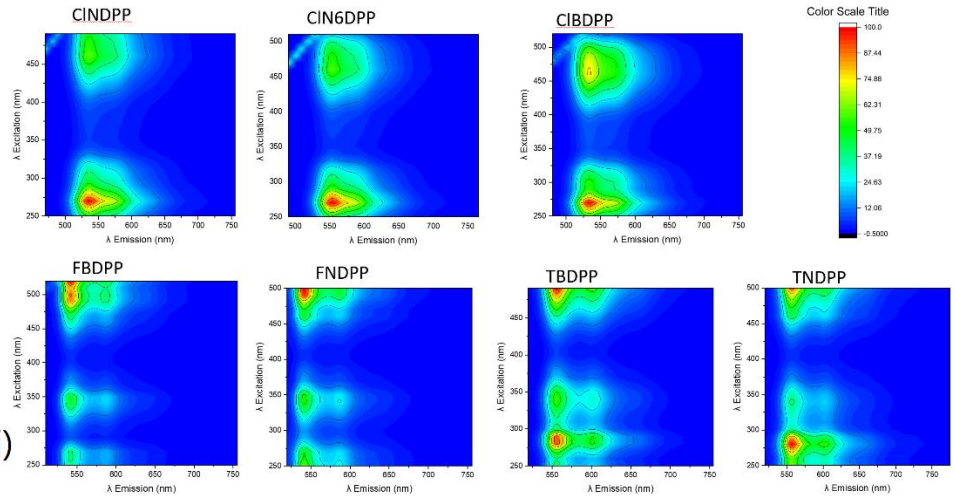


Figure 3.1.8: Normalised absorption (solid line) emission(dashed) spectra of FBDPP (red), FNDPP (pink), TBDPP (green) and TNDPP (black) in acetonitrile.

In contrast to the chlorobenzene substituents, FB/FNDPP and TB/TNDPP all exhibit vibronic progression on both their absorption and emission spectra as well as smaller Stokes shift. The latter is an important parameter to study the excited state of a fluorophore. The rigidity of furan and thiophene is the reason for the narrow Stokes shift as the more rigid the molecule is, the lower the room for structural re-arrangement when the excited state is generated. It is noteworthy to mention that, although TBDPP has the same Stokes shift in wavelength in acetonitrile and dichloromethane, which were 15 nm, however, their Stokes shift in wavenumber were 499 cm^{-1} in acetonitrile and 491 cm^{-1} in the less polar solvent dichloromethane. This shows that reporting Stokes shift in the unit of nm is not appropriate and these should be given in units which are proportional to energy, such as cm^{-1}. Besides, for reference, studies have found that iodinated thiophene DPP were reported to have about 22% higher absorption factor as well as smaller stokes shift (10 nm/300 cm^{-1}) than the non-iodinated 2-thienyl DPP (14 nm/455 cm^{-1}). This is an important finding as the absorption factor of the DPP can be improved by introducing iodinated thiophene into the system. The

iodinated thiophene DPP also shows a bathochromic shift in the absorption maximum.[213,214] This information is interesting because the intensity of the fluorescence should be lower as the fluorescence is quenched with heavy atom effect as iodine is a heavy atom.[211] However, if the derivative with the iodine substitution does not show a decrease in the fluorescence quantum yield, then it means that the heavy atom effect is not observed in these systems. Previous studies also shown that high rigidity and planarity furan-based and thiophene-based DPPs have sharper absorption emission spectra and narrow Stokes shifts.[81,176,178,223-225] Similar to the chlorinated DPPs, the emission spectra in FNDPP, FBDPP, TNDPP and TBDPP also show singlet emitter and only contain one fluorescence emission species. This is shown in the excitation-emission maps (Figure 3.1.9), where the fluorescence emission shown highest saturation (according to the colour scale) at the maximum emission wavelength.

(i)



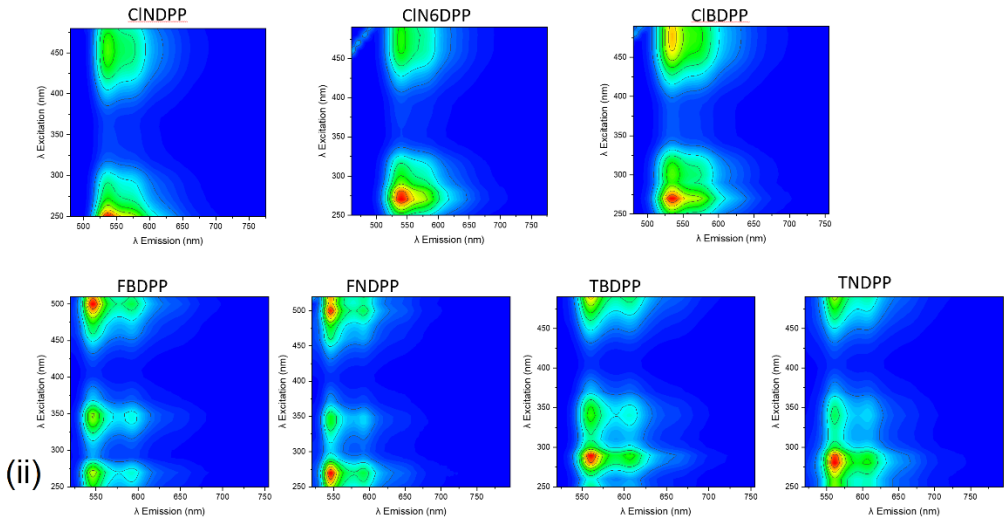


Figure 3.1.9: 3D contour plots of the excitation-emission maps for the DPPs in (i) acetonitrile and (ii) dichloromethane.

Other than Stokes shift and emission maximum, the lifetime, τ, and quantum yield, ϕ, also denote important parameters to characterize a fluorophore. Lifetimes are presented in Table 3.1.1. It should be noted that the quantum yield of the chromophores was not studied in this work. With respect to solvent effects, the lifetime of ClBDPP, ClN6DPP and ClNDPP were longer in the less polar DCM while FNDPP, TBDPP and TNDPP have longer lifetimes in higher polarity acetonitrile. These effects may be caused by the stability of the solute and polarity of solvent, which might affect the lifetime of the fluorophores. For example, ClBDPP, ClN6DPP and ClNDPP are more stabilised in ground state when surrounded by lower polarity DCM while FBDPP, FNDPP, TBDPP and TNDPP are less stabilised in DCM at S_0 – this also explain the results obtained from the absorption measurement that furan-substituted DPPs need less energy to promote to S_1 in DCM than in acetonitrile. However, more studies have to be done to prove this.

The lifetime of FBDPP was not determined on this work, however, according to the trend shown in ClBDPP/ClNDPP and TBDPP/TNDPP, also, since FNDPP has lower lifetimes than TBDPP and TNDPP, herein we predict that FBDPP has higher lifetime than FNDPP as well as lower lifetime than TBDPP/TNDPP. Lifetimes between 5.50 to 7.46 ns have been reported for thiophene-based DPPs in different organic solvents such as toluene, orthochlorobenzene, 2-methyltetrahydrofuran and benzonitrile.[226] Therefore, the estimation lifetime of FBDPP will

be 5.65 ns in acetonitrile and 5.82 ns in DCM. Previous studies have reported fluorescence lifetimes of DPPs in different solvents ranges from 0.01 ns to 9.65 ns.[206-208] Fluorescence lifetimes are needed to calculate quenching rate constant (k_q). Calculated k_q values will be stated in following subsection 3.2.1 and 3.2.2. These values are needed to study the quenching efficiency of these materials – they will be discussed around the diffusion-controlled rate constants in the solvents to study the quenching efficiency of the DPPs. The relationship of DPPs and quenchers will be investigated along with the quenching rate constant of DPPs in depth in section 3.2.

3.2 Sensing of nitroaromatic compounds

There were four nitroaromatic compounds studied (please refer to Figure 2.1.2 in section 2.1) in this work. They were classified into two different groups – non-phenol (section 3.2.1) and phenol-based (section 3.2.2) nitroaromatic compounds. Section 3.2 will be discussing about the quenching of diketopyrrolopyrroles with nitrobenzene (NB), 2,4-dinitrotoluene (2,4-DNT), p-nitrophenol (p-NP) and 2,4-dinitrophenol (2,4-DNP). The quenching efficiency of the DPPs will be explained and discussed based on the quenching rate constant (k_q).

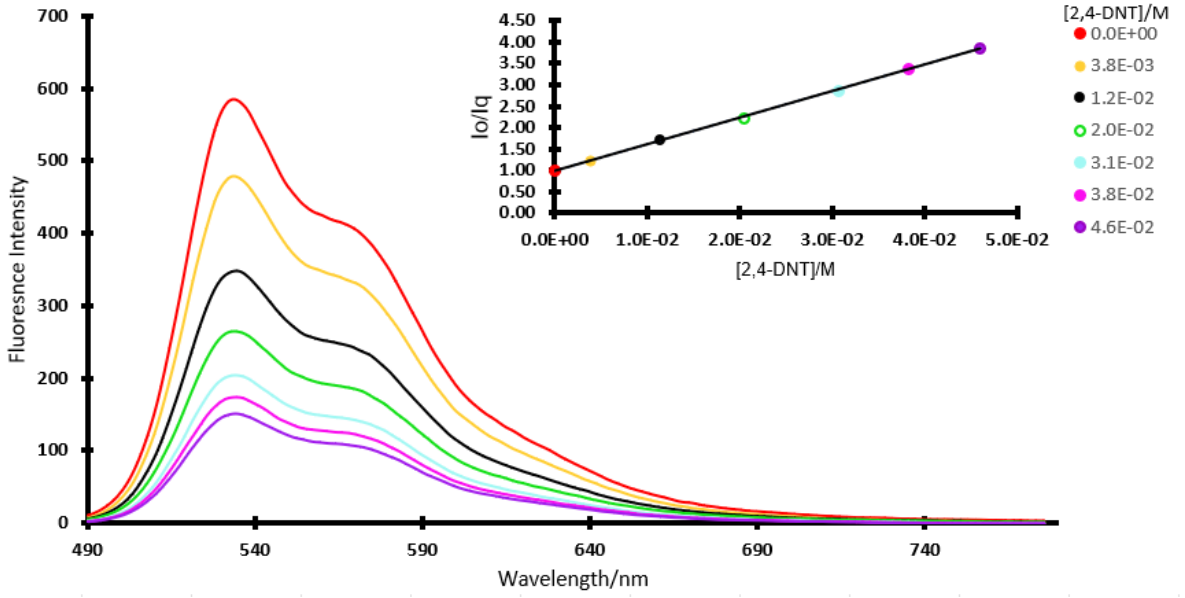


Figure 3.2.1: Fluorescence emission spectra of ClNDPP with increasing concentrations of 2,4-DNT. Inset illustrates the linear relationship observed as a function of the quencher concentration with r^2 value 0.9996 within the Stern-Volmer formalism.

The fluorescence intensity should show decreasing in fluorescence intensity when in contact with NB, 2,4-DNT, p-NP and 2,4-DNP as the fluorescence will show a "turn-off" sensing upon the detection of nitroaromatic compounds. As shown in Figure 3.2.1, fluorescence intensity decreases as the concentration of the quencher increases. Results will be discussed thoroughly in the following subsections. It was of interest to determine how the substitution of DPPs can affect the quenching efficiency in different nitroaromatic compounds.

3.2.1 Detection of non-phenol based nitroaromatic compounds

Table 3.2.1.1: Stern-Volmer and quenching rate constant of DPPs in acetonitrile (ACN) and dichloromethane (DCM).

	Quenching rate constant, k_q / x10^9 M^{-1} s^{-1}	
NAC / **DPP**	**NB**	**2,4-DNT**
	ACN / DCM	**ACN / DCM**
ClBDPP	8.03 / ---	10.61 / ---
ClN6DPP	8.75 / 4.72	11.3 / 7.25
ClNDPP	8.61 / 4.45	10.7 / 6.96
FBDPP*	x > 9.66 / ---	15.60 > x > 13.30 / ---
FNDPP	9.66 / 6.29	15.6 / 12.4
TBDPP	8.46 / ---	12.8 / ---
TNDPP	8.24 / 4.37	13.3 / 9.80

*The quenching rate of FBDPP were not experimentally determined due to missing fluorescence lifetime for this compound.

Table 3.2.1.1 shows the results obtained from the quenching experiments with nitrobenzene (NB) and 2,4-dinitrotoluene (2,4-DNT). Based on the lifetimes provided and the K_{SV} obtained, the range of quenching rate constant of our DPPs detecting nitrobenzene in acetonitrile was 8.03 x 10^9 up to 9.66 x 10^9 $M^{-1}s^{-1}$. However, if the prediction of FBDPP based on its Stern-Volmer constant was correct, then the quenching rate constant of detecting nitrobenzene could be up to at least 11.78 x 10^9 $M^{-1}s^{-1}$in acetonitrile. Then, the k_q of DPPs detecting 2,4-DNT in acetonitrile was 1.06 x 10^{10} — 1.56 x 10^{10} $M^{-1}s^{-1}$ and 6.96 x 10^9 — 10.24 x 10^9 $M^{-1}s^{-1}$ in DCM. The quenching results in acetonitrile and DCM were presented in Figure 3.2.1.1. The results will be discussed mainly with two parameters, the lifetimes and quenching rate constant (k_q).

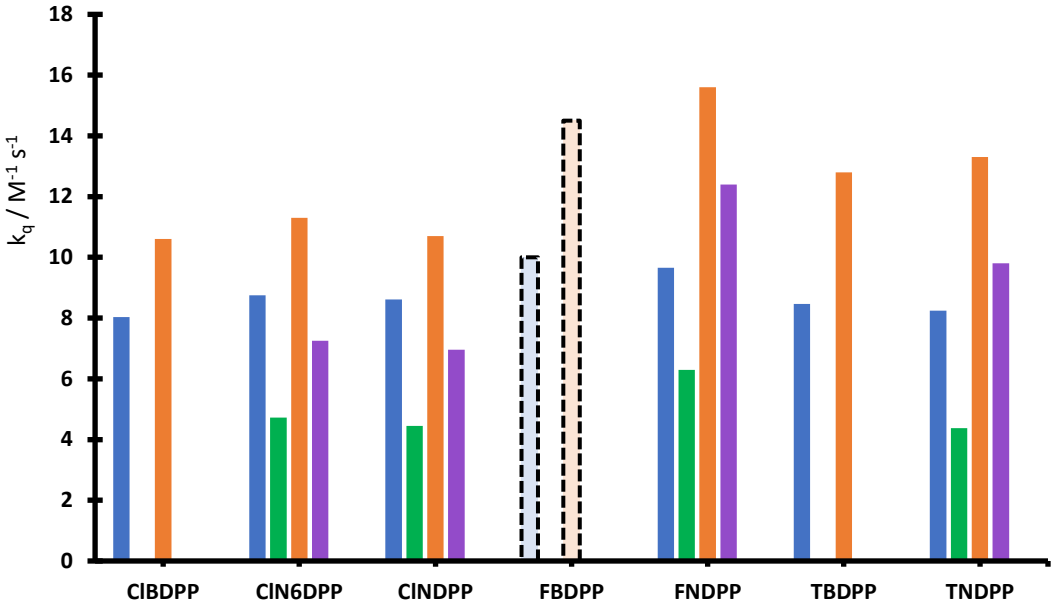


Figure 3.2.1.1: Quenching rate constant (blue: ACN, NB; orange: ACN, 2,4-DNT; green: DCM, NB; purple: DCM, 2,4-DNT) of DPPs quenched by nitrobenzene and 2,4-dinitrotoluene in acetonitrile and dichloromethane obtained from the Stern-Volmer plots. The faded orange and blue bars are the predicted k_q values of FBDPP.

The DPPs show higher K_{SV} values and k_q when detecting higher reduction potential electron withdrawing nitroaromatic groups – DPPs have higher quenching efficiency when sensing 2,4-DNT than nitrobenzene because 2,4-DNT has more nitro groups (NO_2) that increases the electron withdrawing effect as well as the reduction potential. Besides, TBDPP and TNDPP have overall lower quenching rate constant than other DPPs. If the predicted lifetime of FBDPP in acetonitrile was accurate, then FBDPP is a highly efficient fluorescence sensor for nitrobenzene, with quenching rate constant at least 1.18 x 10^{10} $M^{-1}s^{-1}$, which approach the diffusion-controlled rate in acetonitrile (2 x 10^{10} $M^{-1}s^{-1}$)[227,228]. Results show that the quenching efficiencies of these DPPs are higher in acetonitrile than in DCM, where the diffusion-controlled rate of DCM is 1.6 x 10^{10} $M^{-1}s^{-1}$.[229] In all cases, we observed quenching rate constants approaching diffusion-controlled limits in both solvents. These outcomes may be caused of the systems have higher driving force in acetonitrile than in DCM, which benefits the electron transfer.[230] Quenchers with higher reduction potential tend to

have higher ability to withdraw electron from the donor. The addition of nitro groups decreases the electron density on the aromatic rings and increases the overall electron affinity[137] thus a significant enhance on the quenching efficiency – quenching rate constant has increased 24 – 61.5% in acetonitrile and 53.6 – 124% in DCM. This also indicate that 2,4-DNT has better electron transfer driving force to these fluorophores compared to nitrobenzene, especially towards FNDPP.

$$K_{sv} = \tau_0 \cdot k_q \quad \text{Equation 1.4.13}$$

Quenching efficiency can be discussed with Equation 1.4.13, the Stern-Volmer Equation. The main parameters, fluorescence lifetime and quenching rate constant are important measurement to determine the quality of a sensing material through quenching mechanism. For example, the longer the fluorescence lifetime at the exciting state the higher chances a fluorophore can engage in photoinduced electron transfer reactions. The quenching rate constant is as important as the lifetime of a chromophore as it determines the rate at which the fluorescence emission of the fluorophore is quenched by the quencher. In other word, these parameters can determine the effectiveness of a fluorescence sensing material in tracing nitroaromatic by means of fluorescence quenching. Furthermore, although π-conjugation can affect the electron donating properties of a chromophore[179], redox potential is also a critical element to evaluate the performance of a sensing material. For instance, ClN6DPP, ClNDPP, FNDPP and TNDPP have greater conjugation than their counterparts ClBDPP, FBDPP and TBDPP, respectively. Therefore, they can have higher electron density at the core and hence are better electron donors. A good electron donor also indicates that the fluorophore has high oxidation potential, as the energy required to take an electron out is lower. However, for example, ClN6DPP has lower K_{SV} and k_q than FBDPP when detecting nitrobenzene, despite having more π-conjugation and longer lifetime in acetonitrile. This can be explained because of the longer alkyl chain on the lactam nitrogen atoms which diminishes the effect of the naphthalene groups. Thus, FBDDPP is actually more conjugated throughout the long molecular axis than ClN6DPP due to the furan vs chlorobenzene substitution as previously explained. Moreover, although the oxidation potentials of the DPPs

were not calculated in this work, this may be caused by the excessive oxidation rate in ClN6DPP than the reduction potential of nitrobenzene, hence it is easier to pull the electrons from FBDPP than ClN6DPP. Besides, the larger chlorobenzene in ClN6DPP than the furan in FBDPP could also be one of the reasons that affect the quenching result, as smaller moiety has higher planarity than large moiety therefore the former has more interaction between the core and the quencher. This result highlights that FBDPP has higher binding affinity to nitrobenzene hence has higher ability to donate electron to nitrobenzene.

According to the results obtained, the shortest lifetime determined for FNDPP did not translate into this being the least efficient sensing material. Instead, we calculated the largest quenching rate constant for this derivative when quenched by both nitrobenzene (DCM) and 2,4-DNT (acetonitrile and DCM). In contrast to ClNDPP and ClN6DPP, where ClN6DPP has a long 6 carbon long chains, which could have affected the π-π interactions and quenching effect as it may increase the fluorophore-analyte distance. However, as ClN6DPP has longer lifetimes than ClNDPP, this would benefit the excited electron to have higher chance to perform photoinduced electron transfer with the quenchers. The results of chlorinated DPPs also supported the statement and clearly show that fluorescence lifetime is not always an advantage in raising the efficiency of a fluorophore, at least in this study, lifetimes of the fluorophores did not seem to be a significant factor in affecting the quenching results.

Furthermore, one of the hypotheses made in this study was the N-naphthyl substituted DPPs would have a better quenching efficiency as they would have greater π-π interactions with the nitroaromatic compounds and thus enhanced electron transfer. By comparing the substitutions without including FBDPP, the DPPs show consistency in the quenching results, except for TB/TNDPP – the N-naphthyl substitution DPPs have better quenching rate constant. The furan-substituted DPPs had the largest K_{SV} and k_q values in detecting the non-phenolic nitroaromatics. As explained in section 3.1, furan was expected to have higher planarity than thiophene and chlorobenzene, therefore can have larger π-π interactions with the quenchers and followed by better quenching efficiency. Then, by comparing the TBDPP and TNDPP have slightly higher k_q values than the chlorinated DPPs in the quenching study of 2,4-DNT, whereas when quenched by nitrobenzene their quenching rate constant were lower than in ClNDPP and ClN6DPP. An assumption has made based on the results, that TB/TNDPP have undergo a different mechanism when quenching with

nitrobenzene and 2,4-DNT. Besides, this could be caused by the methyl ($–CH_3$) of the 2,4-DNT allows the π- π stacking interactions with TNDPP – the $–CH_3$ in 2,4-DNT favours high electron transfer between the quencher and the fluorophore therefore enhanced quenching efficiency in 2,4-DNT than in nitrobenzene. FNDPP and FBDPP have presented as better electron donor with good quenching rates to nitrobenzene and 2,4-DNT compared to the other DPP derivatives in this study. The next section will be discussing the quenching of DPPs by phenol-based nitroaromatic compounds.

3.2.2 Detection of phenol-based nitroaromatic compounds

Table 3.2.2.1: Stern-Volmer and quenching rate constant of DPPs in acetonitrile (ACN).

	Quenching rate constant, k_q / x10^9 M^{-1} s^{-1}	
NAC / **DPP**	**p-NP**	**2,4-DNP**
ClBDPP	7.55	12.30
ClN6DPP	7.92	13.20
ClNDPP	6.34	12.50
FBDPP*	6.90	16.30
FNDPP	6.29	17.10
TBDPP	5.64	15.50
TNDPP	6.00	18.80

*The quenching rate constants of FBDPP were not experimentally determined.

Phenol-based nitroaromatic compounds p-nitrophenol and 2,4-dinitrophenol have a hydroxyl group (–OH) instead of the methyl substitution on the toluene based nitroaromatics in 3.2.1. The electron donating nature of this group from resonance effects (weakly electron withdrawing nature by inductive effects) could possibly have an effect on the quenching processes. For instance, the K_{SV} and k_q values of DPPs quenched by p-nitrophenol were lower than nitrobenzene – the electron-donating OH attached on the nitrophenol compound increases the electron density at the aromatic ring thus p-NP has potentially become electron richer than nitrobenzene as reflected in the overall lower quenching rate.

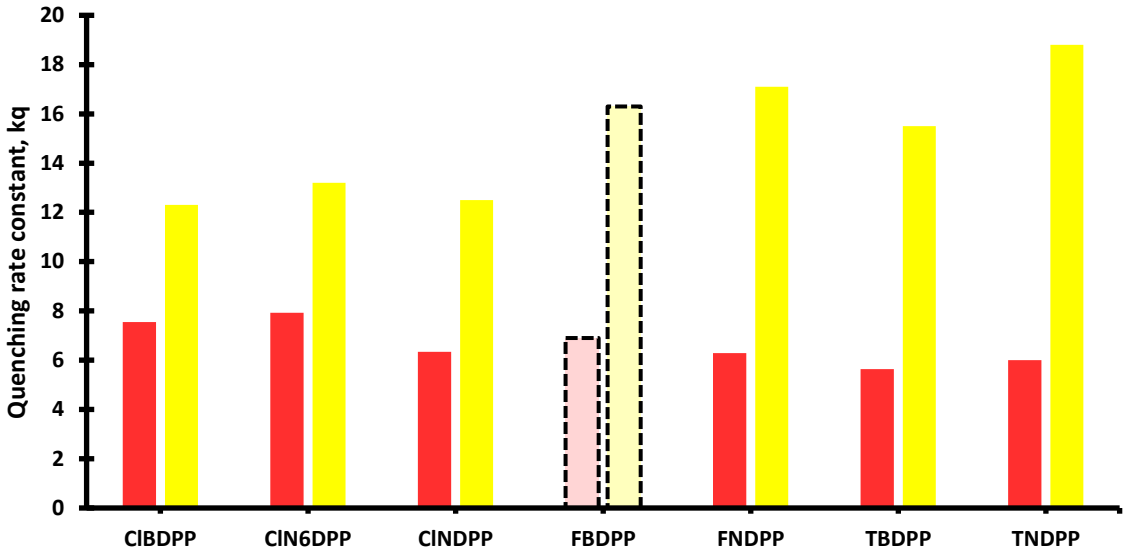


Figure 3.2.2.1: Quenching rate constant (red: p-NP; yellow: 2,4-DNP) of DPPs quenched by p-nitrophenol and 2,4-dinitrophenol in acetonitrile obtained from the Stern-Volmer plots. The faded red and yellow bars shown in FBDPP are the predicted k_q values.

The quenching rate constant results in p-NP were significantly different from the results obtained in non-phenolic NACs. ClN6DPP and ClBDPP, characterized with the longest fluorescence lifetime had the first and second larger quenching rate which corresponds to longer fluorescence lifetime could benefit on the quenching result as the fluorophores can have higher chance to perform fluorescence quenching, if the quenching mechanism was PET dynamic quenching, which the electron transfer happens at the excited state. Also, ClNDPP with the third longest lifetime will have the third highest k_q after ClBDPP, if excluding the estimated quenching rate constant of FBDPP. Meanwhile, by means of the photophysical properties obtained in Section 3.1, the chlorobenzyl-substituted DPPs have lower molar absorptivity as to FNDPP, FBDPP and TBDPP. This shows that ClBDPP, ClN6DPP and ClNDPP are possibly having less electron-donating ability, which could be a reason that they have lower quenching rate constants in detecting nitrobenzene, 2,4-DNT and 2,4-DNP. If these possibilities were omitted, then the hypothesis should be oxidation potential of ClBDPP, ClN6DPP and ClNDPP were lower than the reduction potential of p-NP thus it is easier for the phenol nitroaromatic to withdraw the electrons from these DPPs compared to the other DPPs that has very high oxidation potential. When the reduction potential of the quencher is much

lower than the oxidation rate of fluorophores, the quencher could have lower tendency in accepting electrons from another species hence affecting the quenching rate.

The additional nitro group of 2,4-DNP instantly increases the quenching efficiency from p-NP as the quenching effect can be improved which caused by the decreased electron density on the aromatic ring of the quencher, hence drives higher chance for photoinduced electron transfer to perform in the system. Furthermore, despite 2,4-DNP having same numbers of nitro groups as 2,4-DNT, higher quenching rates were shown in 2,4-DNP, and this was different from our hypothesis – we predicted that the quenching rates of the DPPs in sensing toluene-based 2,4-DNT will have performed better than detecting 2,4-DNP, since the hydroxyl group in 2,4-DNP has higher electron donating capacity due to the two lone pairs in the oxygen than the methyl group ($–CH_3$) in 2,4-DNT. In regards of this, if the quenching mechanism was the same, the quenching efficiencies of the toluene-based NAC should have higher quenching rates than the phenol-based NAC. This outcome could be caused of both cases were applying different quenching mechanism. We can make a hypothesis by assuming that the DPP core is electron deficient due to the carbonyls – the electron density at the carbonyls connected to the core is higher and electron is pulling towards the oxygen molecule hence electron deficient at the DPP core. As there is electron deficiency at the core, it required more electrons to stable the compound, hence withdrawing electrons from the quencher, and in this case, it accepts electrons from 2,4-DNP. Thus, if the quenching mechanism applied was different, then the DPPs fluorescence sensor would act as the electron acceptors and the quencher 2,4-DNP would be the electron donor when performing fluorescence quenching. Yet, we could not make any conclusions before conducting further studies on the quenching parameters such as the redox potential of the fluorophores and quenchers. The outcomes of the detection of phenol-based nitroaromatic compounds by DPPs were the same as the quenching of benzene-based nitroaromatic compounds, they were approaching diffusion control as the bimolecular quenching rate constant were conspicuously less than the diffusion-controlled in acetonitrile.

There was one noteworthy pattern shown from ClNDPP/ClN6DPP and TNDPP/TBDPP in the detection of non-phenol and phenol-based nitroaromatic compounds in acetonitrile. The chlorobenzene substituted DPPs have higher quenching rate when sensing p-NP and NB than the thiophene-substituted DPPs and having lower readings than TBDPP/TNDPP when they were sensing 2,4-DNT and 2,4-DNP which consists of two nitro functional groups. Higher planarity and closer π- π stacking between the chlorinated-DPPs and the single nitro group NACs (NB and p-NP) than the two nitro groups NACs (2,4-DNT and 2,4-DNP) could be one of the reasons that causes the increased quenching efficiency. Meanwhile for ClBDPP with single benzene side ring always having the least quenching rate constants, except when detecting p-NP. The reason could be p-NP is more prone to withdrawing electrons from ClBDPP. For example, p-NP has higher withdrawing potential to ClBDPP therefore it is easier for ClBDPP to donate the electrons to the nitroaromatic compound. Besides, one important factor that can affect the electron transfer rate in PET mechanism is the distance between fluorophore and quencher[231-234]. For example, the bond length or angle between the electron donor and acceptor. The planarity of DPPs play a key role in their detection efficiency, the shorter the distance between the electron donor and acceptor can form a closer and stronger π-π stacking thus enabling effective electron transfer between the chromophores and quenchers.[231,233] In this case, it could be p-NP–ClBDPP has shorter distance compared to other quenchers, as the result shows that ClBDPP has higher efficiency in detecting p-NP than NB, 2,4-DNT and 2,4-DNP. Meanwhile for TN/TBDPP, they have the lowest k_q values in detecting p-NP, and TNDPP has slightly higher efficiency than TBDPP which can be seen similar trends in detecting 2,4-DNT and 2,4-DNP. Not to mention, they have the same fluorescence lifetimes in acetonitrile, and this indicates that TNDPP is a better fluorophore in detecting 2,4-DNT, p-NP and 2,4-DNP as well as having higher oxidation potential than TBDPP for donating electron to the quenchers, as a result, the better quenching efficiency.

Furthermore, the detection efficiencies can be evaluated with the redox potential of electron donor and acceptor, by Rehm-Weller equation given in Equation 1.4.3. Rehm-Weller equation, which determines the thermodynamic driving force or free energy needed for photoinduced electron separation[234], hence redox potentials directly affect the efficiencies in fluorescence quenching.[235] By comparing the quenching results with the fluorescence lifetimes, FNDPP with the shortest lifetime has higher k_q values than TBDPP/TNDPP when

quenched by p-NP. The three DPPs are having the same trend in their quenching rates when detecting non-phenolic and phenol-based NACs, which shows that FNDPP has higher quenching rates than TB/TNDPP. It also shows that FNDPP has higher tendency in donating electrons compared to the chlorinated and thiophene-substituted DPPs. In other way, this can also be explained as FNDPP has high negative reduction potential, and the quenchers have high positive reduction potential, which allow the quenchers to easily accept electron from FNDPP. Additionally, the free energy or driving force are also important to determine the quenching efficiency.[236] The thermodynamic driving force for electron transfer stated here can be explain by the free energy difference between the LUMO and HOMO states of the DPPs and quenchers.[237] Effective PET requires larger gaps between LUMO and HOMO as this could potentially increase the efficiency of the electron transfer between the donor and acceptors therefore enhanced quenching efficiency. The quenching constant results shown above explain that less energy is required to remove or extract an electron from FNDPP, which also can be explained that the redox potential of FNDPP is higher (more negative) that it has higher driving force for electron transfer in the quenching system, hence has higher energy to perform fluorescence quenching. The distance and redox potentials however will not be further discussed as these factors were not measured in this study.

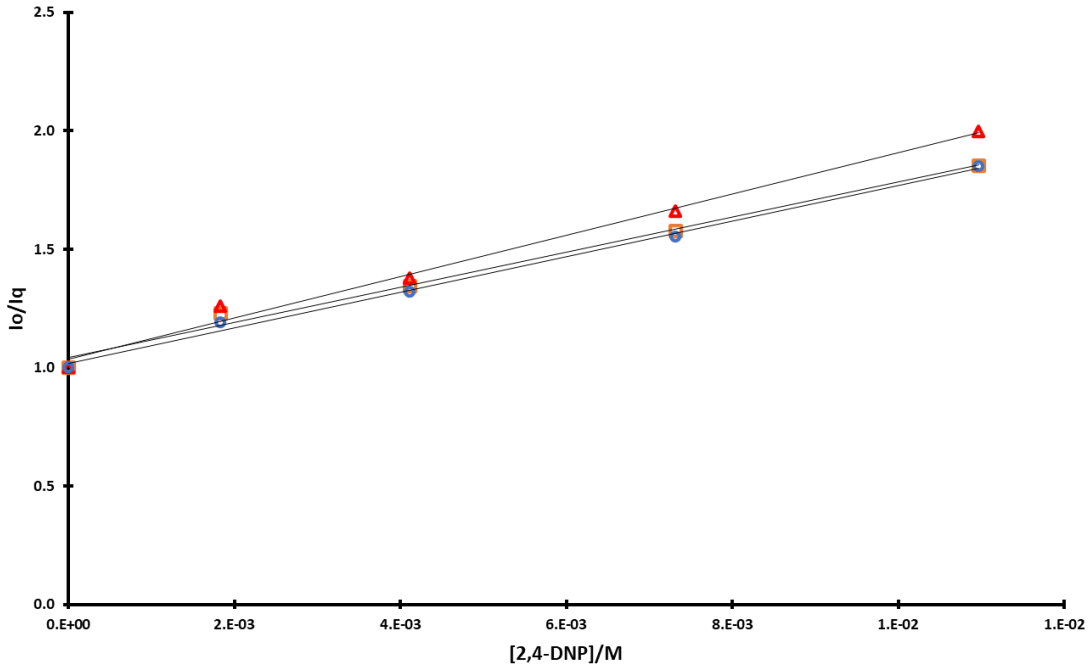


Figure 3.2.2.2: The Stern-Volmer plots of ClBDPP, ClN6DPP and ClNDPP in acetonitrile with increasing concentration of 2,4-DNP.

The Stern-Volmer plots in Figure 3.2.2.2 has r^2 value of ≥ 0.9893. One noteworthy observation was recognized – the second of the three plots were slightly above the linear trendline. When the second data was removed from the plots, they are having r^2= 0.9989 (ClBDPP), 0.9996 (ClNDPP) and 1.0 (ClN6DPP). This shows that the second plot was not an error or coincidence, there must be some reactions between the fluorophores and the quencher at that concentration. This is interesting and should carry out an in-depth study in the future. The quenching of ClBDPP, ClN6DPP and ClNDPP were less efficient with 2,4-DNP when compared to p-NP. These DPPs also have the same outcomes when applied as fluorescence sensor for 2,4-DNT. If the hypothesis made above were matched, this can be caused by the chlorinated-DPPs are having higher oxidation potential (more positive) than 2,4-DNP as well as other DPPs, hence it has lower chance to accept electrons from 2,4-DNP. On the other hand, the detection of phenol-based NACs shows very huge contrast in the quenching of TNDPP, FNDPP and the chlorinated-DPPs. TNDPP has the highest k_q in detecting 2,4-DNP and second lowest quenching rate for the detection of p-NP. Meanwhile, FNDPP has second highest k_q when quenched by 2,4-DNP and got third lowest k_q in sensing p-NP. To

explain along with the hypothesis, it shows that the furan-substituted DPPs have high reduction potential, hence they have high k_q in detecting 2,4-DNP and lower k_q when sensing p-NP. With the exception of detecting p-NP, FNDPP always have the highest quenching rate constants.

4 Conclusions and Future perspectives

To conclude, we have studied seven structurally related diketopyrrolopyrroles. These bear different substitutions on the core rings, namely p-chlorobenzene, furan, and thiophene as well as on lactam nitrogen atoms, including benzyl and naphthalene. Their photophysical properties in solution were experimentally determined. These were characterized by strong absorption in the visible spectral region, with absorption maximum and factors in line with their distinct substitution patterns. Absorption maxima in acetonitrile were 469 – 542 nm and 473 – 546 nm in DCM while the emission maxima ranged from 533 – 556 nm in acetonitrile and 534 – 561 nm in DCM. In all cases, we observed bathochromically shifted absorption and fluorescence emission spectra in the case of furan and thiophene DPPs, which can be attributed to the enhanced planarity of the core rings with respect to the core structure. As a result of this, these systems were also characterized by greater vibronic structure and smaller Stokes shifts when compared to their phenyl counterparts. They have fluorescence lifetimes from 5.56 to 6.62 ns, consistent with previously studied DPP-based materials. These DPPs were evaluated in their ability to act as optical sensors for nitroaromatic compounds, namely nitrobenzene, 2,4-dinitrophenol, p-nitrophenol and 2,4-dinitrophenol. The study of the detection for non-phenolic nitroaromatics have demonstrated solvent polarity could affect photoinduced electron transfer, with higher quenching efficiencies observed in acetonitrile than in dichloromethane. In all cases, quenching rate constant approaching diffusion-controlled rates were observed, indicating successful behaviour for the sought application. The absence of spectral features consistent with the presence of ground state complex is, in the absence of time-dependent quenching analysis, consistent with dynamic quenching processes in all cases.

As hypothesised, the quenching efficiency of the systems positively correlates with the electron withdrawing ability of the nitroaromatic compounds in the order of 2,4-DNP > p-NP and 2,4-DNT > nitrobenzene. When comparing the properties in these nitroaromatic compounds, we know that toluene quencher, 2,4-DNT with the methyl group should have lower electron donating strength compared to the hydroxyl group in 2,4-DNP, where the quenching efficiencies should be lower in the latter, just like the p-NP having lower quenching efficiency than the nitrobenzene, if they all are sharing the same quenching mechanism.

However, 2,4-DNP showed higher quenching rate constants in all cases, it could be caused of the redox potential that affected the outcome or have undergone different quenching mechanism. Further studies like measuring the fluorescence and quenching lifetimes should be done to draw conclusions on this statement.

Overall, furan-substituted diketopyrrolopyrrole was chosen to be the most suitable sensing material for the nitroaromatic compounds tested in this study. FNDPP presented efficient sensing for the NACs and is a good option to detect nitrobenzene, 2,4-DNT and 2,4-DNP. The furan substitution in FB/FNDPP has made them a better option especially with high reduction quenchers. Also, the small molecular size of furan and its planarity can positively impact the distance between the fluorophore and the nitroaromatics – they can form closer and stronger π-π stacking to enhance the quenching process. It has excellent absorption factor as well as good detecting properties even with its short fluorescence lifetime. With the convenient, sensitive, and rapid fluorescence-based method, the DPP substituents could be potentially used as the sensing materials at the forefront to detect nitrobenzene, 2,4-dinitrotoluene, p-nitrophenol and 2,4-dinitrophenol and even other nitroaromatic compounds.

As a result, it is anticipated that in order to fully account for these observations, further studies on the HOMO/LUMO energies and the redox potential should be done for an in-depth review towards the quenching efficiency of these DPPs. Then, computational calculation such as the distance between the quencher and the DPPs should be studied to explain more on the quenching results. Other than that, quenching lifetimes between the fluorophores and nitroaromatics should be carried out in the future to confirm the quenching mechanism.

5 References

1 Al-Kindy, S., Badía, R., Suárez-Rodríguez, J. L., & Díaz-García, M. E. (2000). Molecularly Imprinted Polymers and Optical Sensing Applications. Critical Reviews in Analytical Chemistry, 30(4), 291–309.

2 Li, Z., Askim, J. R., & Suslick, K. S. (2018). The Optoelectronic Nose: Colorimetric and Fluorometric Sensor Arrays. Chemical Reviews, 119(1), 231–292.

3 Díaz-García, M. E., & Badía, R. (2000). Molecularly Imprinted Polymers for Optical Sensing Devices. In R. Narayanaswamy & O. S. Wolfbeis (Eds.), Optical Sensors: Industrial Environmental and Diagnostic Applications (pp. 35–50).

4 Zhu, Z. (2017). An Overview of Carbon Nanotubes and Graphene for Biosensing Applications. Nano-Micro Letters, 9(3), 25.

5 Lodish, H., Berk, A., Zipursky, S. L., Matsudaira, P., Baltimore, D., & Darnell, J. (2000). Molecular Cell Biology (4th ed.). W. H. Freeman.

6 Basabe-Desmonts, L., Reinhoudt, D. N., & Crego-Calama, M. (2007). Design of fluorescent materials for chemical sensing. Chemical Society Reviews, 36(6), 993–1017.

7 Hahn, Y.-B., Ahmad, R., & Tripathy, N. (2012). Chemical and biological sensors based on metal oxide nanostructures. Chemical Communications, 48(84), 10369–10385.

8 Chen, D., Xu, J., Xie, Z., & Shen, G. (2011). Nanowires Assembled SnO2 Nanopolyhedrons with Enhanced Gas Sensing Properties. ACS Applied Materials & Interfaces, 3(6), 2112–2117.

9 Lobnik, A., Turel, M., & Urek, Š. K. (2012). Optical Chemical Sensors:Design and Applications. Advances in Chemical Sensors.

10 Ray, A. K. (2017). Organic Materials for Chemical Sensing. In S. Kasap & P. Capper (Eds.), Springer Handbook of Electronic and Photonic Materials (pp. 1281–1310). Springer International Publishing.

11 Fu, Y., & Finney, N. S. (2018). Small-molecule fluorescent probes and their design. RSC Advances, 8(51), 29051–29061.

12 McKeown, N. B. (1998). Phthalocyanine materials: Synthesis, structure, and function. Cambridge University Press.

13 Nalwa, H. (Ed.). (2001). Supramolecular Photosensitive and Electroactive Materials—1st Edition. Academic Press

14 Guilard, R., Kadish, K., & Smith, K. (Eds.). (2012). The Porphyrin Handbook—1st Edition (Vol. 11). Academic Press.

15 de la Torre, G., Vázquez, P., Agulló-López, F., & Torres, T. (2004). Role of Structural Factors in the Nonlinear Optical Properties of Phthalocyanines and Related Compounds. Chemical Reviews, 104(9), 3723–3750.

16 D'Souza, F., & Ito, O. (2009). Supramolecular donor–acceptor hybrids of porphyrins/phthalocyanines with fullerenes/carbon nanotubes: Electron transfer, sensing, switching, and catalytic applications. Chemical Communications, 33, 4913–4928.

17 Sun, Q., Feng, W., Yang, P., You, G., & Chen, Y. (2018). Highly selective room-temperature NO2 sensors based on a fluoroalkoxy-substituted phthalocyanine. New Journal of Chemistry, 42(9), 6713–6718.

18 Kotlowski, C., Aspermair, P., Khan, H. U., Reiner-Rozman, C., Breu, J., Szunerits, S., Kim, J.-J., Bao, Z., Kleber, C., Pelosi, P., & Knoll, W. (2018). Electronic biosensing with flexible organic transistor devices. Flexible and Printed Electronics, 3(3), 034003.

19 Torsi, L., Magliulo, M., Manoli, K., & Palazzo, G. (2013). Organic field-effect transistor sensors: A tutorial review. Chemical Society Reviews, 42(22), 8612–8628.

20 Klug, A., Denk, M., Bauer, T., Sandholzer, M., Scherf, U., Slugovc, C., & List, E. J. W. (2013). Organic field-effect transistor based sensors with sensitive gate dielectrics used for low-concentration ammonia detection. Organic Electronics, 14(2), 500–504.

21 Knopfmacher, O., Hammock, M. L., Appleton, A. L., Schwartz, G., Mei, J., Lei, T., Pei, J., & Bao, Z. (2014). Highly stable organic polymer field-effect transistor sensor for selective detection in the marine environment. Nature Communications, 5(1), 1–9.

22 Rochat, S., & Swager, T. M. (2013). Conjugated amplifying polymers for optical sensing applications. ACS applied materials & interfaces, 5(11), 4488–4502.

23 Thomas, S. W., Joly, G. D., & Swager, T. M. (2007). Chemical Sensors Based on Amplifying Fluorescent Conjugated Polymers. Chemical Reviews, 107(4), 1339–1386.

24 Feng, X., Liu, L., Wang, S., & Zhu, D. (2010). Water-soluble fluorescent conjugated polymers and their interactions with biomacromolecules for sensitive biosensors. Chemical Society Reviews, 39(7), 2411–2419.

25 Feng, L., Zhu, C., Yuan, H., Liu, L., Lv, F., & Wang, S. (2013). Conjugated polymer nanoparticles: Preparation, properties, functionalization and biological applications. Chemical Society Reviews, 42(16), 6620–6633.)

26 Guan, W., Zhou, W., Lu, J., & Lu, C. (2015). Luminescent films for chemo- and biosensing. Chemical Society Reviews, 44(19), 6981–7009.

27 Wang, B., Jing, M., & Xiangmei, M. (2020). Synthesis, characterization and fluorescent performance studies of noveldiphenyl sulfone-functionalized water-soluble polymer. Journal of the Serbian Chemical Society, 00, 41–41.

28 Qu, Y., Ren, G., Yu, L., Zhu, B., Chai, F., & Chen, L. (2019). The carbon dots as colorimetric and fluorescent dual-readout probe for 2-nitrophenol and 4-nitrophenol detection. Journal of Luminescence, 207, 589–596.

29 Han, L., Liu, S. G., Liang, J. Y., Ju, Y. J., Li, N. B., & Luo, H. Q. (2019). PH-mediated reversible fluorescence nanoswitch based on inner filter effect induced fluorescence quenching for selective and visual detection of 4-nitrophenol. Journal of Hazardous Materials, 362, 45–52.

30 Bogale, R. F., Chen, Y., Ye, J., Yang, Y., Rauf, A., Duan, L., Tian, P., & Ning, G. (2017). Highly selective and sensitive detection of 4-nitrophenol and Fe3+ ion based on a luminescent layered terbium (III) coordination polymer. Sensors and Actuators B: Chemical, 245, 171–178.

31 Qu, F., Chen, P., Zhu, S., & You, J. (2017). High selectivity of colorimetric detection of p-nitrophenol based on Ag nanoclusters. Spectrochimica Acta Part A: Molecular and Biomolecular Spectroscopy, 171, 449–453.

32 Wang, J., Zha, Q., Qin, G., & Ni, Y. (2020). A novel Zn(II)-based metal-organic framework as a high selective and sensitive sensor for fluorescent detections of aromatic nitrophenols and antibiotic metronidazole. Talanta, 211, 120742.

33 Shi, X., Qu, X., Chai, J., Tong, C., Fan, Y., & Wang, L. (2019). Stable coordination polymers with linear dependence color tuning and luminescent properties for detection of metal ions and explosives. Dyes and Pigments, 170, 107583.

34 Zhang, J., Yang, P. L., & Gray, N. S. (2009). Targeting cancer with small molecule kinase inhibitors. Nature Reviews. Cancer, 9(1), 28–39.

35 Wang, W. U., Chen, C., Lin, K., Fang, Y., & Lieber, C. M. (2005). Label-free detection of small-molecule-protein interactions by using nanowire nanosensors. Proceedings of the National Academy of Sciences of the United States of America, 102(9), 3208–3212.

36 Strausberg, R. L., & Schreiber, S. L. (2003). From knowing to controlling: A path from genomics to drugs using small molecule probes. Science (New York, N.Y.), 300(5617), 294–295.

37 Kenakin, T., & Christopoulos, A. (2013). Signalling bias in new drug discovery: Detection, quantification and therapeutic impact. Nature Reviews. Drug Discovery, 12(3), 205–216.

38 Holliger, P., & Hudson, P. J. (2005). Engineered antibody fragments and the rise of single domains. Nature Biotechnology, 23(9), 1126–1136.

39 O'Neill, E. M., Mucyn, T. S., Patteson, J. B., Finkel, O. M., Chung, E.-H., Baccile, J. A., Massolo, E., Schroeder, F. C., Dangl, J. L., & Li, B. (2018). Phevamine A, a small molecule that suppresses plant immune responses. Proceedings of the National Academy of Sciences of the United States of America, 115(41), E9514–E9522.

40 Caron, T., Pasquinet, E., van der Lee, A., Pansu, R. B., Rouessac, V., Clavaguera, S., Bouhadid, M., Serein-Spirau, F., Lère-Porte, J.-P., & Montméat, P. (2014). Efficient Sensing of Explosives by Using Fluorescent Nonporous Films of Oligophenyleneethynylene Derivatives Thanks to Optimal Structure Orientation and Exciton Migration. Chemistry – A European Journal, 20(46), 15069–15076.

41 Zhao, Y., Hao, W., Ma, W., Zang, Z., Zhang, H., Liu, X., Zou, S., Zhang, H., Liu, W., & Gao, J. (2014). Easily-soluble heteroacene bis(benzothieno)silole derivatives for sensing of nitro explosives. New Journal of Chemistry, 38(12), 5754–5760.

42 Bhalla, V., Gupta, A., Kumar, M., Rao, D. S. S., & Prasad, S. K. (2013). Self-Assembled Pentacenequinone Derivative for Trace Detection of Picric Acid. ACS Applied Materials & Interfaces, 5(3), 672–679.

43 Kaur, S., Gupta, A., Bhalla, V., & Kumar, M. (2014). Pentacenequinone derivatives: Aggregation-induced emission enhancement, mechanism and fluorescent aggregates for superamplified detection of nitroaromatic explosives. Journal of Materials Chemistry C, 2(35), 7356–7363.

44 Bhalla, V., Gupta, A., & Kumar, M. (2012). Fluorescent Nanoaggregates of Pentacenequinone Derivative for Selective Sensing of Picric acid in Aqueous Media. Organic Letters, 14(12), 3112–3115.

45 Shanmugaraju, S., & Mukherjee, P. S. (2015). π-Electron rich small molecule sensors for the recognition of nitroaromatics. Chemical Communications, 51(89), 16014–16032.

46 Zyryanov, G., Kopchuk, D., Kovalev, I., Nosova, E., Rusinov, V., & Chupakhin, O. (2014). Chemosensors for detection of nitroaromatic compounds (explosives). Russian Chemical Reviews, 83, 783.

47 Meaney, M. S., & McGuffin, V. L. (2008). Investigation of common fluorophores for the detection of nitrated explosives by fluorescence quenching. Analytica Chimica Acta, 610(1), 57–67.

48 Sriyab, S., Jorn-Iat, K., Prompinit, P., Wolschann, P., Hannongbua, S., & Suramitr, S. (2018). Photophysical properties of 1-pyrene-based derivatives for nitroaromatic explosives detection: Experimental and theoretical studies. Journal of Luminescence, 203, 492–499.

49 Kalyanasundaram, K., & Thomas, J. K. (1977). Environmental effects on vibronic band intensities in pyrene monomer fluorescence and their application in studies of micellar systems. Journal of the American Chemical Society, 99(7), 2039–2044.

50 Somerharju, P. (2002). Pyrene-labeled lipids as tools in membrane biophysics and cell biology. Chemistry and Physics of Lipids, 116(1–2), 57–74.

51 Jagtap, S. B., Potphode, D. D., Ghorpade, T. K., Palai, A. K., Patri, M., & Mishra, S. P. (2014). TButyl pyrene containing poly(arylene ethynylene)s for highly sensitive and selective sensing of TNT. Polymer, 55(12), 2792–2798.

52 Mikroyannidis, J. A., Fenenko, L., Yahiro, M., & Adachi, C. (2007). Alternating copolyfluorenevinyles with polynuclear aromatic moieties: Synthesis, photophysics, and electroluminescence. Journal of Polymer Science, Part A: Polymer Chemistry, 45(20), 4661–4670.

53 Thomas, S. W., Joly, G. D., & Swager, T. M. (2007). Chemical Sensors Based on Amplifying Fluorescent Conjugated Polymers. Chemical Reviews, 107(4), 1339–1386.

54 Pan, J., Cha, T.-G., Chen, H., & Choi, J. H. (2013). 10—Carbon nanotube-based optical platforms for biomolecular detection. In S. Yamashita, Y. Saito, & J. H. Choi (Eds.), Carbon Nanotubes and Graphene for Photonic Applications (pp. 270–303e). Woodhead Publishing.

55 Gründler, P. (2007). Chemical Sensors: An Introduction for Scientists and Engineers (1st ed.). Springer-Verlag.

56 McDonagh, C., Burke, C. S., & MacCraith, B. D. (2008). Optical Chemical Sensors. Chemical Reviews, 108(2), 400–422.

57 Peixoto, A. C., & Silva, A. F. (2017). 11 - Smart devices: Micro- and nanosensors. In L. Rodrigues & M. Mota (Eds.), Bioinspired Materials for Medical Applications (pp. 297–329). Woodhead Publishing.

58 Yang, Y., Jiang, J., Shen, G., & Yu, R. (2009). An optical sensor for mercury ion based on the fluorescence quenching of tetra(p-dimethylaminophenyl)porphyrin. Analytica Chimica Acta, 636(1), 83–88.

59 Cha, T.-G., Baker, B. A., Sauffer, M. D., Salgado, J., Jaroch, D., Rickus, J. L., Porterfield, D. M., & Choi, J. H. (2011). Optical Nanosensor Architecture for Cell-Signaling Molecules Using DNA Aptamer-Coated Carbon Nanotubes. ACS Nano, 5(5), 4236–4244.

60 Lamprecht, B., Abel, T., Kraker, E., Haase, A., Konrad, C., Tscherner, M., Köstler, S., Ditlbacher, H., & Mayr, T. (2010). Integrated fluorescence sensor based on ring-shaped organic photodiodes. Physica Status Solidi (RRL) – Rapid Research Letters, 4(7), 157–159.

61 Wang, X., & Wolfbeis, O. S. (2016). Fiber-Optic Chemical Sensors and Biosensors (2013–2015). Analytical Chemistry, 88(1), 203–227.

62 Caucheteur, C., Guo, T., Liu, F., Guan, B.-O., & Albert, J. (2016). Ultrasensitive plasmonic sensing in air using optical fibre spectral combs. Nature Communications, 7(1), 1–8.

63 Walt, D. R. (2009). Fibre optic microarrays. Chemical Society Reviews, 39(1), 38–50.

64 Dutta, A. (2016). Introduction to Planar Waveguide Optical Sensor. In A. Dutta, B. Deka, & P. Pratim Sahu (Eds.), Planar Waveguide Optical Sensors: From Theory to Applications (pp. 1–8). Springer International Publishing.

65 Schlücker, S. (2014). Surface-Enhanced Raman Spectroscopy: Concepts and Chemical Applications. Angewandte Chemie International Edition, 53(19), 4756–4795.

66 Haynes, C. L., McFarland, A. D., & Van Duyne, R. P. (2005). Surface-Enhanced Raman Spectroscopy. Analytical Chemistry, 77(17), 338 A-346 A.

67 Ding, S.-Y., You, E.-M., Tian, Z.-Q., & Moskovits, M. (2017). Electromagnetic theories of surface-enhanced Raman spectroscopy. Chemical Society Reviews, 46(13), 4042–4076.

68 Narayanaswamy, R., & Wolfbeis, O. S. (Eds.). (2004). Optical Sensors: Industrial Environmental and Diagnostic Applications.

69 Wang, Z., Yang, M., Chen, C., Zhang, L., & Zeng, H. (2016). Selectable Ultrasensitive Detection of Hg2+ with Rhodamine 6G-Modified Nanoporous Gold Optical Sensor. Scientific Reports, 6(1), 1–7.

70 Physicochemical and Environmental Plant Physiology—4th Edition (4th ed.). (2009). Academic Press.

71 Demchenko, A. P. (Ed.). (2009). Fluorescence Detection Techniques. In Introduction to Fluorescence Sensing (pp. 65–118). Springer Netherlands.

72 Wang, Z., Luo, M., Mao, C., Wei, Q., Zhao, T., Li, Y., Huang, G., & Gao, J. (2017). A Redox-Activatable Fluorescent Sensor for the High-Throughput Quantification of Cytosolic Delivery of Macromolecules. Angewandte Chemie (International Ed. in English), 56(5), 1319–1323.

73 Tainaka, K., Sakaguchi, R., Hayashi, H., Nakano, S., Liew, F. F., & Morii, T. (2010). Design Strategies of Fluorescent Biosensors Based on Biological Macromolecular Receptors. Sensors (Basel, Switzerland), 10(2), 1355–1376.

74 De Acha, N., Elosúa, C., Corres, J. M., & Arregui, F. J. (2019). Fluorescent Sensors for the Detection of Heavy Metal Ions in Aqueous Media. Sensors, 19(3), 599.

75 Ding, Y., Zhao, C., Ding, Y., & Zhao, C. (2018). A highly selective fluorescent sensor for detection of trilavent metal ions based on a sample schiff-base. Química Nova, 41(6), 623–627.

76 Li, Y., Yuan, J., & Xu, Z. (2019). A Sensitive Fluorescence Biosensor for Silver Ions (Ag+) Detection Based on C-Ag+-C Structure and Exonuclease III-Assisted Dual-Recycling Amplification. Journal of Analytical Methods in Chemistry, 2019, 3712032.

77 Baslak, C., & Kursunlu, A. N. (2018). A naked-eye fluorescent sensor for copper(II) ions based on a naphthalene conjugate Bodipy dye. Photochemical & Photobiological Sciences, 17(8), 1091–1097.

74 Chen, X., Zhou, Y., Peng, X., & Yoon, J. (2010). Fluorescent and colorimetric probes for detection of thiols. Chemical Society Reviews, 39(6), 2120–2135.

75 Kumar, V., Maiti, B., Chini, M. K., De, P., & Satapathi, S. (2019). Multimodal Fluorescent Polymer Sensor for Highly Sensitive Detection of Nitroaromatics. Scientific Reports, 9.

76 Nath, S., Pathak, S. K., Pradhan, B., Gupta, R. K., Reddy, K. A., Krishnamoorthy, G., & Achalkumar, A. S. (2018). A sensitive and selective sensor for picric acid detection with a fluorescence switching response. New Journal of Chemistry, 42(7), 5382–5394.

77 Valeur, B. (2001). Molecular Fluorescence Principles and Applications. Wiley-VCH Verlag GmbH & Co. KGaA.

78 Kessler, R. W., Kessler, W., & Zikulnig‐Rusch, E. (2016). A Critical Summary of Spectroscopic Techniques and their Robustness in Industrial PAT Applications. Chemie Ingenieur Technik, 88(6), 710–721.

79 Vessman, J., Stefan, R. I., van Staden, J. F., Danzer, K., Linder, W., Burns, D. T., Fajgelj, A., & Müller, H. (2001). Pure and Applied Chemistry. 73(8), 1381–1386.

80 Qu, W., Yang, L., Hang, Y., Zhang, X., Qu, Y., & Hua, J. (2015). Photostable red turn-on fluorescent diketopyrrolopyrrole chemodosimeters for the detection of cysteine in living cells. Sensors and Actuators B: Chemical, 211, 275–282.

81 Grzybowski, M., & Gryko, D. T. (2015). Diketopyrrolopyrroles: Synthesis, Reactivity, and Optical Properties. Advanced Optical Materials, 3(3), 280–320.

82 Wallquist, O., & Lenz, R. (2009). Diketopyrrolopyrrole (DPP) Pigments. In High Performance Pigments (pp. 165–194). John Wiley & Sons, Ltd.

83 Wallquist, O., & Lenz, R. (2002). 20 years of DPP pigments – future perspectives. Macromolecular Symposia, 187(1), 617–630.

84 Farnum, D. G., Mehta, G., Moore, G. G. I., & Siegal, F. P. (1974). Attempted reformatskii reaction of benzonitrile, 1,4-diketo-3,6-diphenylpyrrolo[3,4-C]pyrrole. A lactam analogue of pentalene. Tetrahedron Letters, 15(29), 2549–2552.

85 General. (2005). In Industrial Organic Pigments (pp. 1–181). John Wiley & Sons, Ltd.

86 Iqbal, A., Jost, M., Kirchmayr, R., Pfenninger, J., Rochat, A., & Wallquist, O. (1988). The synthesis and properties of 1,4-diketo-pyrrolo[3,4-C]pyrroles. Bulletin Des Sociétés Chimiques Belges, 97(8–9), 615–644.

87 Hao, Z., & Iqbal, A. (1997). Some aspects of organic pigments. Chemical Society Reviews, 26(3), 203–213.

88 LENZ, R., & WALLQUIST, O. (2002). DPP chemistry: Continuous innovation. DPP Chemistry: Continuous Innovation, 85(1), 19–26.

89 David, J., Weiter, M., Vala, M., Vyňuchal, J., & Kučerík, J. (2011). Stability and structural aspects of diketopyrrolopyrrole pigment and its N-alkyl derivatives. Dyes and Pigments, 89(2), 137–143.

90 Zollinger, H. (2003). Color chemistry: syntheses, properties, and applications of organic dyes and pigments. John Wiley & Sons.

91 Zhang, H., Deng, R., Wang, J., Li, X., Chen, Y.-M., Liu, K., Taubert, C. J., Cheng, S. Z. D., & Zhu, Y. (2017). Crystalline Organic Pigment-Based Field-Effect Transistors. ACS Applied Materials & Interfaces, 9(26), 21891–21899.

92 Potrawa, T., & Langhals, H. (1987). Fluorescent dyes with large stokes shifts – soluble dihydropyrrolopurroldiones. 120(7), 1075–1078.

93 Colonna, G., Pilati, T., Rusconi, F., & Zecchi, G. (2007). Synthesis and properties of some new N,N′-disubstituted 2,5-dihydro-1,4-dioxo-3,6-diphenylpyrrolo[3,4-c]pyrroles. Dyes and Pigments, 75(1), 125–129.

94 Raju, M. V. R., & Lin, H.-C. (2013). A Novel Diketopyrrolopyrrole (DPP)-Based [2]Rotaxane for Highly Selective Optical Sensing of Fluoride. Organic Letters, 15(6), 1274–1277.

95 Hang, Y., Wang, J., Jiang, T., Lu, N., & Hua, J. (2016). Diketopyrrolopyrrole-Based Ratiometric/Turn-on Fluorescent Chemosensors for Citrate Detection in the Near-Infrared Region by an Aggregation-Induced Emission Mechanism. Analytical Chemistry, 88(3), 1696–1703.

96 Lim, B., Sun, H., Lee, J., & Noh, Y.-Y. (2017). High Performance Solution Processed Organic Field Effect Transistors with Novel Diketopyrrolopyrrole-Containing Small Molecules. Scientific Reports, 7(1), 1–8.

97 Takaya, T., Mamo, M. D., Karakawa, M., & Noh, Y.-Y. (2018). Donor unit effect on DPP based organic field-effect transistor performance. Dyes and Pigments, 158, 306–311.

98 Heinrichová, P., Pospíšil, J., Stříteský, S., Vala, M., Weiter, M., Toman, P., Rais, D., Pfleger, J., Vondráček, M., Šimek, D., Fekete, L., Horáková, P., Dokládalová, L., Kubáč, L., & Kratochvílová, I. (2019). Diketopyrrolopyrrole-Based Organic Solar Cells Functionality: The Role of Orbital Energy and Crystallinity. The Journal of Physical Chemistry C, 123(18), 11447–11463.

99 A, T., C, Z., J, Y., & E, Z. (2016). Design of Diketopyrrolopyrrole (DPP)-Based Small Molecules for Organic-Solar-Cell Applications. Advanced Materials (Deerfield Beach, Fla.), 29(2).

100 Mahesh, K., Karpagam, S., & Pandian, K. (2019). How to Design Donor–Acceptor Based Heterocyclic Conjugated Polymers for Applications from Organic Electronics to Sensors. Topics in Current Chemistry, 377(3), 12.

101 Singh, N., & Riaz, U. (2022). Recent trends on synthetic approaches and application studies of conducting polymers and copolymers: A review. Polymer Bulletin.

102 Thomas, S. W., & Swager, T. M. (2009). Chapter 10—Detection of Explosives Using Amplified Fluorescent Polymers. In M. Marshall & J. C. Oxley (Eds.), Aspects of Explosives Detection (pp. 203–221). Elsevier.

103 Stott, T. L., & Wolf, M. O. (2003). Electronic interactions in metallated polythiophenes: What can be learned from model complexes. Coordination Chemistry Reviews, 246(1), 89–101.

104 Zhou, E., Cong, J., Wei, Q., Tajima, K., Yang, C., & Hashimoto, K. (2011). All-Polymer Solar Cells from Perylene Diimide Based Copolymers: Material Design and Phase Separation Control. Angewandte Chemie International Edition, 50(12), 2799–2803.

105 Cortizo-Lacalle, D., Howells, C. T., Pandey, U. K., Cameron, J., Findlay, N. J., Inigo, A. R., Tuttle, T., Skabara, P. J., & Samuel, I. D. W. (2014). Solution processable diketopyrrolopyrrole (DPP) cored small molecules with BODIPY end groups as novel donors for organic solar cells. Beilstein Journal of Organic Chemistry, 10(1), 2683–2695.

106 Walker, B., Kim, C., & Nguyen, T.-Q. (2011). Small Molecule Solution-Processed Bulk Heterojunction Solar Cells. Chemistry of Materials, 23(3), 470–482.

107 Vasa, P. (2019). Strong Light–Matter Interaction. In Digital Encyclopedia of Applied Physics (pp. 1–30). American Cancer Society.

108 Myers, J. A., Curtis, B. S., & Curtis, W. R. (2013). Improving accuracy of cell and chromophore concentration measurements using optical density. BMC Biophysics, 6(1), 4.

109 Einstein, A. B. (1905). On a heuristic point of view concerning the production and transformation of light. Annalen Der Physik, 17, 132–148.

110 Tsuji, M. (1989). 34—Electron Microscopy. In G. Allen & J. C. Bevington (Eds.), Comprehensive Polymer Science and Supplements (pp. 785–840). Pergamon.

111 Soniya, R., Thejokalyani, N., & Dhoble, S. J. (2016). Organic Light-emitting Diodes (OLED): Materials, Technology and Advantages. New York: NOVA Science Publishers.

112 Jabłoński, A. (1935). Über den Mechanismus der Photolumineszenz von Farbstoffphosphoren. Zeitschrift für Physik, 94(1), 38–46.

113 Lakowicz, J. R. (Ed.). (2006). Introduction to Fluorescence. In Principles of Fluorescence Spectroscopy (pp. 1–26).

114 Omary, M. A., & Patterson, H. H. (2017). Luminescence, Theory. In J. C. Lindon, G. E. Tranter, & D. W. Koppenaal (Eds.), Encyclopedia of Spectroscopy and Spectrometry (Third Edition) (pp. 636–653).

115 Molina, P., Arques, A., & Cartagena, I. (2008). 3.09 - Thiophenes and their Benzo Derivatives: Structure. In A. R. Katritzky, C. A. Ramsden, E. F. V. Scriven, & R. J. K. Taylor (Eds.), Comprehensive Heterocyclic Chemistry III (Vol. 3, pp. 625–739). Elsevier.

116 Albani, J. R. (2004). Structure and Dynamics of Macromolecules: Absorption and Fluorescence Studies—1st Edition (1st ed.). Elsevier Science.

117 Schulman, S. G. (1985,1998,1993). Molecular luminescence spectroscopy, parts 1–3. John Wiley & Sons, Incorporated.

118 Baryshnikov, G., Minaev, B., & Ågren, H. (2017). Theory and Calculation of the Phosphorescence Phenomenon. Chemical Reviews, 117(9), 6500–6537.

119 Zhao, Q., Huang, C., & Li, F. (2011). Phosphorescent heavy-metal complexes for bioimaging. Chemical Society Reviews, 40(5), 2508–2524.

120 Lo, K. K.-W., & Li, S. P.-Y. (2014). Utilization of the photophysical and photochemical properties of phosphorescent transition metal complexes in the development of photofunctional cellular sensors, imaging reagents, and cytotoxic agents. RSC Advances, 4(21), 10560–10585.

121 Haddock, S. H. D., Moline, M. A., & Case, J. F. (2010). Bioluminescence in the Sea. Annual Review of Marine Science, 2(1), 443–493.

122 Zhao, Q., Li, F., & Huang, C. (2010). Phosphorescent chemosensors based on heavy-metal complexes. Chemical Society Reviews, 39(8), 3007–3030.

123 Yam, V. W.-W., & Wong, K. M.-C. (2011). Luminescent metal complexes of d6, d8 and d10 transition metal centres. Chemical Communications, 47(42), 11579–11592.

124 Singh-Rachford, T. N., & Castellano, F. N. (2010). Photon upconversion based on sensitized triplet–triplet annihilation. Coordination Chemistry Reviews, 254(21), 2560–2573.

125 Xiang, H., Cheng, J., Ma, X., Zhou, X., & Chruma, J. J. (2013). Near-infrared phosphorescence: Materials and applications. Chemical Society Reviews, 42(14), 6128–6185.

126 Slinker, J., Bernards, D., Houston, P. L., Abruña, H. D., Bernhard, S., & Malliaras, G. G. (2003). Solid-state electroluminescent devices based on transition metal complexes. Chemical Communications, 19, 2392–2399.

127 Costa, R. D., Ortí, E., & Bolink, H. J. (2011). Recent advances in light-emitting electrochemical cells. Pure and Applied Chemistry, 83(12), 2115–2128.

128 Minaev, B., Baryshnikov, G., & Agren, H. (2014). Principles of phosphorescent organic light emitting devices. Physical Chemistry Chemical Physics, 16(5), 1719–1758.

129 Engel, T., & Reid, P. (2006). Physical Chemistry. Pearson Benjamin-Cummings.

130 Lakowicz, J. R. (2006). Principles Of Fluorescence Spectroscopy (Third). Springer.

131 Valeur, B. (2001). Characteristics of Fluorescence Emission. In Molecular Fluorescence (pp. 34–71). John Wiley & Sons, Ltd.

132 Peng, X., Song, F., Lu, E., Wang, Y., Zhou, W., Fan, J., & Gao, Y. (2005). Heptamethine Cyanine Dyes with a Large Stokes Shift and Strong Fluorescence: A Paradigm for Excited-State Intramolecular Charge Transfer. Journal of the American Chemical Society, 127(12), 4170–4171.

133 Verhoeven, J. W. (1996). Glossary of terms used in photochemistry (IUPAC Recommendations 1996). Pure and Applied Chemistry, 68(12), 2223–2286.

!34 Skourtis, S. S., Liu, C., Antoniou, P., Virshup, A. M., & Beratan, D. N. (2016). Dexter energy transfer pathways. Proceedings of the National Academy of Sciences, 113(29), 8115–8120.

135 Albini, A., Fagnoni, M., & Mella, M. (2000). Photoinduced Electron Transfer: Perspectives in Organic Synthesis. In L. Fabbrizzi & A. Poggi (Eds.), Chemistry at the Beginning of the Third Millennium (pp. 83–101). Springer.

136 Meaney, M. S., & McGuffin, V. L. (2008). Investigation of common fluorophores for the detection of nitrated explosives by fluorescence quenching. *Analytica Chimica Acta*, *610*(1), 57–67.

137 Goodpaster, J. V., & McGuffin, V. L. (2001). Fluorescence Quenching as an Indirect Detection Method for Nitrated Explosives. Analytical Chemistry, 73(9), 2004–2011.

138 Levitus, M. (2019). Chapter 1—Photophysics of single-molecule probes. In C. K. Johnson (Ed.), Spectroscopy and Dynamics of Single Molecules (pp. 15–69). Elsevier.

139 Germain, M. E., & Knapp, M. J. (2009). Optical explosives detection: From color changes to fluorescence turn-on. Chemical Society Reviews, 38(9), 2543–2555.

140 Sun, X., Wang, Y., & Lei, Y. (2015). Fluorescence based explosive detection: From mechanisms to sensory materials. Chemical Society Reviews, 44(22), 8019–8061.

141 Germain, M. E., Vargo, T. R., Khalifah, P. G., & Knapp, M. J. (2007). Fluorescent Detection of Nitroaromatics and 2,3-Dimethyl- 2,3-dinitrobutane (DMNB) by a Zinc Complex: (Salophen)Zn. Inorganic Chemistry, 46(11), 4422–4429.

142 Germain, M. E., & Knapp, M. J. (2008). Discrimination of Nitroaromatics and Explosives Mimics by a Fluorescent Zn(salicylaldimine) Sensor Array. Journal of the American Chemical Society, 130(16), 5422–5423.

143 Beyazkilic, P., Yildirim, A., & Bayindir, M. (2014). Formation of Pyrene Excimers in Mesoporous Ormosil Thin Films for Visual Detection of Nitro-explosives. ACS Applied Materials & Interfaces, 6(7), 4997–5004.

144 Ju, K.-S., & Parales, R. E. (2010). Nitroaromatic compounds, from synthesis to biodegradation. Microbiology and Molecular Biology Reviews: MMBR, 74(2), 250–272.

145 Spain, J. C., Hughes, J. B., Knackmuss, H.-J., Hughes, J. B., & Knackmuss, H.-J. (2000). Biodegradation of Nitroaromatic Compounds and Explosives. CRC Press.

146 Ys, K., & Qx, L. (2004). Reduction of nitroaromatic pesticides with zero-valent iron. Chemosphere, 54(3), 255–263.

147 Zyryanov, G. V., Kopchuk, D. S., Kovalev, I. S., Nosova, S., Rusinov, E. V., & Chupakhin, O. N. (20114). Chemosensors for detection of nitroaromatic compounds (explosives). ResearchGate, 83(9), 783–819.

148 Zhou, Q., & Swager, T. M. (1995). Method for enhancing the sensitivity of fluorescent chemosensors: Energy migration in conjugated polymers. Journal of the American Chemical Society, 117(26), 7017–7018.

149 Sohn, H., Sailor, M. J., Magde, D., & Trogler, W. C. (2003). Detection of Nitroaromatic Explosives Based on Photoluminescent Polymers Containing Metalloles. Journal of the American Chemical Society, 125(13), 3821–3830.

150 Zhao, D., & Swager, T. M. (2005). Sensory Responses in Solution vs Solid State: A Fluorescence Quenching Study of Poly(iptycenebutadiynylene)s. Macromolecules, 38(22), 9377–9384.

151 Caron, T., Guillemot, M., Montméat, P., Veignal, F., Perraut, F., Prené, P., & Serein-Spirau, F. (2010). Ultra trace detection of explosives in air: Development of a portable fluorescent detector. Talanta, 81(1–2), 543–548.

152 Chen, S., Zhang, Q., Zhang, J., Gu, J., & Zhang, L. (2010). Synthesis of two conjugated polymers as TNT chemosensor materials. Sensors and Actuators B: Chemical, 149(1), 155–160.

153 Clavaguera, S., Montméat, P., Parret, F., Pasquinet, E., Lère-Porte, J.-P., & Hairault, L. (2010). Comparison of fluorescence and QCM technologies: Example of explosives detection with a π-conjugated thin film. Talanta, 82(4), 1397–1402.

154 Wang, Z., Wang, Z. Y., Ma, J., Bock, W. J., & Ma, D. (2010). Effect of film thickness, blending and undercoating on optical detection of nitroaromatics using fluorescent polymer films. Polymer, 51(4), 842–847.

155 Yang, X., Du, X.-X., Shi, J., & Swanson, B. (2001). Molecular recognition and self-assembled polymer films for vapor phase detection of explosives. Talanta, 54(3), 439–445.

156 Ewing, R. G., Atkinson, D. A., Eiceman, G. A., & Ewing, G. J. (2001). A critical review of ion mobility spectrometry for the detection of explosives and explosive related compounds. Talanta, 54(3), 515–529.

157 Fetterolf, D. & Clark, T. (0). Detection of Trace Explosive Evidence by Ion Mobility Spectrometry. Journal of Forensic Sciences, 38(1), 28-39.

158 Garroway, A. N., Buess, M. L., Miller, J. B., Suits, B. H., Hibbs, A. D., Barrall, G. A., Matthews, R., & Burnett, L. J. (2001). Remote sensing by nuclear quadrupole resonance. IEEE Transactions on Geoscience and Remote Sensing, 39(6), 1108–1118.

159 Caulfield, J. A., Bruno, T. J., & Miller, K. E. (2009). Enthalpy of Solution and Kováts Retention Indices for Nitroaromatic Compounds on Stationary Phases Using Gas Chromatography. Journal of Chemical & Engineering Data, 54(6), 1814–1822.

160 Cook, G. W., LaPuma, P. T., Hook, G. L., & Eckenrode, B. A. (2010). Using Gas Chromatography with Ion Mobility Spectrometry to Resolve Explosive Compounds in the Presence of Interferents*. Journal of Forensic Sciences, 55(6), 1582–1591.

161 Cooks, R. G., Ouyang, Z., Takats, Z., & Wiseman, J. M. (2006). Ambient Mass Spectrometry. Science, 311(5767), 1566–1570.

162 Zhang, Y., Ma, X., Zhang, S., Yang, C., Ouyang, Z., & Zhang, X. (2008). Direct detection of explosives on solid surfaces by low temperature plasma desorption mass spectrometry. Analyst, 134(1), 176–181.

163 Luggar, R. D., Farquharson, M. J., Horrocks, J. A., & Lacey, R. J. (1998). Multivariate analysis of statistically poor EDXRD spectra for the detection of concealed explosives. X-Ray Spectrometry, 27(2), 87–94.

164 Sylvia, J. M., Janni, J. A., Klein, J. D., & Spencer, K. M. (2000). Surface-Enhanced Raman Detection of 2,4-Dinitrotoluene Impurity Vapor as a Marker To Locate Landmines. Analytical Chemistry, 72(23), 5834–5840.

165 Tao, A., Kim, F., Hess, C., Goldberger, J., He, R., Sun, Y., Xia, Y., & Yang, P. (2003). Langmuir−Blodgett Silver Nanowire Monolayers for Molecular Sensing Using Surface-Enhanced Raman Spectroscopy. Nano Letters, 3(9), 1229–1233.

166 Caygill, J. S., Davis, F., & Higson, S. P. J. (2012). Current trends in explosive detection techniques. Talanta, 88, 14–29.

167 Sheaff, C. N., Eastwood, D., & Wai, C. M. (2007). Increasing Selectivity for TNT-Based Explosive Detection by Synchronous Luminescence and Derivative Spectroscopy with Quantum Yields of Selected Aromatic Amines. Applied Spectroscopy, 61(1), 68–73.

168 López-Ruiz, N., Erenas, M. M., de Orbe-Payá, I., Capitán-Vallvey, L. F., Palma, A. J., & Martínez-Olmos, A. (2016, June 29). Computer Vision-Based Portable System for Nitroaromatics Discrimination [Research Article]. Journal of Sensors; Hindawi.

169 Calvo-Castro, J., Maczka, S., Thomson, C., Morris, G., Kennedy, A. R., & McHugh, C. J. (2016). Twist and shout: A surprising synergy between aryl and N-substituents defines the computed charge transport properties in a series of crystalline diketopyrrolopyrroles. CrystEngComm, 18(48), 9382–9390.

170 Calvo-Castro, J., Warzecha, M., Oswald, I. D. H., Kennedy, A. R., Morris, G., McLean, A. J., & McHugh, C. J. (2016). Intermolecular Interactions and Energetics in the Crystalline π–π Stacks and Associated Model Dimer Systems of Asymmetric Halogenated Diketopyrrolopyrroles. Crystal Growth & Design, 16(3), 1531–1542.

171 Sadek, P. C. (2002). The HPLC Solvent Guide, 2nd Edition (Second). John Wiley & Sons.

172 Taniguchi, M., & Lindsey, J. S. (2018). Database of Absorption and Fluorescence Spectra of >300 Common Compounds for use in PhotochemCAD. Photochemistry and Photobiology, 94(2), 290–327.

173 Gerke, K. M., Sidle, R. C., & Mallants, D. (2013). Criteria for selecting fluorescent dye tracers for soil hydrological applications using Uranine as an example. Journal of Hydrology and Hydromechanics, 61(4), 313–325.

174 ElMasry, G., & Nakauchi, S. (2015). Prediction of meat spectral patterns based on optical properties and concentrations of the major constituents. Food Science & Nutrition, 4(2), 269–283.

175 Kaur, M., & Choi, D. H. (2014). Diketopyrrolopyrrole: Brilliant red pigment dye-based fluorescent probes and their applications. Chemical Society Reviews, 44(1), 58–77.

176 Grzybowski, M., Glodkowska-Mrowka, E., Stoklosa, T., & Gryko, D. T. (2012). Bright, Color-Tunable Fluorescent Dyes Based on π-Expanded Diketopyrrolopyrroles. Organic Letters, 14(11), 2670–2673.

177 M. Grzybowski ,D. T. Gryko. (2013). BASF SE, Int. Patent Appl. WO2013/092474

178 Purc, A., Sobczyk, K., Sakagami, Y., Ando, A., Kamada, K., & Gryko, D. T. (2015). Strategy towards large two-photon absorption cross-sections for diketopyrrolopyrroles. Journal of Materials Chemistry C, 3(4), 742–749.

179 Riggs, R. L., Morton, C. J. H., Slawin, A. M. Z., Smith, D. M., Westwood, N. J., Austen, W. S. D., & Stuart, K. E. (2005). Synthetic studies related to diketopyrrolopyrrole (DPP) pigments. Part 3: Syntheses of tri- and tetra-aryl DPPs. Tetrahedron, 61(47), 11230–11243.

180 Yamagata, T., Kuwabara, J., & Kanbara, T. (2012). Synthesis and Characterization of Dioxopyrrolopyrrole Derivatives Having Electron-Withdrawing Groups. European Journal of Organic Chemistry, 2012(27), 5282–5290.

181 Kuwabara, J., Yamagata, T., & Kanbara, T. (2010). Solid-state structure and optical properties of highly fluorescent diketopyrrolopyrrole derivatives synthesized by cross-coupling reaction. Tetrahedron, 66(21), 3736–3741.

182 Dhar, J., Venkatramaiah, N., A, A., & Patil, S. (2014). Photophysical, electrochemical and solid state properties of diketopyrrolopyrrole based molecular materials: importance of the donor group. Journal of Materials Chemistry C, 2(17), 3457–3466.

183 Vala, M., Weiter, M., Vyňuchal, J., Toman, P., & Luňák, S. (2008). Comparative Studies of Diphenyl-Diketo-Pyrrolopyrrole Derivatives for Electroluminescence Applications. Journal of Fluorescence, 18(6), 1181.

184 Luňák, S., Vyňuchal, J., Vala, M., Havel, L., & Hrdina, R. (2009). The synthesis, absorption and fluorescence of polar diketo-pyrrolo-pyrroles. Dyes and Pigments, 82(2), 102–108.

185 Vala, M., Vyňuchal, J., Toman, P., Weiter, M., & Luňák, S. (2010). Novel, soluble diphenyl-diketo-pyrrolopyrroles: Experimental and theoretical study. Dyes and Pigments, 84(2), 176–182.

186 Tamayo, A. B., Tantiwiwat, M., Walker, B., & Nguyen, T.-Q. (2008). Design, Synthesis, and Self-assembly of Oligothiophene Derivatives with a Diketopyrrolopyrrole Core. The Journal of Physical Chemistry C, 112(39), 15543–15552.

187 Bürckstümmer, H., Weissenstein, A., Bialas, D., & Würthner, F. (2011). Synthesis and Characterization of Optical and Redox Properties of Bithiophene-Functionalized Diketopyrrolopyrrole Chromophores. The Journal of Organic Chemistry, 76(8), 2426–2432.

188 Lee, Y., Jo, A., & Park, S. B. (2015). Rational Improvement of Molar Absorptivity Guided by Oscillator Strength: A Case Study with Furoindolizine-Based Core Skeleton. Angewandte Chemie International Edition, 54(52), 15689–15693.

189 Tissue, B. M. (2013). Basics of Analytical Chemistry and Chemical Equilibria. John Wiley & Sons.

190 Grzybowski, M., Hugues, V., Blanchard‐Desce, M., & Gryko, D. T. (2014). Two-Photon-Induced Fluorescence in New π-Expanded Diketopyrrolopyrroles. Chemistry – A European Journal, 20(39), 12493–12501.

191 Fu, L., Fu, W., Cheng, P., Xie, Z., Fan, C., Shi, M., Ling, J., Hou, J., Zhan, X., & Chen, H. (2014). A diketopyrrolopyrrole molecule end-capped with a furan-2-carboxylate moiety: The planarity of molecular geometry and photovoltaic properties. Journal of Materials Chemistry A, 2(18), 6589–6597.

192 Areephong, J., Hendsbee, A. D., & Welch, G. C. (2015). Facile synthesis of unsymmetrical and π-extended furan-diketopyrrolopyrrole derivatives through C–H direct (hetero)arylation using a heterogeneous catalyst system. New Journal of Chemistry, 39(9), 6714–6717.

193 Li, Y., Sonar, P., Singh, S. P., Ooi, Z. E., Lek, E. S. H., & Loh, M. Q. Y. (2012). Poly(2,5-bis(2-octyldodecyl)-3,6-di(furan-2-yl)-2,5-dihydro-pyrrolo[3,4-c]pyrrole-1,4-dione-co-thieno[3,2-b]thiophene): A high performance polymer semiconductor for both organic thin film transistors and organic photovoltaics. Physical Chemistry Chemical Physics, 14(19), 7162–7169.

194 Liu, H., Jia, H., Wang, L., Wu, Y., Zhan, C., Fu, H., & Yao, J. (2012). Intermolecular electron transfer promoted by directional donor–acceptor attractions in self-assembled diketopyrrolopyrrole-thiophene films. Physical Chemistry Chemical Physics, 14(41), 14262–14269.

195 Kanimozhi, C., Naik, M., Yaacobi-Gross, N., Burnett, E. K., Briseno, A. L., Anthopoulos, T. D., & Patil, S. (2014). Controlling Conformations of Diketopyrrolopyrrole-Based Conjugated Polymers: Role of Torsional Angle. The Journal of Physical Chemistry C, 118(22), 11536–11544.

196 Dhar, J., Mukhopadhay, T., Yaacobi-Gross, N., Anthopoulos, T. D., Salzner, U., Swaraj, S., & Patil, S. (2015). Effect of Chalcogens on Electronic and Photophysical Properties of Vinylene-Based Diketopyrrolopyrrole Copolymers. The Journal of Physical Chemistry B, 119(34), 11307–11316.

197 Narayanaswamy, R., & Wolfbeis, O. S. (Eds.). (2004). Optical Sensors: Industrial Environmental and Diagnostic Applications. Springer-Verlag.

198 Karsten, B. P., & Janssen, R. A. J. (2011). Chain Length Dependence in Diketopyrrolopyrrole/Thiophene Oligomers. Macromolecular Chemistry and Physics, 212(5), 515–520.

199 Brédas, J. L., Street, G. B., Thémans, B., & André, J. M. (1985). Organic polymers based on aromatic rings (polyparaphenylene, polypyrrole, polythiophene): Evolution of the electronic properties as a function of the torsion angle between adjacent rings. The Journal of Chemical Physics, 83(3), 1323–1329.

200 Maior, R. M. S., Hinkelmann, K., Eckert, H., & Wudl, F. (1990). Synthesis and characterization of two regiochemically defined poly(dialkylbithiophenes): A comparative study. Macromolecules, 23(5), 1268–1279.

201 Barta, P., Dannetun, P., Stafström, S., Zagórska, M., & Proń, A. (1994). Temperature evolution of the electronic band structure of the undoped and doped regioregular analog of poly(3‐alkylthiophenes): A spectroscopic and theoretical study. The Journal of Chemical Physics, 100(2), 1731–1741.

202 Fell, H. J., Samuelsen, E. J., Mårdalen, J., Bakken, E., & Carlsen, P. H. J. (1995). The effect of stereoregularity on the structure of poly(octylthiophene): An x-ray diffraction study. Synthetic Metals, 69(1), 301–302.

203 Kim, W., Sung, J., Grzybowski, M., Gryko, D. T., & Kim, D. (2016). Modulation of Symmetry-Breaking Intramolecular Charge-Transfer Dynamics Assisted by Pendant Side Chains in π-Linkers in Quadrupolar Diketopyrrolopyrrole Derivatives. The Journal of Physical Chemistry Letters, 7(15), 3060–3066.

204 Morton, CJH., Gilmour, R., Smith, DM., Lightfoot, P., Slawin, A. M. Z., & MacLean, EJ. (2002). Synthetic studies related to diketopyrrolopyrrole (DPP) pigments. Part 1: The search for alkenyl-DPPs. Unsaturated nitriles in standard DPP syntheses: a novel cyclopenta[c]pyrrolone chromophore. Tetrahedron, 58, 5547-5565.

205 Yamagata, T., Kuwabara, J., & Kanbara, T. (2010). Synthesis of highly fluorescent diketopyrrolopyrrole derivative and two-step response of fluorescence to acid. Tetrahedron Letters, 51(12), 1596–1599.

206 Maercker, A., Brieden, W., Schmidt, T., & Lutz, H. D. (1989). Tetraalkylidene-1,4-diboracyclohexanes from 3,4-Dilithio-2,5-dimethyl-2,4-hexadiene; the First "Hetero[6]radialene" with Chair Conformation. Angewandte Chemie International Edition in English, 28(4), 477–478.

207 MacLean, E. J., Tremayne, M., Kariuki, B. M., Harris, K. D. M., Iqbal, A. F. M., & Hao, Z. (2000). Structural understanding of a polymorphic system by structure solution and refinement from powder X-ray diffraction data: The α and β phases of the latent pigment DPP-Boc. Journal of the Chemical Society, Perkin Transactions 2, 7, 1513–1519.

208 Jin, Y., Xu, Y., Liu, Y., Wang, L., Jiang, H., Li, X., & Cao, D. (2011). Synthesis of novel diketopyrrolopyrrole-based luminophores showing crystallization-induced emission enhancement properties. Dyes and Pigments, 90(3), 311–318.

209 Kim, C., Liu, J., Lin, J., Tamayo, A. B., Walker, B., Wu, G., & Nguyen, T.-Q. (2012). Influence of Structural Variation on the Solid-State Properties of Diketopyrrolopyrrole-Based Oligophenylenethiophenes: Single-Crystal Structures, Thermal Properties, Optical Bandgaps, Energy Levels, Film Morphology, and Hole Mobility. Chemistry of Materials, 24(10), 1699–1709.

210 Szabadai, R. S., Roth-Barton, J., Ghiggino, K. P., White, J. M., & Wilson, D. J. D. (2014). Solvatochromism in Diketopyrrolopyrrole Derivatives: Experimental and Computational Studies. Australian Journal of Chemistry, 67(9), 1330–1337.

211 Richert, S., Mosquera Vazquez, S., Grzybowski, M., Gryko, D. T., Kyrychenko, A., & Vauthey, E. (2014). Excited-state dynamics of an environment-sensitive push-pull diketopyrrolopyrrole: Major differences between the bulk solution phase and the dodecane/water interface. The Journal of Physical Chemistry. B, 118(33), 9952–9963.

212 Wang, L., Yang, L., Li, L., & Cao, D. (2016). The synthesis and highly sensitive detection of water content in THF using a novel solvatochromic AIE polymer containing diketopyrrolopyrrole and triphenylamine. New Journal of Chemistry, 40(8), 6706–6713.

213 Nigam, S., & Rutan, S. (2001). Principles and Applications of Solvatochromism. Applied Spectroscopy, 55(11), 362A-370A.

214 Buss, V., & Eggers, L. (1999). Dyes and Indicators, Use of UV-Visible Absorption Spectroscopy. In J. C. Lindon (Ed.), Encyclopedia of Spectroscopy and Spectrometry (pp. 388–396). Elsevier.

215 Khan, M. R. R., Khalilian, A., & Kang, S.-W. (2016). Fast, Highly-Sensitive, and Wide-Dynamic-Range Interdigitated Capacitor Glucose Biosensor Using Solvatochromic Dye-Containing Sensing Membrane. Sensors, 16(2), 265.

216 Kulinich, A. V., Mikitenko, E. K., & Ishchenko, A. A. (2016). Scope of negative solvatochromism and solvatofluorochromism of merocyanines. Physical Chemistry Chemical Physics, 18(5), 3444–3453.

217 Cartwright, S. J. (2016). Solvatochromic dyes detect the presence of homeopathic potencies. Homeopathy, 105(1), 55–65.

218 Deye, J. F., Berger, T. A., & Anderson, A. G. (1990). Nile Red as a solvatochromic dye for measuring solvent strength in normal liquids and mixtures of normal liquids with supercritical and near critical fluids. Analytical Chemistry, 62(6), 615–622.

219 Buncel, E., & Rajagopal, S. (1990). Solvatochromism and solvent polarity scales. Accounts of Chemical Research, 23(7), 226–231.

220 Adeloye, A. O., & Ajibade, P. A. (2011). A High Molar Extinction Coefficient Mono-Anthracenyl Bipyridyl Heteroleptic Ruthenium(II) Complex: Synthesis, Photophysical and Electrochemical Properties. Molecules, 16(6), 4615–4631.

221 Paquot, C. (2013). Standard Methods for the Analysis of Oils, Fats and Derivatives. Elsevier.

222 Yin, N., Wang, L., Lin, Y., Yi, J., Yan, L., Dou, J., Yang, H.-B., Zhao, X., & Ma, C.-Q. (2016). Effect of the π-conjugation length on the properties and photovoltaic performance of A–π–D–π–A type oligothiophenes with a 4,8-bis(thienyl)benzo[1,2-b:4,5-b′]dithiophene core. Beilstein Journal of Organic Chemistry, 12(1), 1788–1797.

223 Chen, S., Yu, Y.-L., & Wang, J.-H. (2018). Inner filter effect-based fluorescent sensing systems: A review. Analytica Chimica Acta, 999, 13–26.

224 Territo, P. R., Heil, J., Bose, S., Evans, F. J., & Balaban, R. S. (2007). Fluorescence Absorbance Inner-Filter Decomposition: The Role of Emission Shape on Estimates of Free Ca2+ Using Rhod-2. Applied Spectroscopy, 61(2), 138–147.

225 Purc, A., Koszarna, B., Iachina, I., H. Friese, D., Tasior, M., Sobczyk, K., Pędziński, T., Brewer, J., & T. Gryko, D. (2017). The impact of interplay between electronic and steric effects on the synthesis and the linear and non-linear optical properties of diketopyrrolopyrrole bearing benzofuran moieties. Organic Chemistry Frontiers, 4(5), 724–736.

226 Kirkus, M. (2013). Diketopyrrolopyrrole based molecular materials: Synthesis, optical characterization, and application in photovoltaics.

227 Aaron, J. J. (2009). Bioactive Heterocycles VII: Flavonoids and Anthocyanins in Plants, and Latest Bioactive Heterocycles II. Springer Science & Business Media.

228 Eisenthal, K. B., Turro, N. J., Sitzmann, E. V., Gould, I. R., Hefferon, G., Langan, J., & Cha, Y. (1985). Singlet-triplet interconversion of diphenylmethylene. Energetics, dynamics and reactivities of different spin states. Tetrahedron, 41(8), 1543–1554.

229 Montalti, M., Credi, A., Prodi, L., & Gandolfi, M. T. (2006). Handbook of Photochemistry (Third). CRC Press.

230 Nançoz, C., Rumble, C., Rosspeintner, A., & Vauthey, E. (2020). Bimolecular photoinduced electron transfer in non-polar solvents beyond the diffusion limit. The Journal of Chemical Physics, 152(24), 244501.

231 H, N., & M, S. (2004). Using photoinduced charge transfer reactions to study conformational dynamics of biopolymers at the single-molecule level. Current Pharmaceutical Biotechnology, 5(3), 285–298.

232 Doose, S., Neuweiler, H., & Sauer, M. (2009). Fluorescence Quenching by Photoinduced Electron Transfer: A Reporter for Conformational Dynamics of Macromolecules. ChemPhysChem, 10(9–10), 1389–1398.

233 Dirian, K., Herranz, M. Á., Katsukis, G., Malig, J., Rodríguez-Pérez, L., Romero-Nieto, C., Strauss, V., Martín, N., & Guldi, D. M. (2013). Low dimensional nanocarbons – chemistry and energy/electron transfer reactions. Chemical Science, 4(12), 4335–4353.

234 Rehm, D., & Weller, A. (1970). Kinetics of Fluorescence Quenching by Electron and H-Atom Transfer. Israel Journal of Chemistry, 8(2), 259–271.

235 Ward, A. J., Ruseckas, A., Kareem, M. M., Ebenhoch, B., Serrano, L. A., Al‐Eid, M., Fitzpatrick, B., Rotello, V. M., Cooke, G., & Samuel, I. D. W. (2015). The Impact of Driving Force on Electron Transfer Rates in Photovoltaic Donor–Acceptor Blends. Advanced Materials, 27(15), 2496–2500.

236 Electron transfers in chemistry and biology. (1985). Biochimica et Biophysica Acta (BBA) - Reviews on Bioenergetics, 811(3), 265–322.

237 Niamnont, N., Kimpitak, N., Wongravee, K., Rashatasakhon, P., Baldridge, K. K., Siegel, J. S., & Sukwattanasinitt, M. (2012). Tunable star-shaped triphenylamine fluorophores for fluorescence quenching detection and identification of nitro-aromatic explosives. Chemical Communications, 49(8), 780–782.

Appendix A

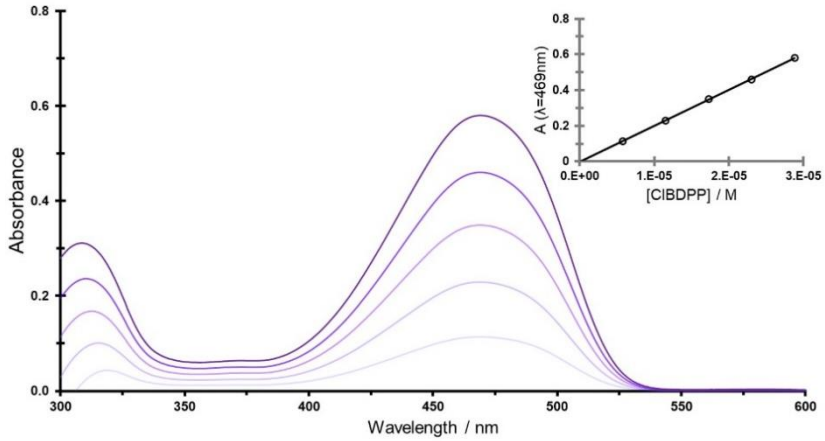


Figure A1.1: Absorption spectra of increasing concentration ClBDPP in acetonitrile at 469 nm. Inset illustrates the linear Beer-Lambert plot for absorbance at 469 nm.

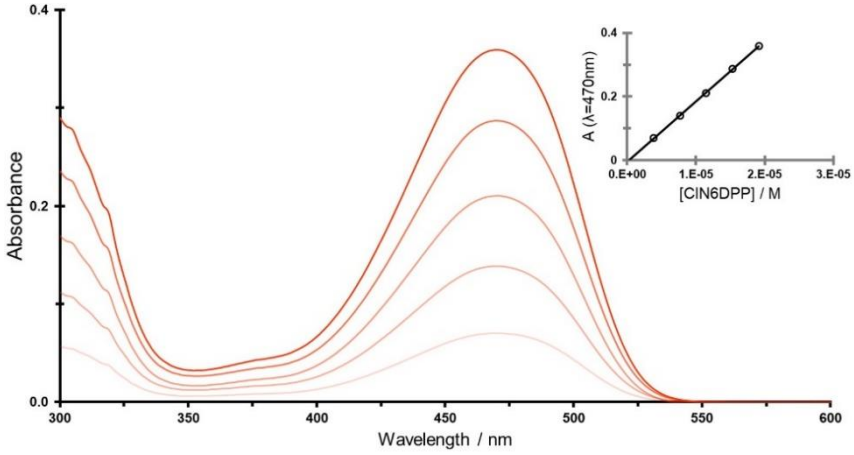


Figure A1.2: Absorption spectra of increasing concentration ClN6DPP in acetonitrile at 470 nm. Inset illustrates the linear Beer-Lambert plot for absorbance at 470 nm.

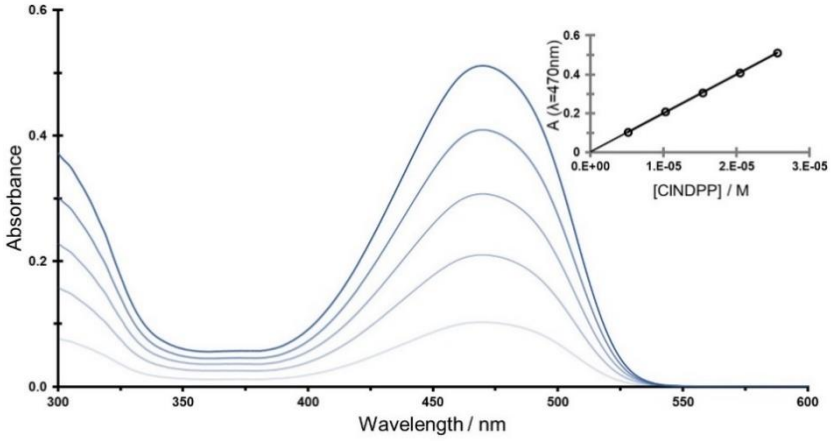


Figure A1.2: Absorption spectra of increasing concentration ClN6DPP in acetonitrile at 470 nm. Inset illustrates the linear Beer-Lambert plot for absorbance at 470 nm.

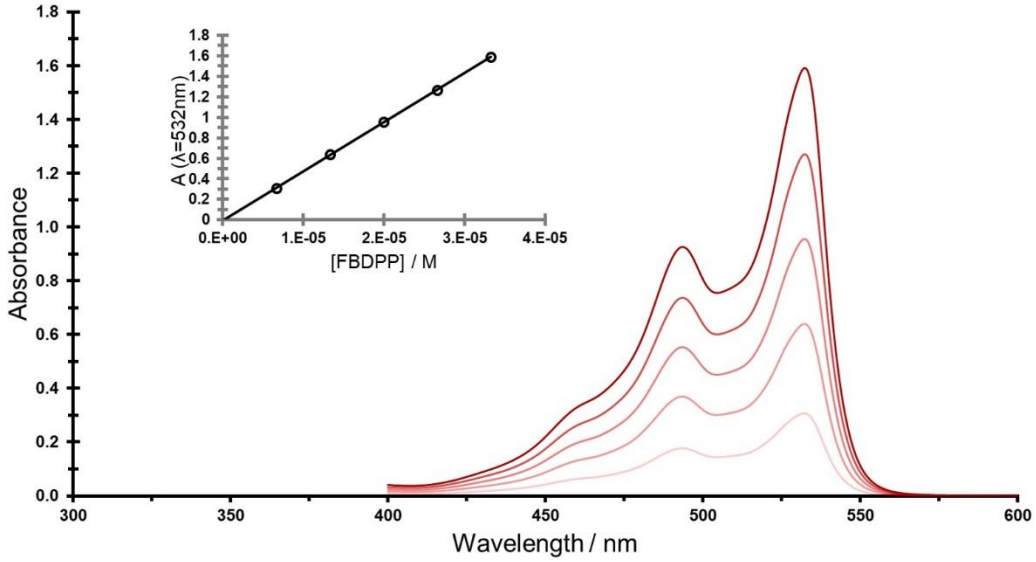


Figure A1.4: Absorption spectra of increasing concentration FBDPP in acetonitrile at 532 nm. Inset illustrates the linear Beer-Lambert plot for absorbance at 532 nm.

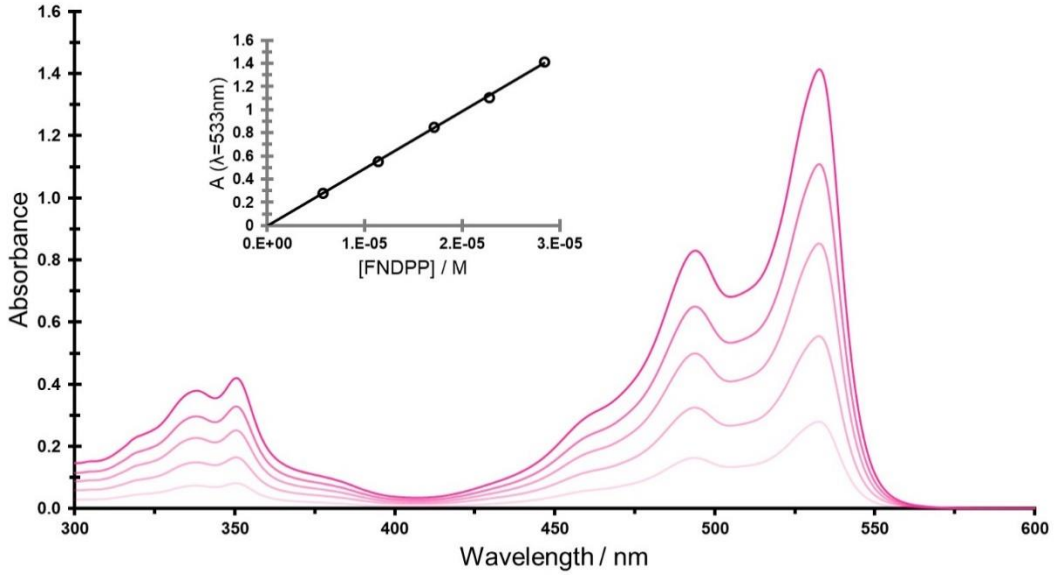


Figure A1.5: Absorption spectra of increasing concentration FNDPP in acetonitrile at 533 nm. Inset illustrates the linear Beer-Lambert plot for absorbance at 533 nm.

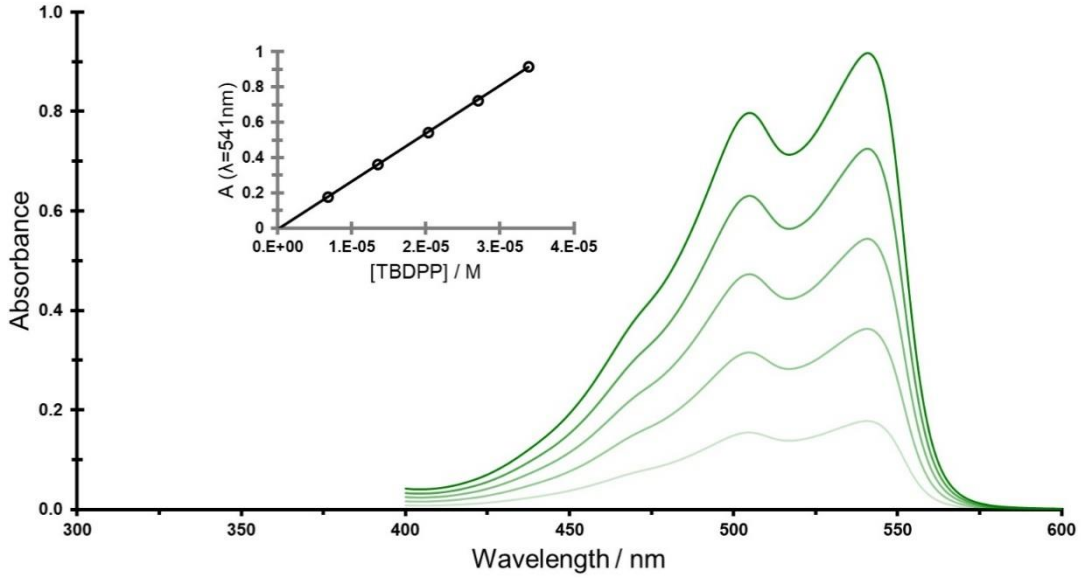


Figure A1.6: Absorption spectra of increasing concentration FNDPP in acetonitrile at 541 nm. Inset illustrates the linear Beer-Lambert plot for absorbance at 541 nm.

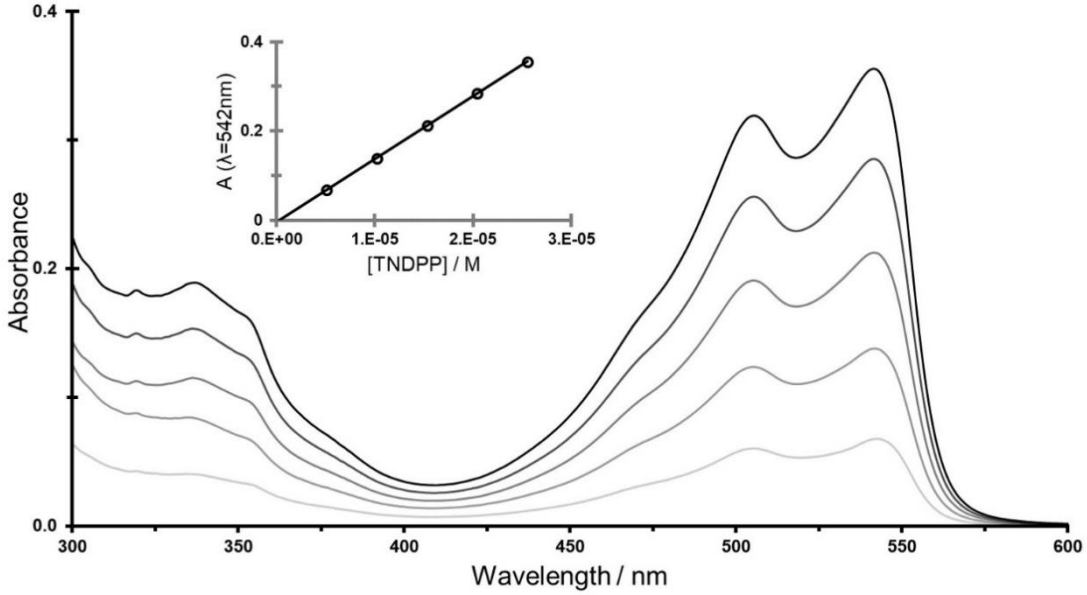


Figure A1.7: Absorption spectra of increasing concentration FNDPP in acetonitrile at 542 nm. Inset illustrates the linear Beer-Lambert plot for absorbance at 542 nm.

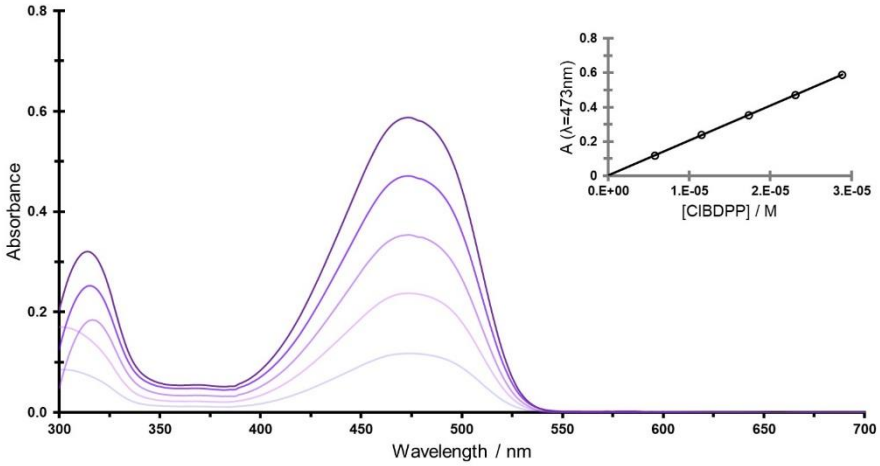


Figure A1.8: Absorption spectra of increasing concentration ClBDPP in dichloromethane at 473 nm. Inset illustrates the linear Beer-Lambert plot for absorbance at 473 nm.

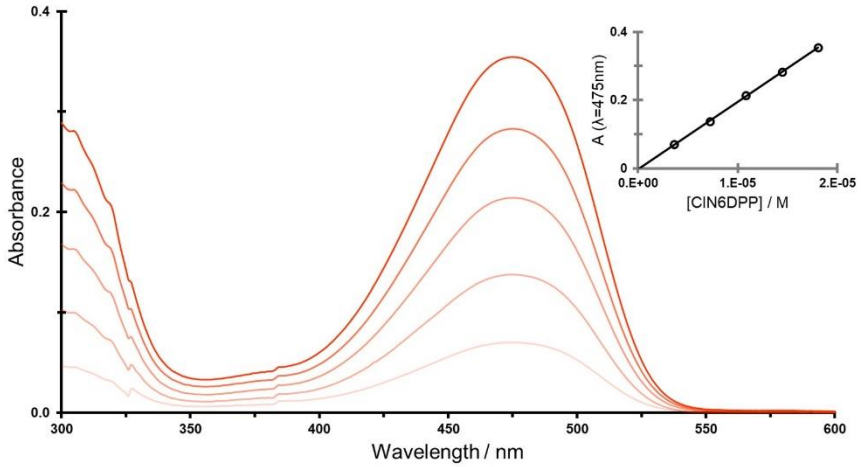


Figure A1.9: Absorption spectra of increasing concentration ClN6DPP in dichloromethane at 475 nm. Inset illustrates the linear Beer-Lambert plot for absorbance at 475 nm.

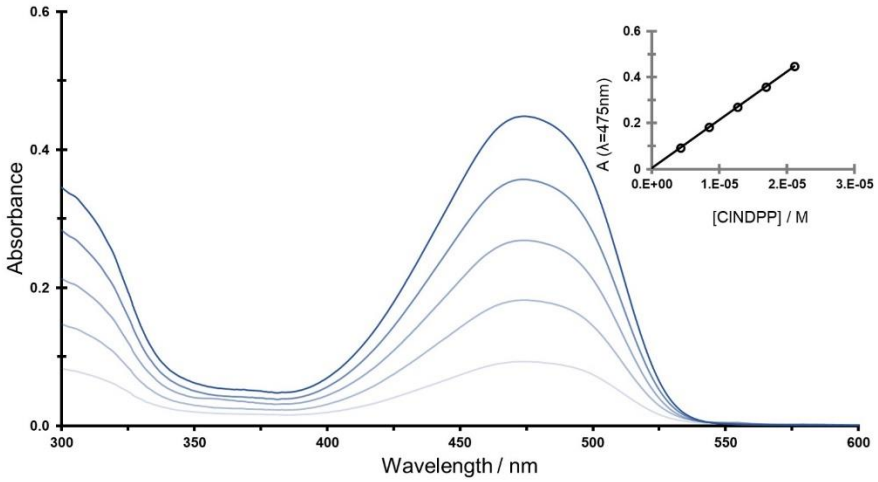


Figure A1.10: Absorption spectra of increasing concentration ClNDPP in dichloromethane at 475 nm. Inset illustrates the linear Beer-Lambert plot for absorbance at 475 nm.

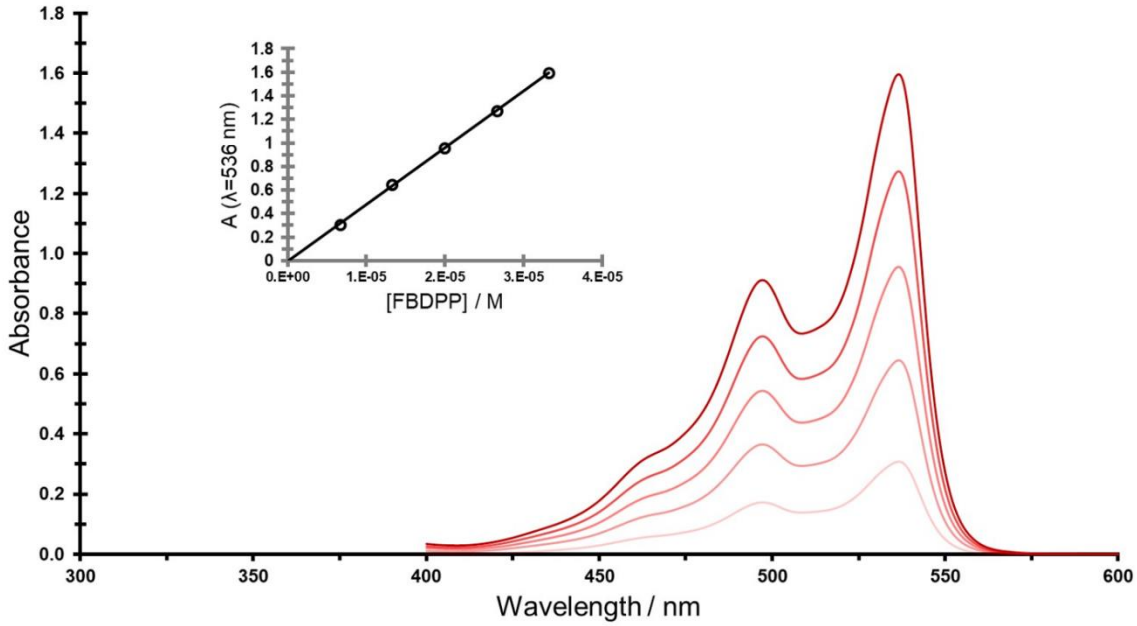


Figure A1.11: Absorption spectra of increasing concentration FBDPP in dichloromethane at 536 nm. Inset illustrates the linear Beer-Lambert plot for absorbance at 536 nm.

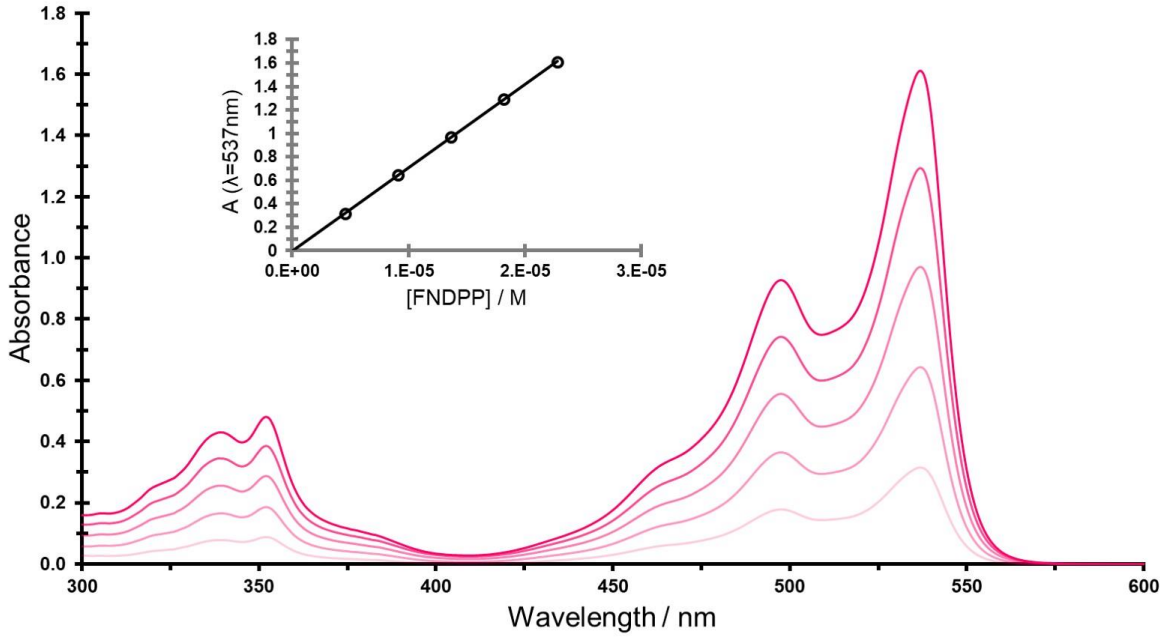


Figure A1.12: Absorption spectra of increasing concentration FNDPP in dichloromethane at 537 nm. Inset illustrates the linear Beer-Lambert plot for absorbance at 537 nm.

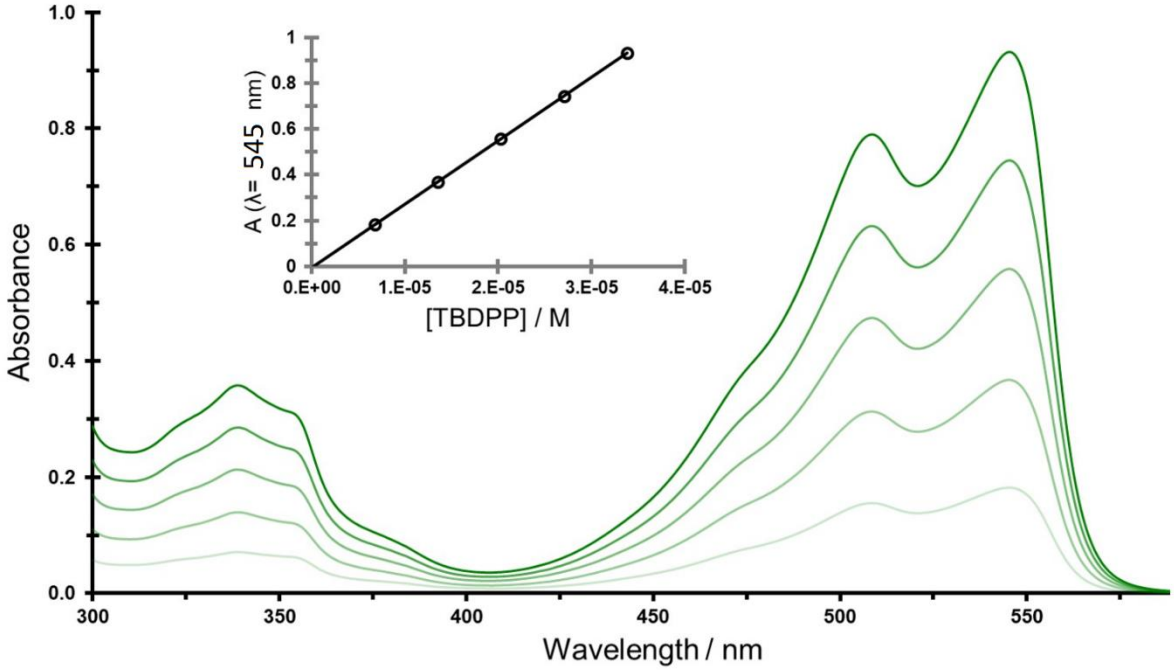


Figure A1.13: Absorption spectra of increasing concentration TBDPP in dichloromethane at 545 nm. Inset illustrates the linear Beer-Lambert plot for absorbance at 545 nm.

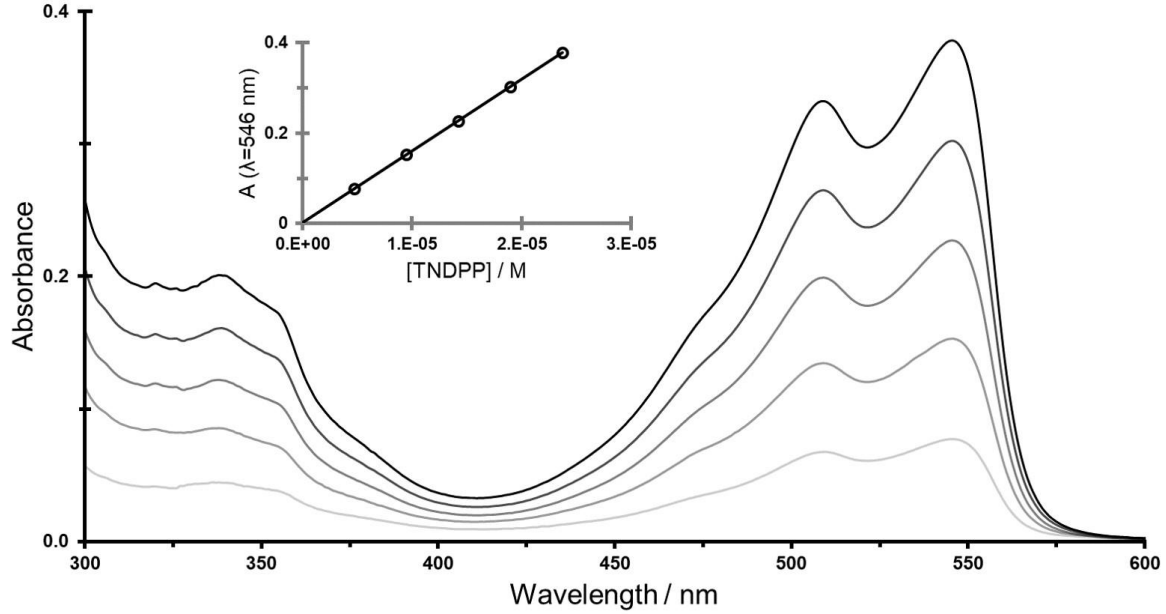


Figure A1.14: Absorption spectra of increasing concentration TNDPP in dichloromethane at 546 nm. Inset illustrates the linear Beer-Lambert plot for absorbance at 546 nm.

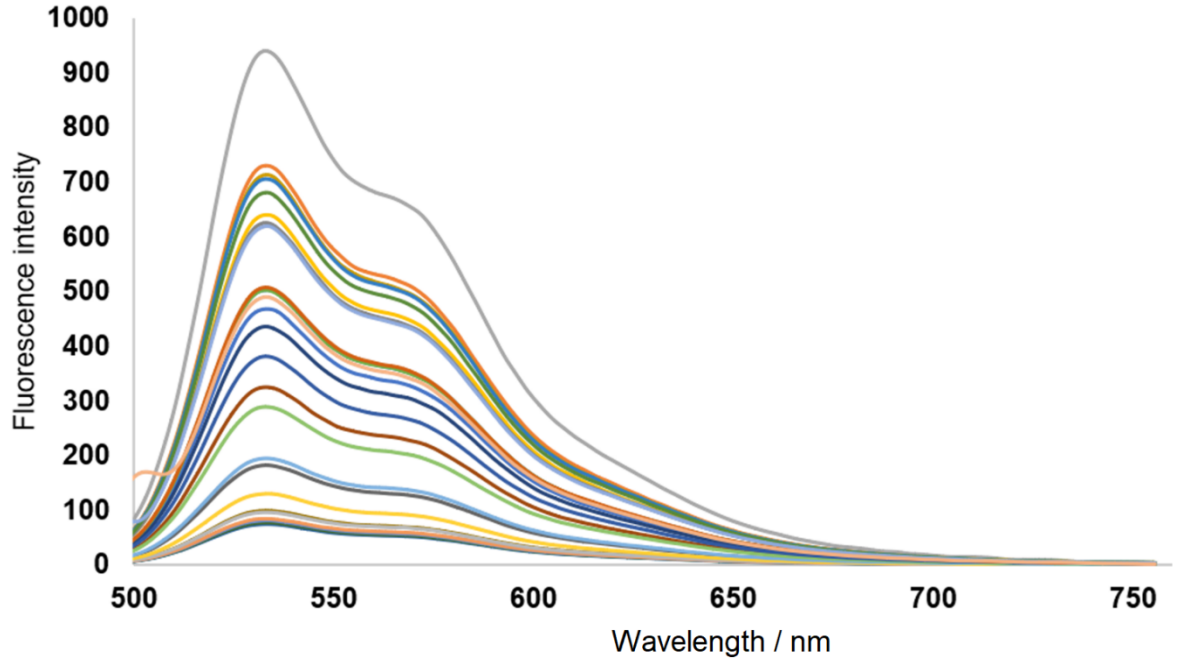


Figure A2.1: Fluorescence emission spectra of ClBDPP in acetonitrile at different excitation wavelengths.

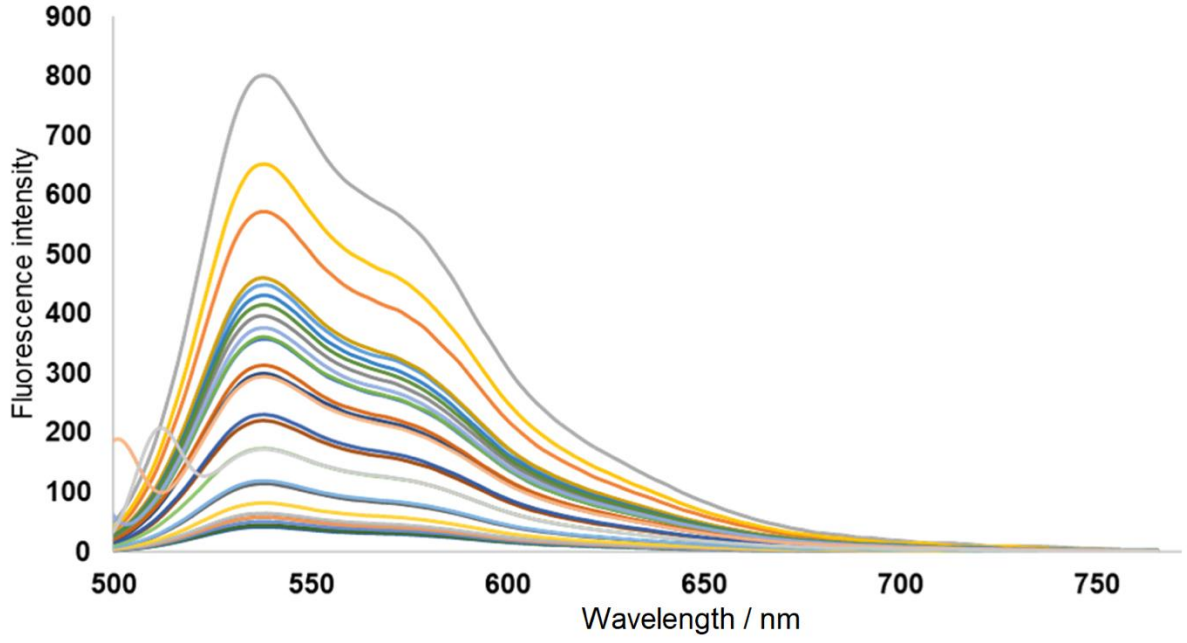


Figure A2.2: Fluorescence emission spectra of ClN6DPP in acetonitrile at different excitation wavelengths.

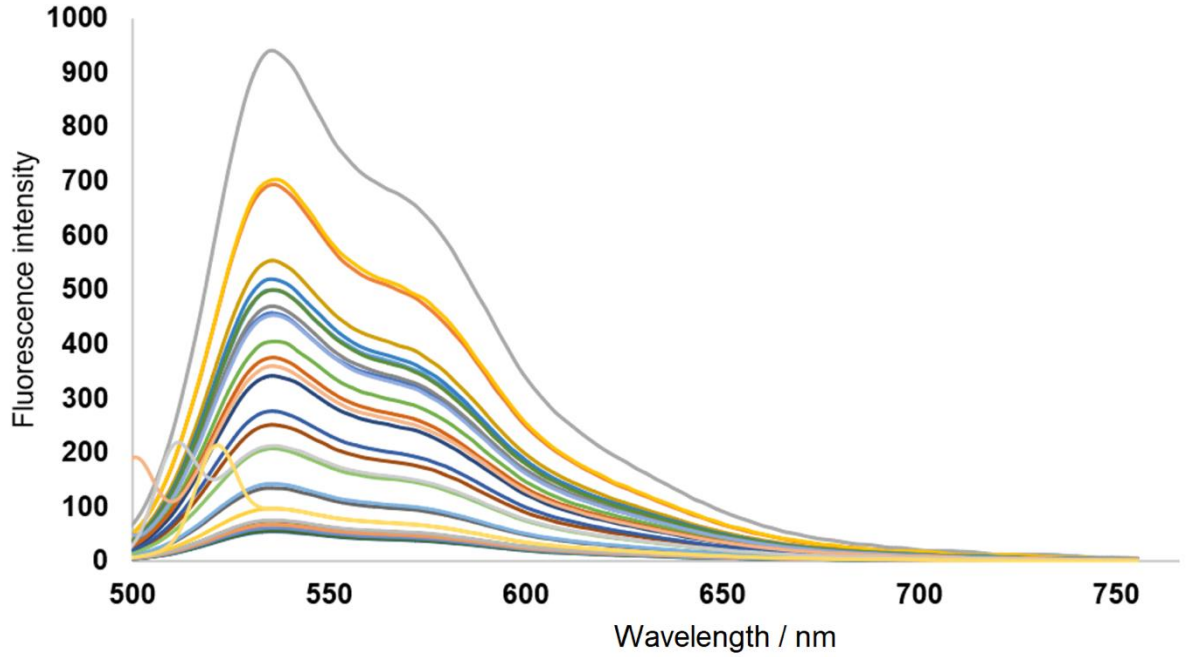


Figure A2.3: Fluorescence emission spectra of ClNDPP in acetonitrile at different excitation wavelengths.

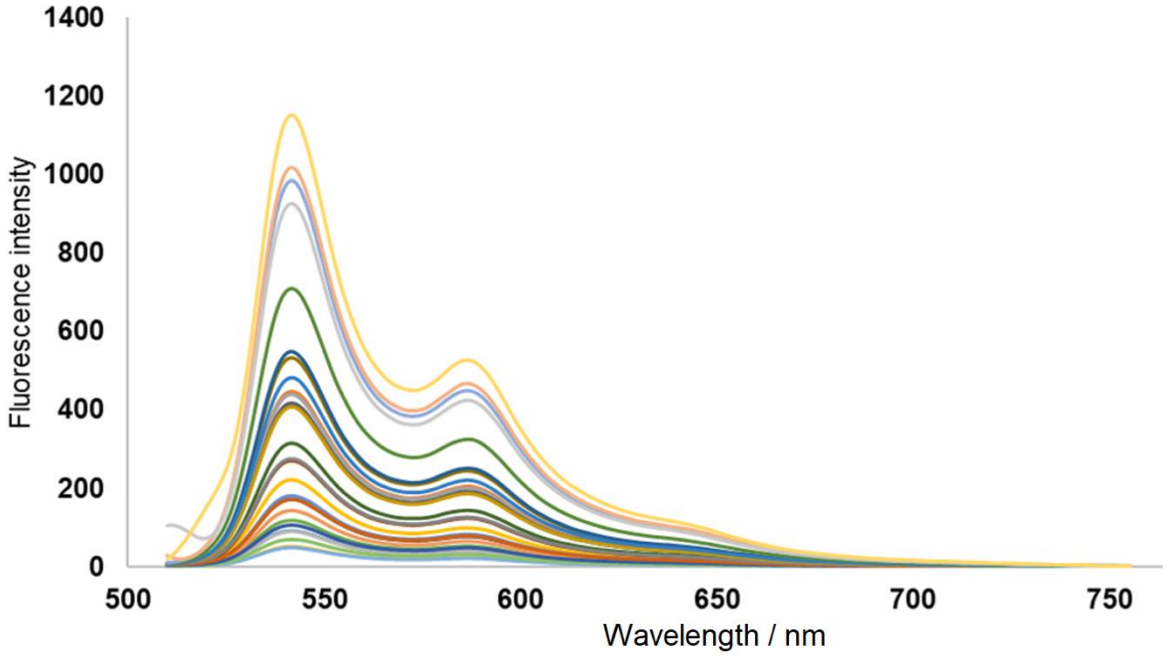


Figure A2.4: Fluorescence emission spectra of FBDPP in acetonitrile at different excitation wavelengths.

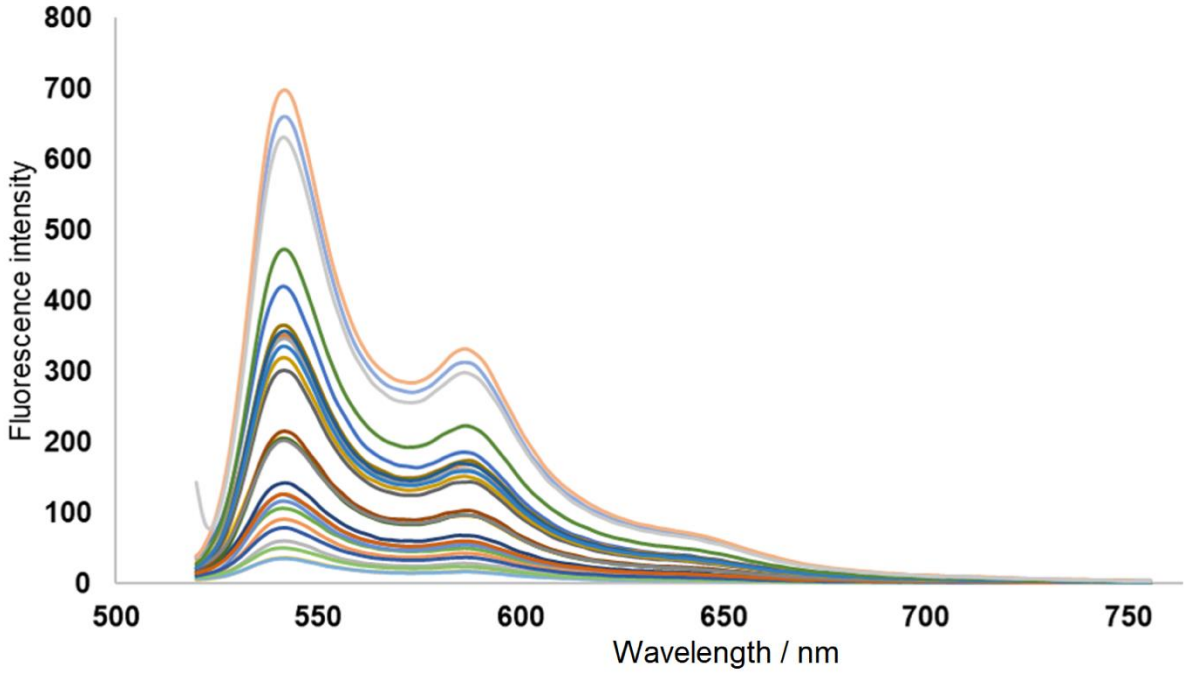


Figure A2.5: Fluorescence emission spectra of FNDPP in acetonitrile at different excitation wavelengths.

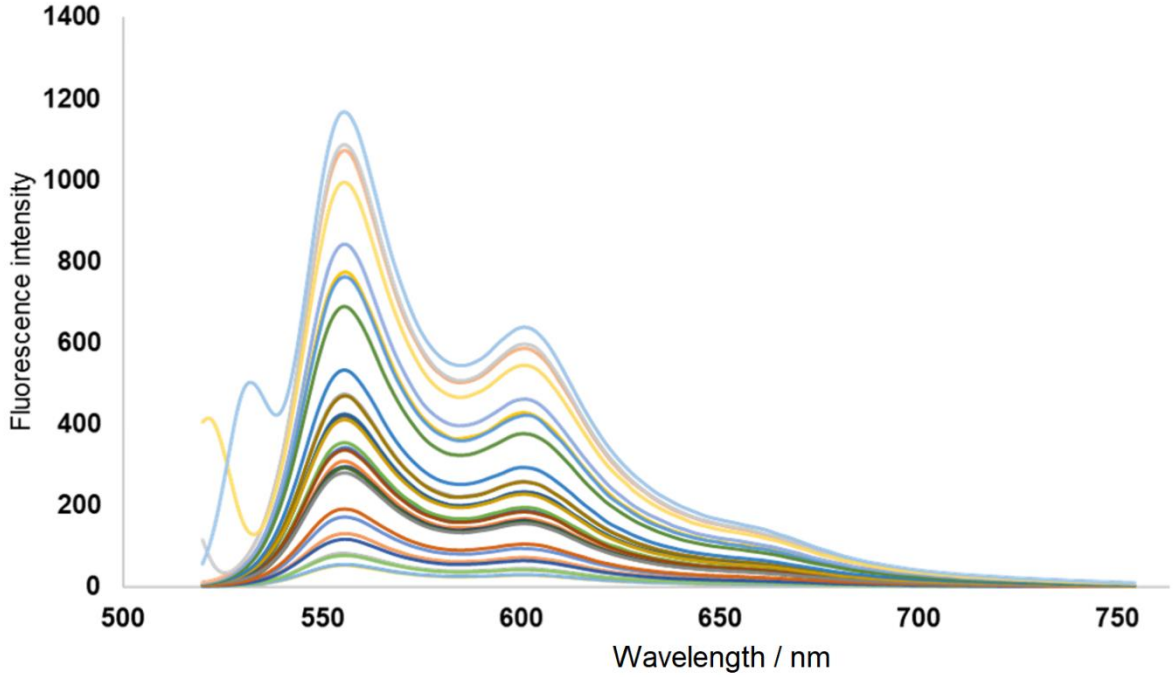


Figure A2.6: Fluorescence emission spectra of TBDPP in acetonitrile at different excitation wavelengths.

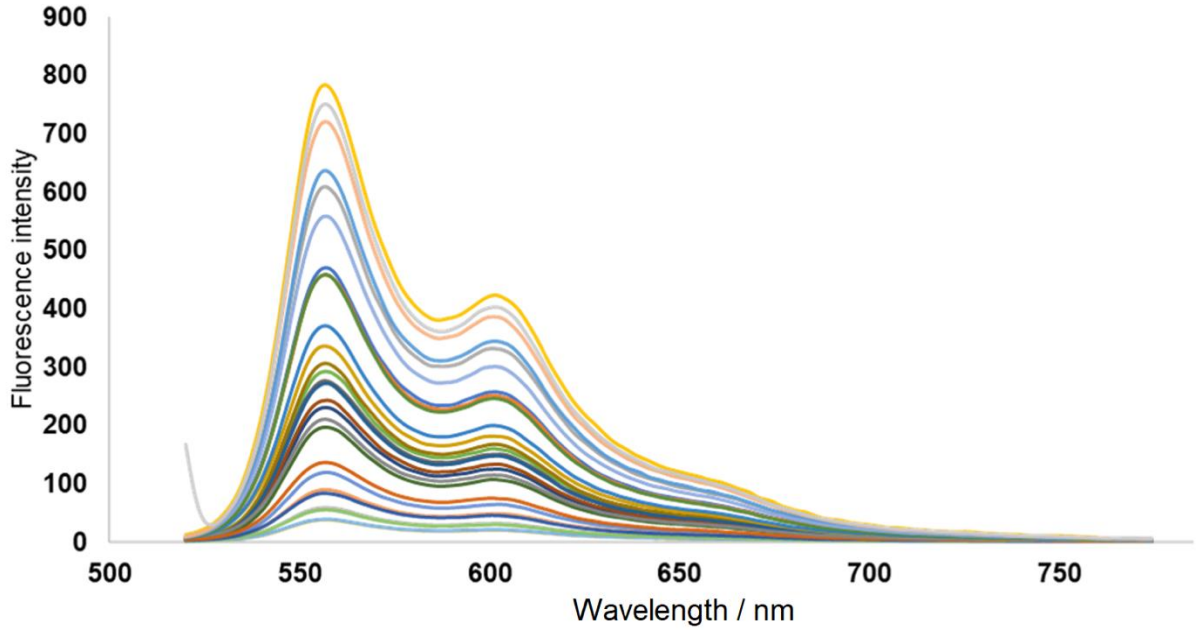


Figure A2.7: Fluorescence emission spectra of TNDPP in acetonitrile at different excitation wavelengths.

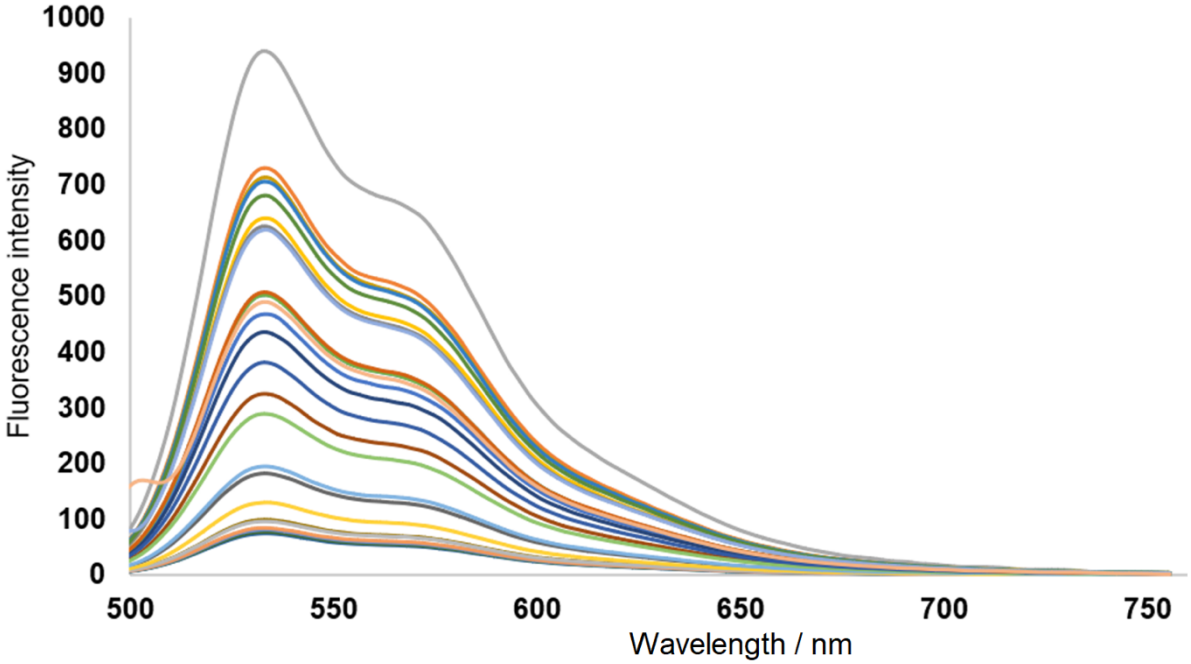


Figure A2.9: Fluorescence emission spectra of ClBDPP in dichloromethane at different excitation wavelengths.

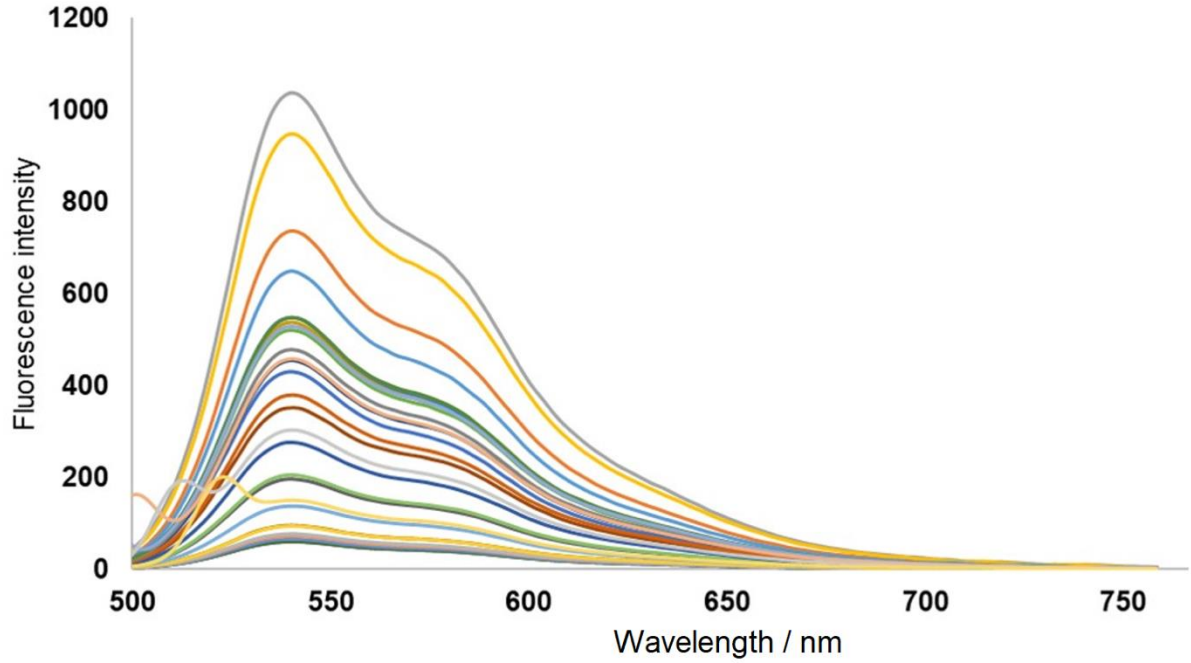


Figure A2.10: Fluorescence emission spectra of ClN6DPP in dichloromethane at different excitation wavelengths.

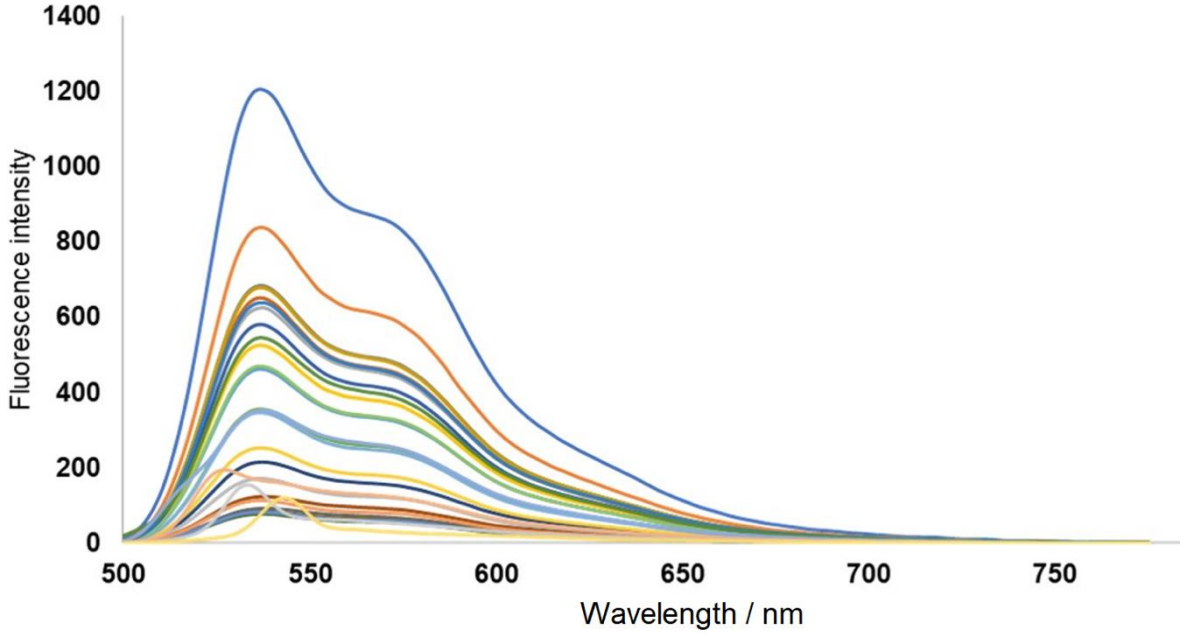


Figure A2.11: Fluorescence emission spectra of ClN6DPP in dichloromethane at different excitation wavelengths.

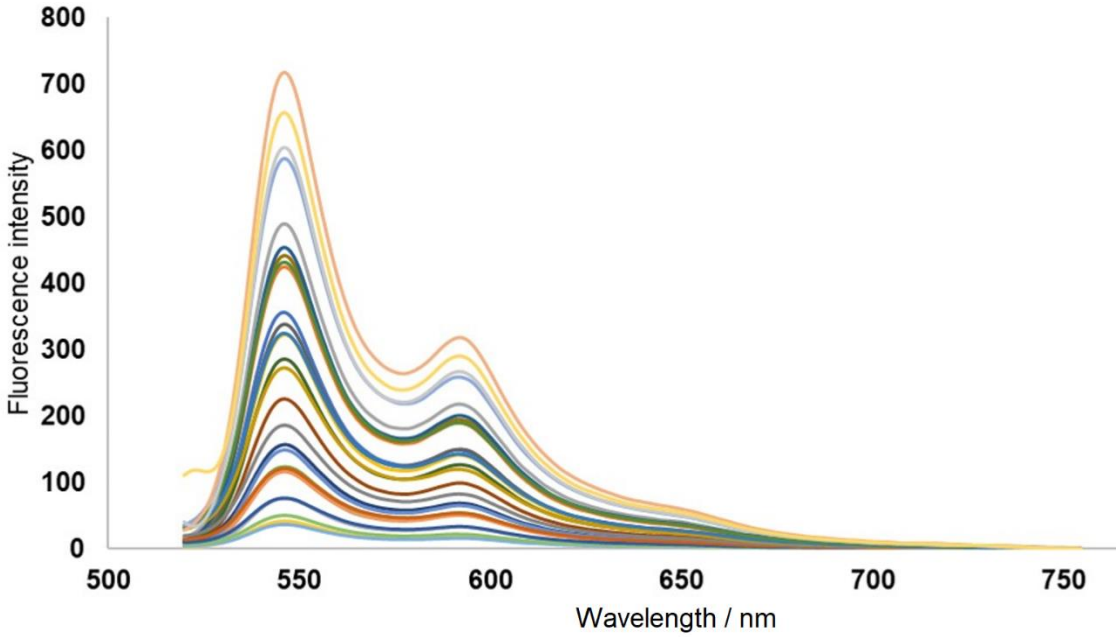


Figure A2.12: Fluorescence emission spectra of FBDPP in dichloromethane at different excitation wavelengths.

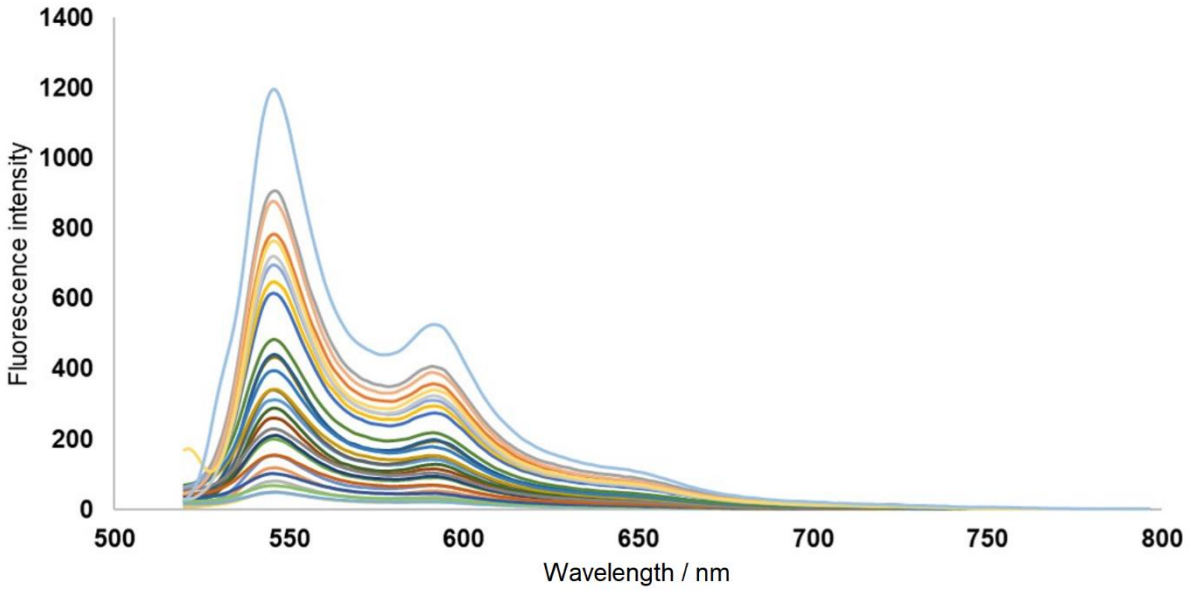


Figure A2.13: Fluorescence emission spectra of FNDPP in dichloromethane at different excitation wavelengths.

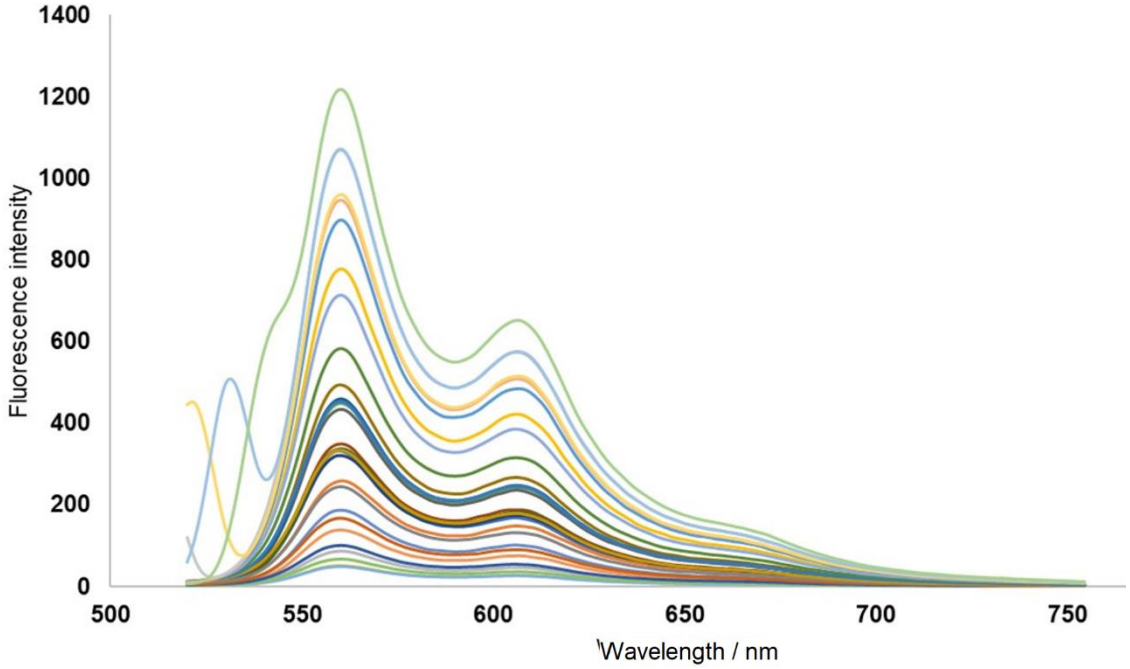


Figure A2.14: Fluorescence emission spectra of TBDPP in dichloromethane at different excitation wavelengths.

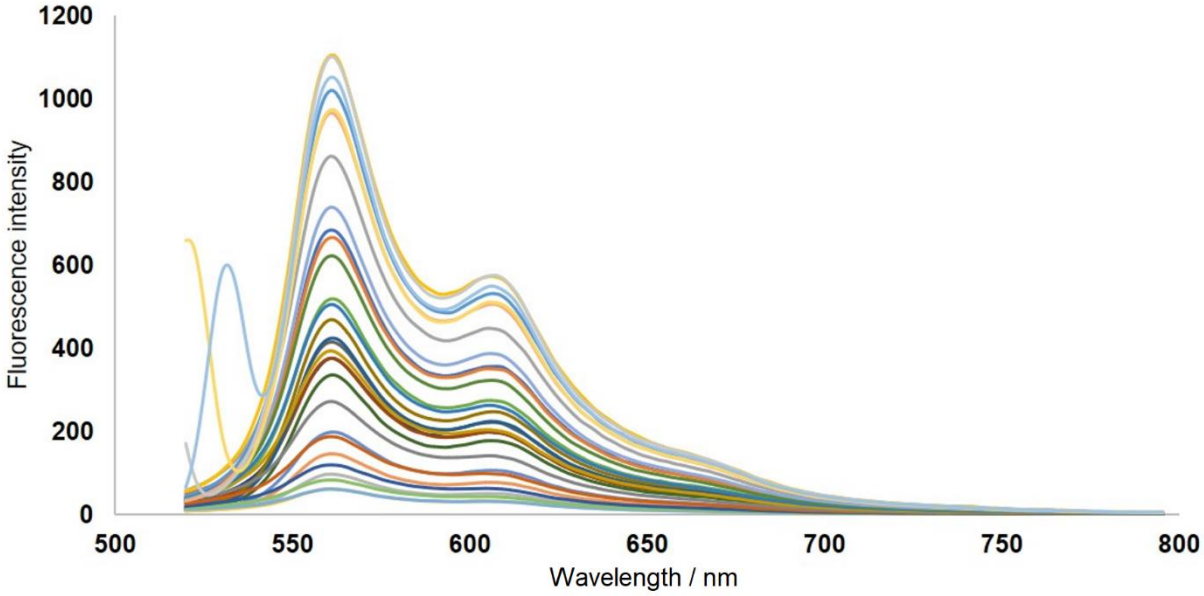


Figure A2.15: Fluorescence emission spectra of TNDPP in dichloromethane at different excitation wavelengths.

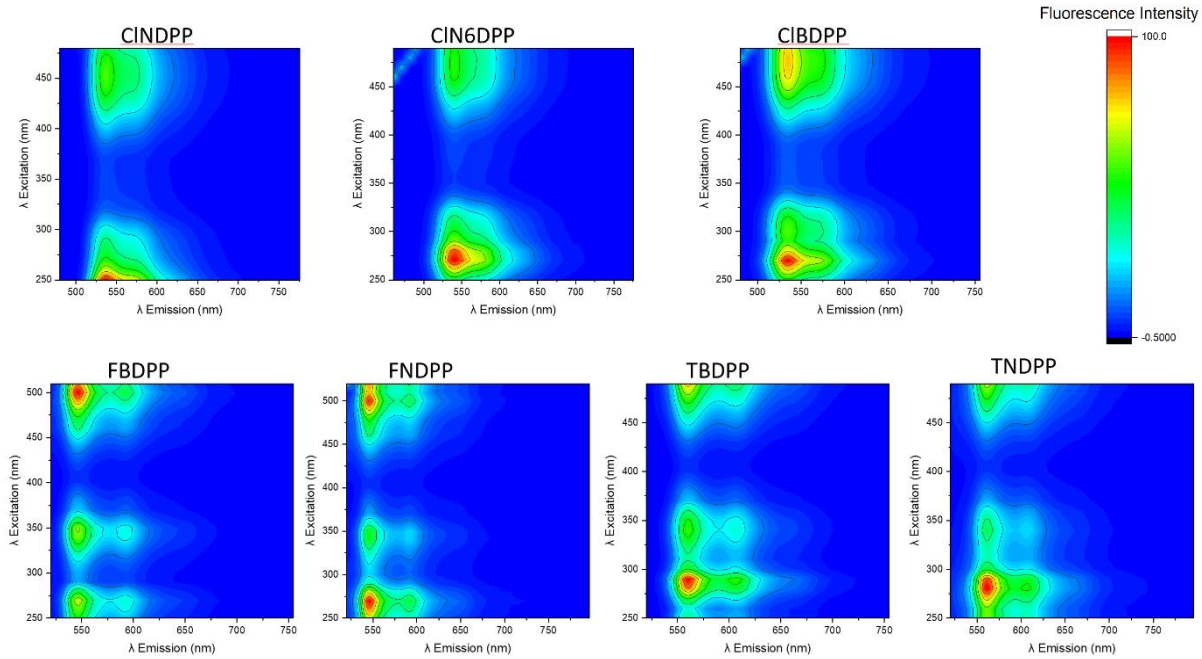


Figure A2.16: 3D contour plots of DPPs in dichloromethane.

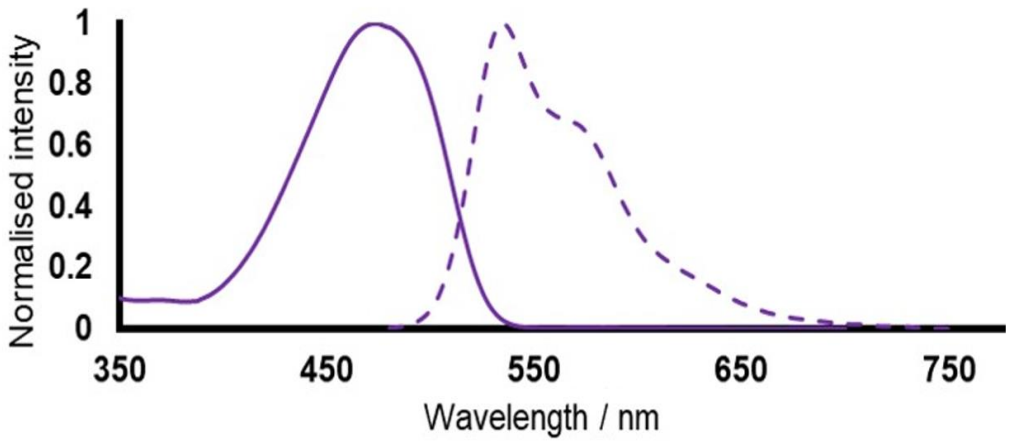


Figure A2.17: Normalised absorption and fluorescence emission spectra of ClBDPP in dichloromethane.

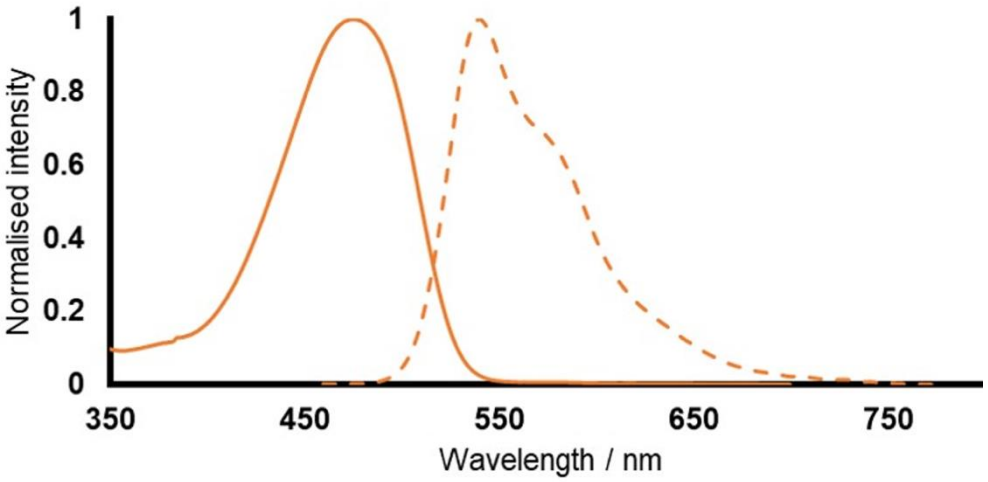


Figure A2.18: Normalised absorption and fluorescence emission spectra of ClN6DPP in dichloromethane.

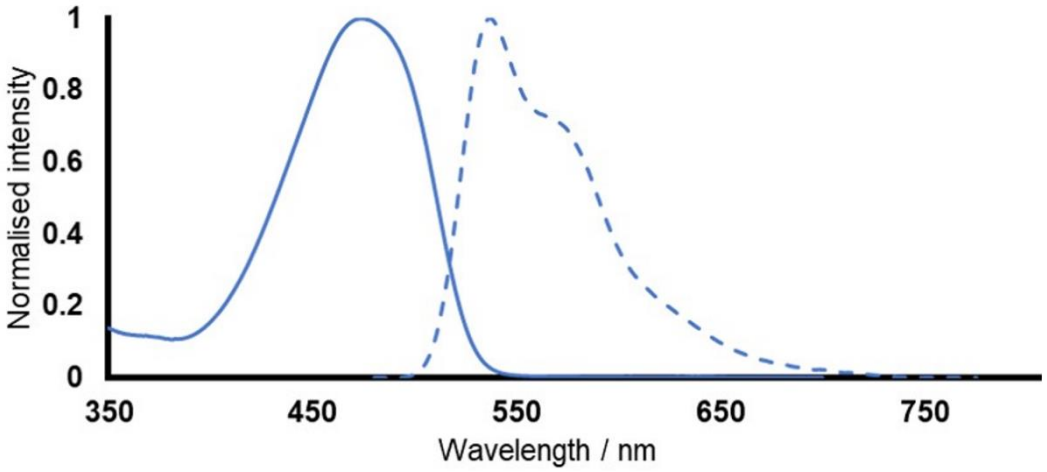


Figure A2.19: Normalised absorption and fluorescence emission spectra of ClNDPP in dichloromethane.

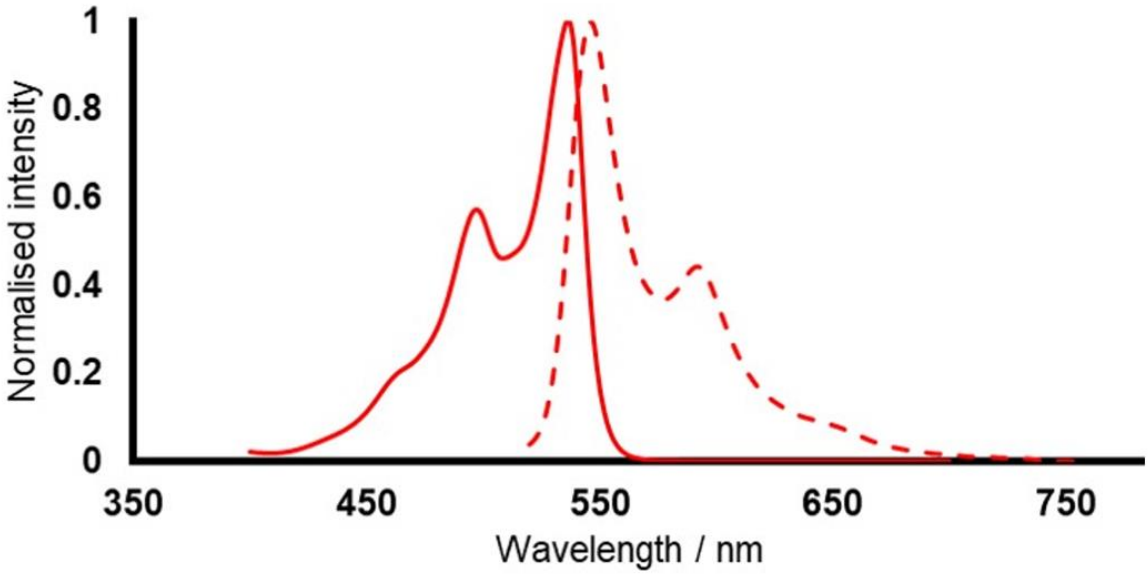


Figure A2.20: Normalised absorption and fluorescence emission spectra of FBDPP in dichloromethane.

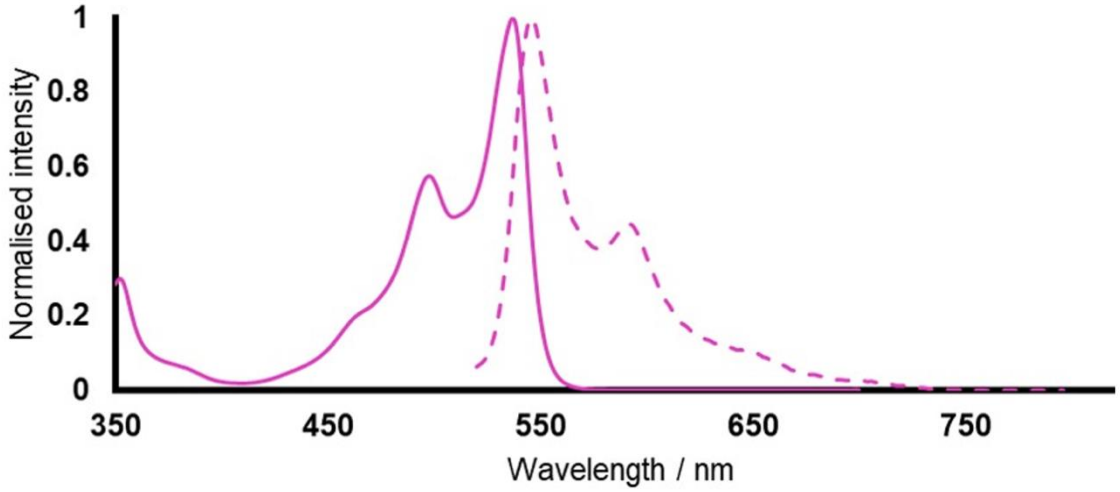


Figure A2.21: Normalised absorption and fluorescence emission spectra of FNDPP in dichloromethane.

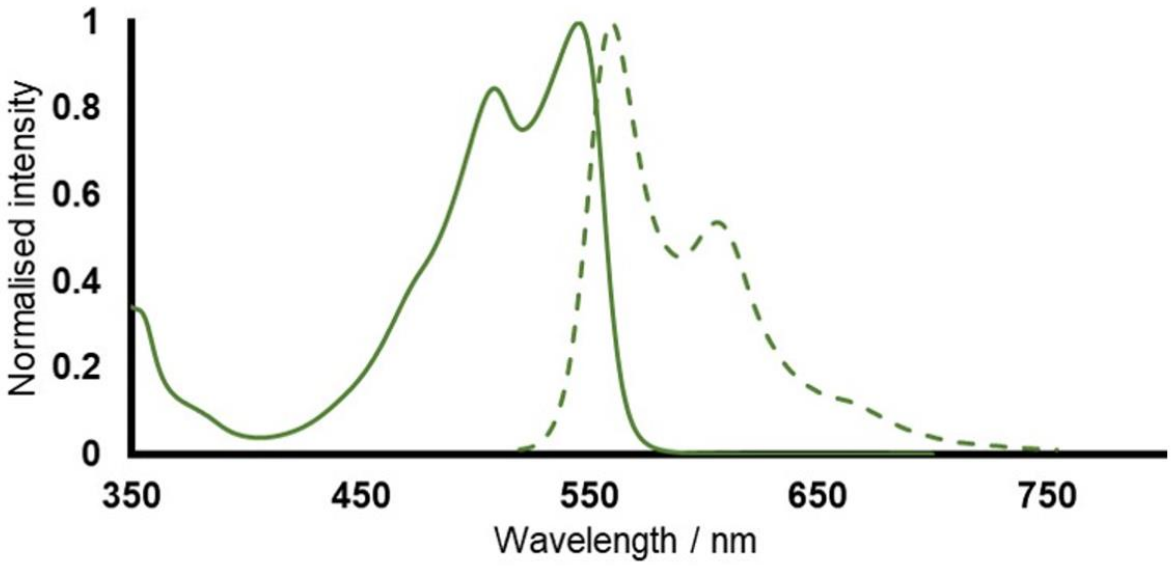


Figure A2.22: Normalised absorption and fluorescence emission spectra of TBDPP in dichloromethane.

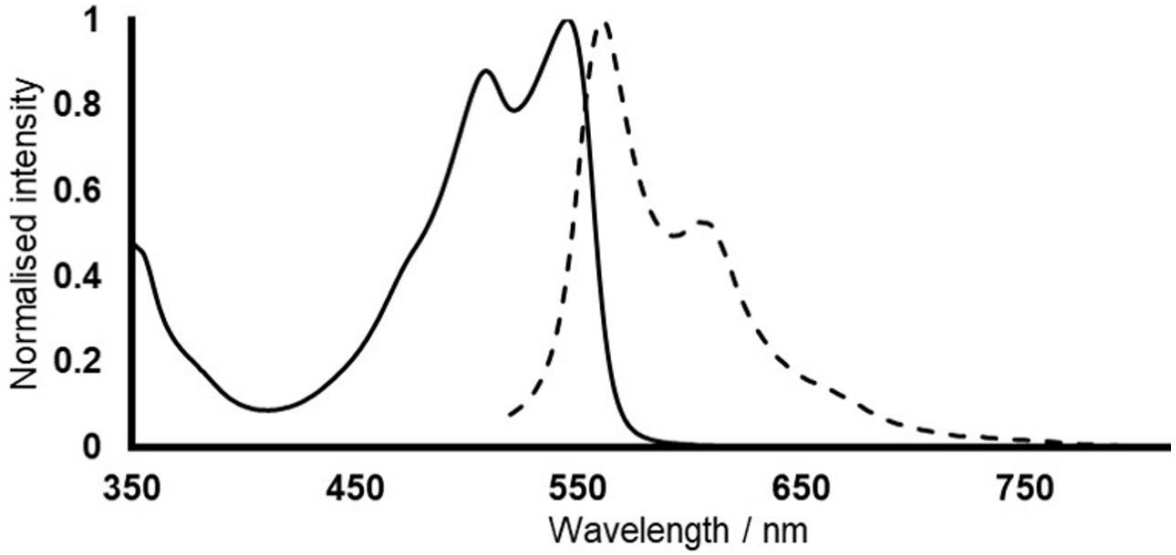


Figure A2.23: Normalised absorption and fluorescence emission spectra of TNDPP in dichloromethane.

Appendix B

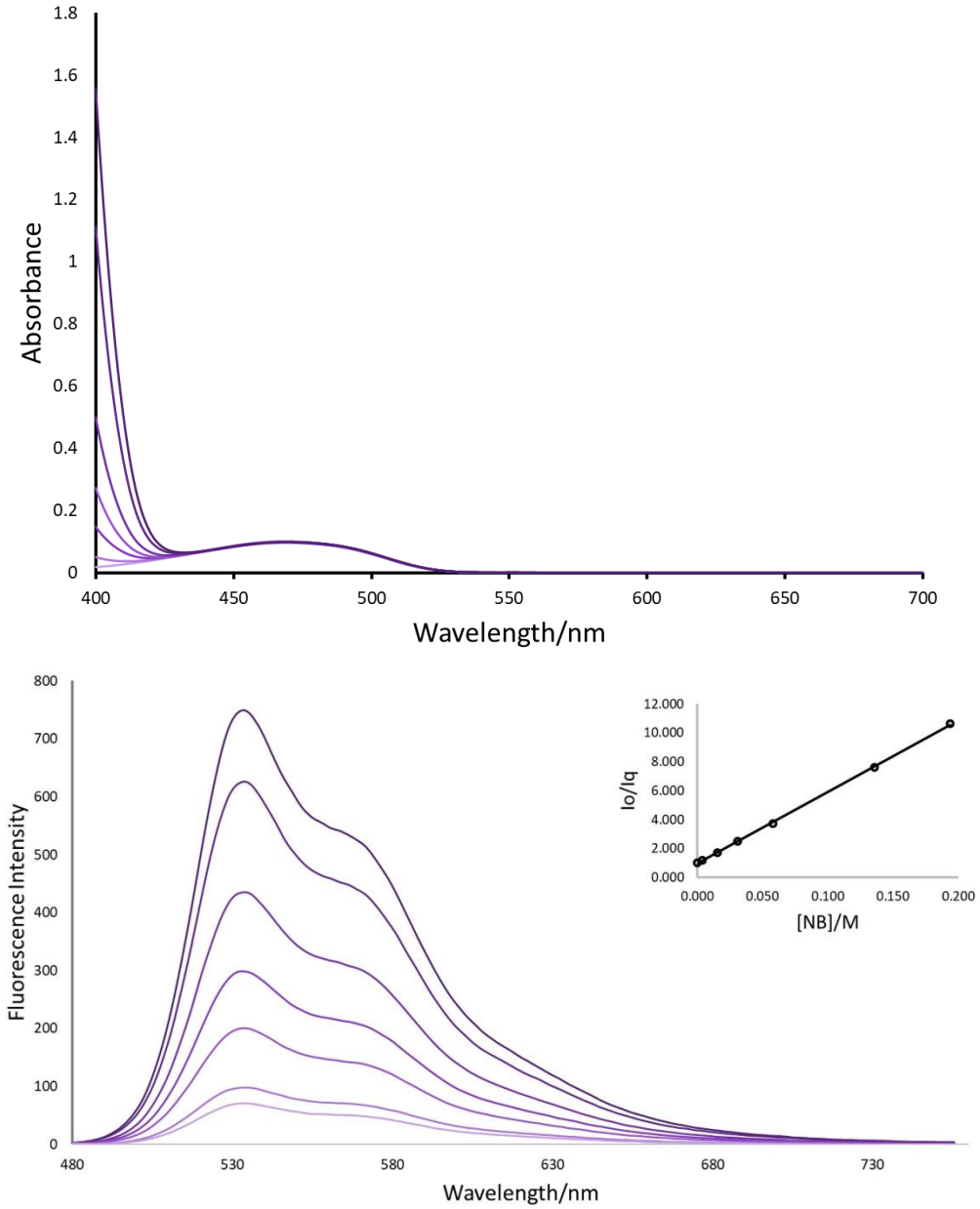


Figure B1.1: Top: Absorption spectra of ClBDPP in acetonitrile with nitrobenzene. Bottom: Fluorescence emission spectra of ClBDPP in acetonitrile with increasing concentration of nitrobenzene.

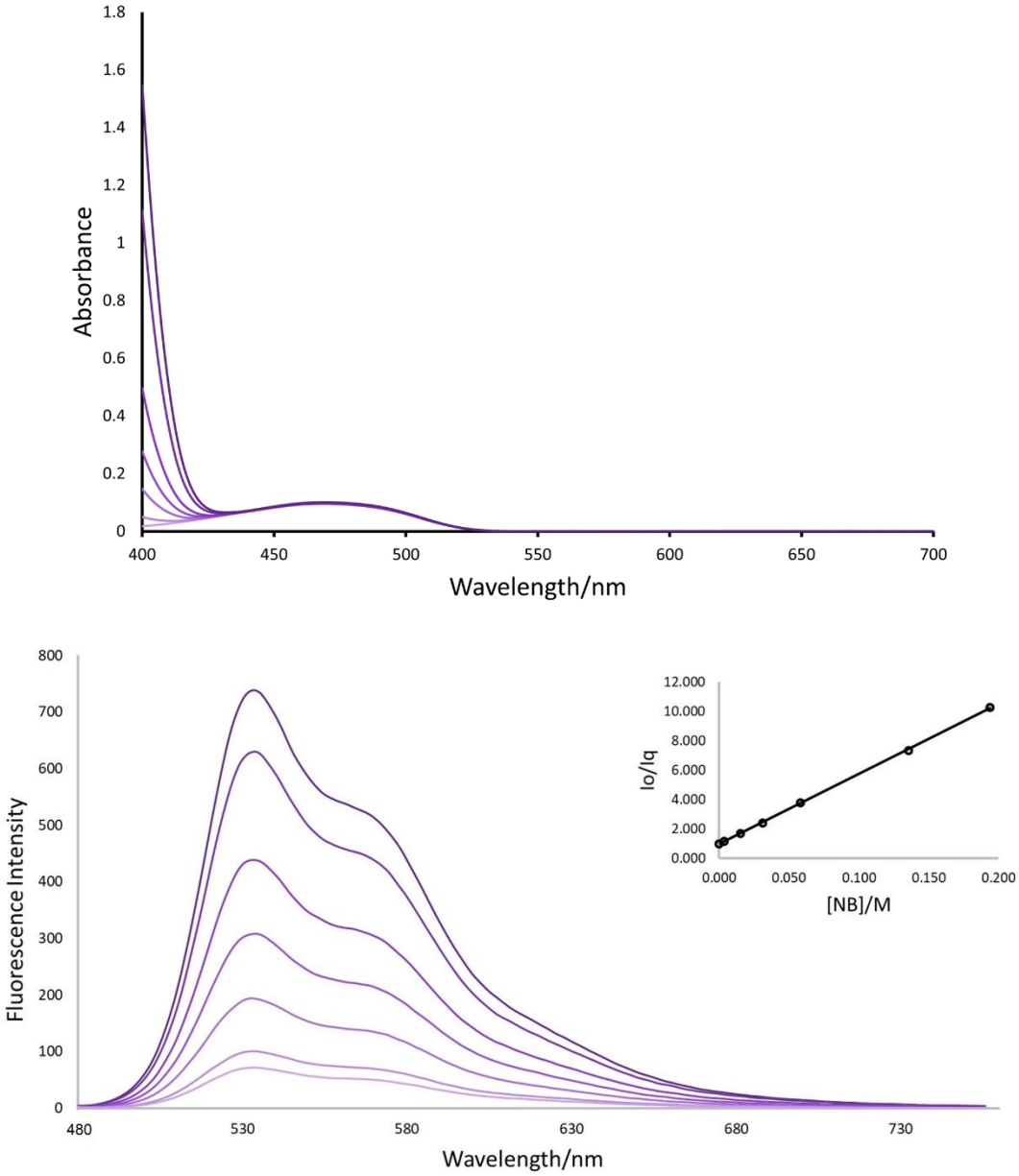


Figure B1.2: Top: Duplicate absorption spectra of ClBDPP in acetonitrile with nitrobenzene. Bottom: Duplicate fluorescence emission spectra of ClBDPP in acetonitrile with increasing concentration of nitrobenzene.

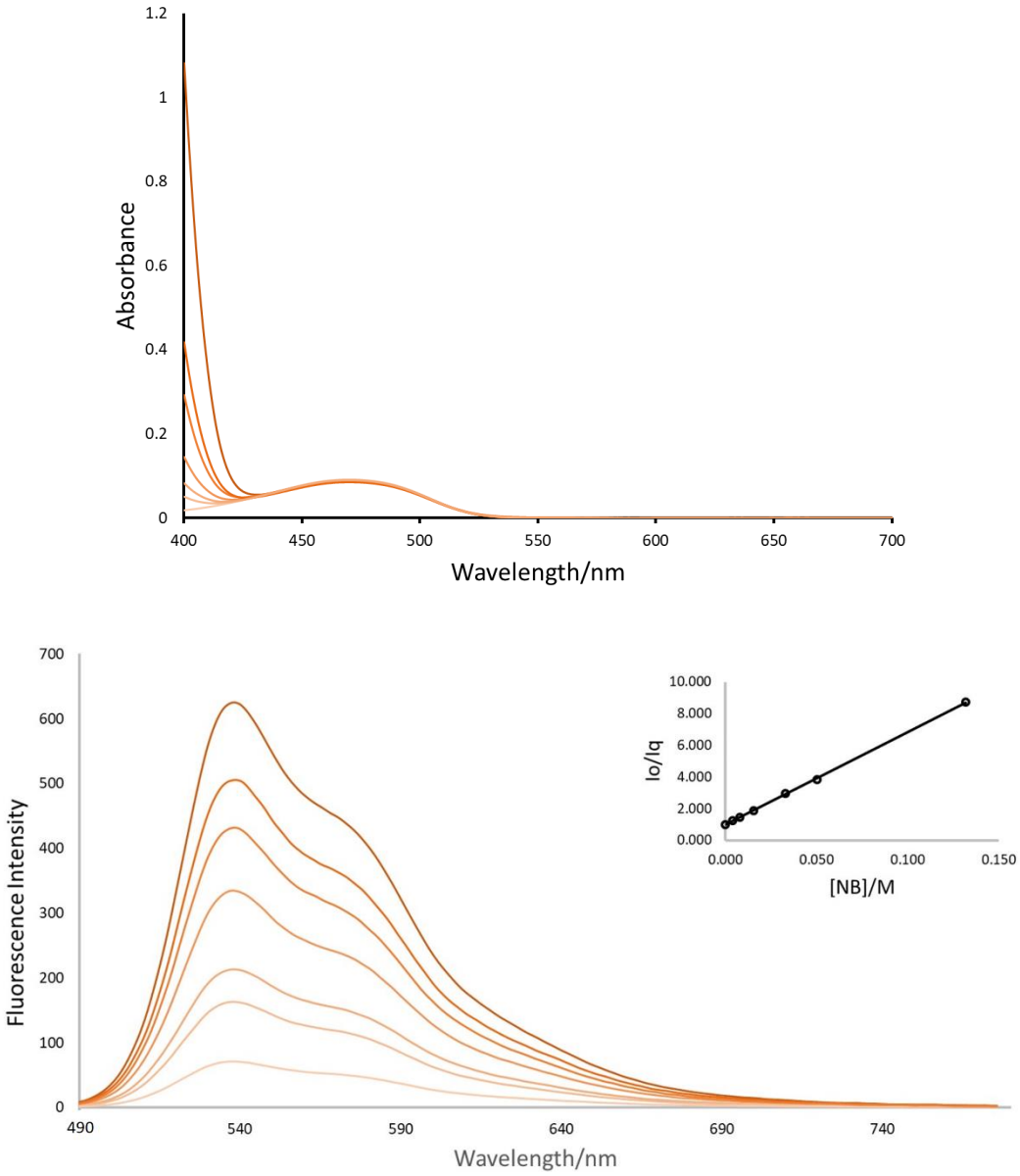


Figure B1.3: Top: Absorption spectra of ClN6DPP in acetonitrile with nitrobenzene. Bottom: Fluorescence emission spectra of ClN6DPP in acetonitrile with increasing concentration of nitrobenzene.

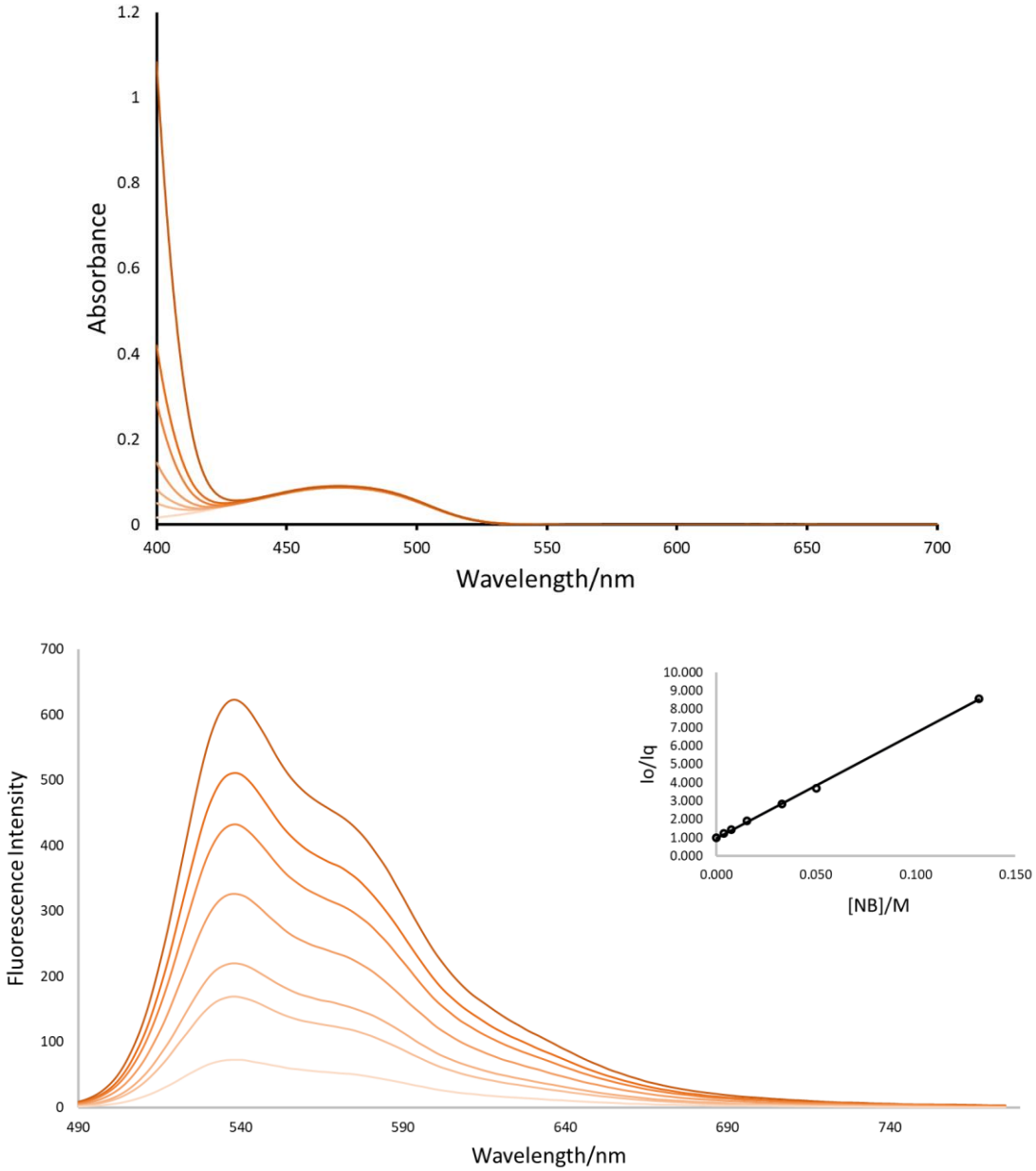


Figure B1.4: Top: Duplicate absorption spectra of ClN6DPP in acetonitrile with nitrobenzene. Bottom: Duplicate fluorescence emission spectra of ClN6DPP in acetonitrile with increasing concentration of nitrobenzene.

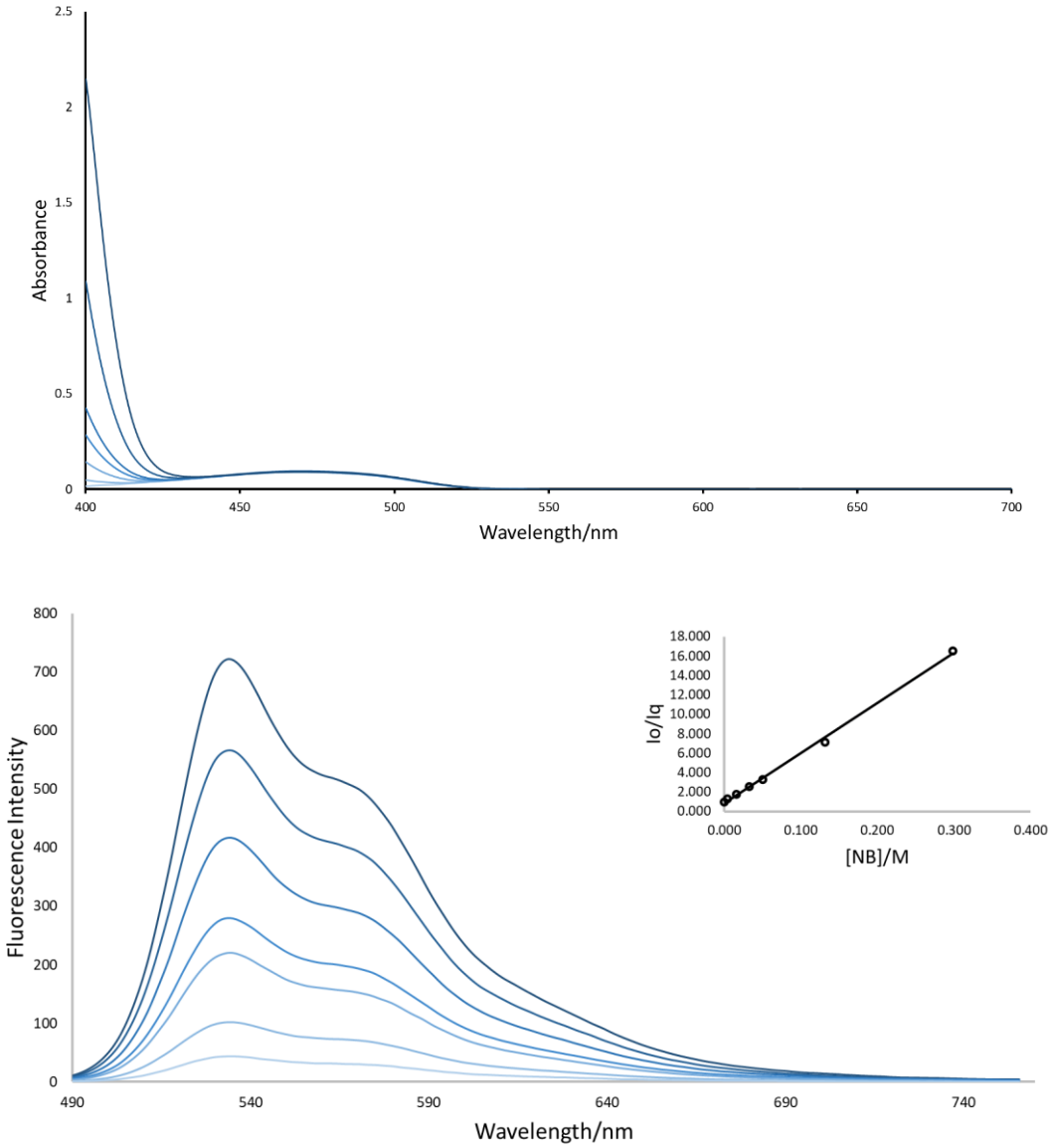


Figure B1.5: Top: Absorption spectra of ClNDPP in acetonitrile with nitrobenzene. Bottom: Fluorescence emission spectra of ClNDPP in acetonitrile with increasing concentration of nitrobenzene.

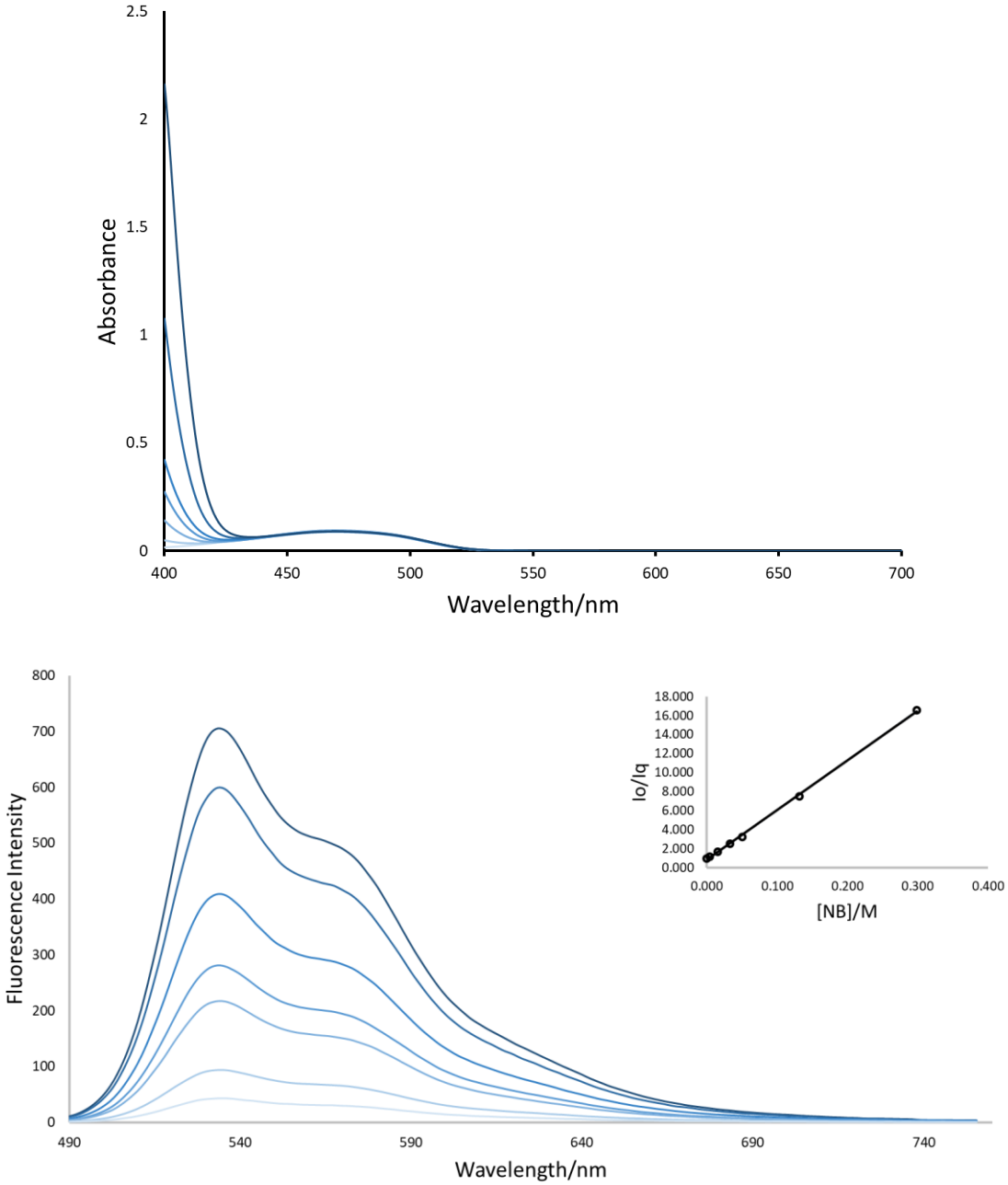


Figure B1.6: Top: Duplicate absorption spectra of ClNDPP in acetonitrile with nitrobenzene. Bottom: Duplicate fluorescence emission spectra of ClNDPP in acetonitrile with increasing concentration of nitrobenzene.

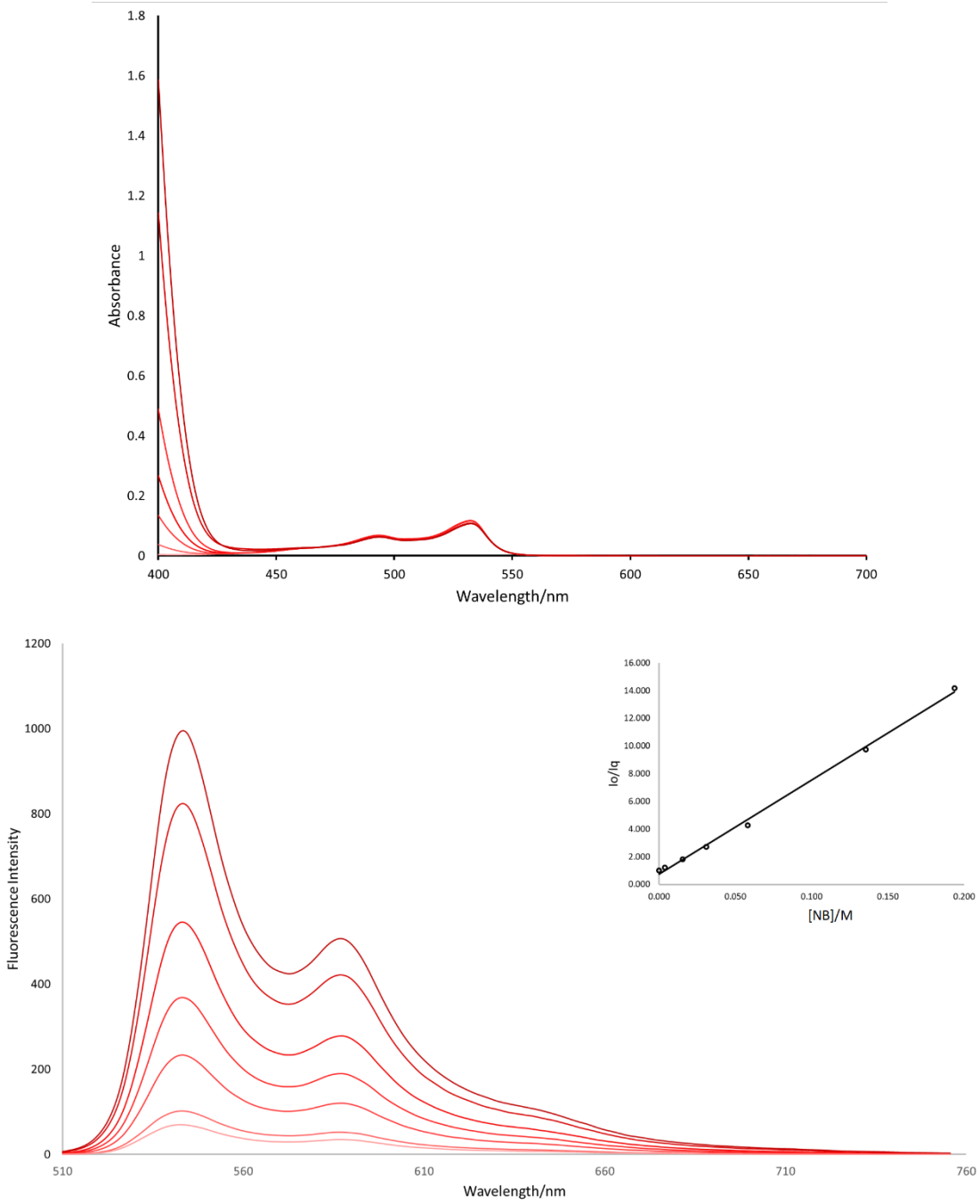


Figure B1.7: Top: Absorption spectra of FBDPP in acetonitrile with nitrobenzene. Bottom: Fluorescence emission spectra of FBDPP in acetonitrile with increasing concentration of nitrobenzene.

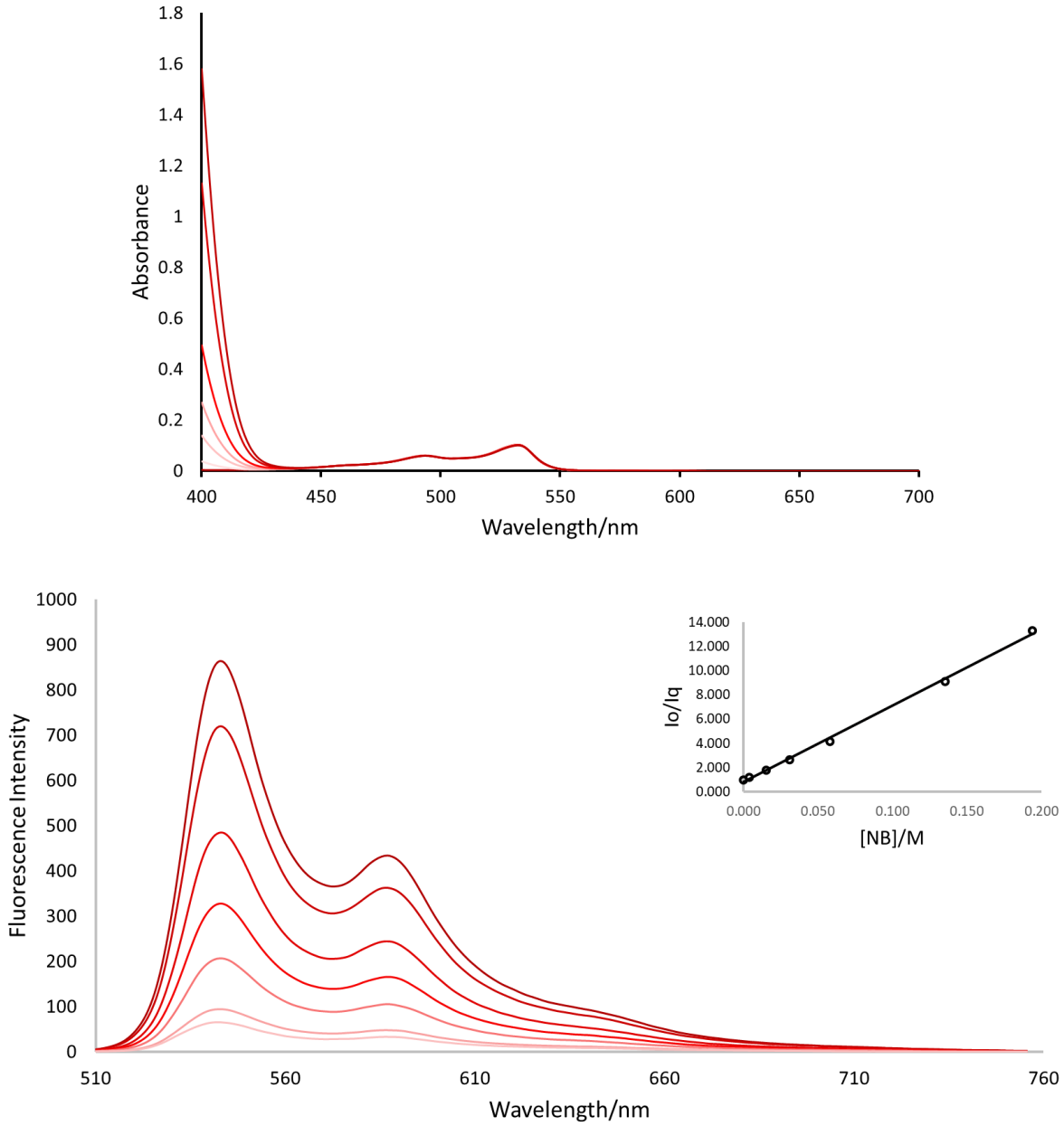


Figure B1.8: Top: Duplicate absorption spectra of FBDPP in acetonitrile with nitrobenzene. Bottom: Duplicate fluorescence emission spectra of FBDPP in acetonitrile with increasing concentration of nitrobenzene.

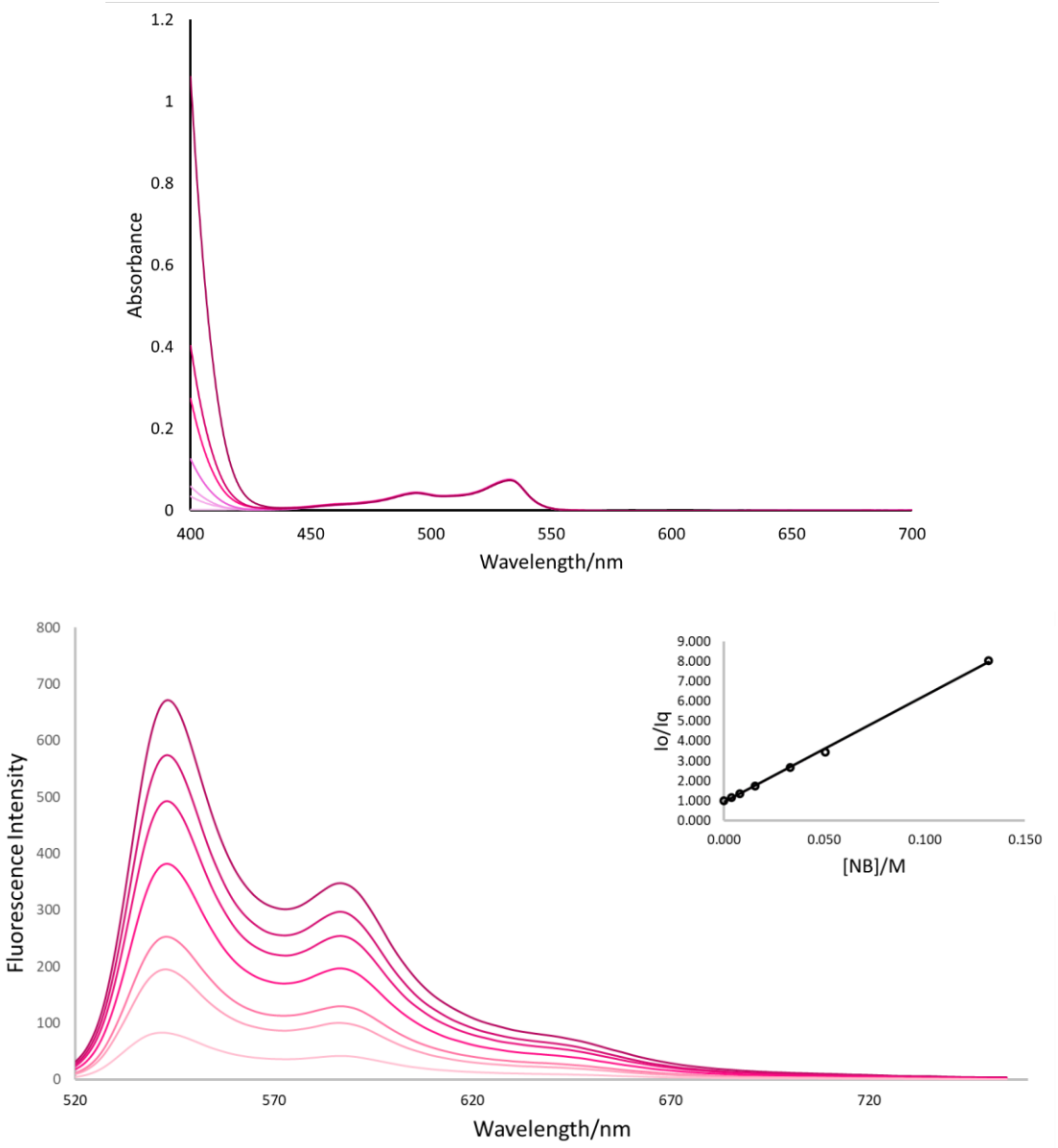


Figure B1.9: Top: Absorption spectra of FNDPP in acetonitrile with nitrobenzene. Bottom: Fluorescence emission spectra of FNDPP in acetonitrile with increasing concentration of nitrobenzene.

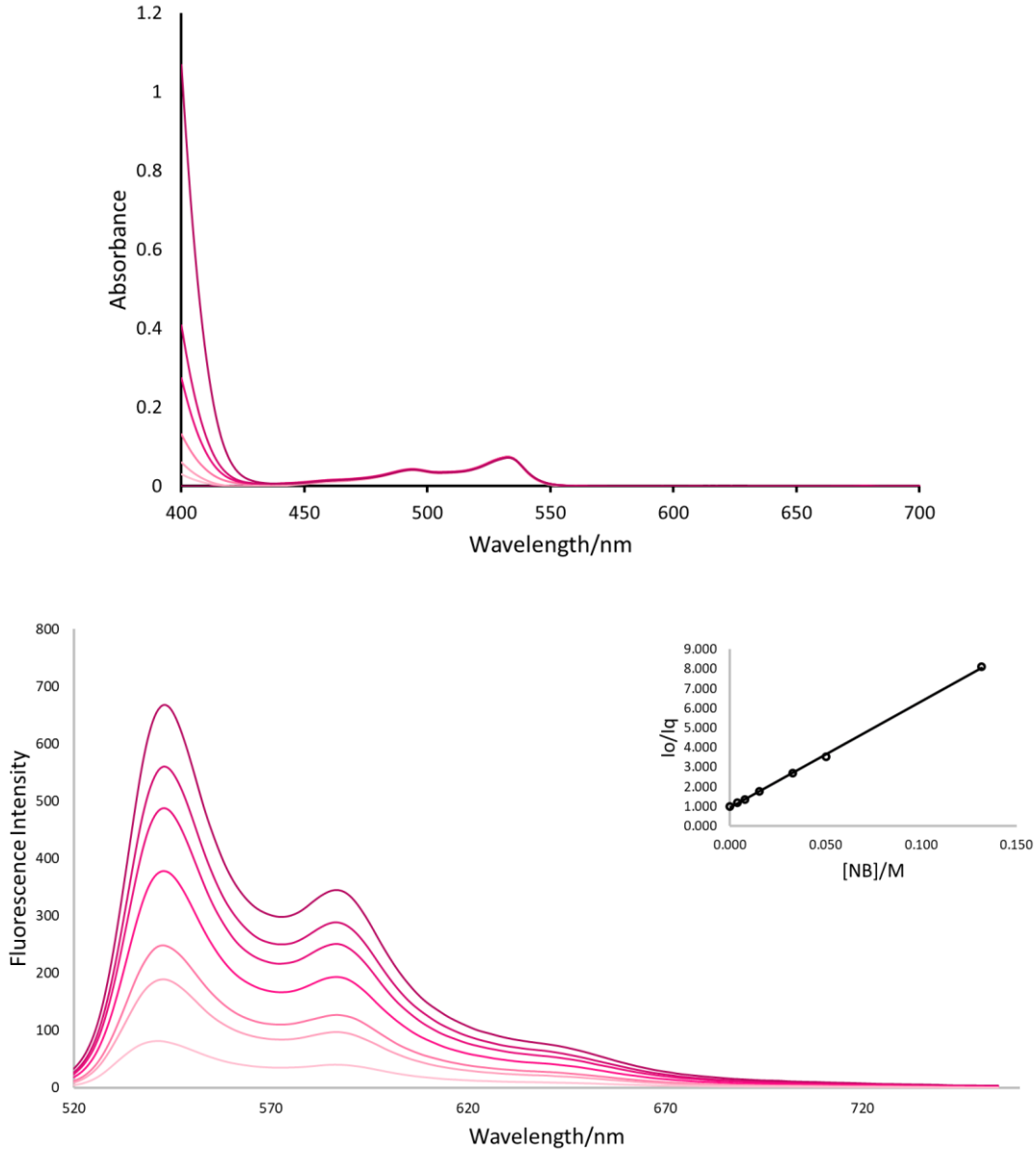


Figure B1.10: Top: Duplicate absorption spectra of FNDPP in acetonitrile with nitrobenzene. Bottom: Duplicate fluorescence emission spectra of FNDPP in acetonitrile with increasing concentration of nitrobenzene.

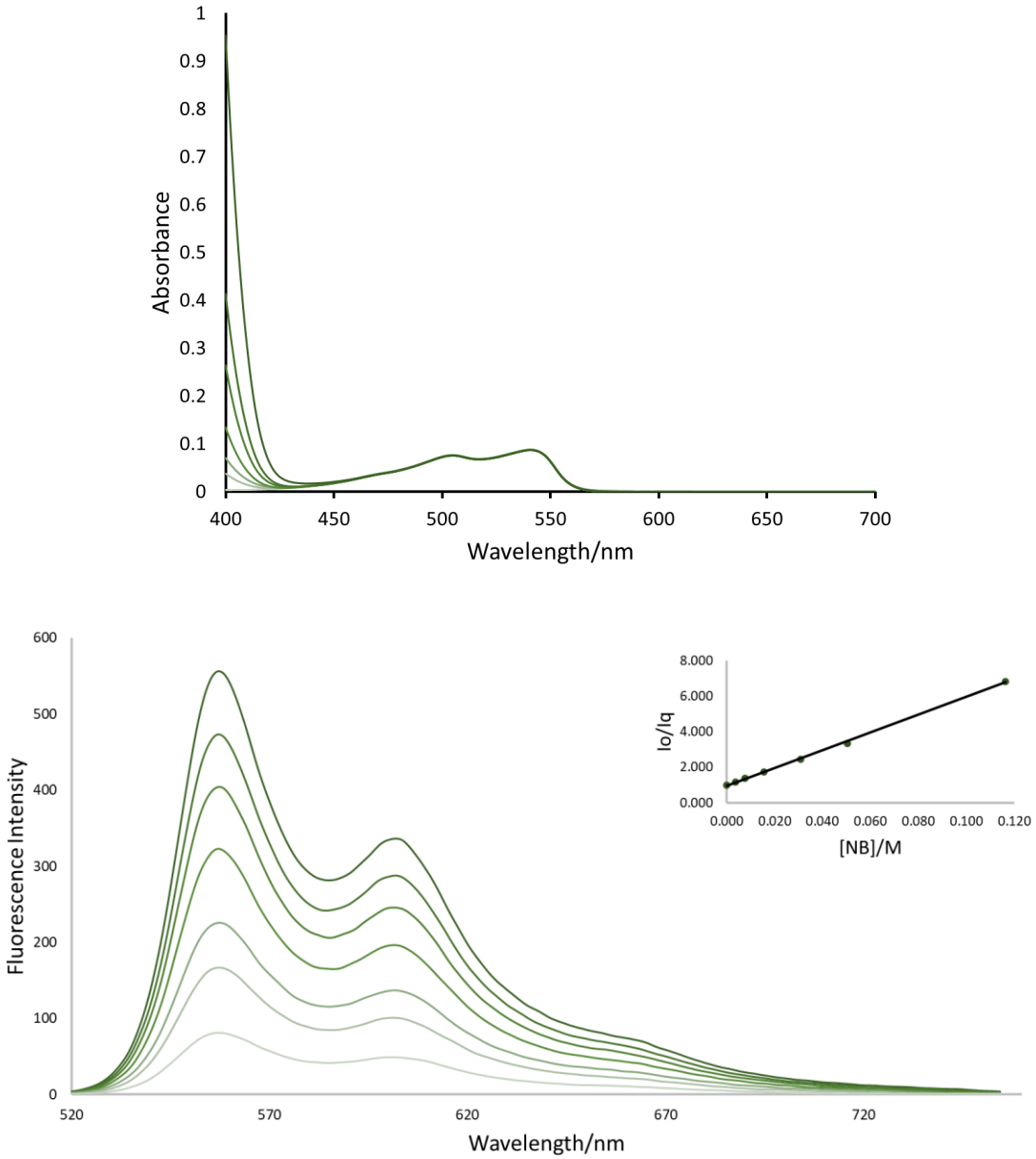


Figure B1.11: Top: Absorption spectra of TBDPP in acetonitrile with nitrobenzene. Bottom: Fluorescence emission spectra of TBDPP in acetonitrile with increasing concentration of nitrobenzene.

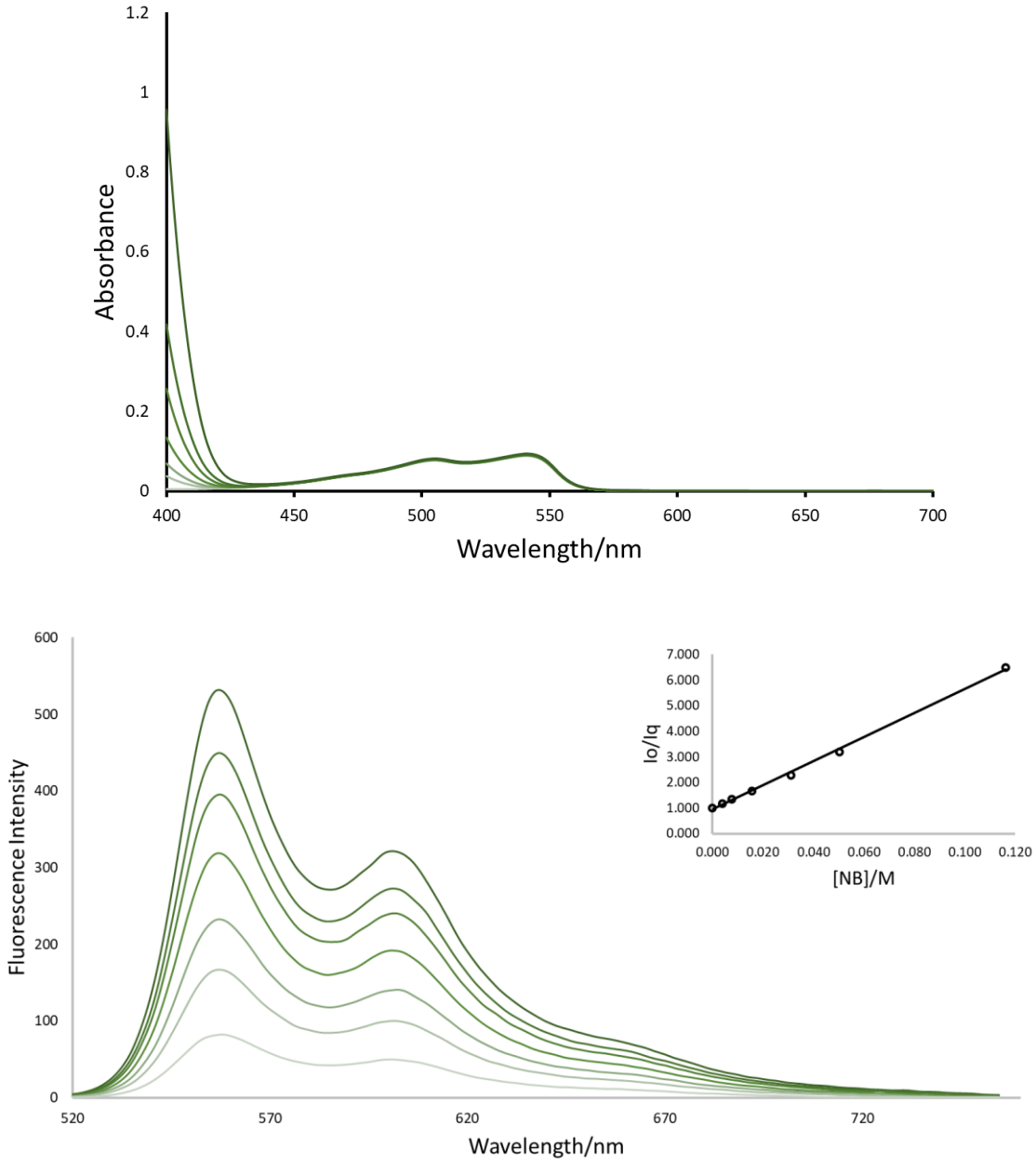


Figure B1.12: Top: Duplicate absorption spectra of TBDPP in acetonitrile with nitrobenzene. Bottom: Duplicate fluorescence emission spectra of TBDPP in acetonitrile with increasing concentration of nitrobenzene.

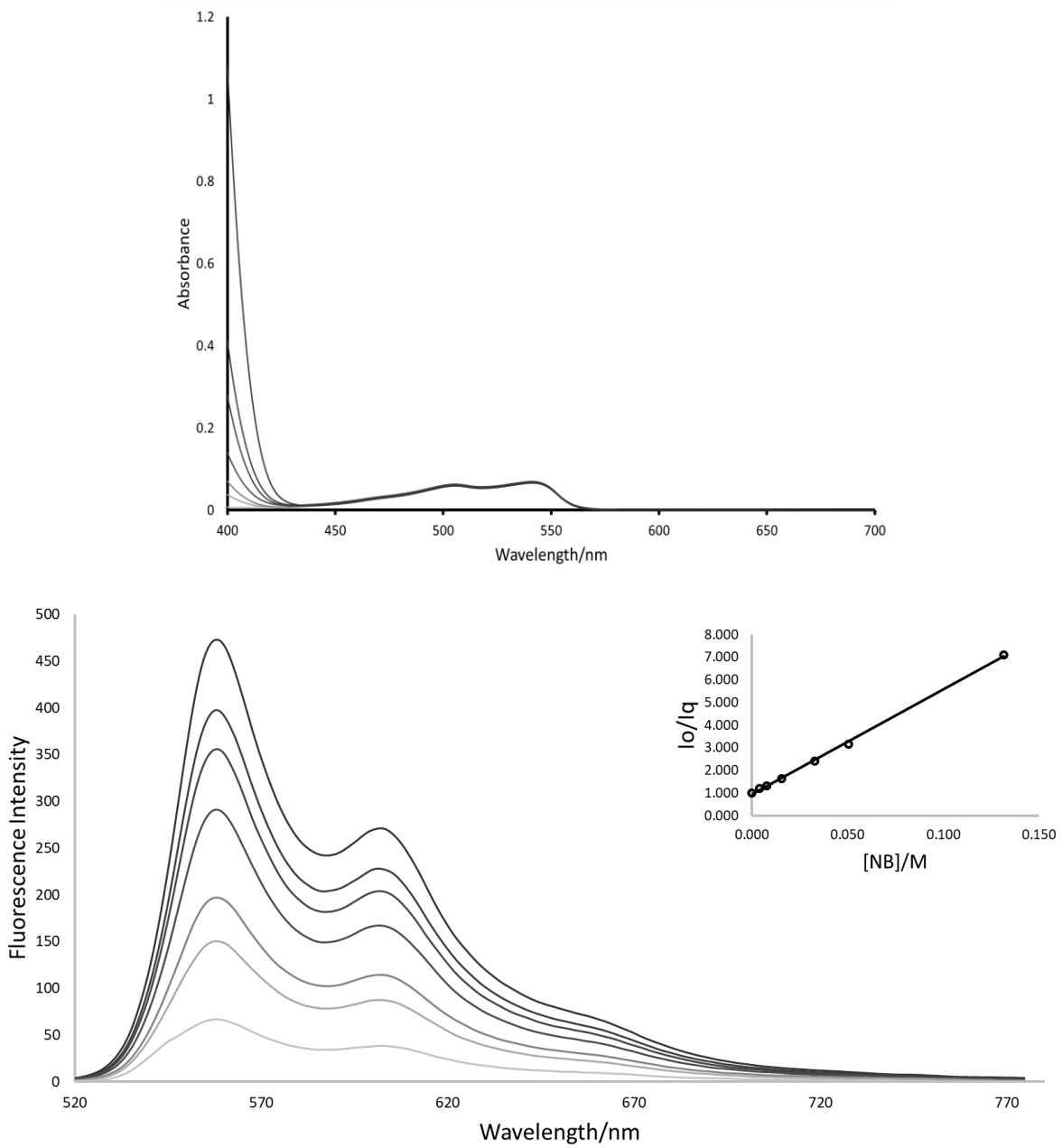


Figure B1.13: Top: Absorption spectra of TNDPP in acetonitrile with nitrobenzene. Bottom: Fluorescence emission spectra of TNDPP in acetonitrile with increasing concentration of nitrobenzene.

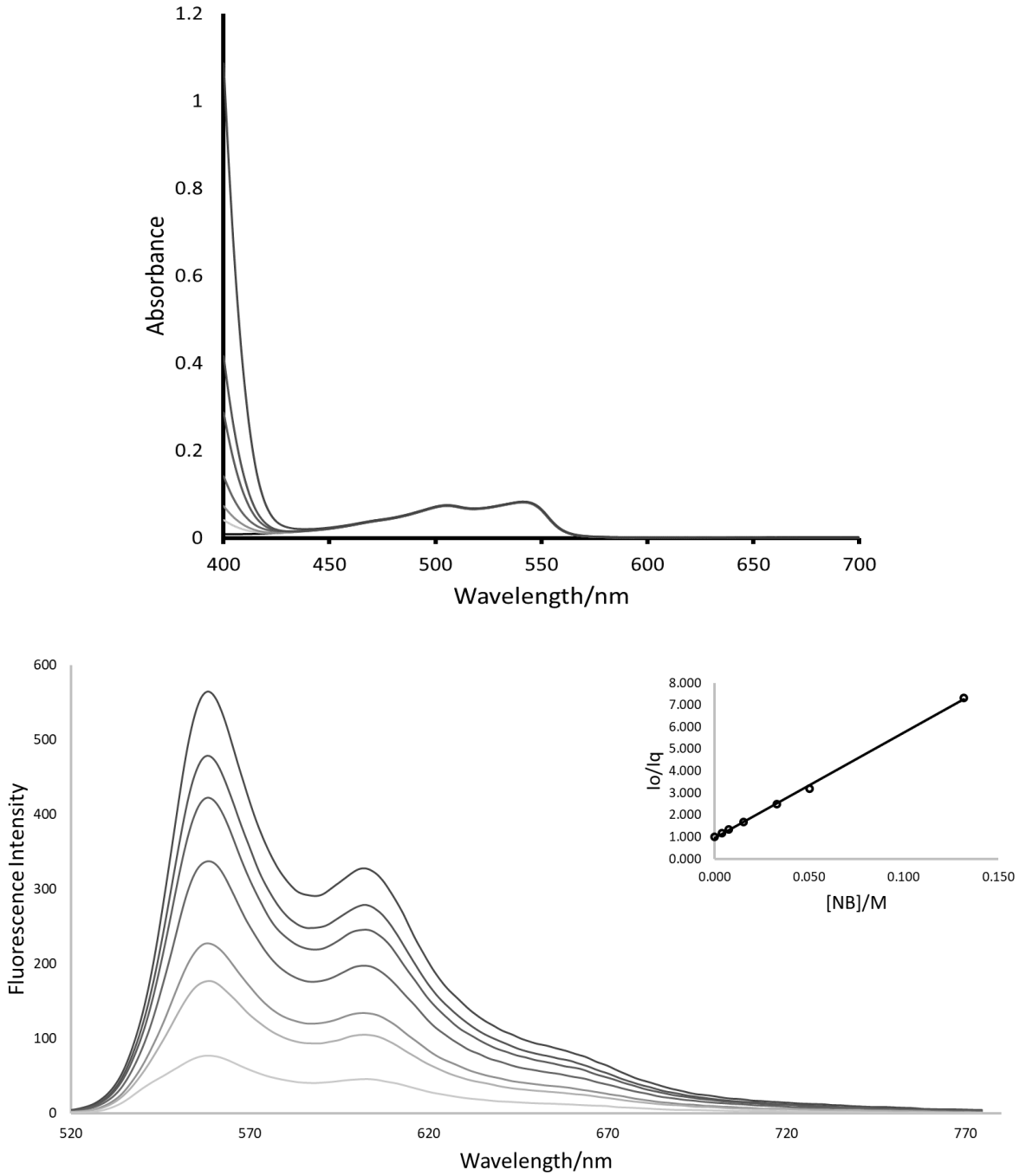


Figure B1.14: Top: Duplicate absorption spectra of TNDPP in acetonitrile with nitrobenzene. Bottom: Duplicate fluorescence emission spectra of TNDPP in acetonitrile with increasing concentration of nitrobenzene.

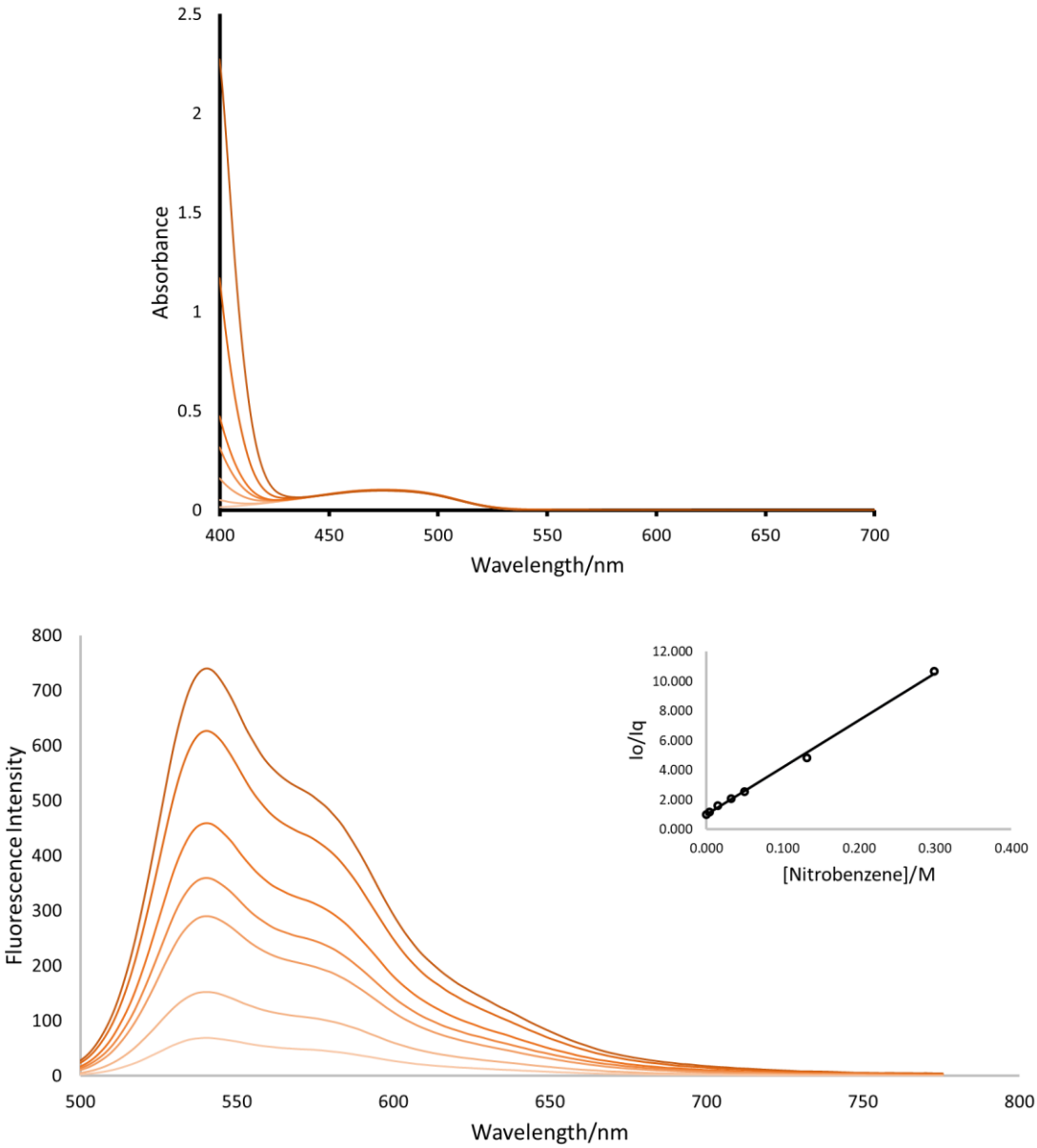


Figure B1.15: Top: Absorption spectra of ClN6DPP in dichloromethane with nitrobenzene. Bottom: Fluorescence emission spectra of ClN6DPP in dichloromethane with increasing concentration of nitrobenzene.

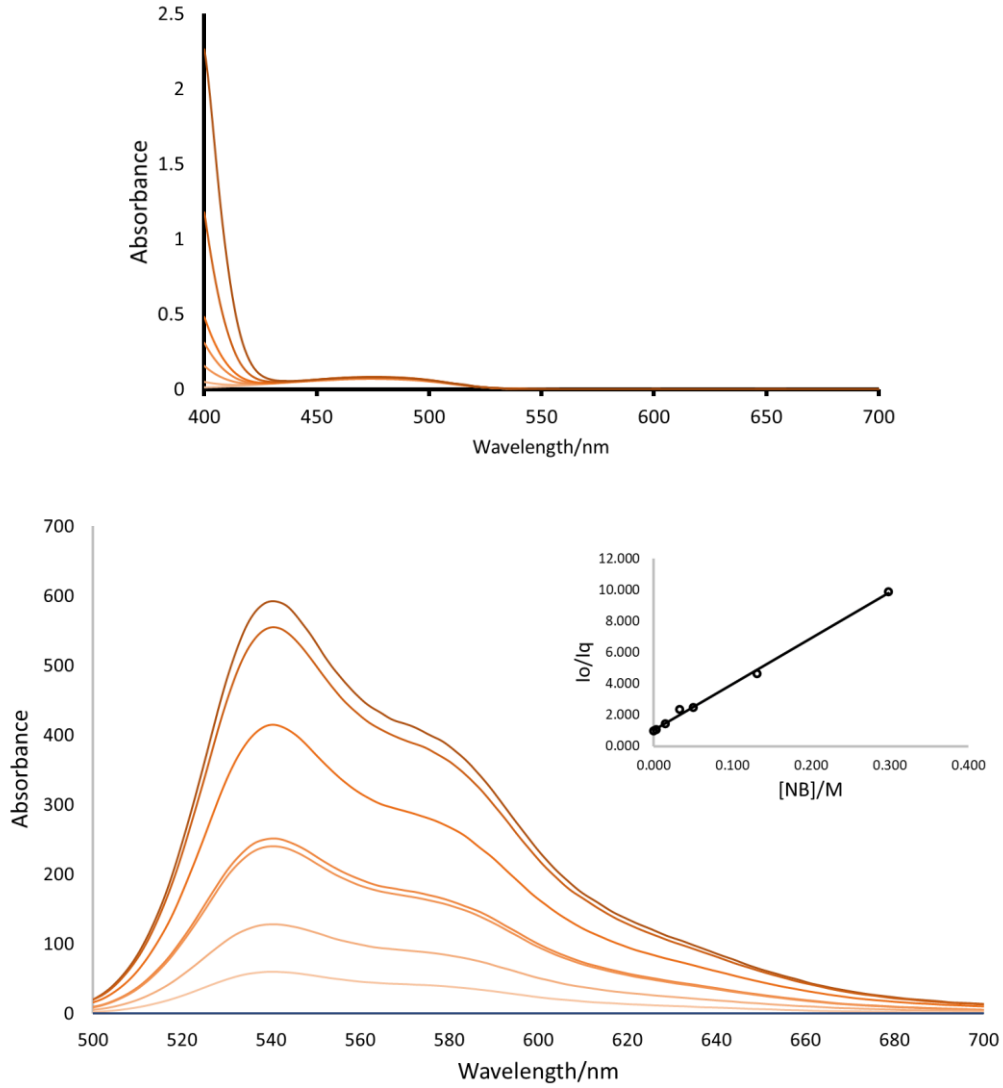


Figure B1.16: Top: Duplicate absorption spectra of ClN6DPP in dichloromethane with nitrobenzene. Bottom: Duplicate fluorescence emission spectra of ClN6DPP in dichloromethane with increasing concentration of nitrobenzene.

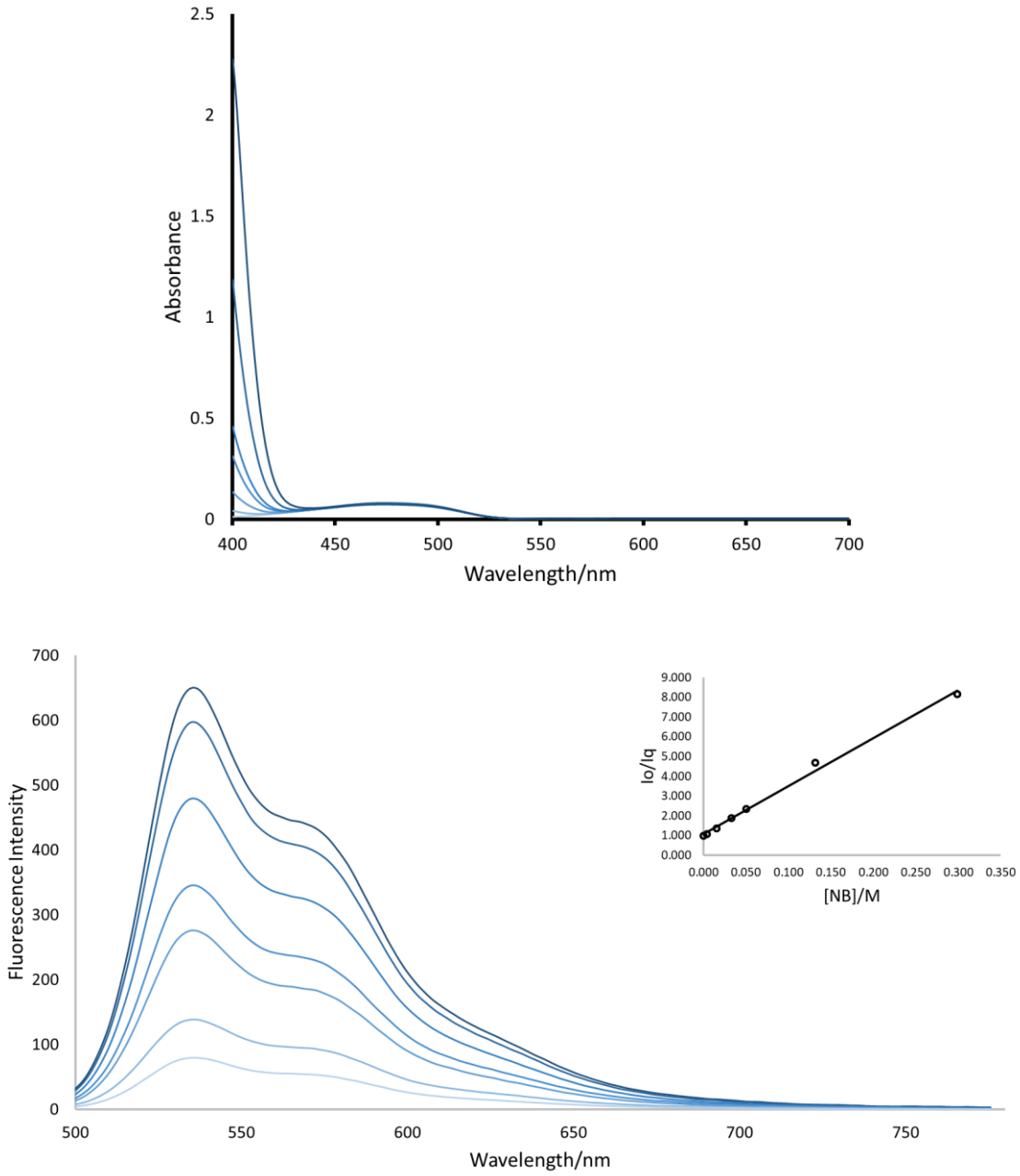


Figure B1.17: Top: Absorption spectra of ClNDPP in dichloromethane with nitrobenzene. Bottom: Fluorescence emission spectra of ClNDPP in dichloromethane with increasing concentration of nitrobenzene.

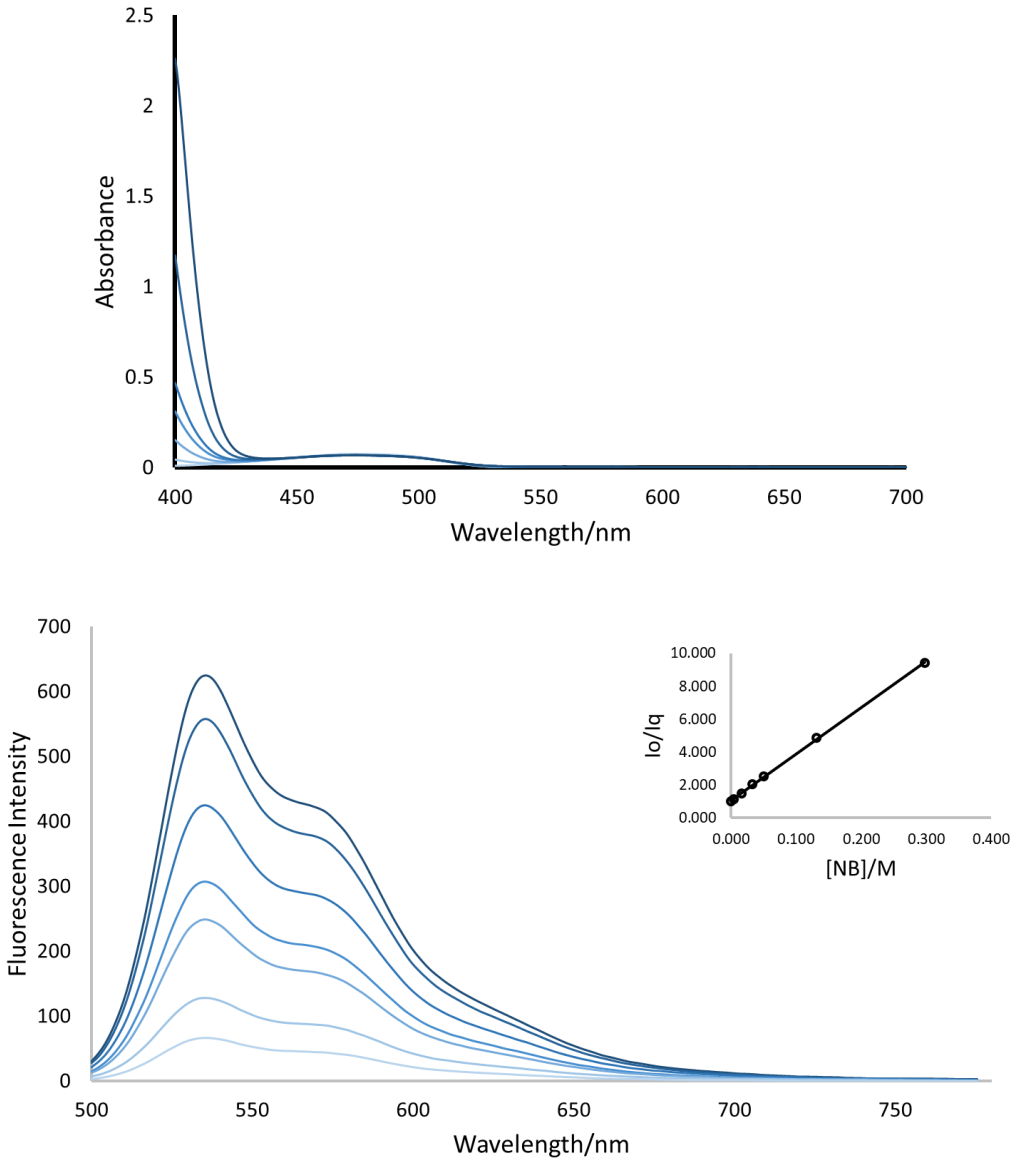


Figure B1.18: Top: Duplicate absorption spectra of ClNDPP in dichloromethane with nitrobenzene. Bottom: Duplicate fluorescence emission spectra of ClNDPP in dichloromethane with increasing concentration of nitrobenzene.

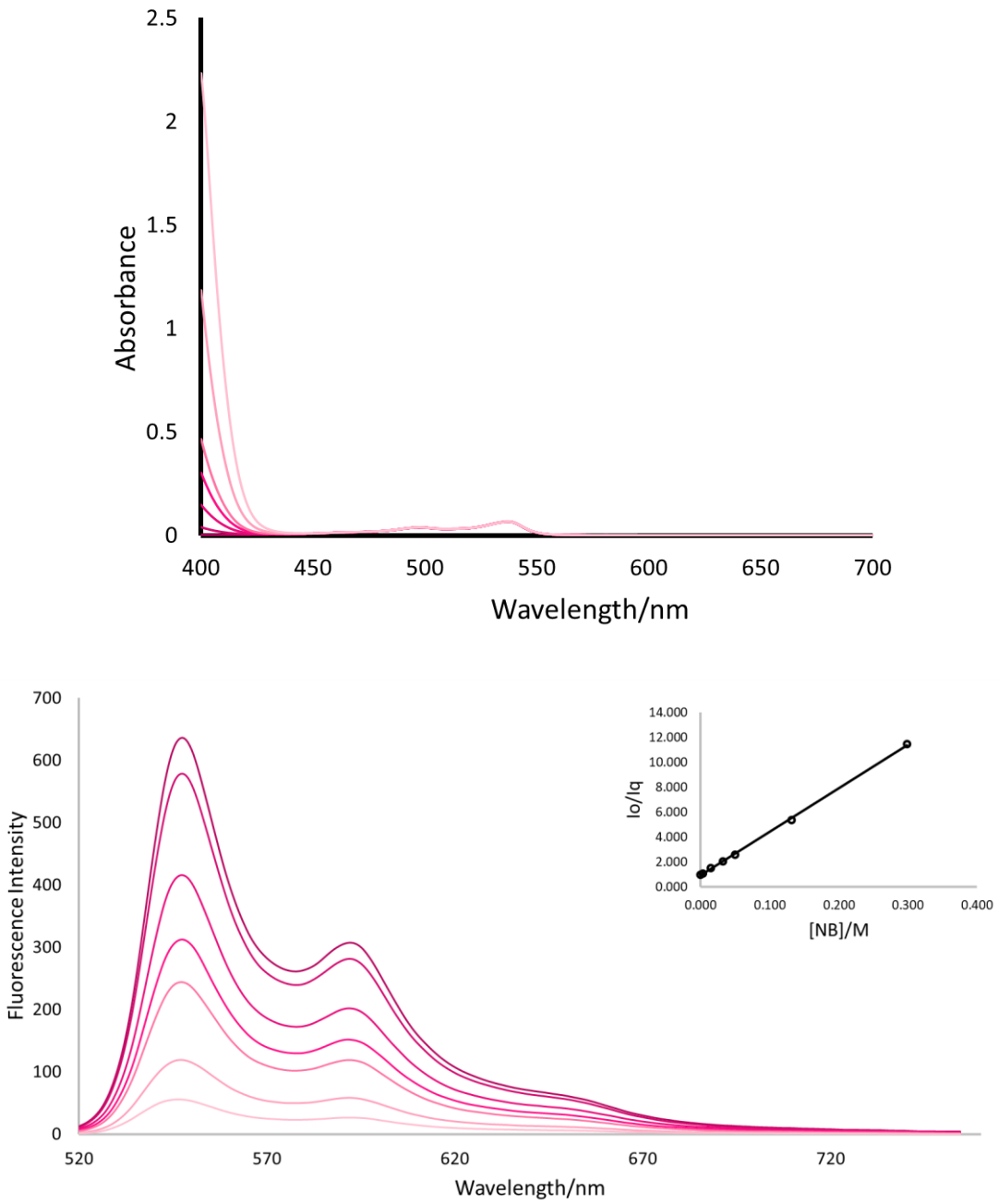


Figure B1.19: Top: Absorption spectra of FNDPP in dichloromethane with nitrobenzene. Bottom: Fluorescence emission spectra of FNDPP in dichloromethane with increasing concentration of nitrobenzene.

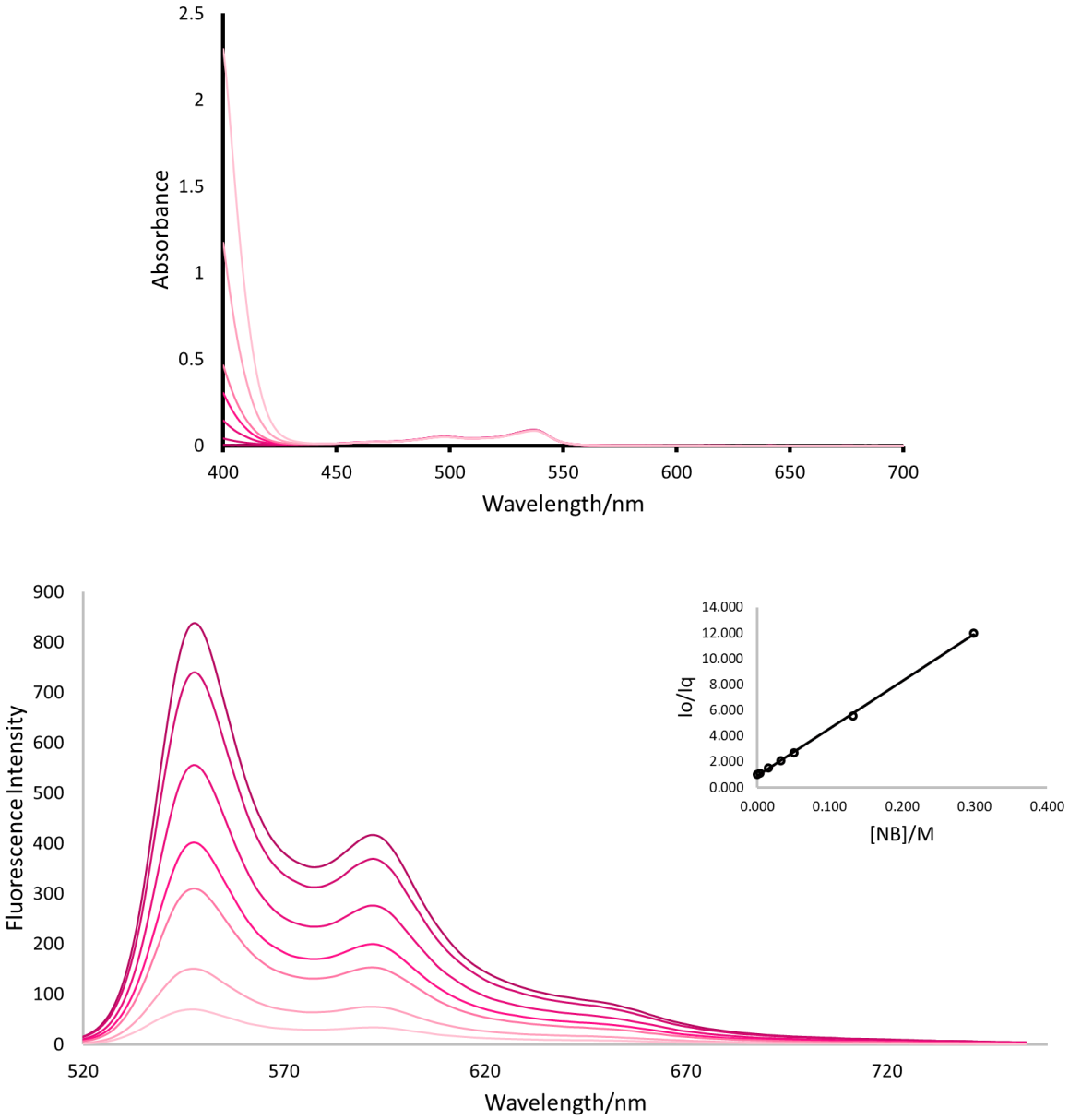


Figure B1.20: Top: Duplicate absorption spectra of FNDPP in dichloromethane with nitrobenzene. Bottom: Duplicate fluorescence emission spectra of FNDPP in dichloromethane with increasing concentration of nitrobenzene.

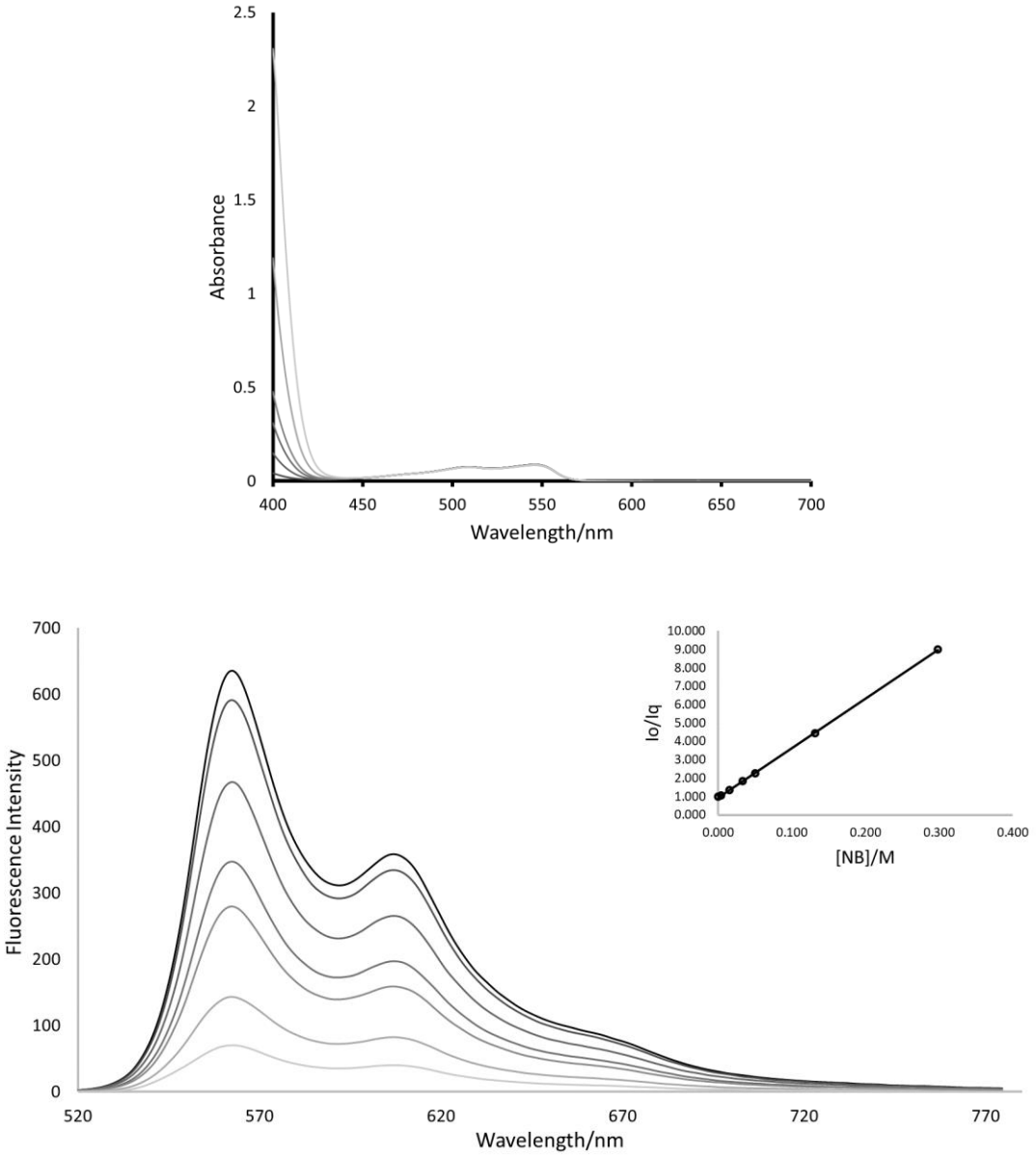


Figure B1.21: Top: Absorption spectra of TNDPP in dichloromethane with nitrobenzene. Bottom: Fluorescence emission spectra of TNDPP in dichloromethane with increasing concentration of nitrobenzene.

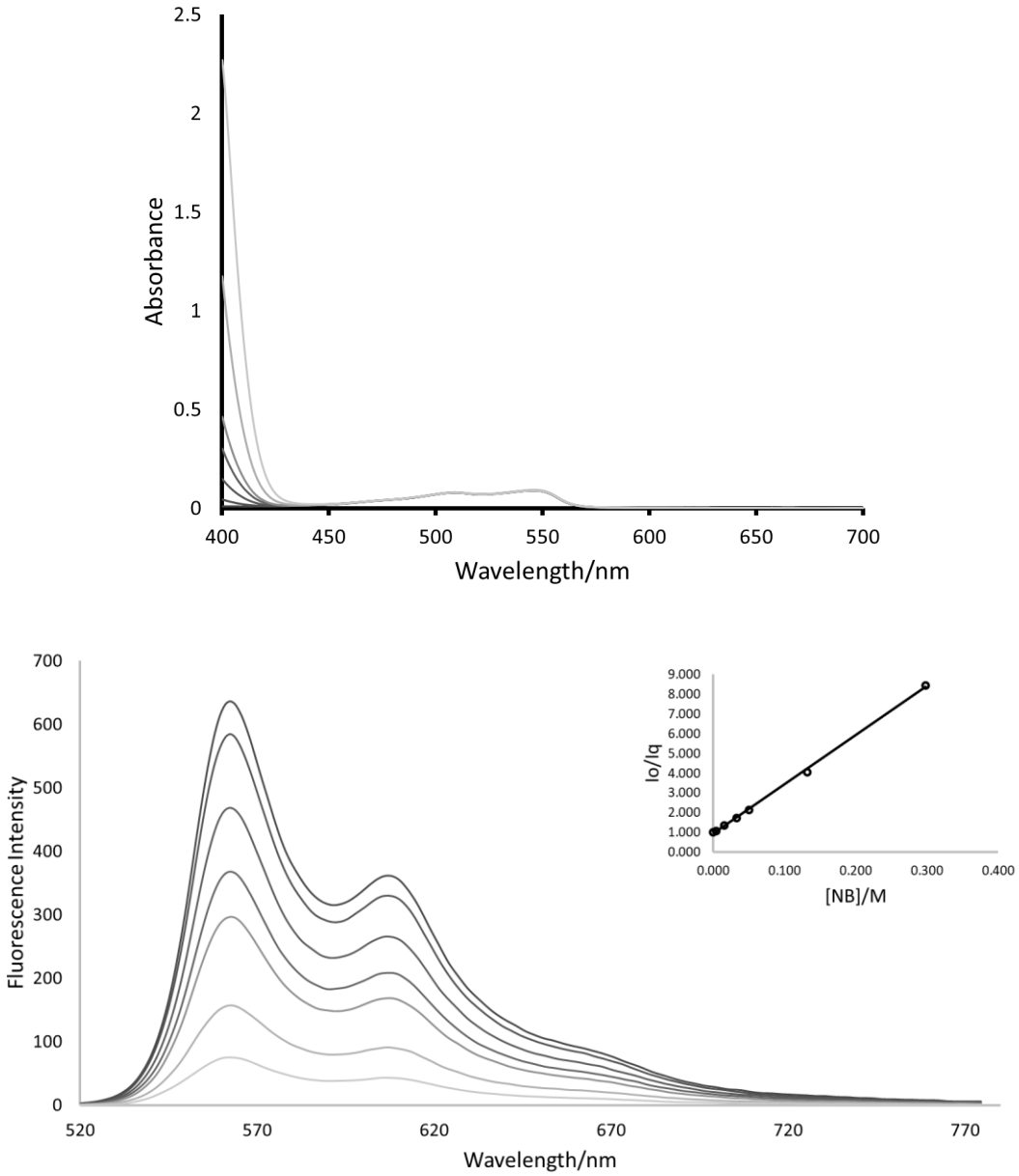


Figure B1.22: Top: Duplicate absorption spectra of TNDPP in dichloromethane with nitrobenzene. Bottom: Duplicate fluorescence emission spectra of TNDPP in dichloromethane with increasing concentration of nitrobenzene.

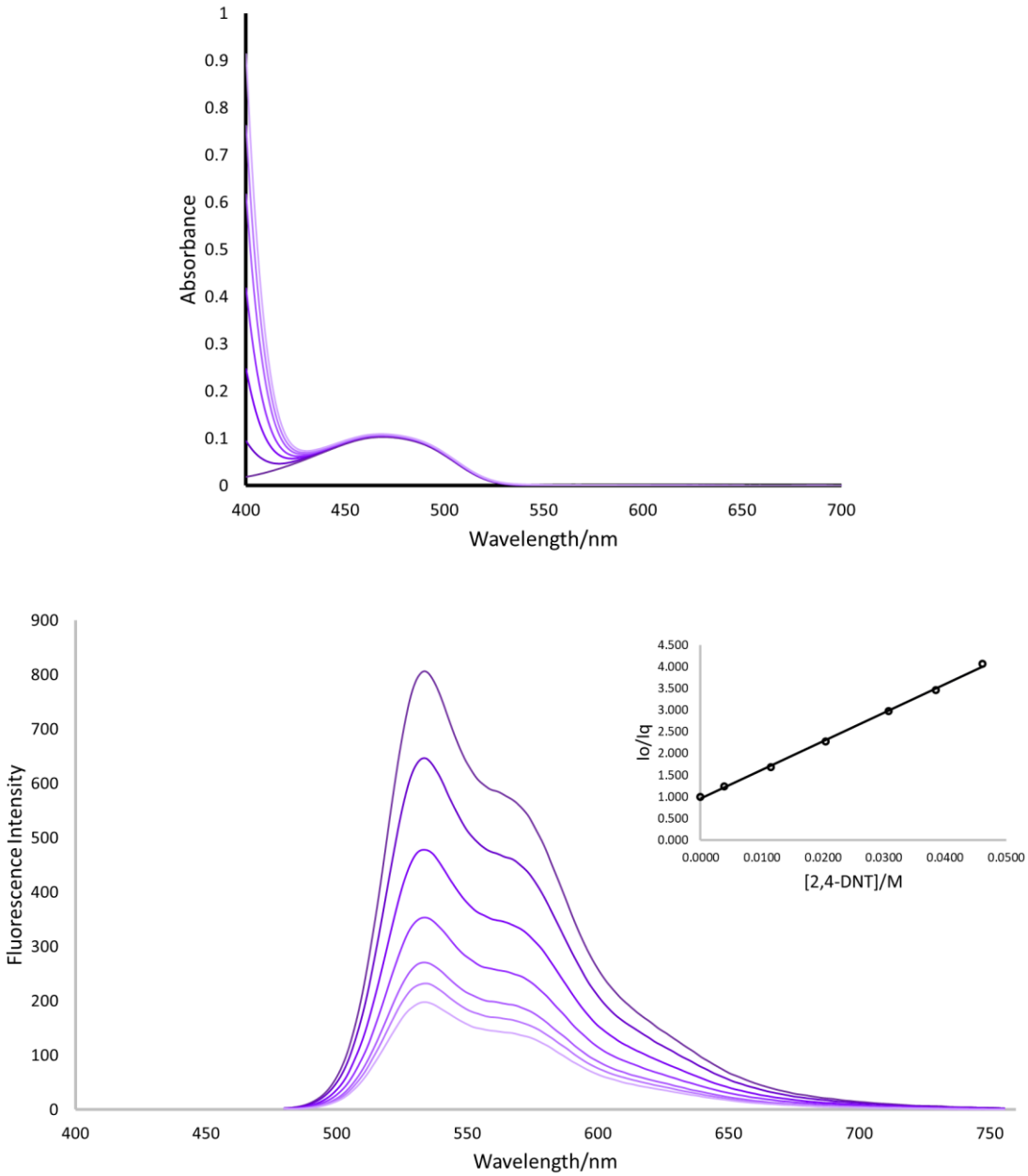


Figure B2.1: Top: Absorption spectra of ClBDPP in acetonitrile with 2,4-dinitrotoluene. Bottom: Fluorescence emission spectra of ClBDPP in acetonitrile with increasing concentration of 2,4-dinitrotoluene.

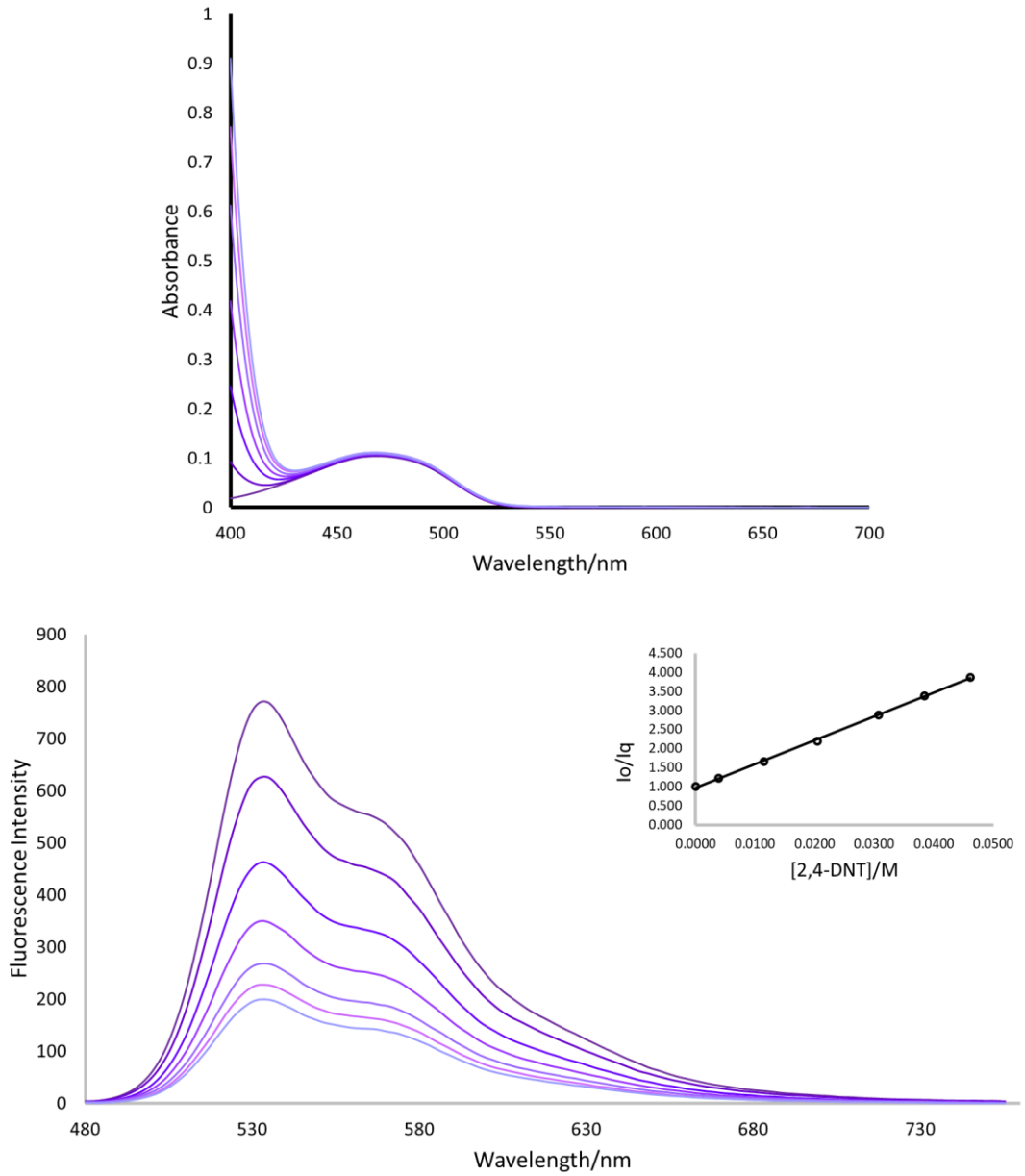


Figure B2.2: Top: Duplicate absorption spectra of ClBDPP in acetonitrile with 2,4-dinitrotoluene. Bottom: Duplicate fluorescence emission spectra of ClBDPP in acetonitrile with increasing concentration of 2,4-dinitrotoluene.

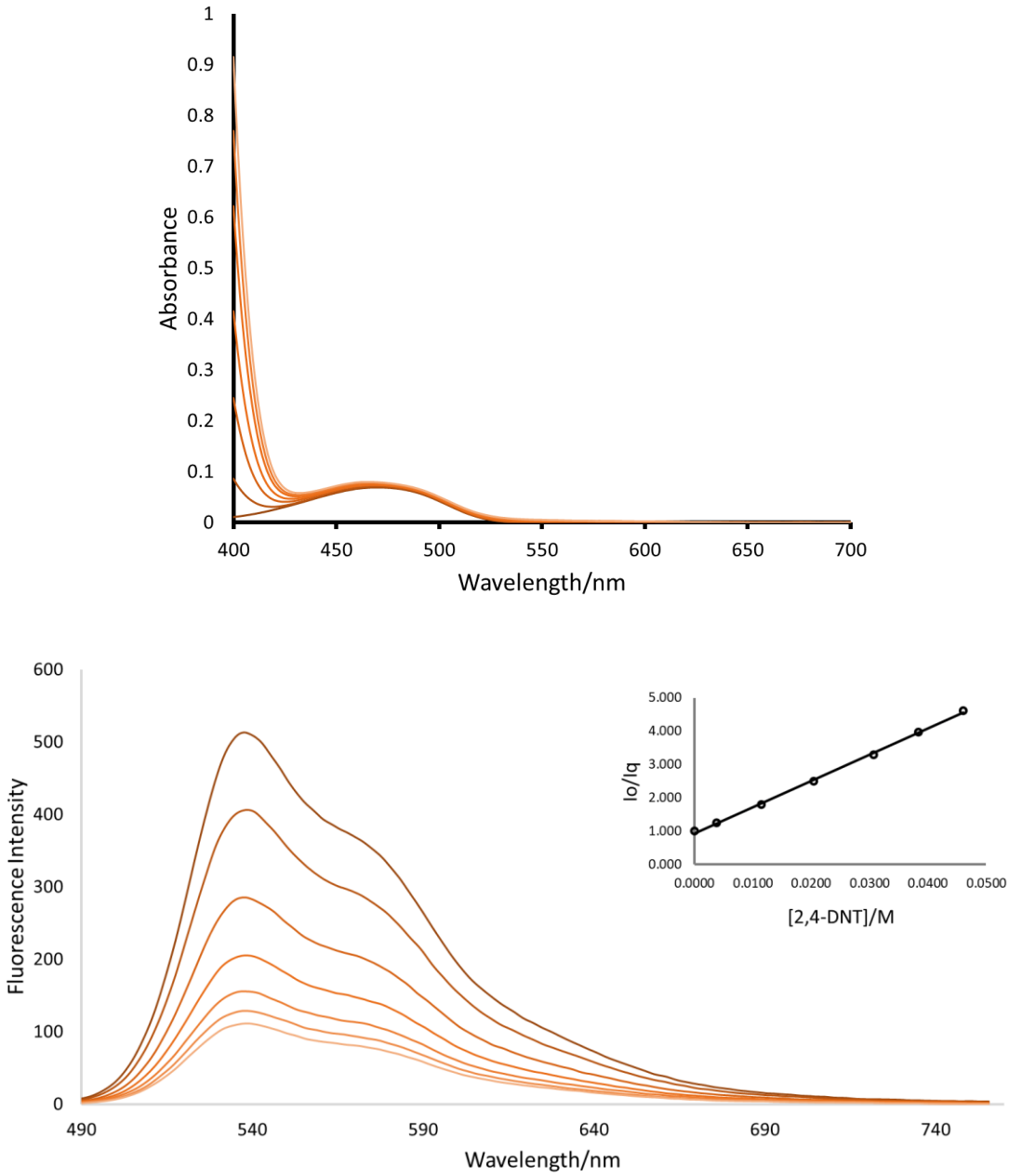


Figure B2.3: Top: Absorption spectra of ClN6DPP in acetonitrile with 2,4-dinitrotoluene. Bottom: Fluorescence emission spectra of ClN6DPP in acetonitrile with increasing concentration of 2,4-dinitrotoluene.

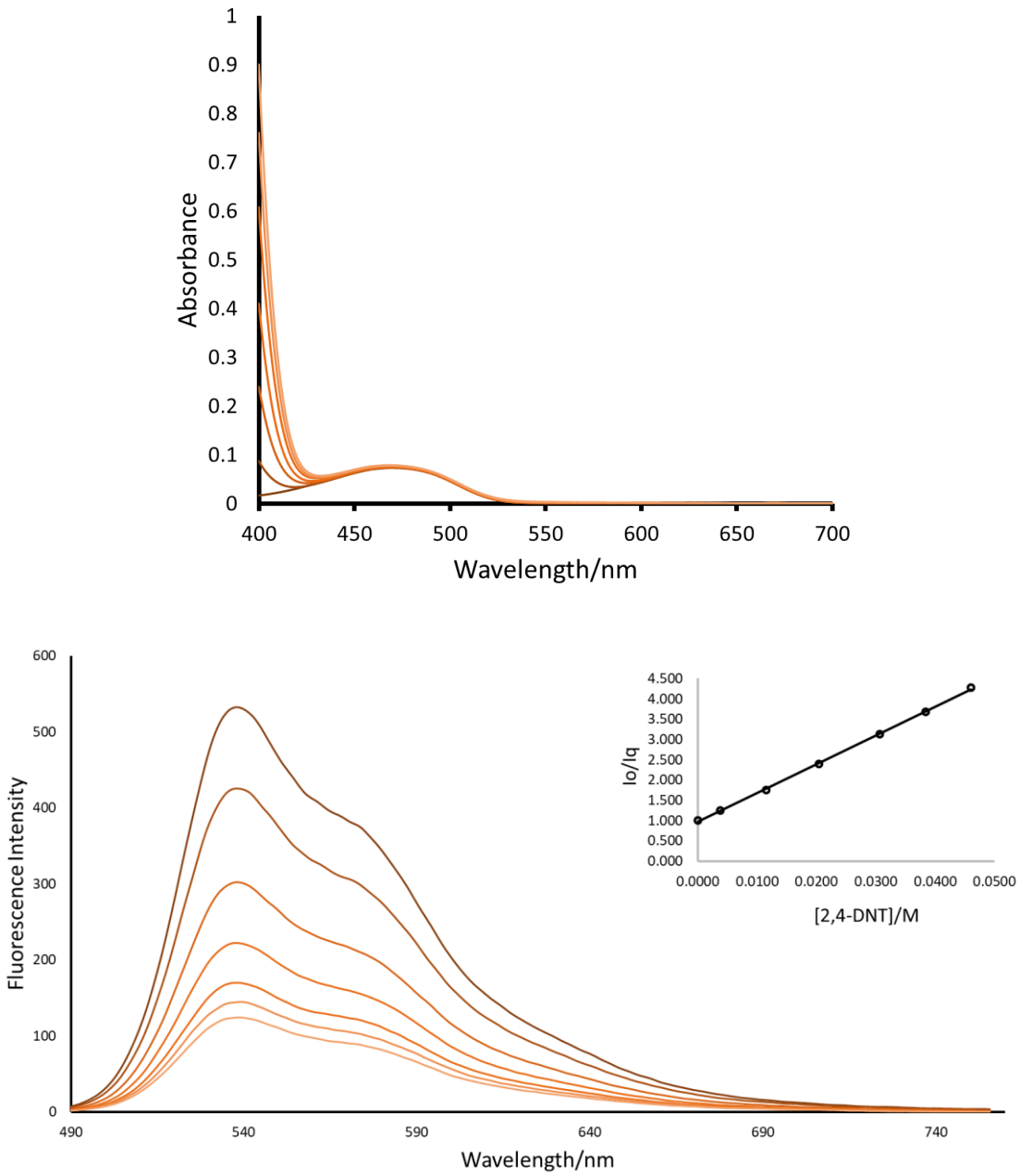


Figure B2.4: Top: Duplicate absorption spectra of ClN6DPP in acetonitrile with 2,4-dinitrotoluene. Bottom: Duplicate fluorescence emission spectra of ClN6DPP in acetonitrile with increasing concentration of 2,4-dinitrotoluene.

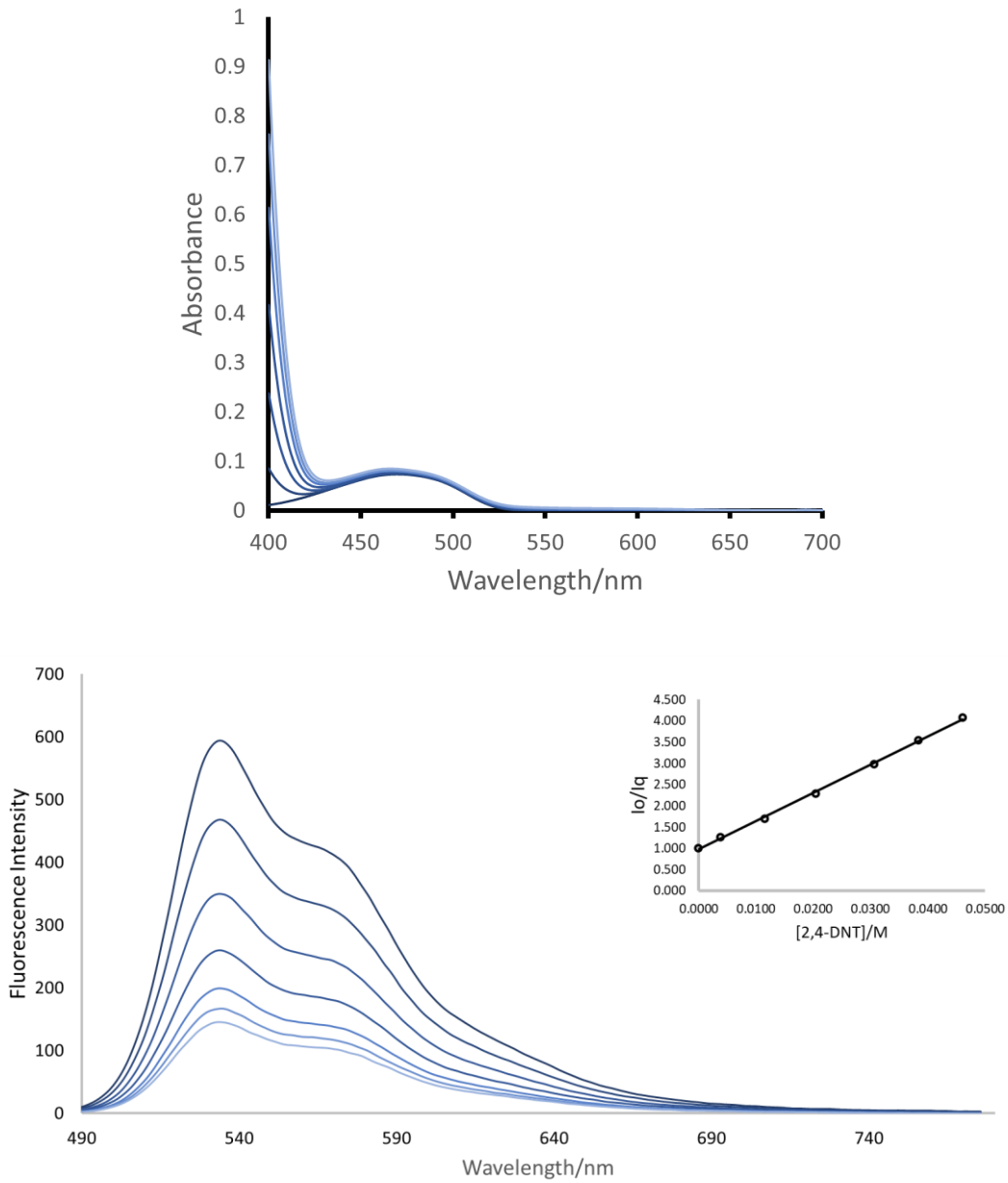


Figure B2.5: Top: Absorption spectra of ClNDPP in acetonitrile with 2,4-dinitrotoluene. Bottom: Fluorescence emission spectra of ClNDPP in acetonitrile with increasing concentration of 2,4-dinitrotoluene.

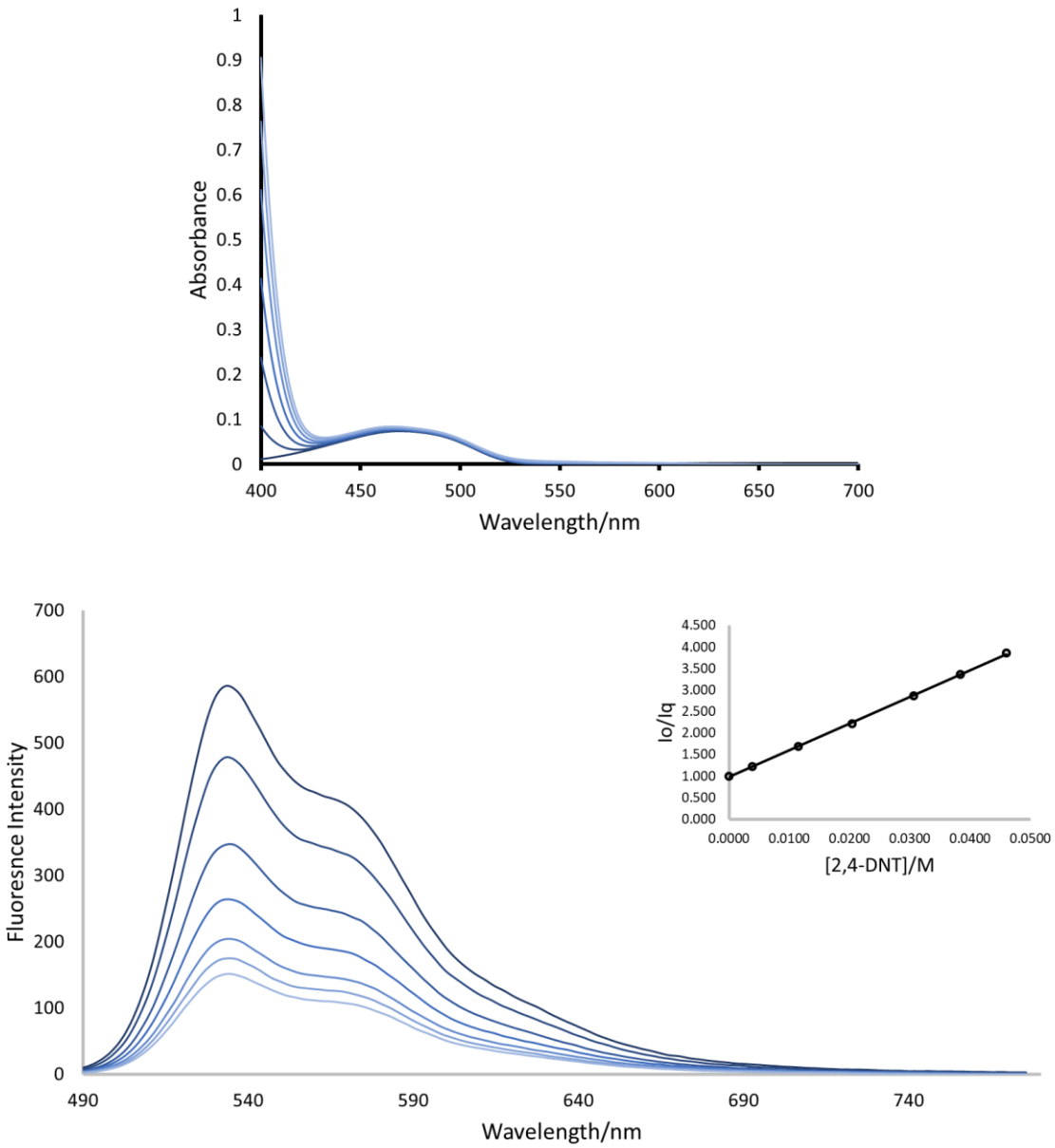


Figure B2.6: Top: Duplicate absorption spectra of ClNDPP in acetonitrile with 2,4-dinitrotoluene. Bottom: Duplicate fluorescence emission spectra of ClNDPP in acetonitrile with increasing concentration of 2,4-dinitrotoluene.

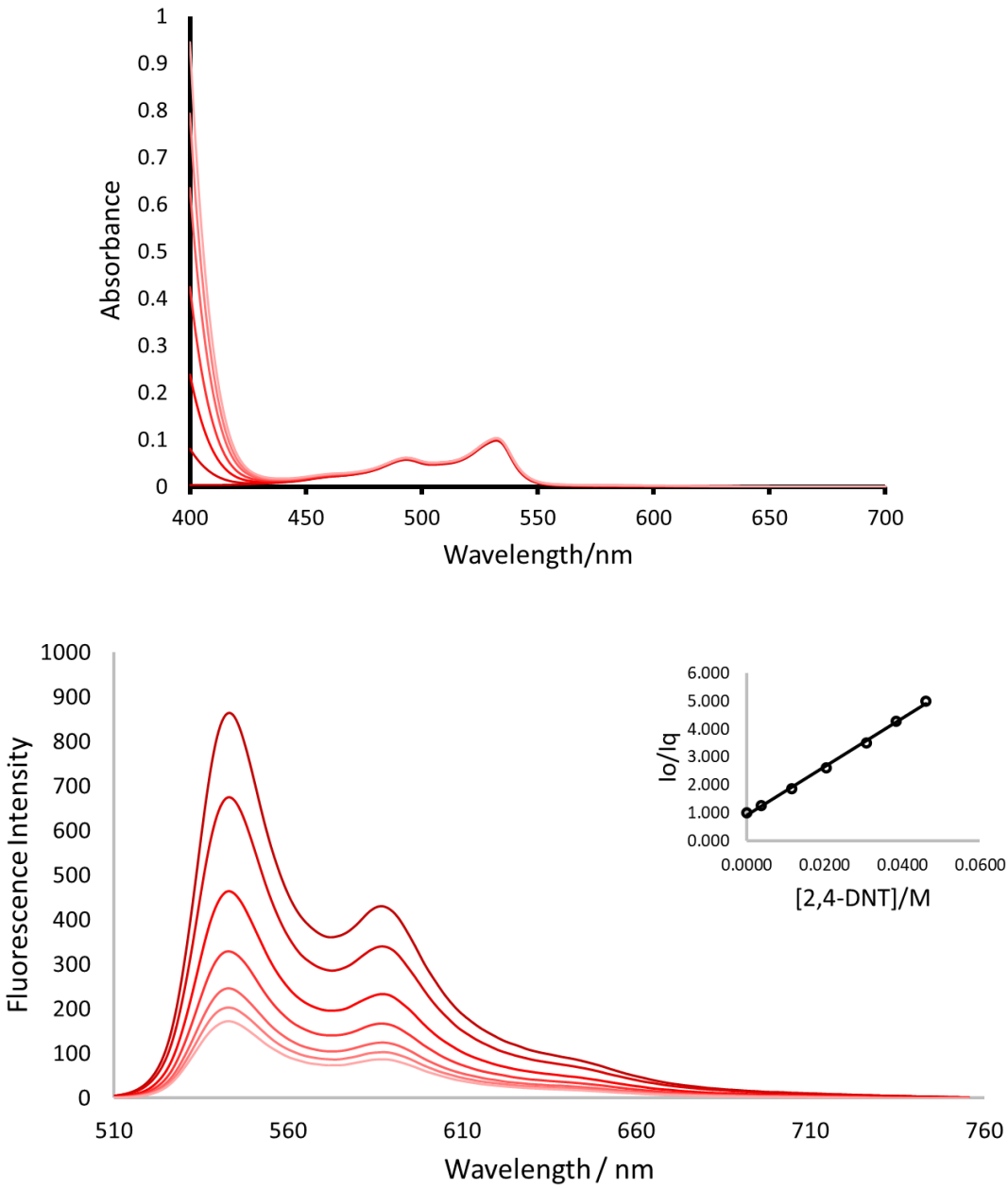


Figure B2.7: Top: Absorption spectra of FBDPP in acetonitrile with 2,4-dinitrotoluene. Bottom: Fluorescence emission spectra of FBDPP in acetonitrile with increasing concentration of 2,4-dinitrotoluene.

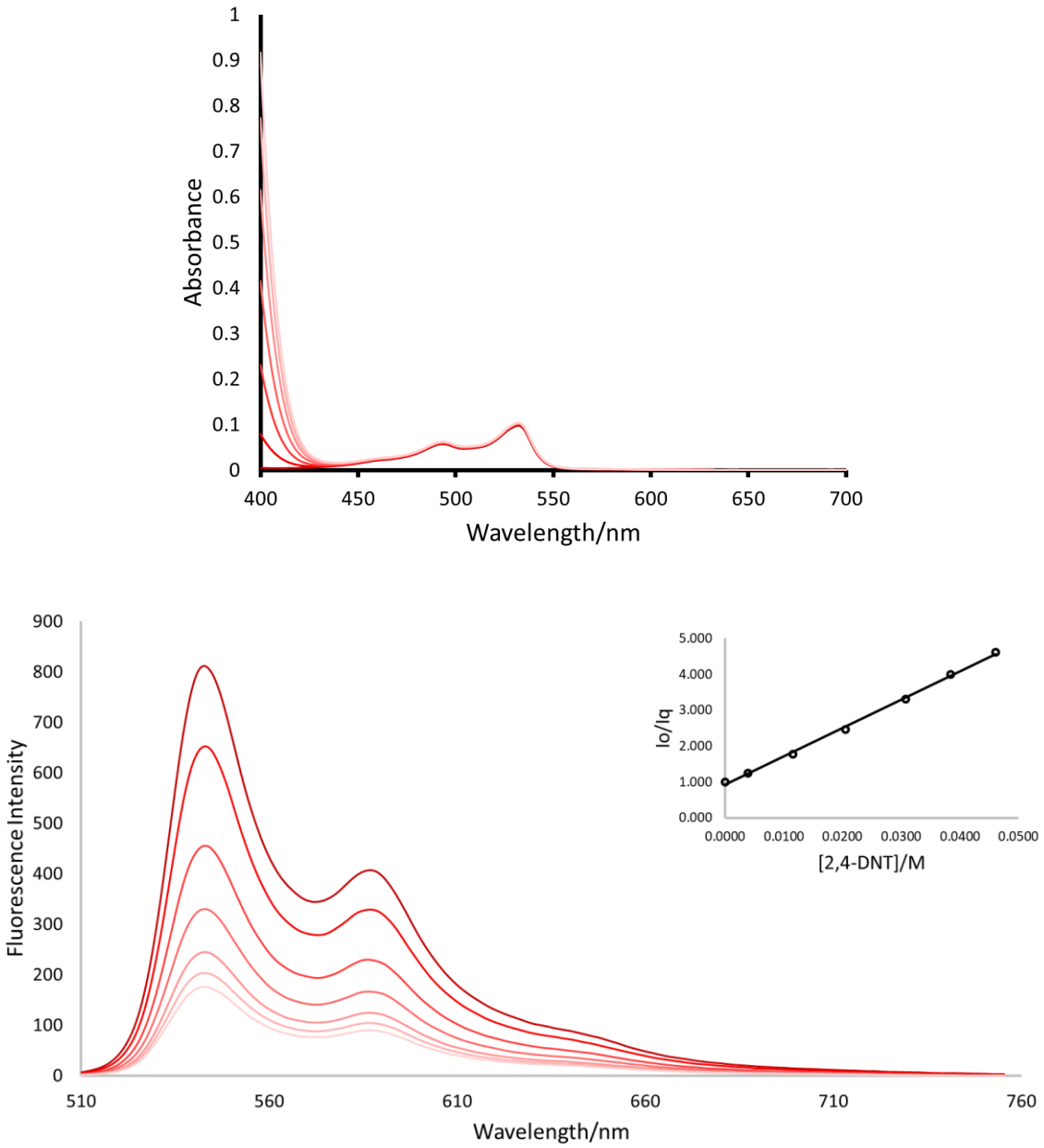


Figure B2.8: Top: Duplicate absorption spectra of FBDPP in acetonitrile with 2,4-dinitrotoluene. Bottom: Duplicate fluorescence emission spectra of FBDPP in acetonitrile with increasing concentration of 2,4-dinitrotoluene.

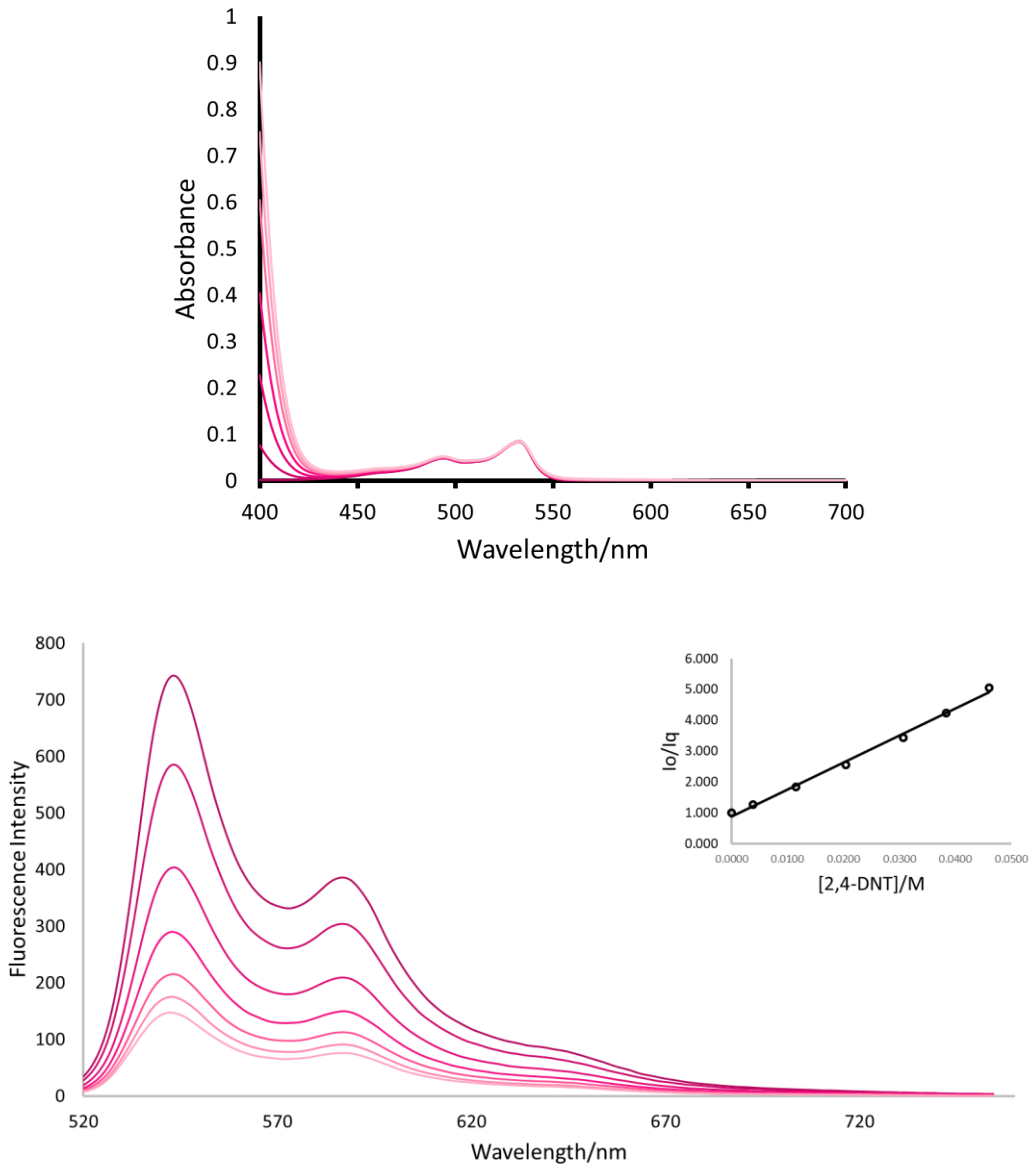


Figure B2.9: Top: Absorption spectra of FNDPP in acetonitrile with 2,4-dinitrotoluene. Bottom: Fluorescence emission spectra of FNDPP in acetonitrile with increasing concentration of 2,4-dinitrotoluene.

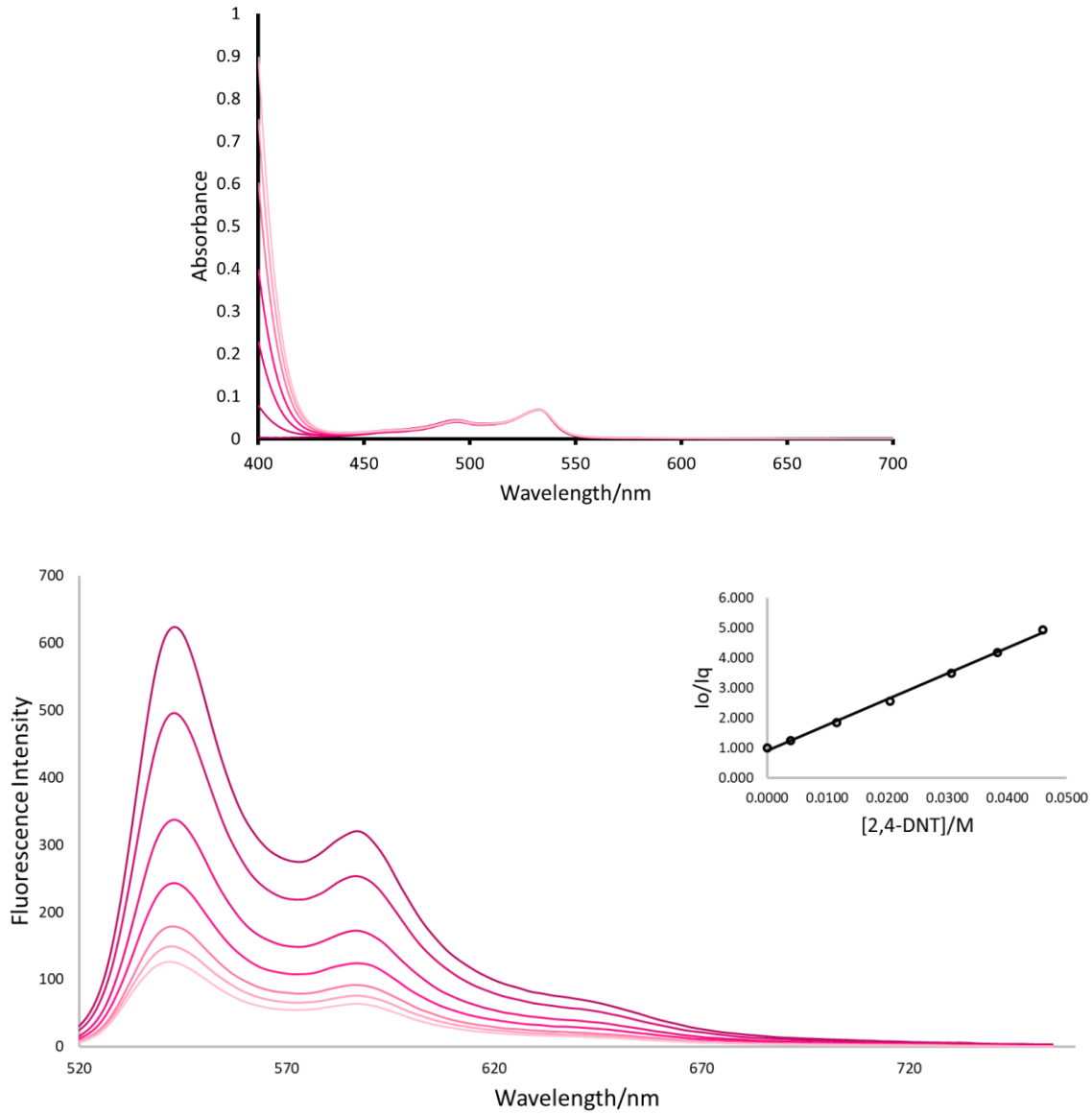


Figure B2.10: Top: Duplicate absorption spectra of FNDPP in acetonitrile with 2,4-dinitrotoluene. Bottom: Duplicate fluorescence emission spectra of FNDPP in acetonitrile with increasing concentration of 2,4-dinitrotoluene.

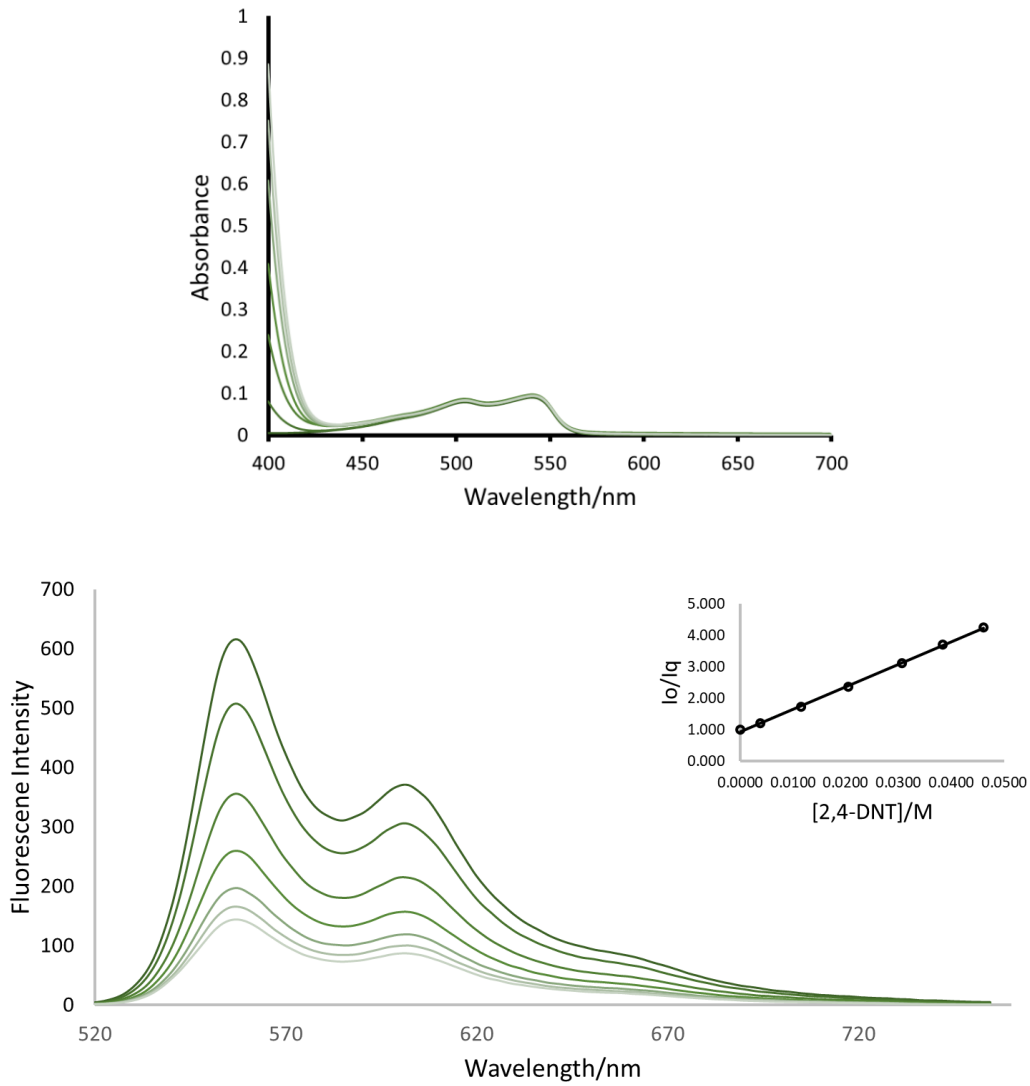


Figure B2.11: Top: Absorption spectra of TBDPP in acetonitrile with 2,4-dinitrotoluene. Bottom: Fluorescence emission spectra of TBDPP in acetonitrile with increasing concentration of 2,4-dinitrotoluene.

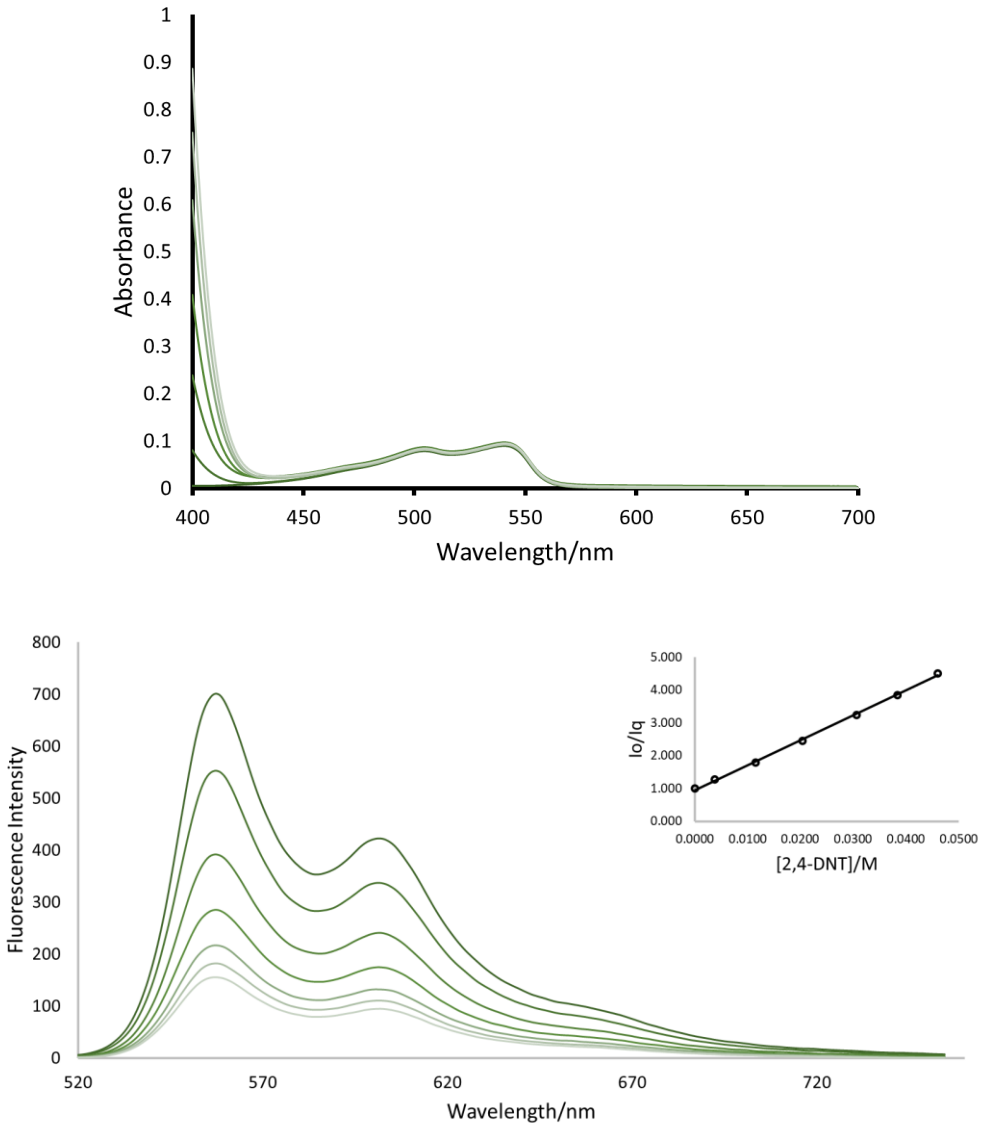


Figure B2.12: Top: Duplicate absorption spectra of TBDPP in acetonitrile with 2,4-dinitrotoluene. Bottom: Duplicate fluorescence emission spectra of TBDPP in acetonitrile with increasing concentration of 2,4-dinitrotoluene.

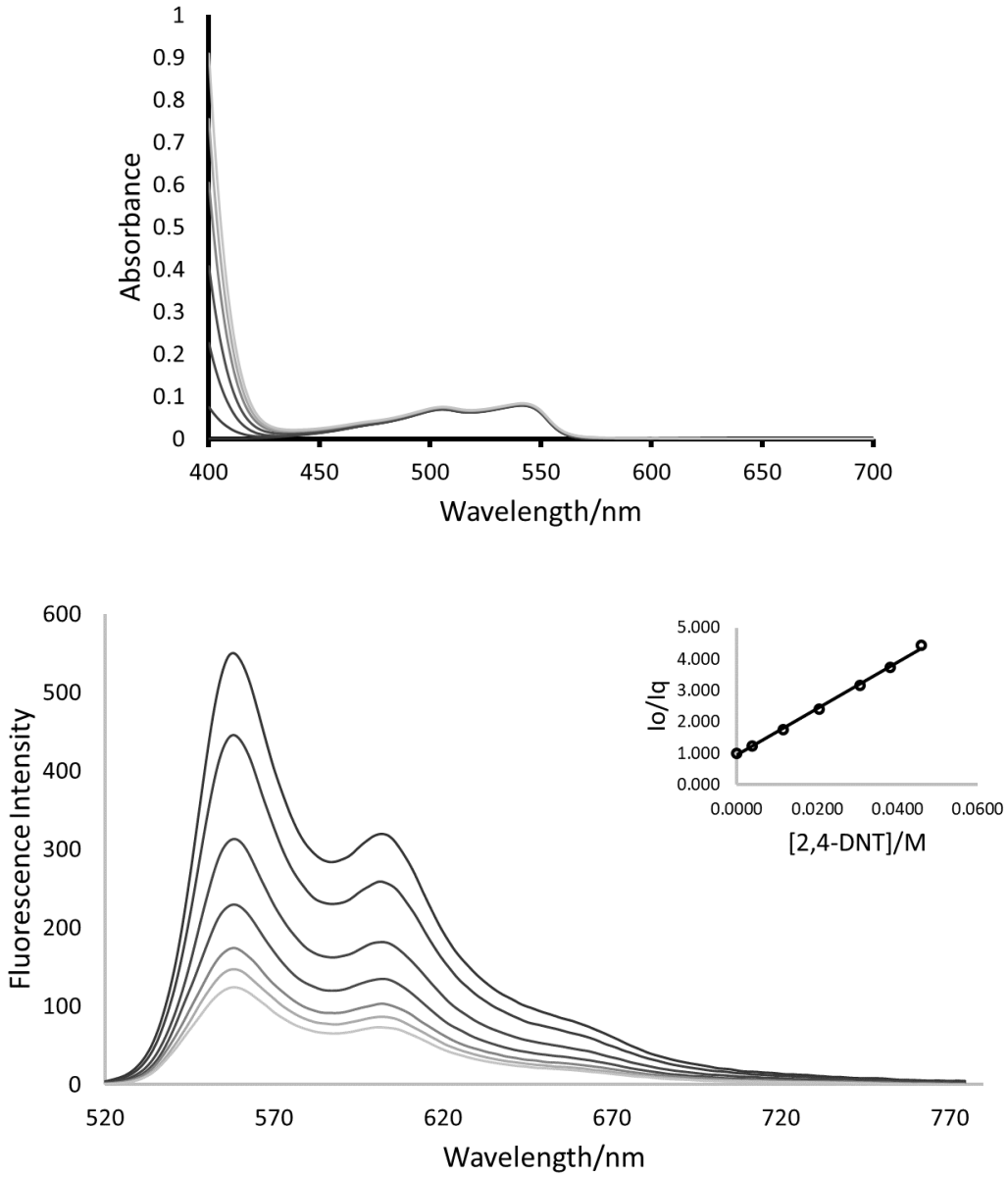


Figure B2.13: Top: Absorption spectra of TNDPP in acetonitrile with 2,4-dinitrotoluene. Bottom: Fluorescence emission spectra of TNDPP in acetonitrile with increasing concentration of 2,4-dinitrotoluene.

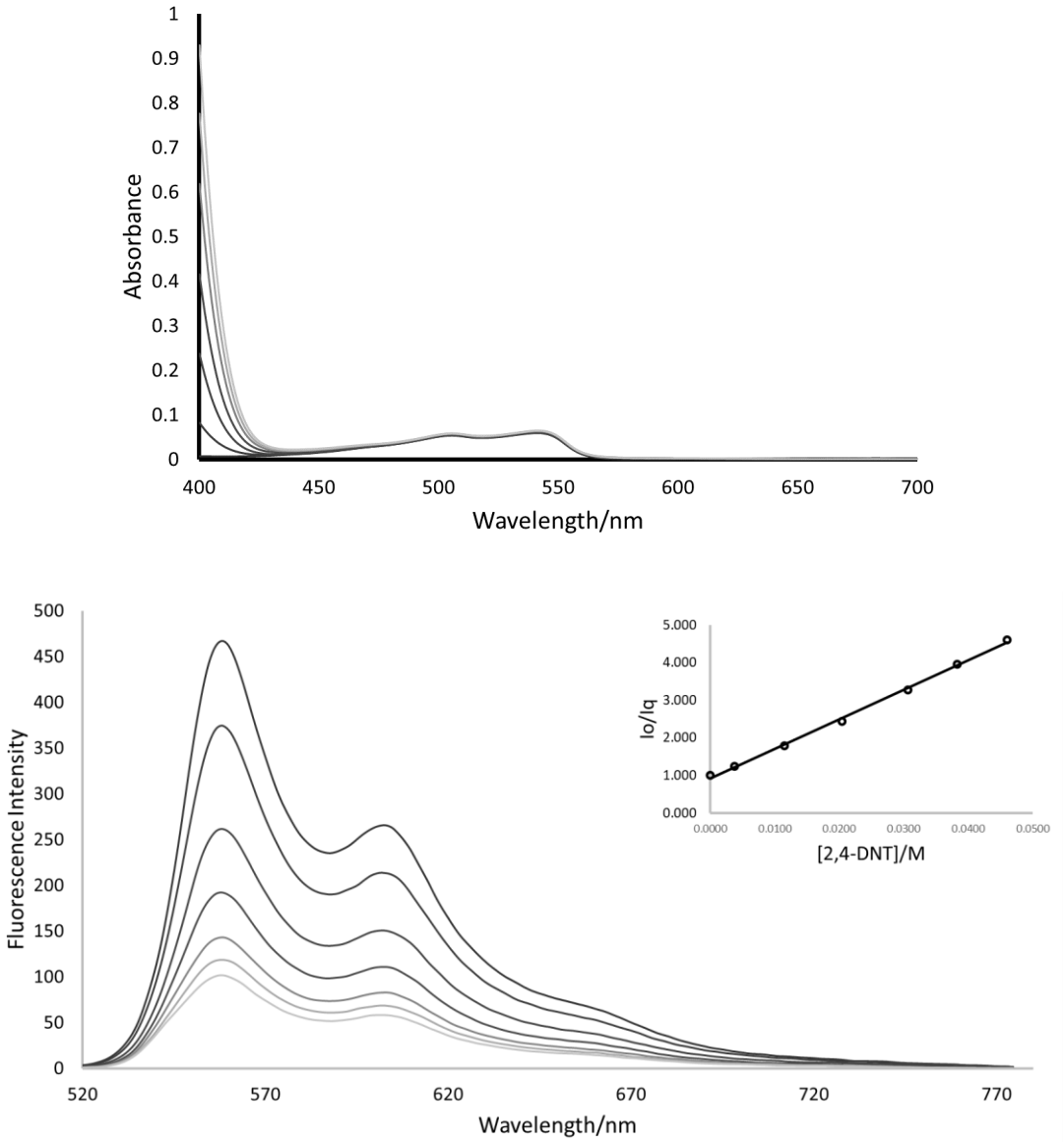


Figure B2.14: Top: Duplication absorption spectra of TNDPP in acetonitrile with 2,4-dinitrotoluene. Bottom: Duplication fluorescence emission spectra of TNDPP in acetonitrile with increasing concentration of 2,4-dinitrotoluene.

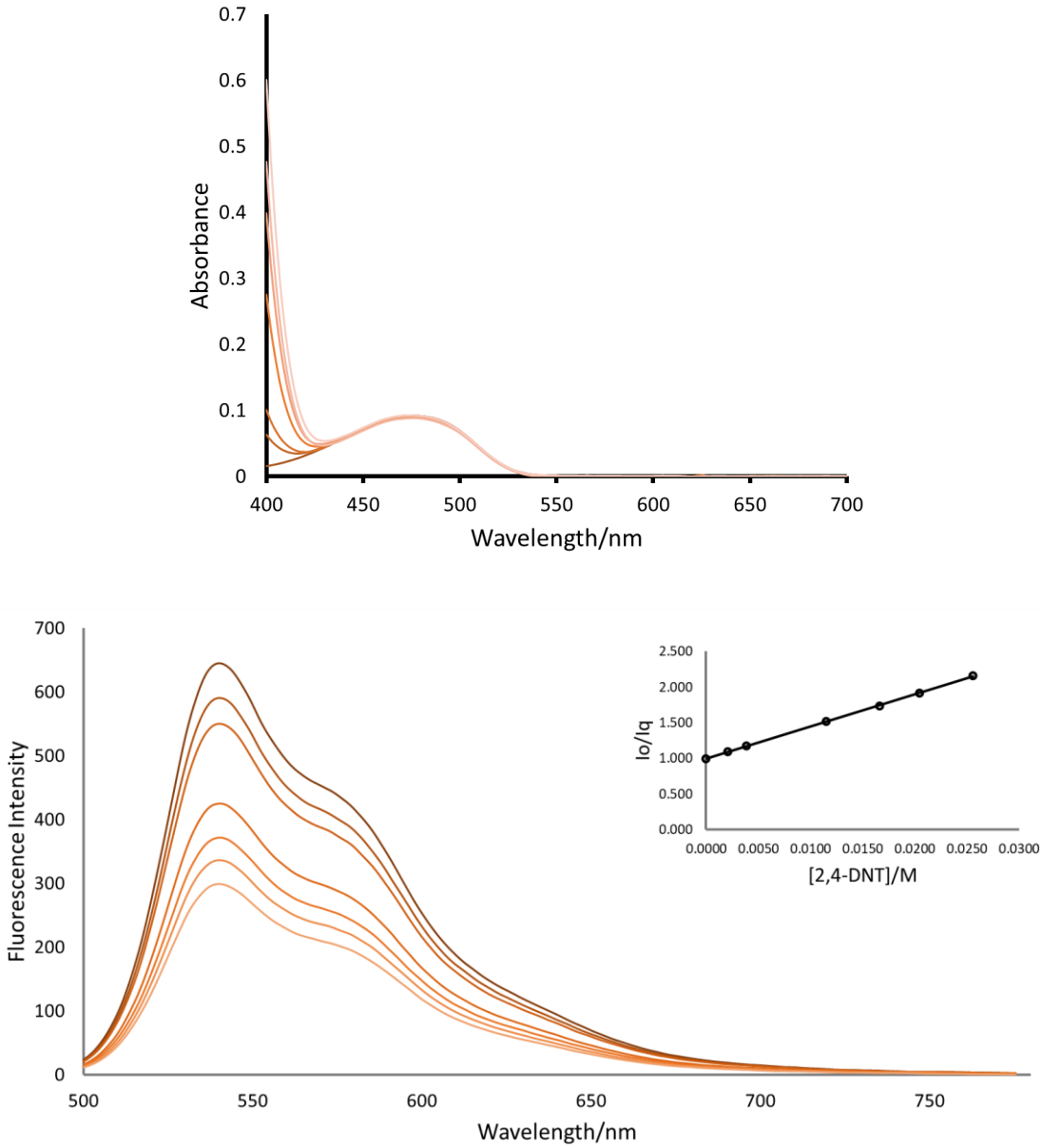


Figure B2.15: Top: Absorption spectra of ClN6DPP in dichloromethane with 2,4-dinitrotoluene. Bottom: Fluorescence emission spectra of ClN6DPP in dichloromethane with increasing concentration of 2,4-dinitrotoluene.

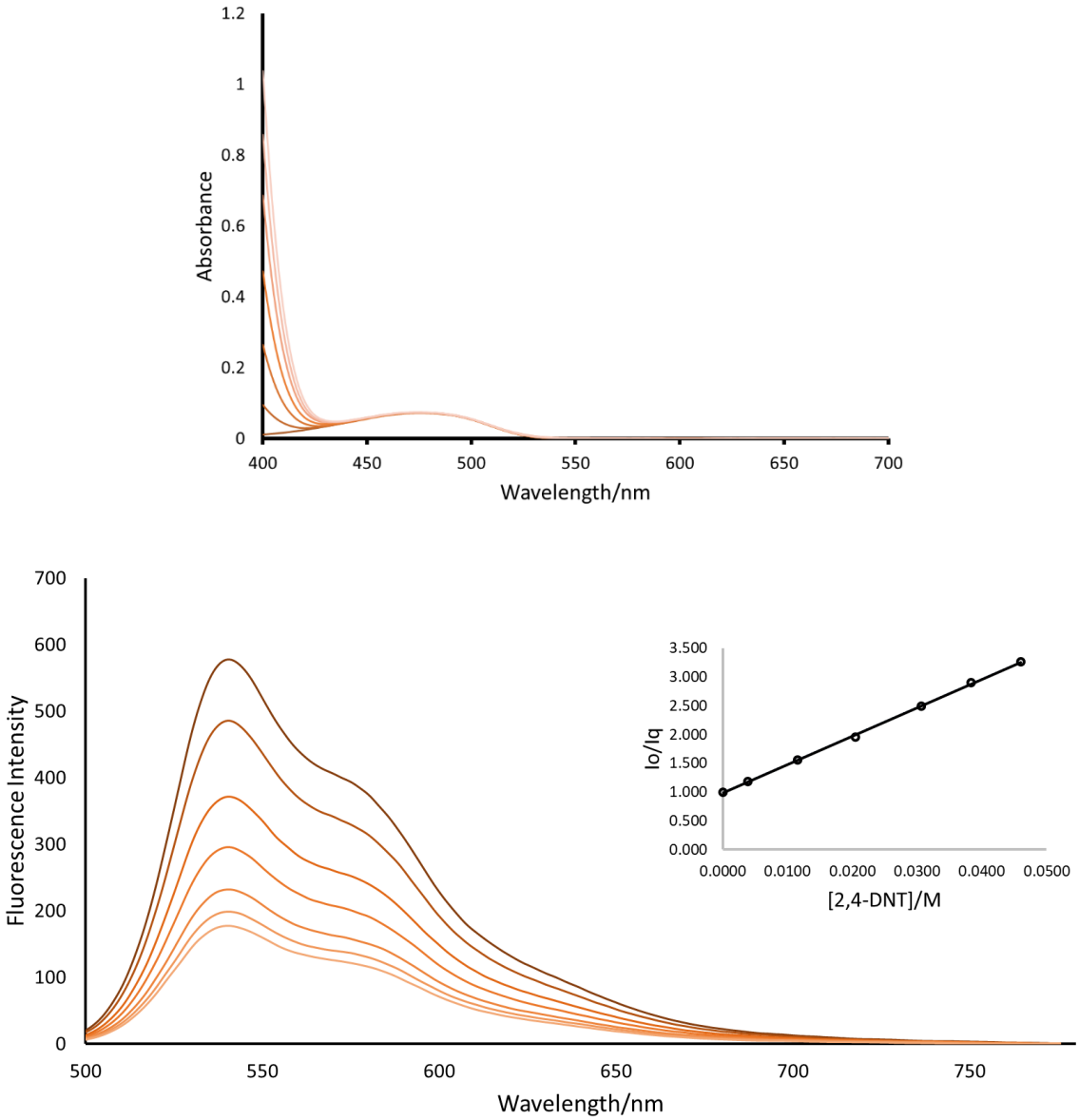


Figure B2.16: Top: Duplicate absorption spectra of ClN6DPP in dichloromethane with 2,4-dinitrotoluene. Bottom: Duplicate fluorescence emission spectra of ClN6DPP in dichloromethane with increasing concentration of 2,4-dinitrotoluene.

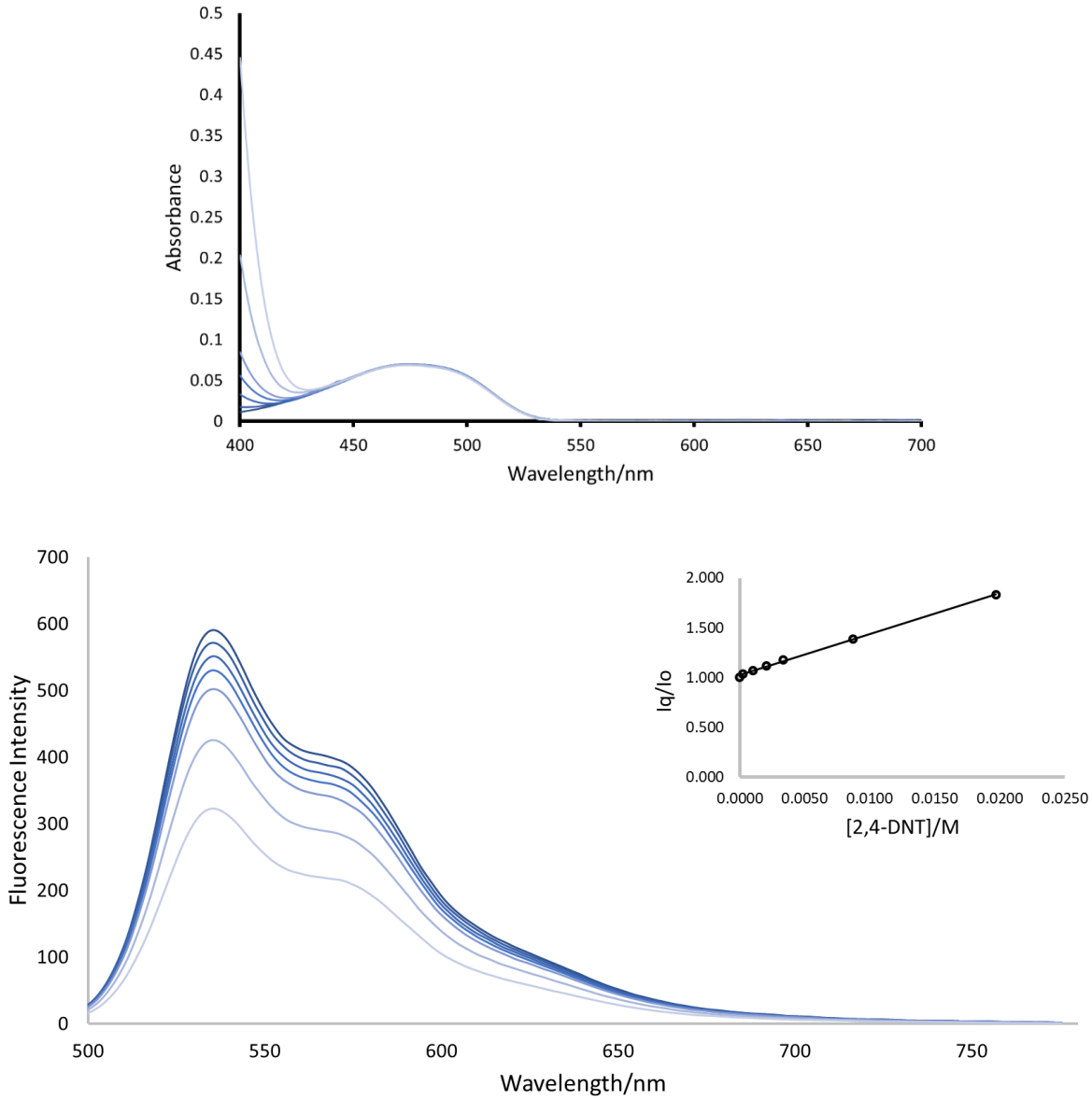


Figure B2.17: Top: Absorption spectra of ClNDPP in dichloromethane with 2,4-dinitrotoluene. Bottom: Fluorescence emission spectra of ClNDPP in dichloromethane with increasing concentration of 2,4-dinitrotoluene.

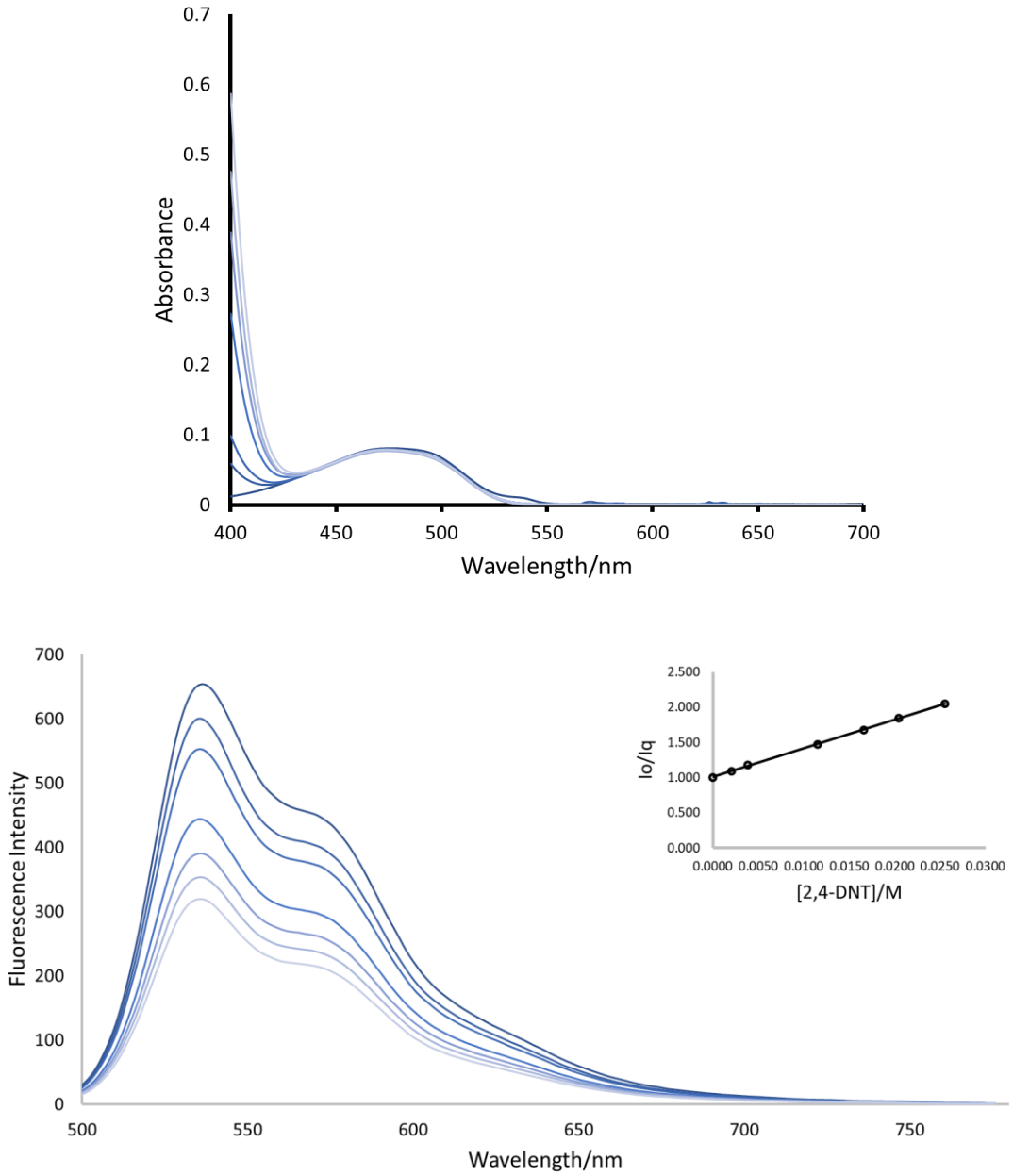


Figure B2.18: Top: Duplicate absorption spectra of ClNDPP in dichloromethane with 2,4-dinitrotoluene. Bottom: Duplicate fluorescence emission spectra of ClNDPP in dichloromethane with increasing concentration of 2,4-dinitrotoluene.

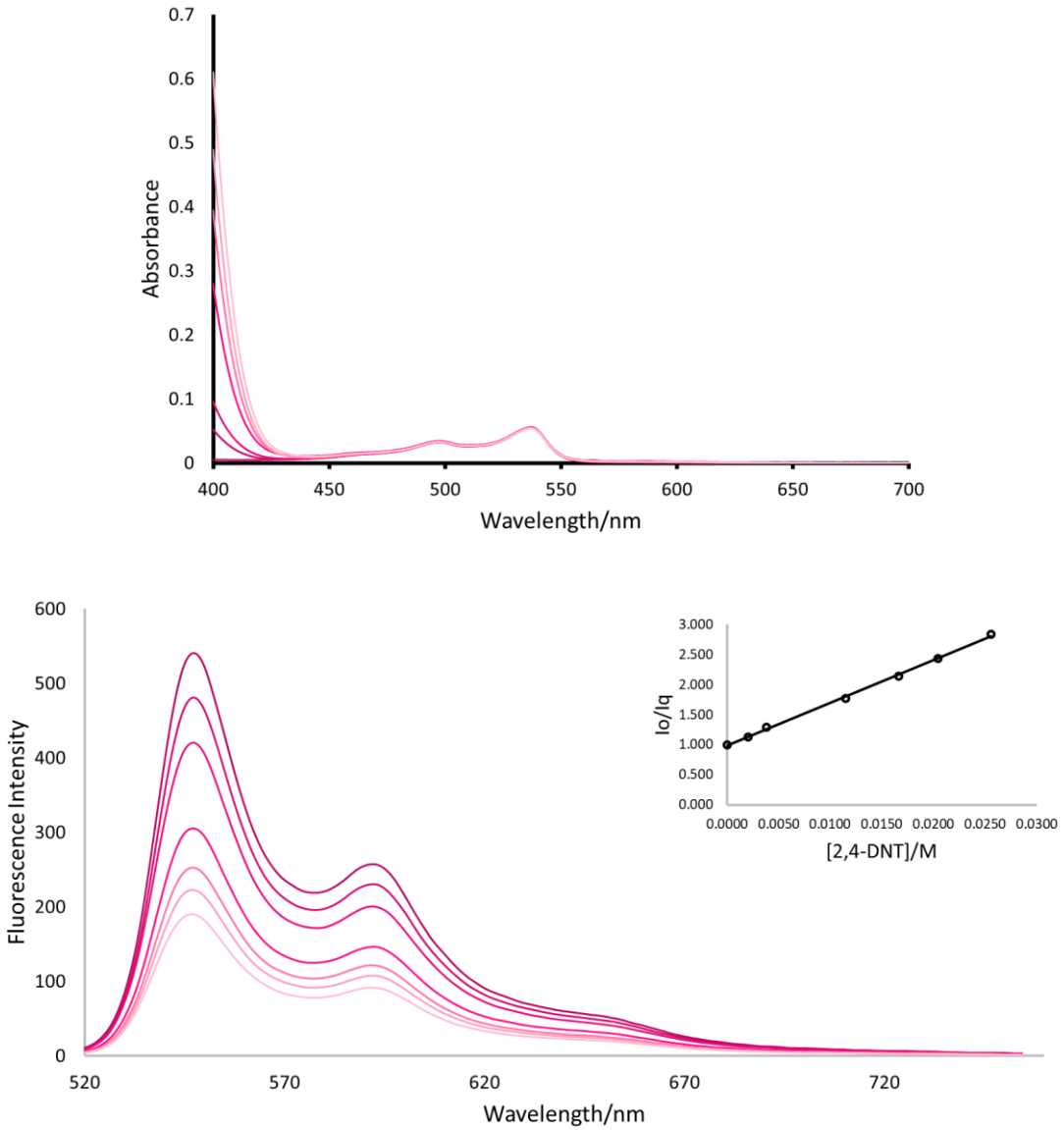


Figure B2.19: Top: Absorption spectra of FNDPP in dichloromethane with 2,4-dinitrotoluene. Bottom: Fluorescence emission spectra of FNDPP in dichloromethane with increasing concentration of 2,4-dinitrotoluene.

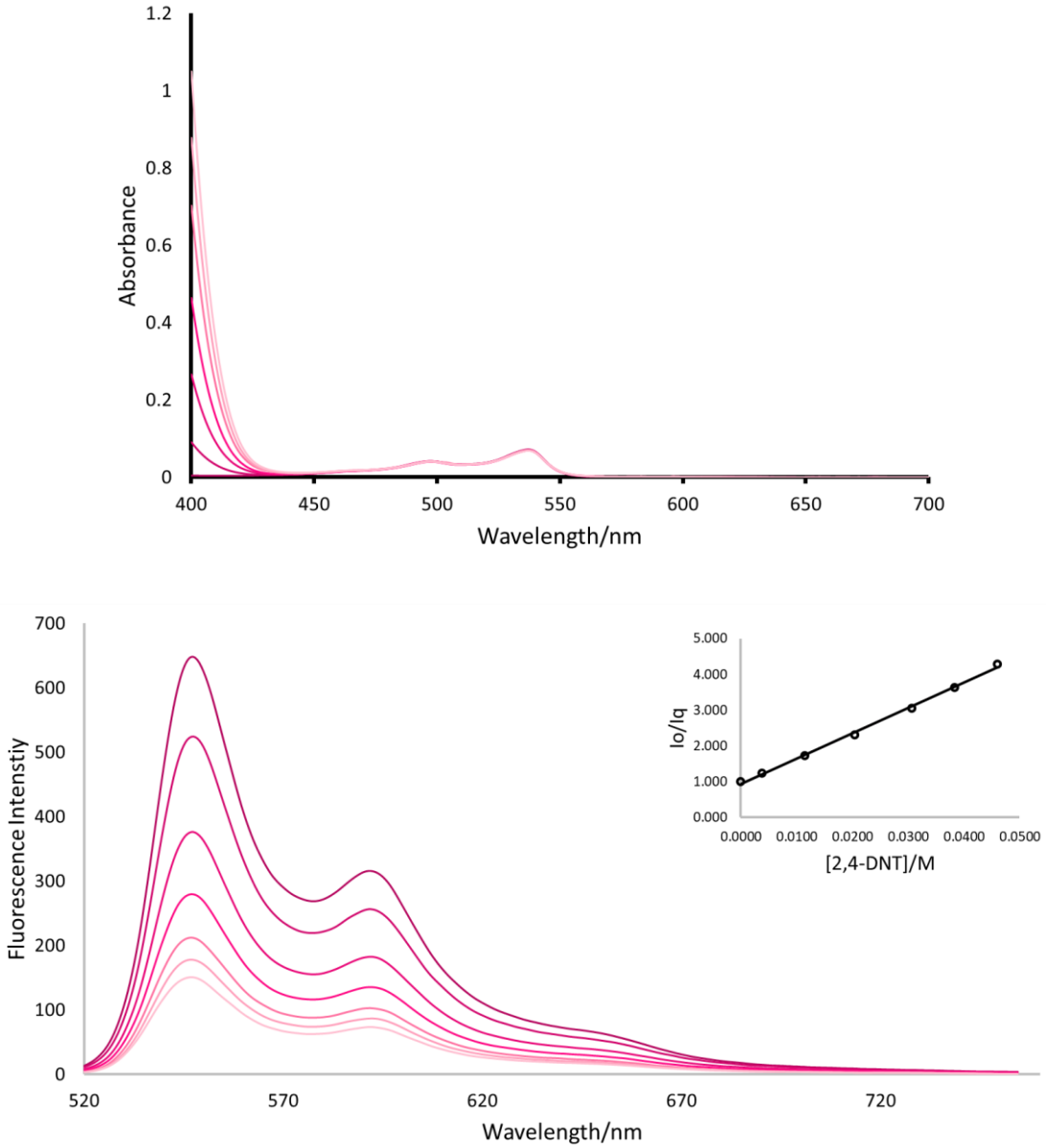


Figure B2.20: Top: Duplicate absorption spectra of FNDPP in dichloromethane with 2,4-dinitrotoluene. Bottom: Duplicate fluorescence emission spectra of FNDPP in dichloromethane with increasing concentration of 2,4-dinitrotoluene.

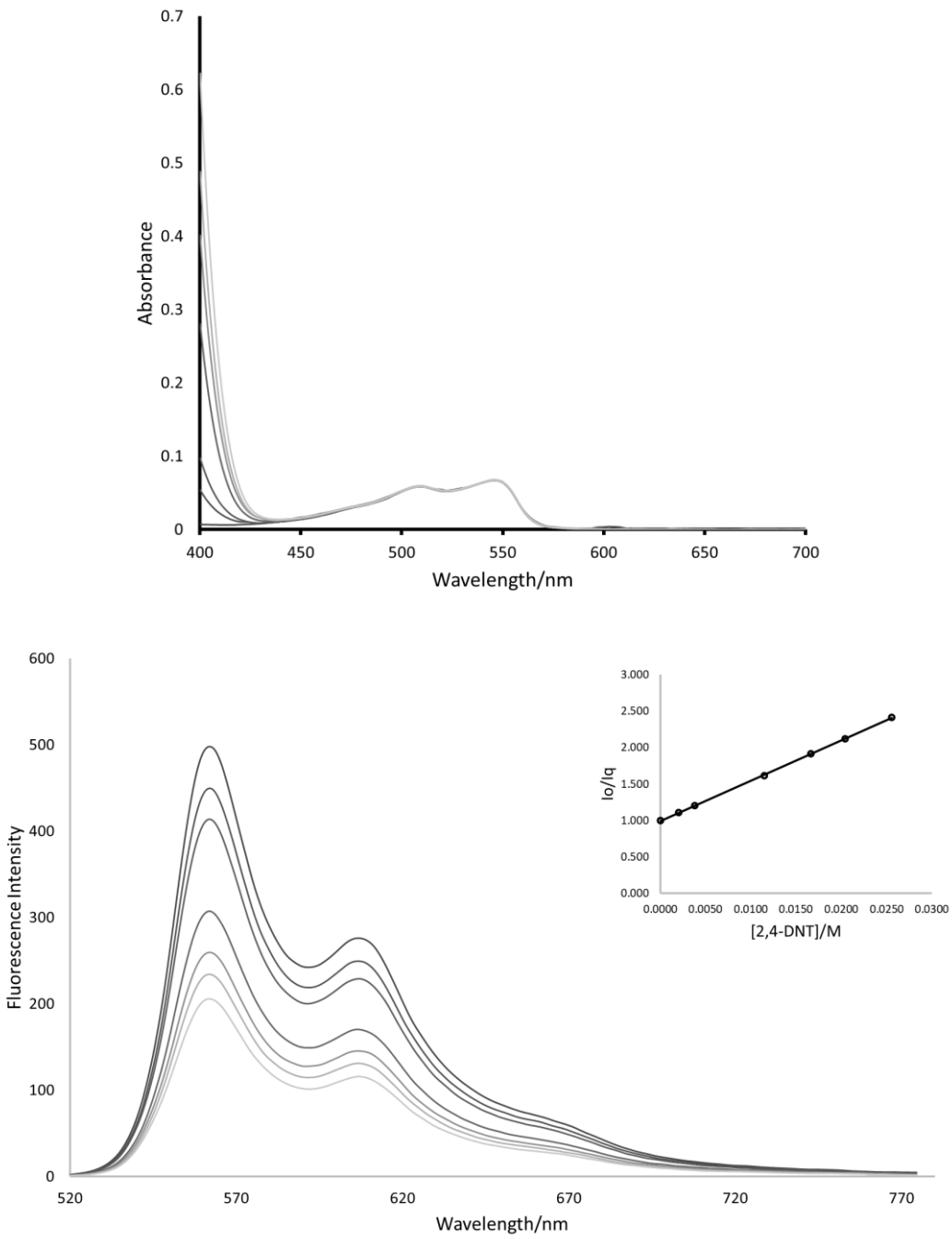


Figure B2.21: Top: Absorption spectra of TNDPP in dichloromethane with 2,4-dinitrotoluene. Bottom: Fluorescence emission spectra of TNDPP in dichloromethane with increasing concentration of 2,4-dinitrotoluene.

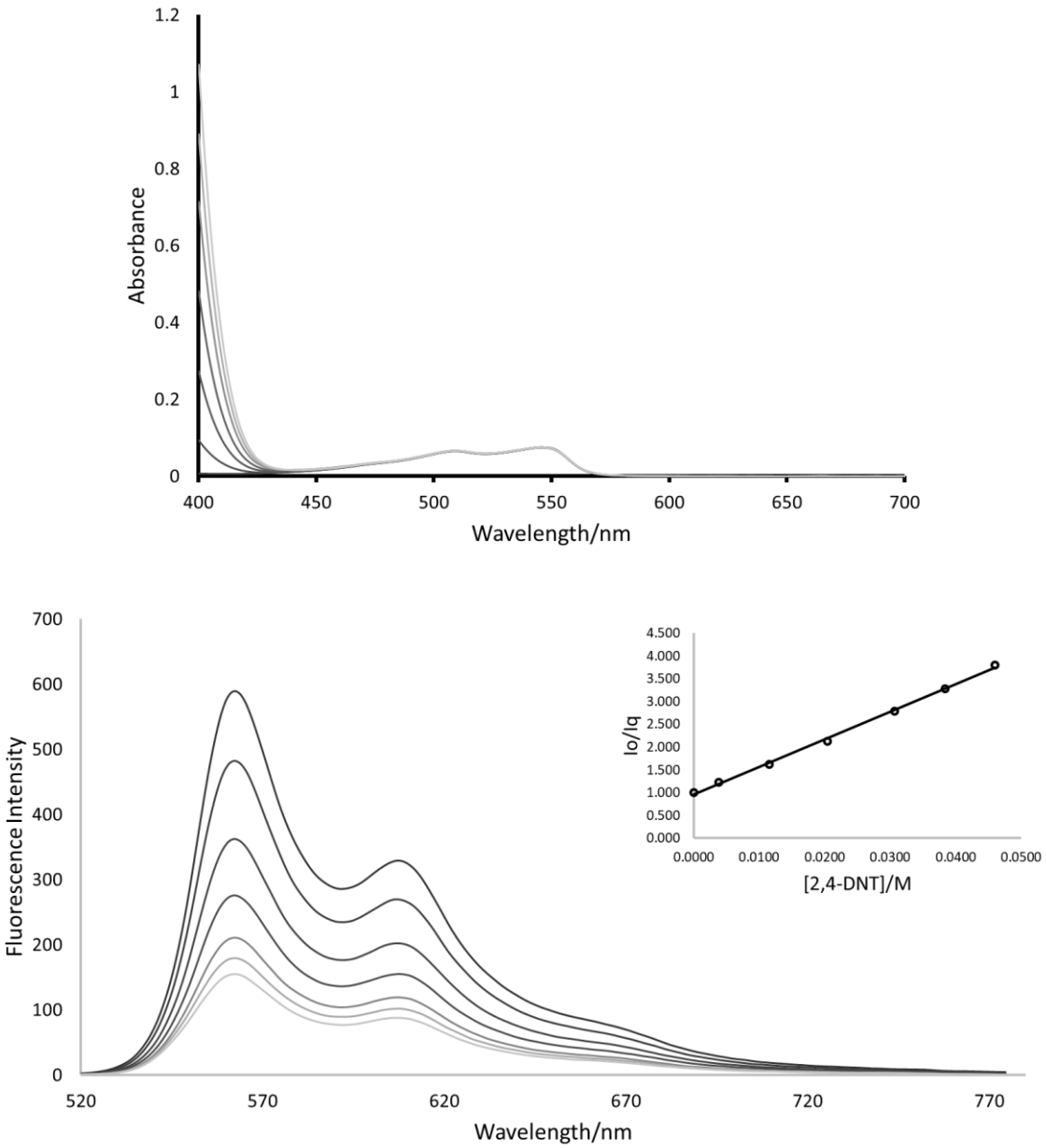


Figure B2.22: Top: Duplicate absorption spectra of TNDPP in dichloromethane with 2,4-dinitrotoluene. Bottom: Duplicate fluorescence emission spectra of TNDPP in dichloromethane with increasing concentration of 2,4-dinitrotoluene.

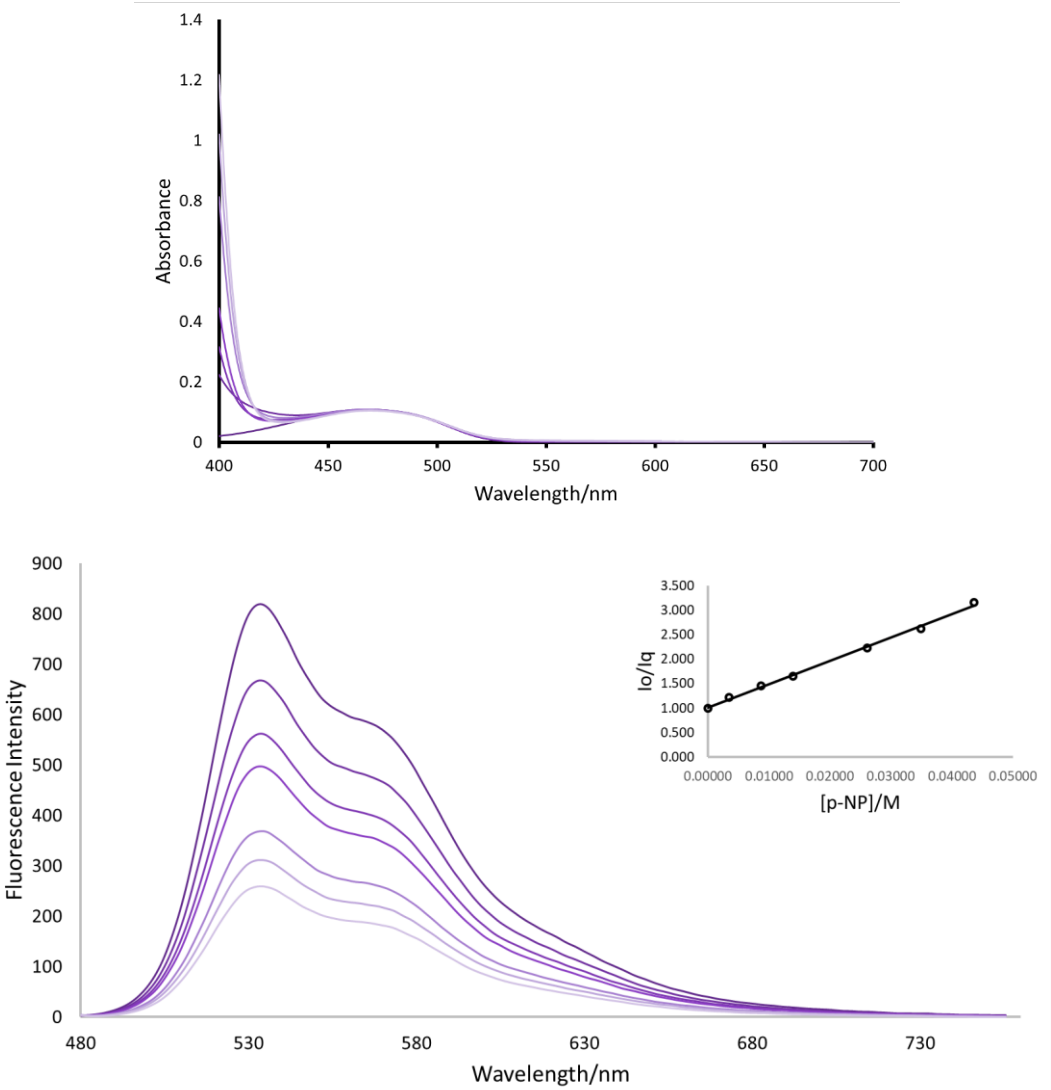


Figure B3.1: Top: Absorption spectra of ClBDPP in acetonitrile with p-nitrophenol. Bottom: Fluorescence emission spectra of ClBDPP in acetonitrile with increasing concentration of p-nitrophenol.

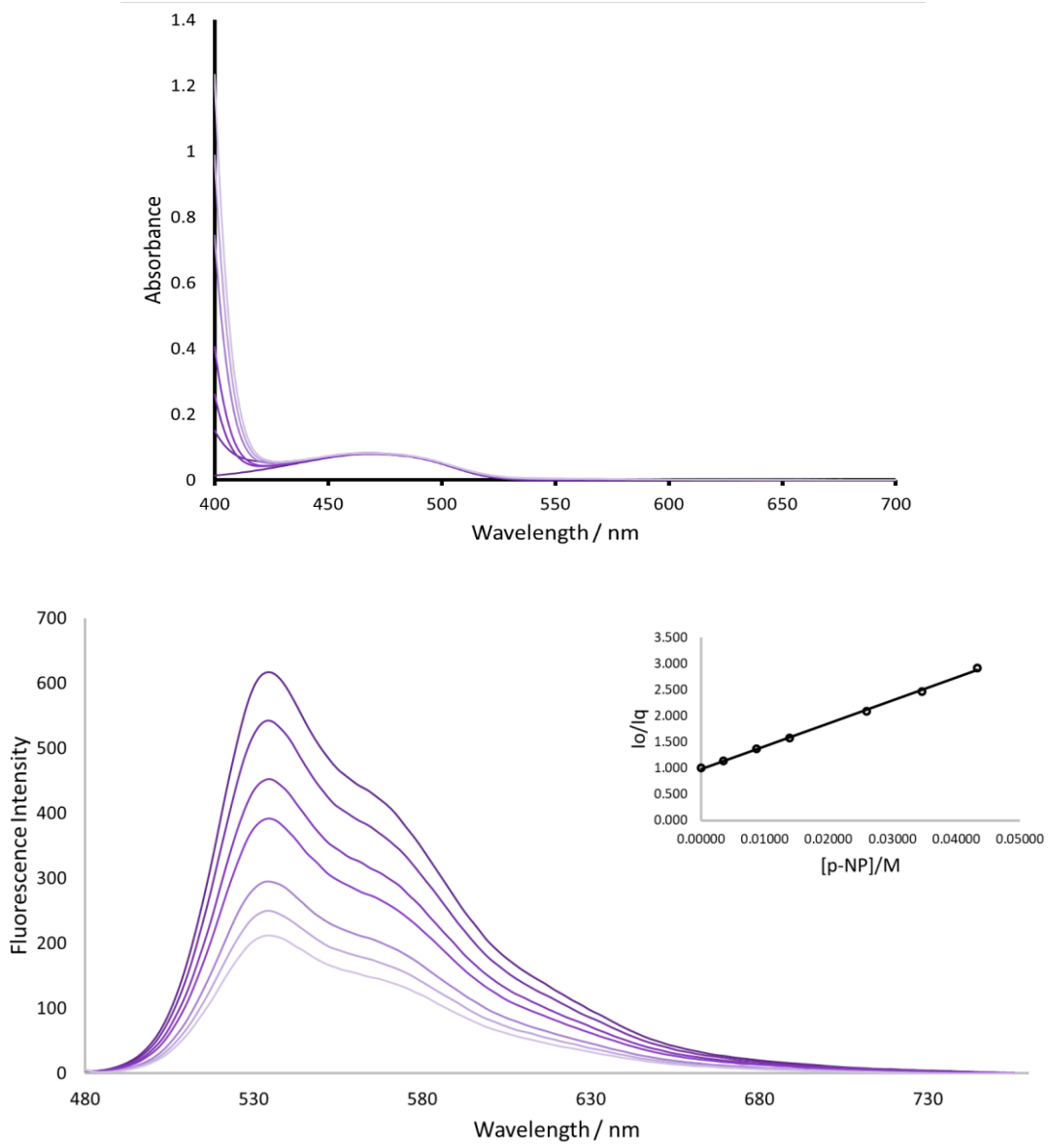


Figure B3.2: Top: Duplicate absorption spectra of ClBDPP in acetonitrile with p-nitrophenol. Bottom: Duplicate fluorescence emission spectra of ClBDPP in acetonitrile with increasing concentration of p-nitrophenol.

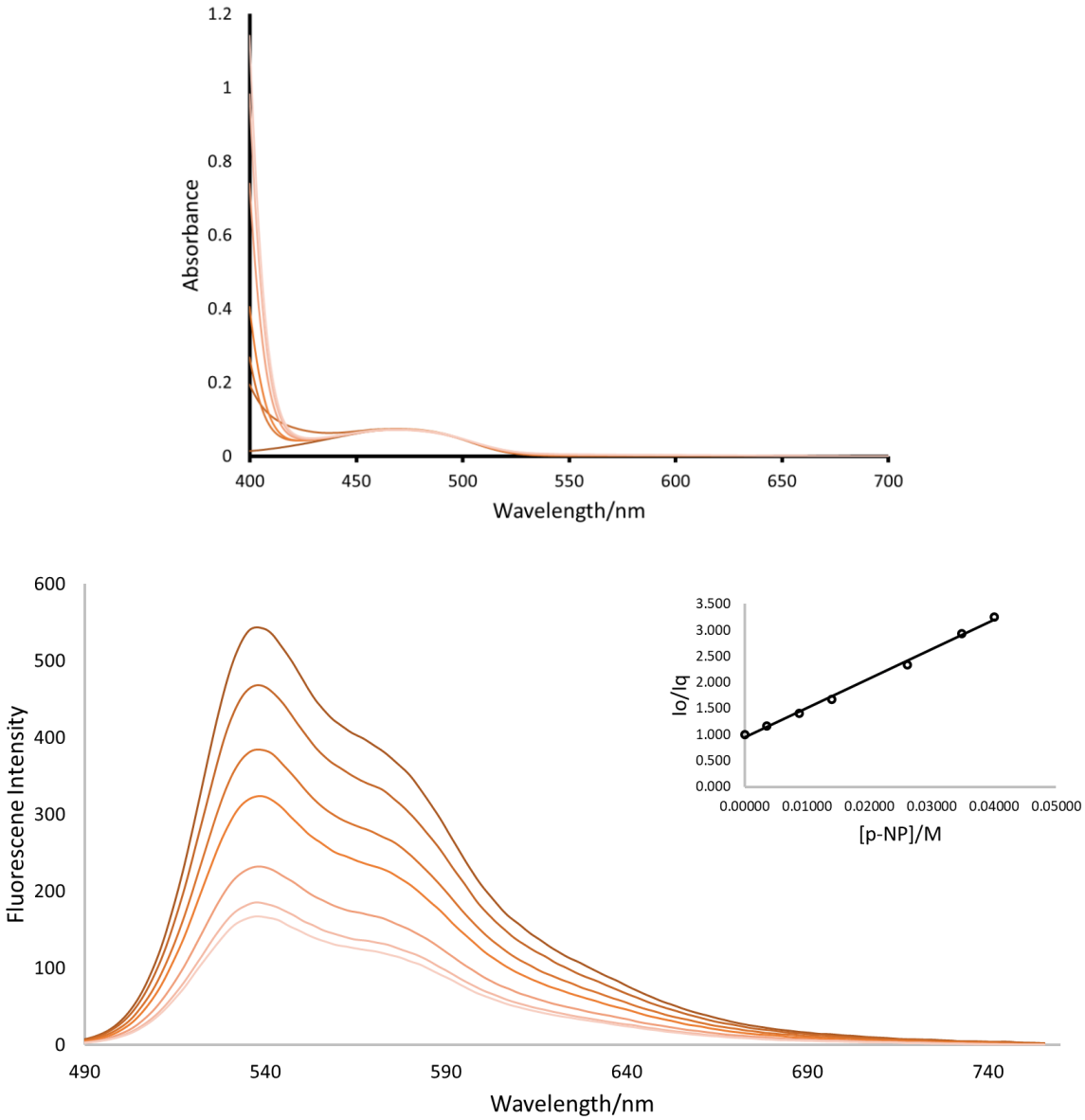


Figure B3.3: Top: Absorption spectra of ClN6DPP in acetonitrile with p-nitrophenol. Bottom: Fluorescence emission spectra of ClN6DPP in acetonitrile with increasing concentration of p-nitrophenol.

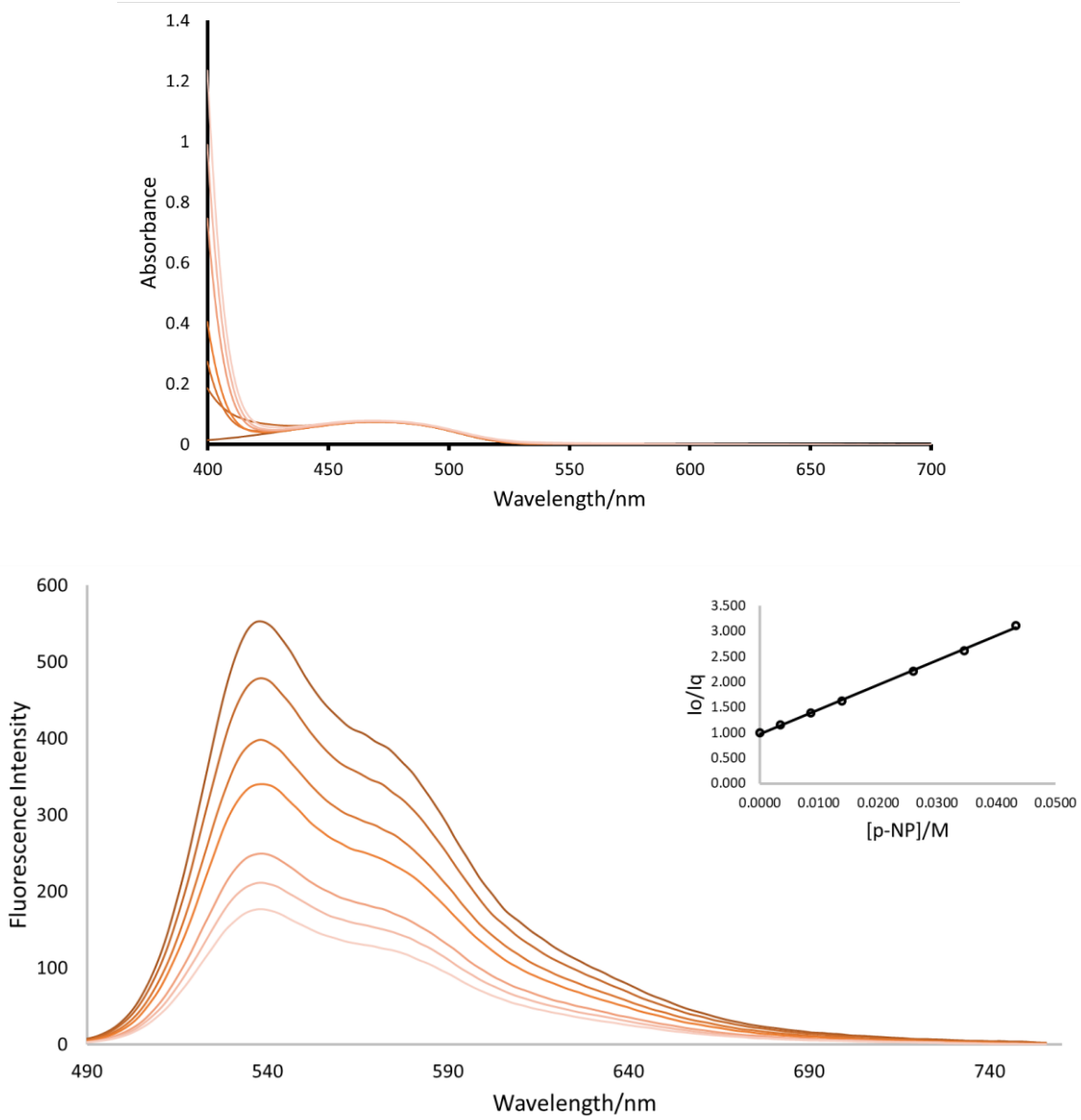


Figure B3.4: Top: Duplicate absorption spectra of ClN6DPP in acetonitrile with p-nitrophenol. Bottom: Duplicate fluorescence emission spectra of ClN6DPP in acetonitrile with increasing concentration of p-nitrophenol.

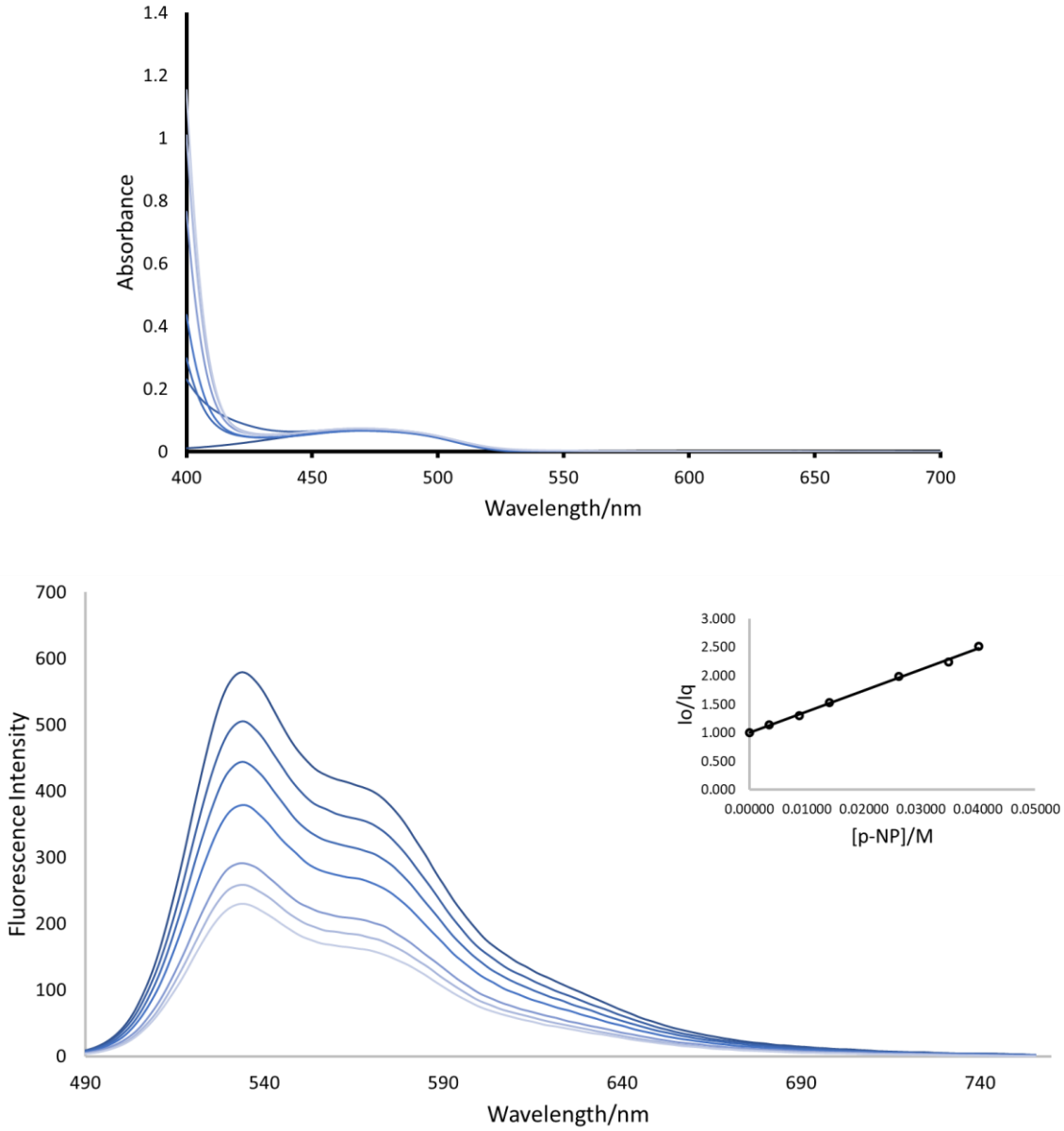


Figure B3.5: Top: Absorption spectra of ClNDPP in acetronitrile with p-nitrophenol. Bottom: Fluorescence emission spectra of ClNDPP in acetonitrile with increasing concentration of p-nitrophenol.

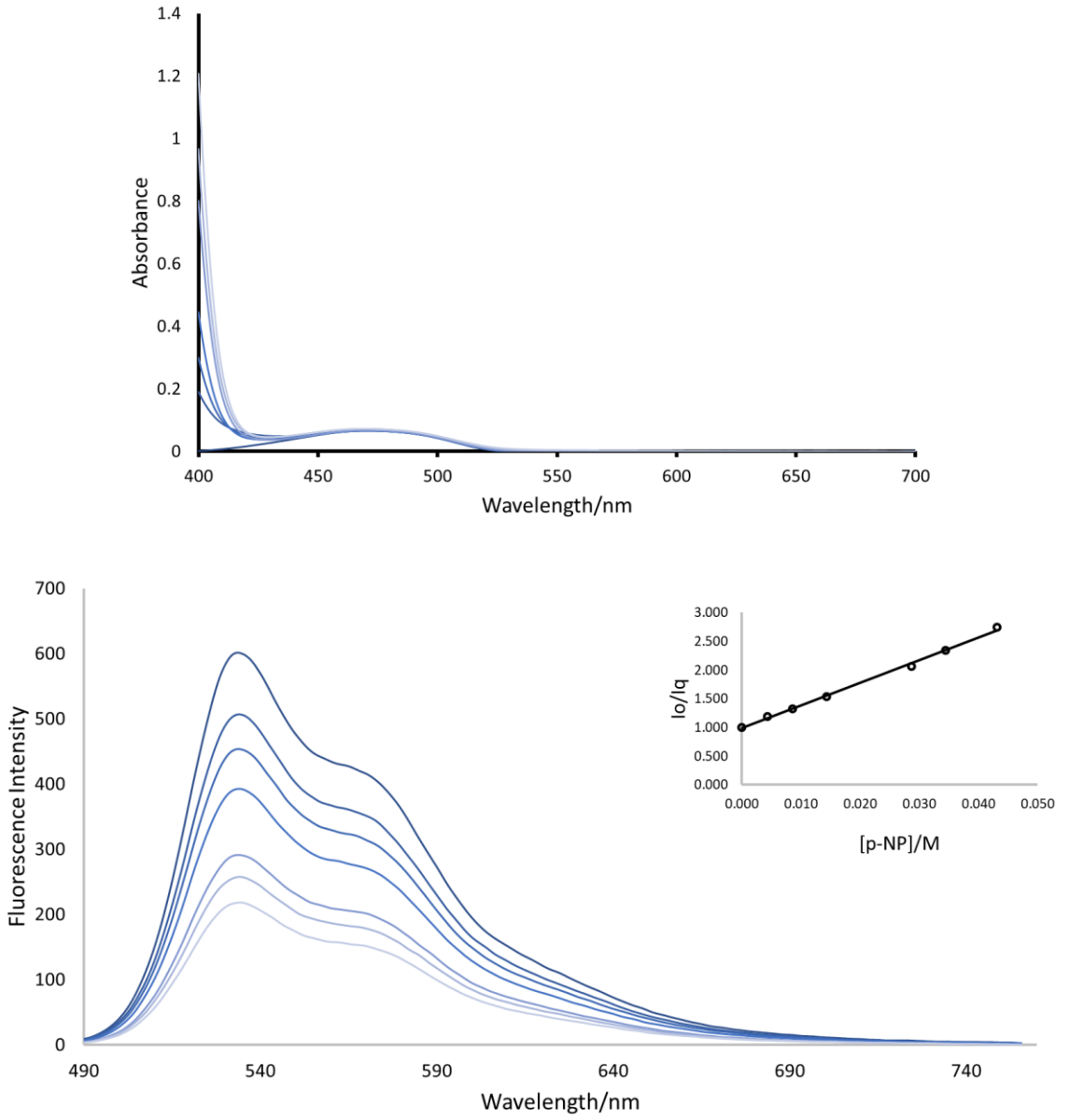


Figure B3.6: Top: Duplicate absorption spectra of ClNDPP in acetonitrile with p-nitrophenol. Bottom: Duplicate fluorescence emission spectra of ClNDPP in acetonitrile with increasing concentration of p-nitrophenol.

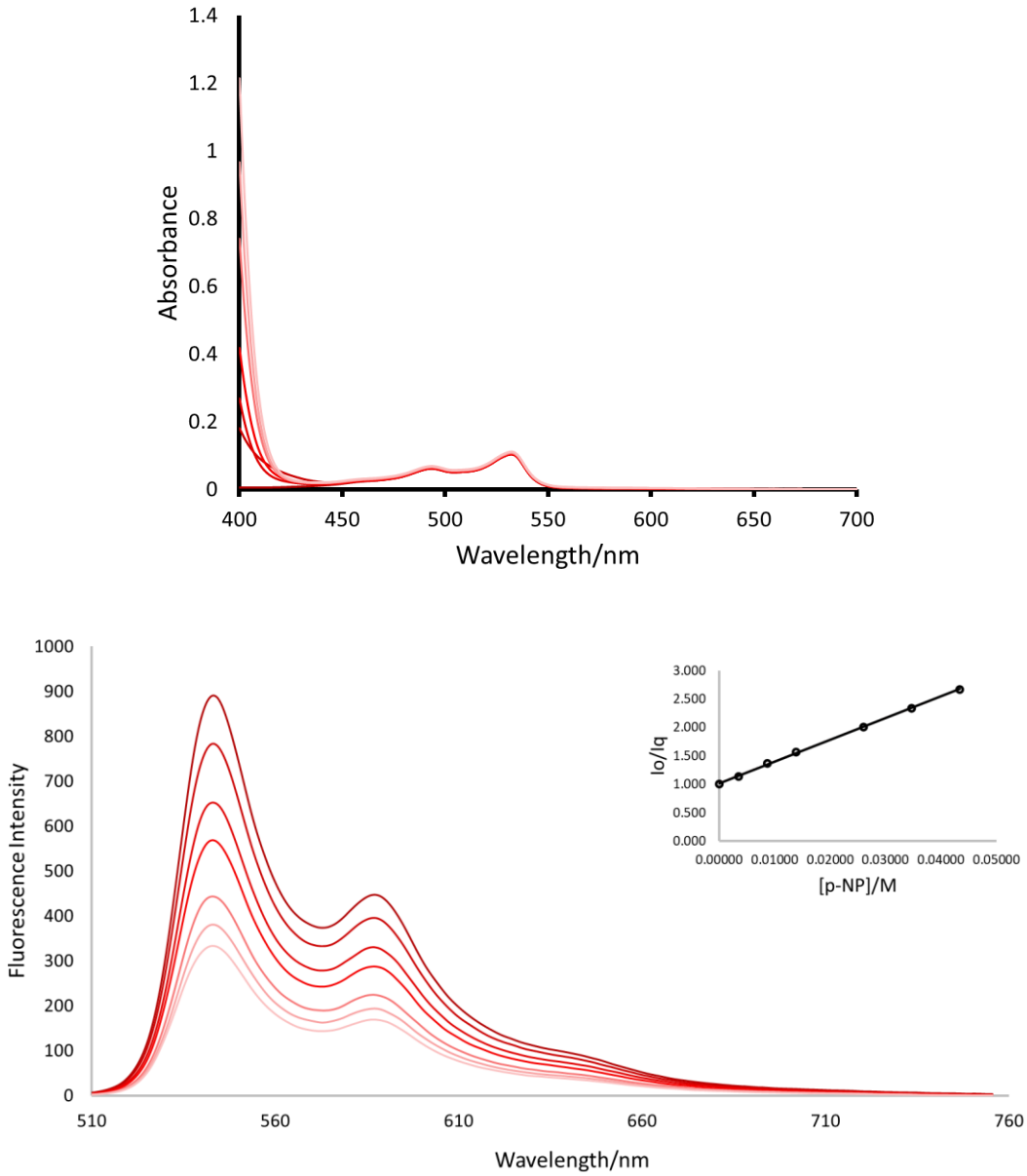


Figure B3.7: Top: Absorption spectra of FBDPP in acetonitrile with p-nitrophenol. Bottom: Fluorescence emission spectra of FBDPP in acetonitrile with increasing concentration of p-nitrophenol.

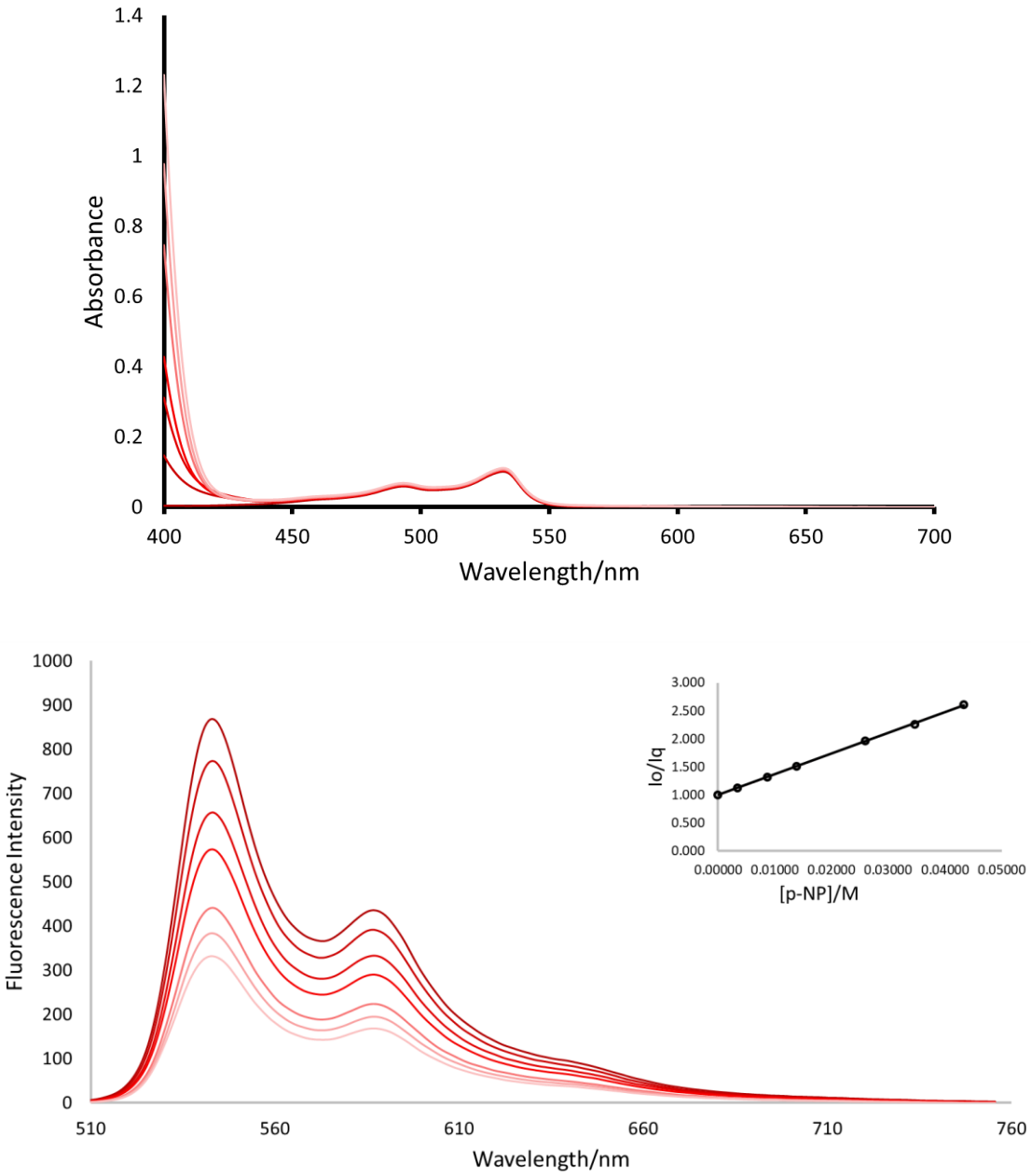


Figure B3.8: Top: Duplicate absorption spectra of FBDPP in acetonitrile with p-nitrophenol. Bottom: Duplicate fluorescence emission spectra of FBDPP in acetonitrile with increasing concentration of p-nitrophenol.

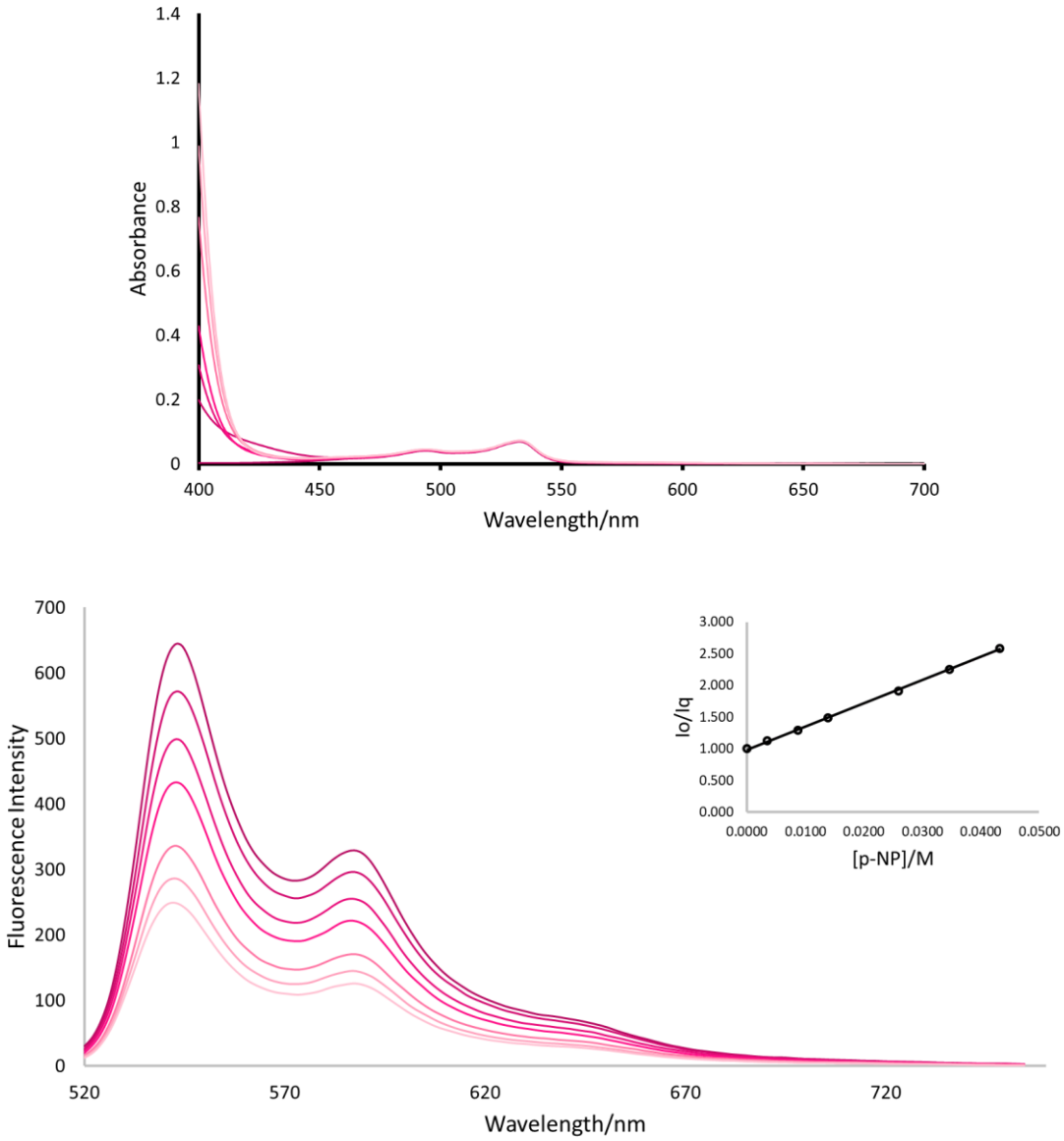


Figure B3.9: Top: Absorption spectra of FNDPP in acetonitrile with p-nitrophenol. Bottom: Fluorescence emission spectra of FNDPP in acetonitrile with increasing concentration of p-nitrophenol.

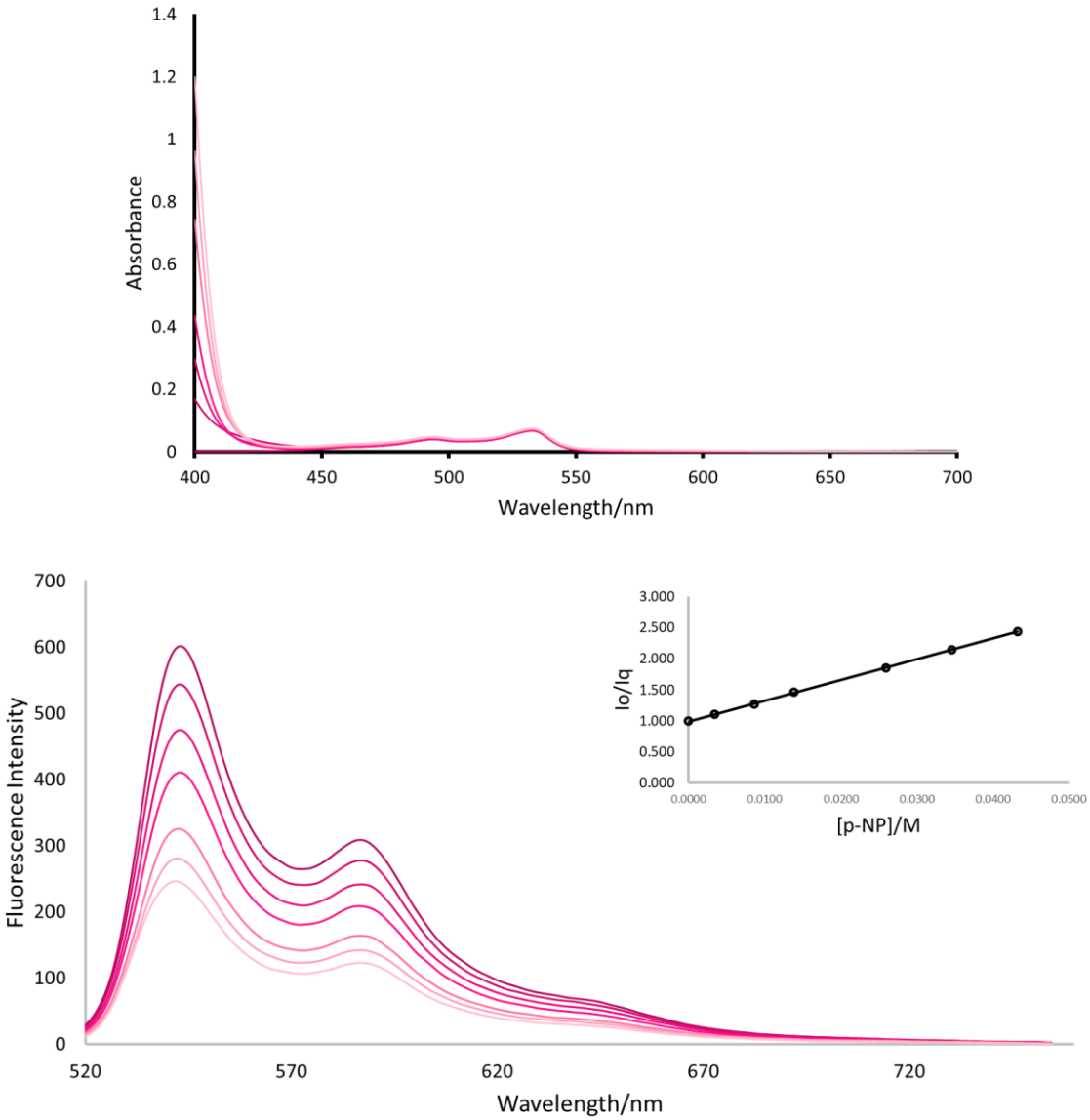


Figure B3.10: Top: Duplicate absorption spectra of FNDPP in acetonitrile with p-nitrophenol. Bottom: Duplicate fluorescence emission spectra of FNDPP in acetonitrile with increasing concentration of p-nitrophenol.

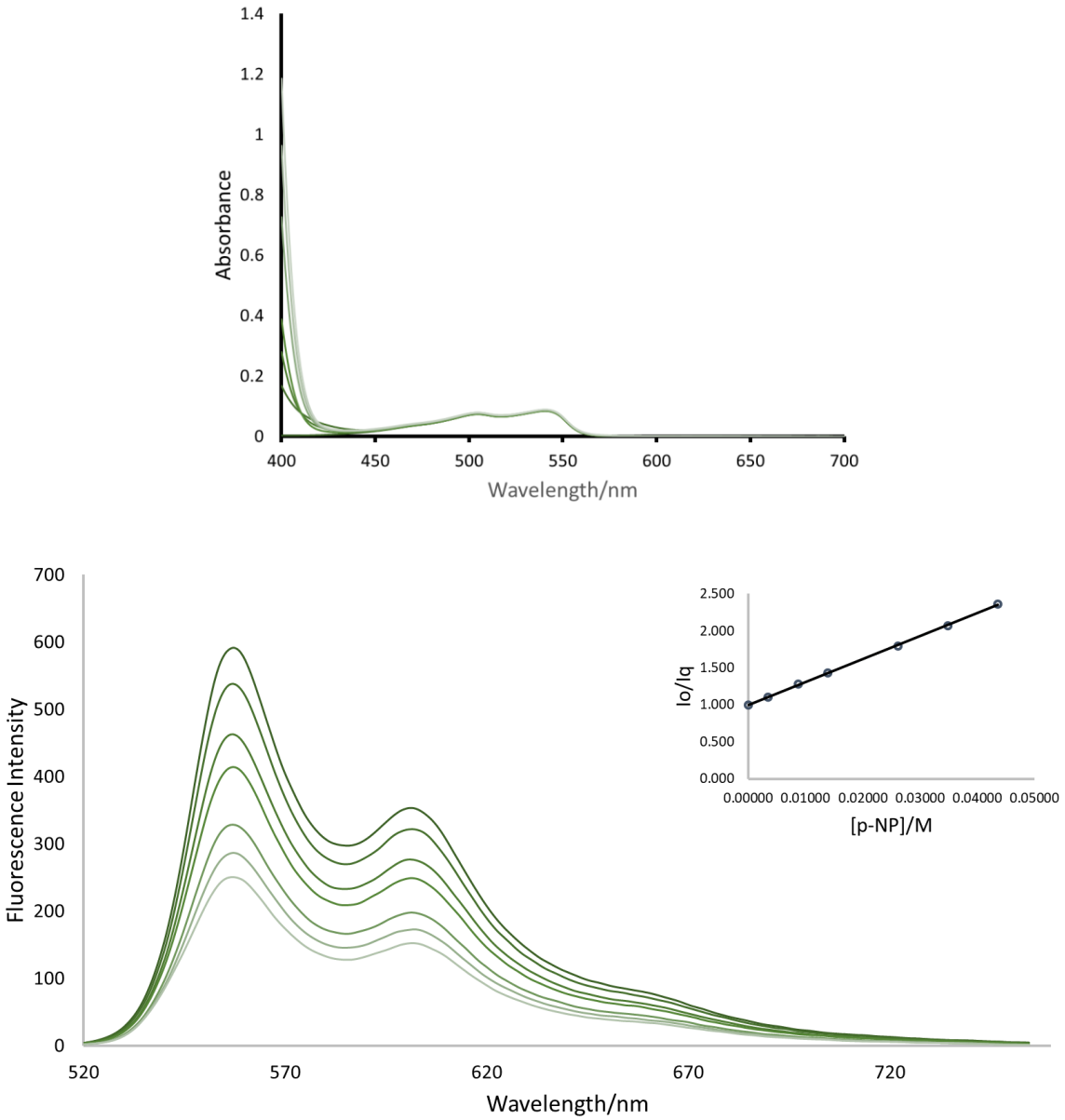


Figure B3.11: Top: Absorption spectra of TBDPP in acetonitrile with p-nitrophenol. Bottom: Fluorescence emission spectra of TBDPP in acetonitrile with increasing concentration of p-nitrophenol.

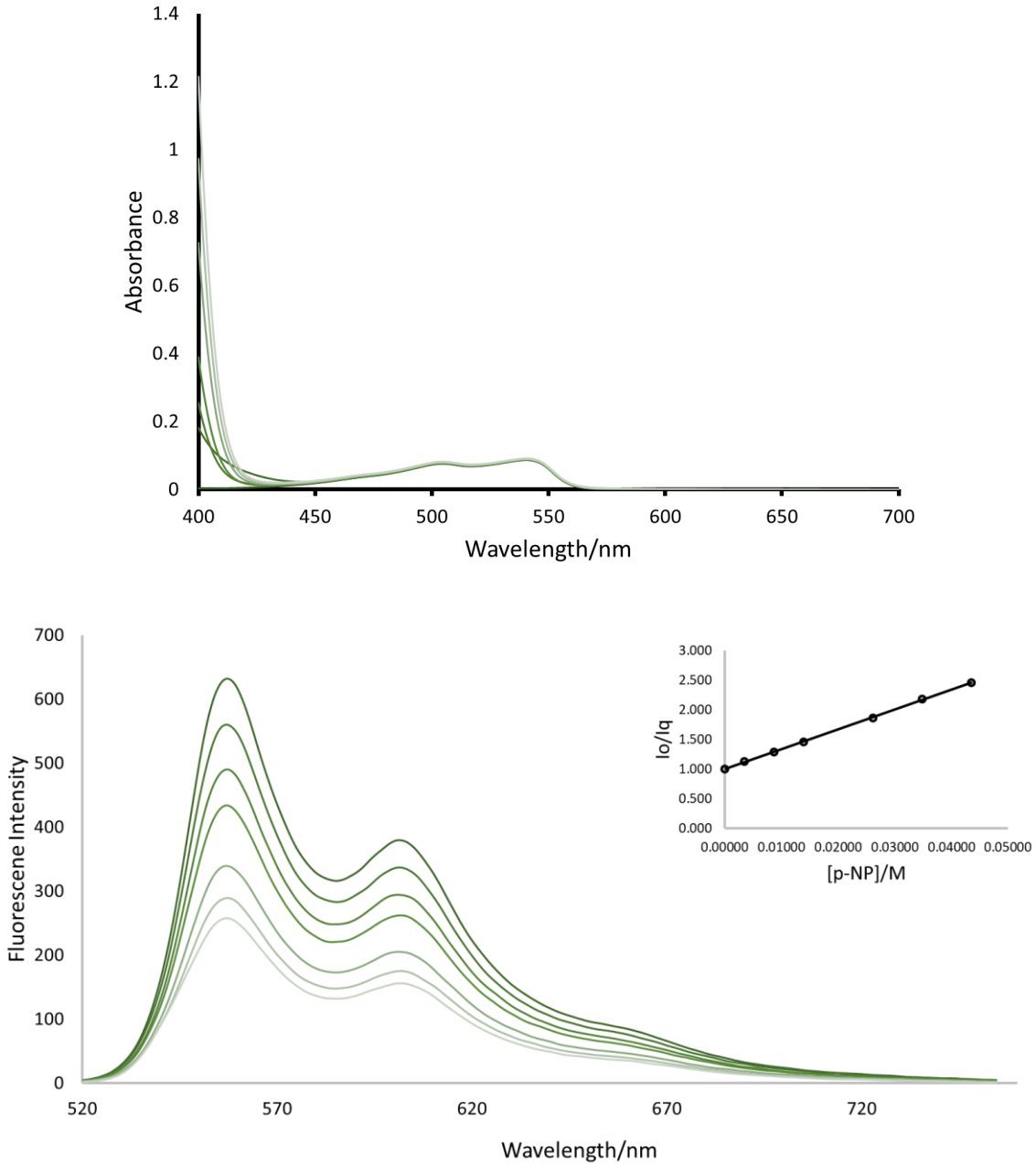


Figure B3.12: Top: Duplicate absorption spectra of TBDPP in acetonitrile with p-nitrophenol. Bottom: Duplicate fluorescence emission spectra of TBDPP in acetonitrile with increasing concentration of p-nitrophenol.

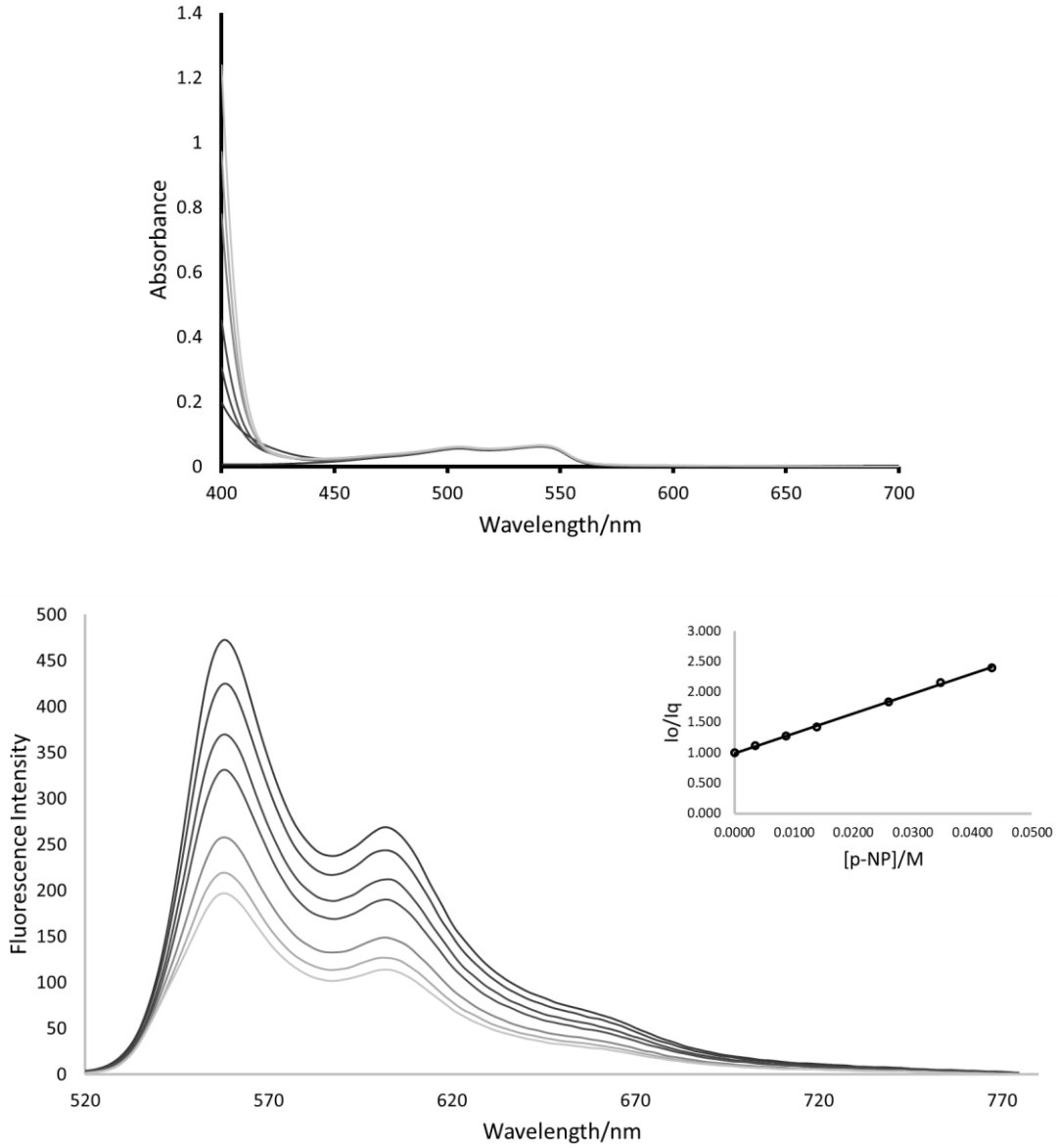


Figure B3.13: Top: Absorption spectra of TNDPP in acetonitrile with p-nitrophenol. Bottom: Fluorescence emission spectra of TNDPP in acetonitrile with increasing concentration of p-nitrophenol.

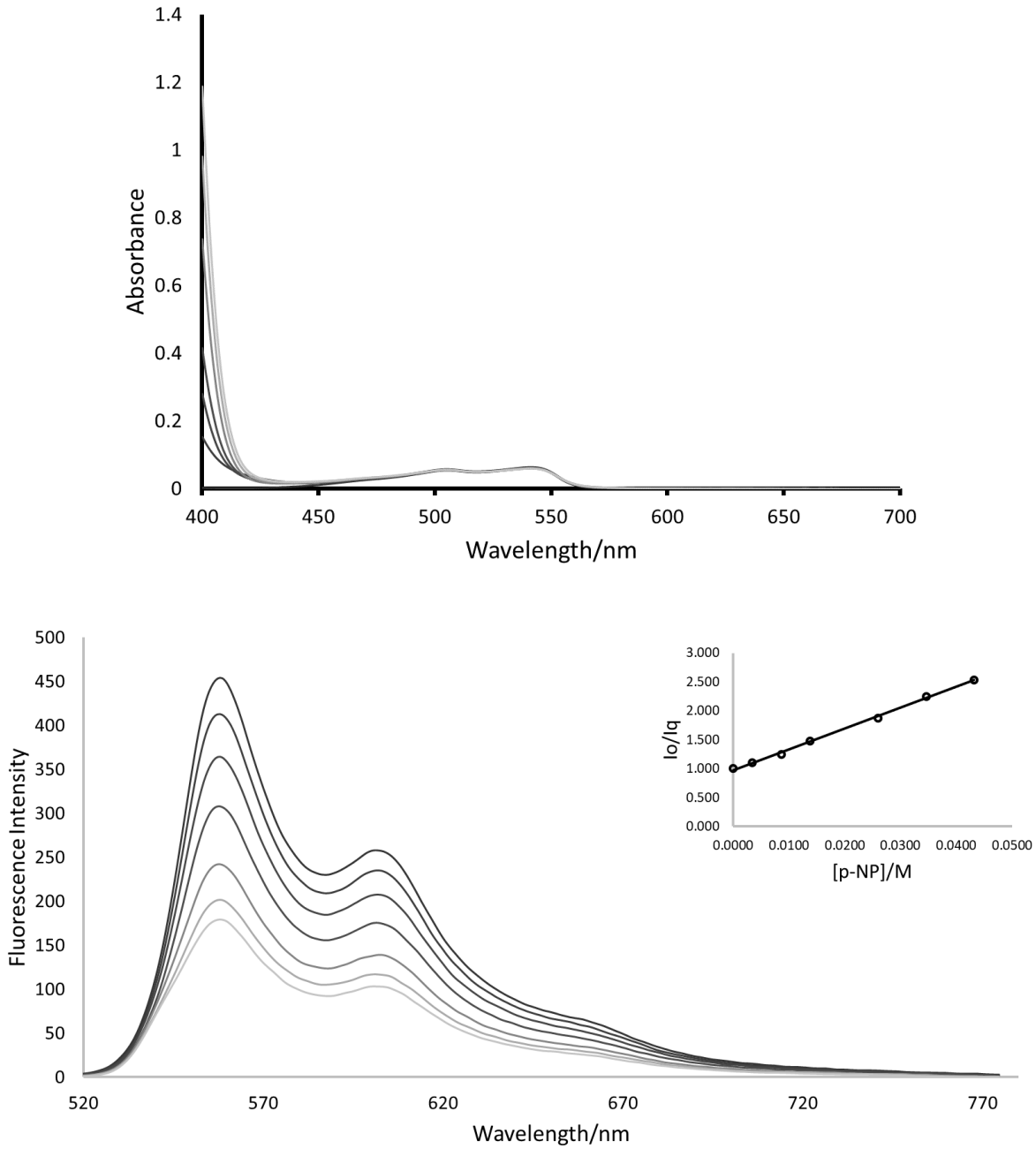


Figure B3.14: Top: Duplicate absorption spectra of TNDPP in acetonitrile with p-nitrophenol. Bottom: Duplicate fluorescence emission spectra of TNDPP in acetonitrile with increasing concentration of p-nitrophenol.

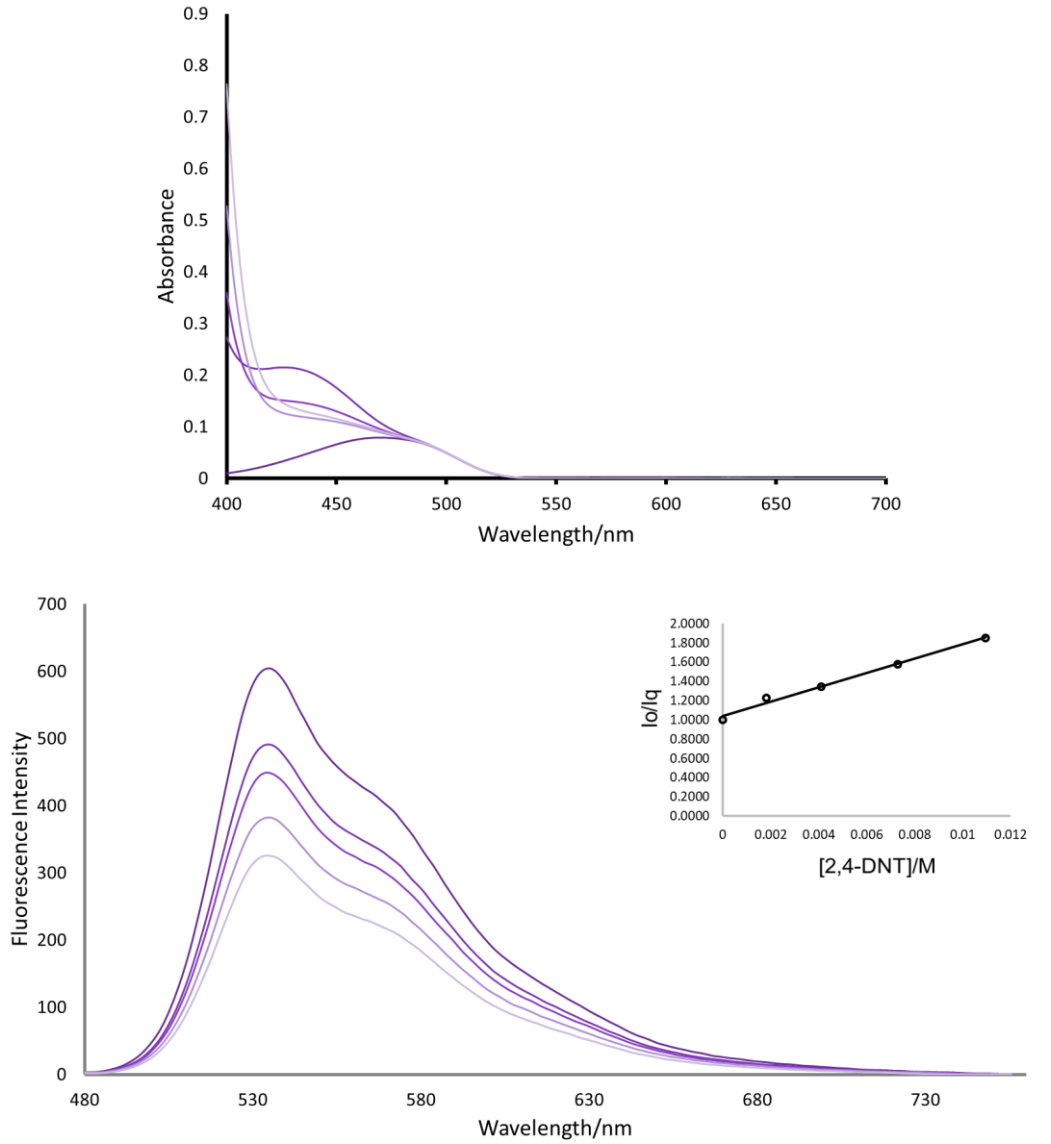


Figure B4.1: Top: Absorption spectra of ClBDPP in acetonitrile with 2,4-dinitrophenol. Bottom: Fluorescence emission spectra of ClBDPP in acetonitrile with increasing concentration of 2,4-dinitrophenol.

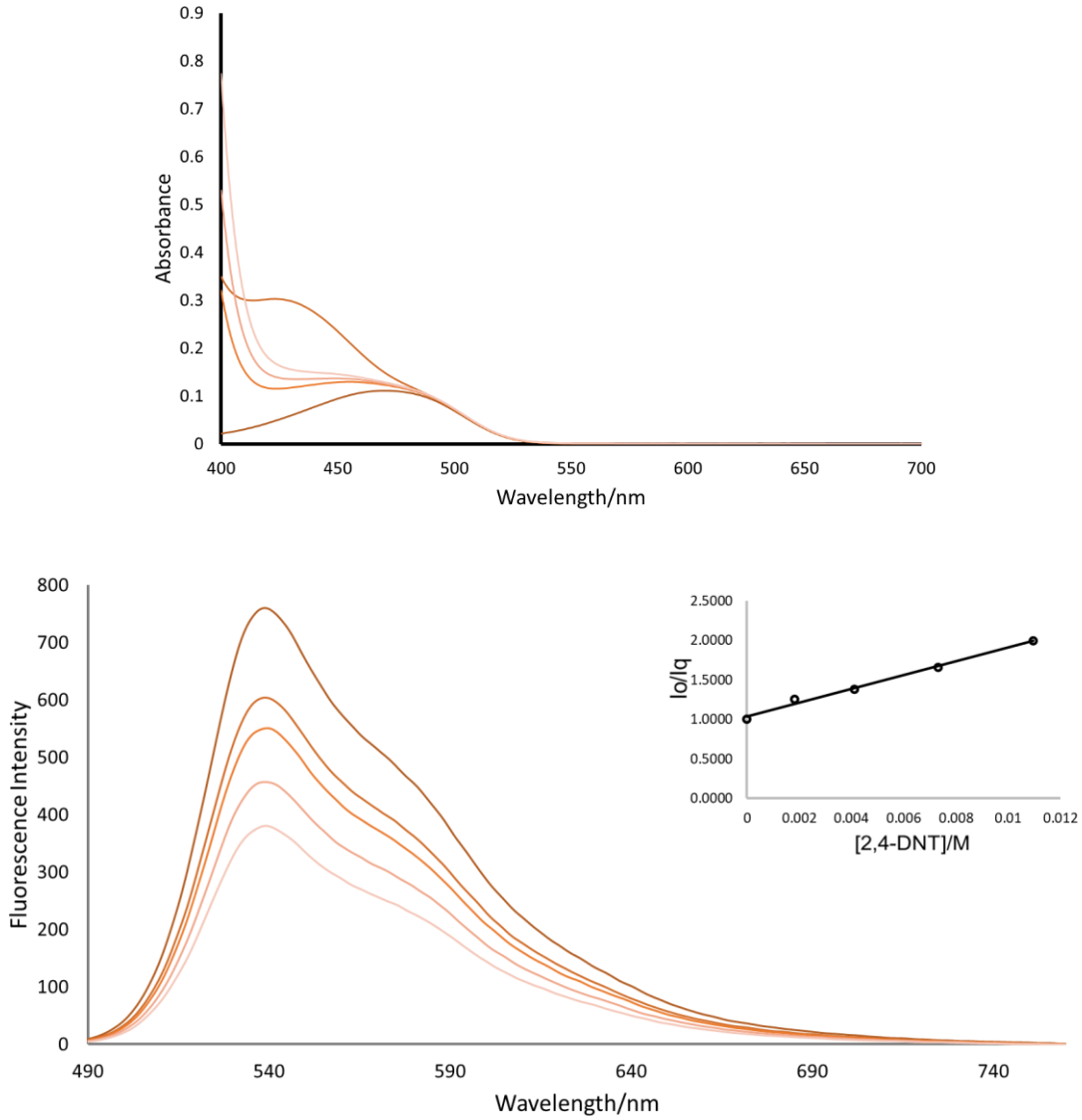


Figure B4.2: Top: Absorption spectra of ClN6DPP in acetonitrilewith 2,4-dinitrophenol. Bottom: Fluorescence emission spectra of ClN6DPP in acetonitrile with increasing concentration of 2,4-dinitrophenol.

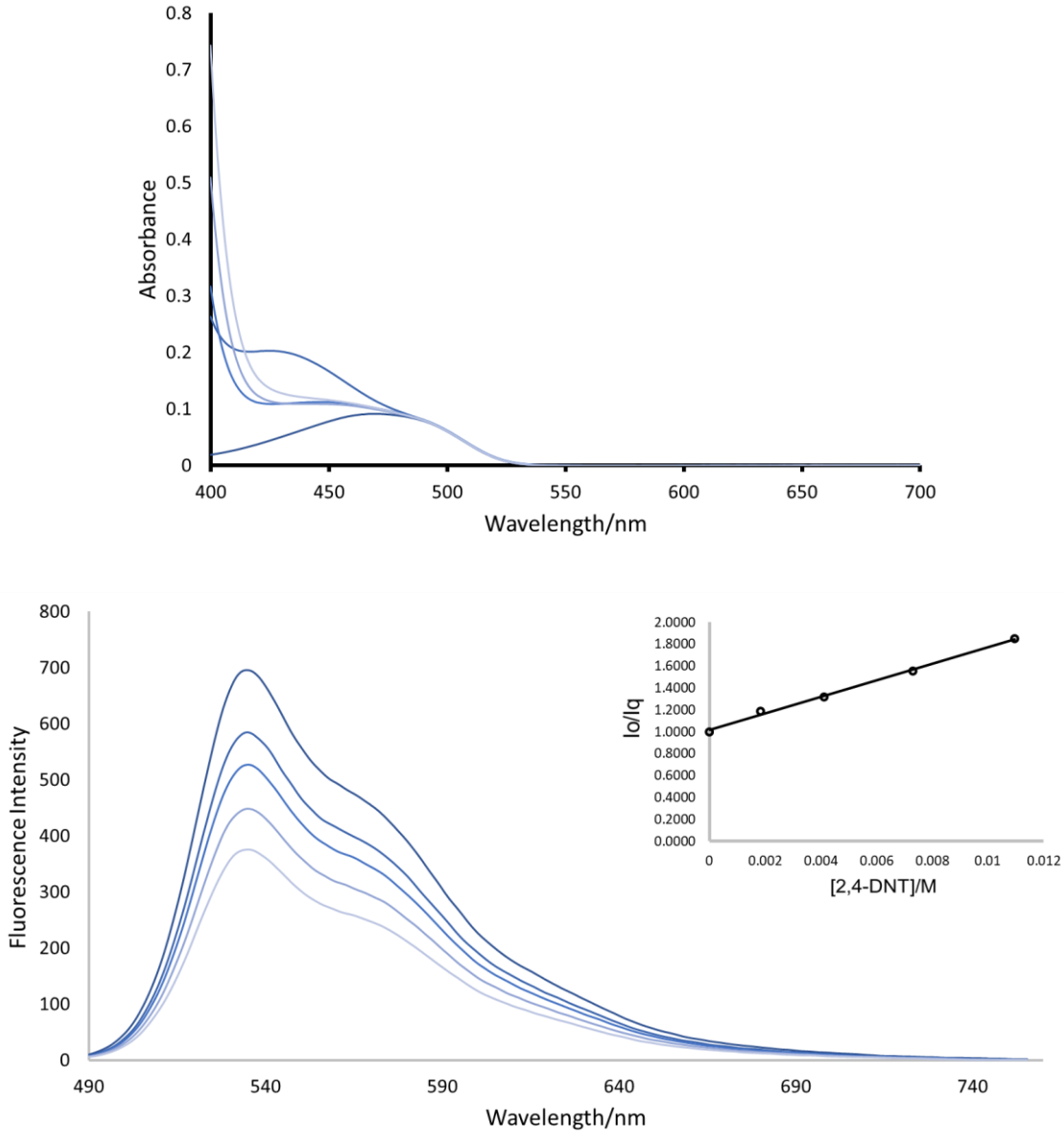


Figure B4.3: Top: Absorption spectra of ClNDPP in acetonitrile with 2,4-dinitrophenol. Bottom: Fluorescence emission spectra of ClNDPP in acetonitrile with increasing concentration of 2,4-dinitrophenol.

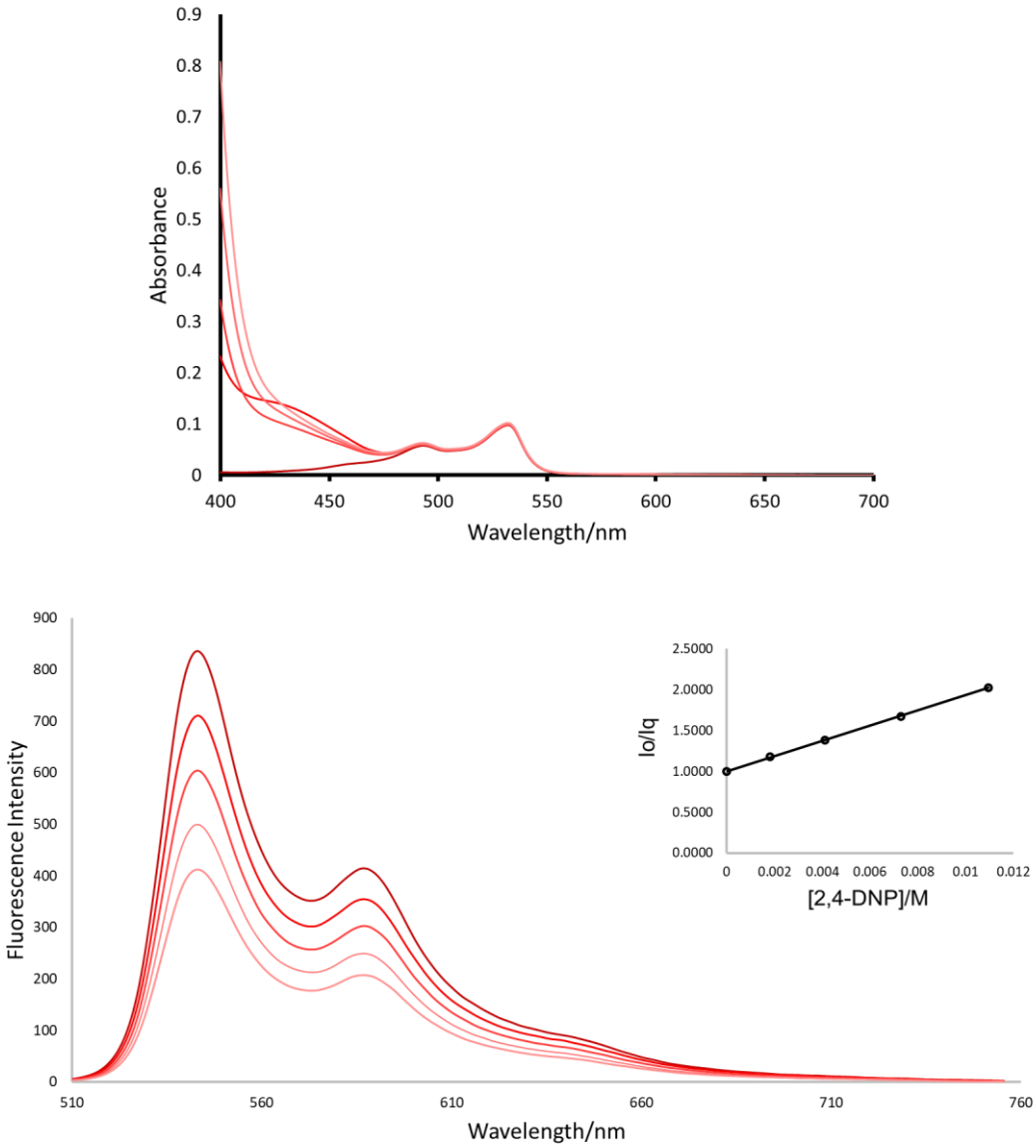


Figure B4.4: Top: Absorption spectra of FBDPP in acetonitrile with 2,4-dinitrophenol. Bottom: Fluorescence emission spectra of FBDPP in acetonitrile with increasing concentration of 2,4-dinitrophenol.

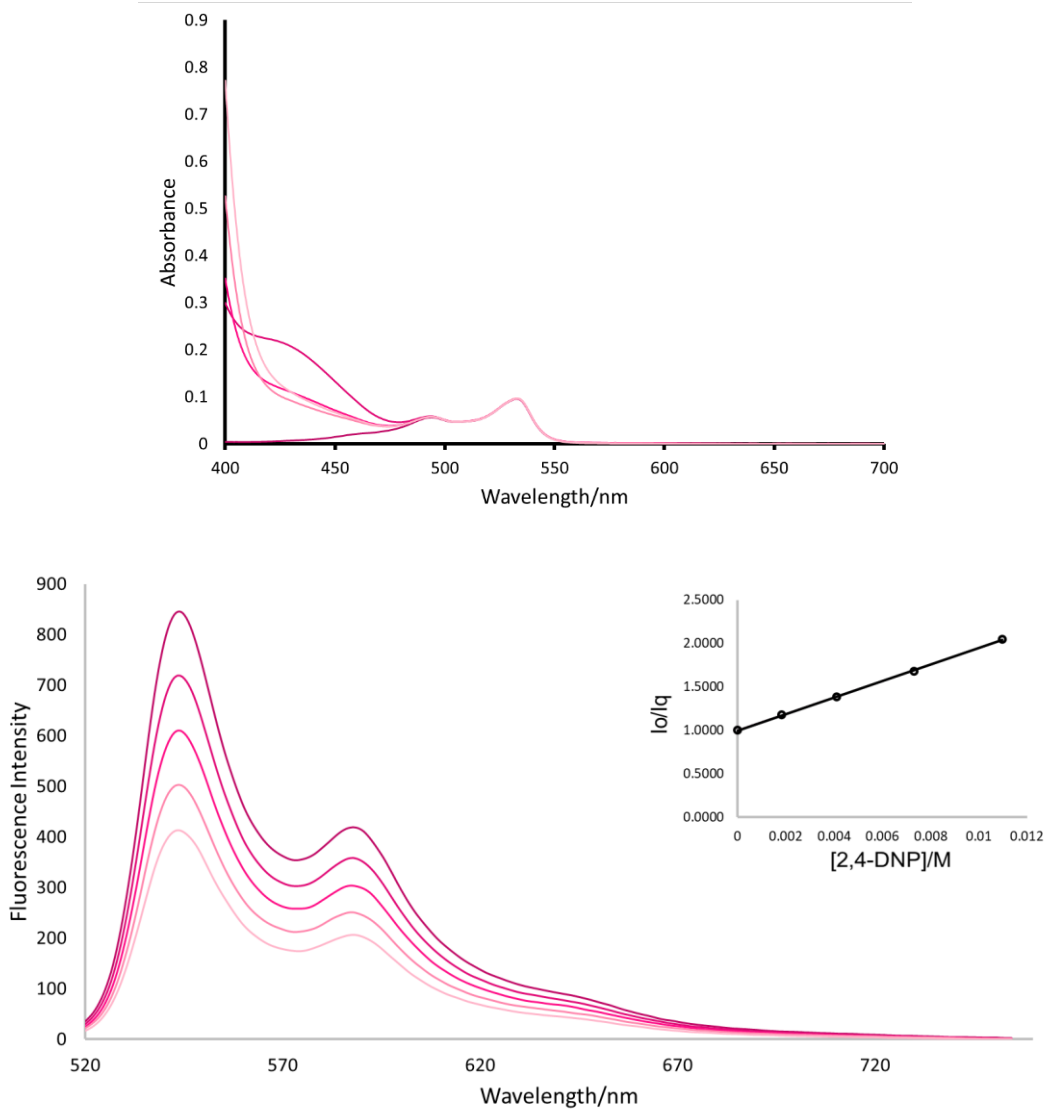


Figure B4.5: Top: Absorption spectra of FNDPP in acetonitrile with 2,4-dinitrophenol. Bottom: Fluorescence emission spectra of FNDPP in acetonitrile with increasing concentration of 2,4-dinitrophenol.

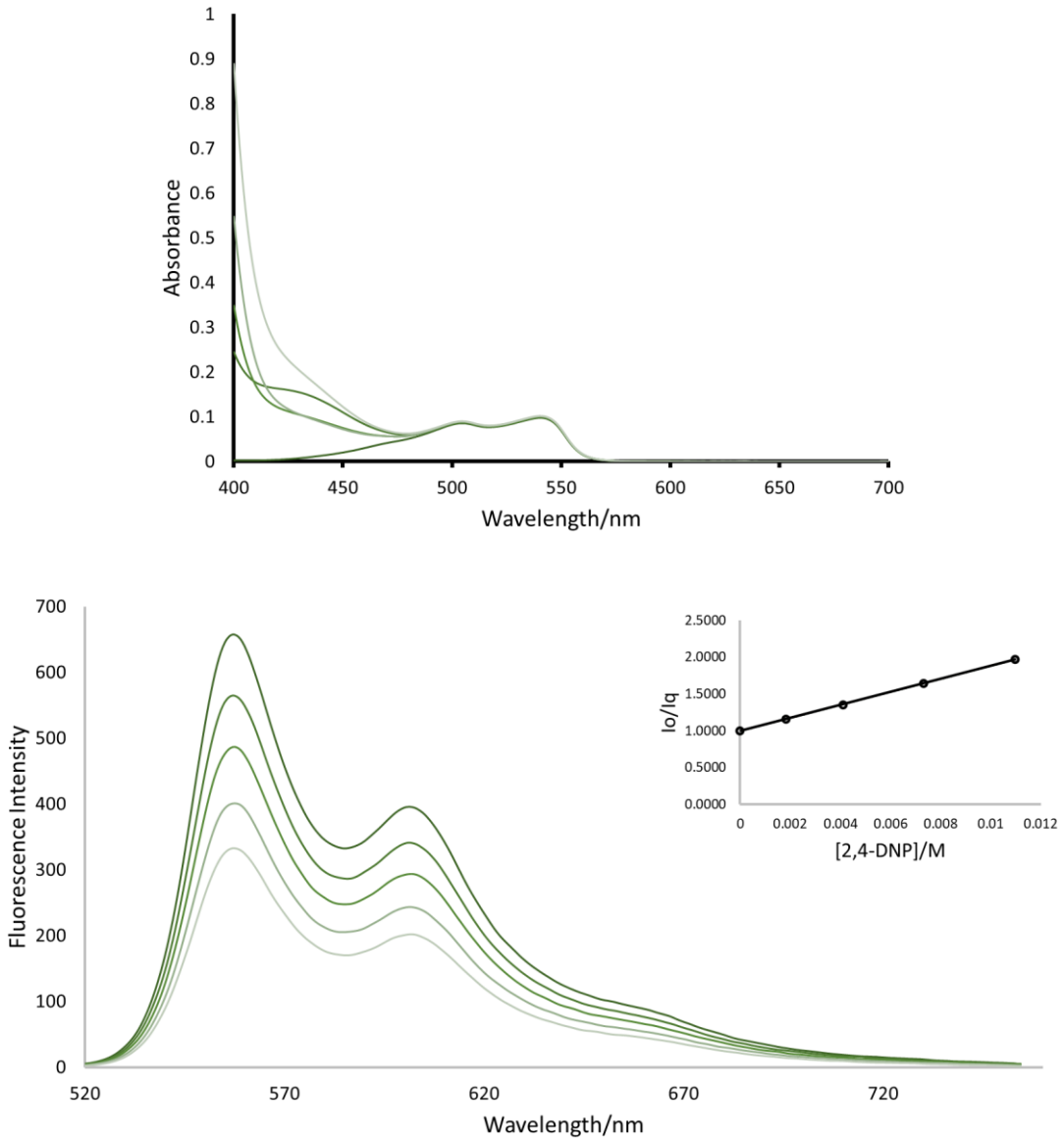


Figure B4.6: Top: Absorption spectra of TBDPP in acetonitrile with 2,4-dinitrophenol. Bottom: Fluorescence emission spectra of TBDPP in acetonitrile with increasing concentration of 2,4-dinitrophenol.

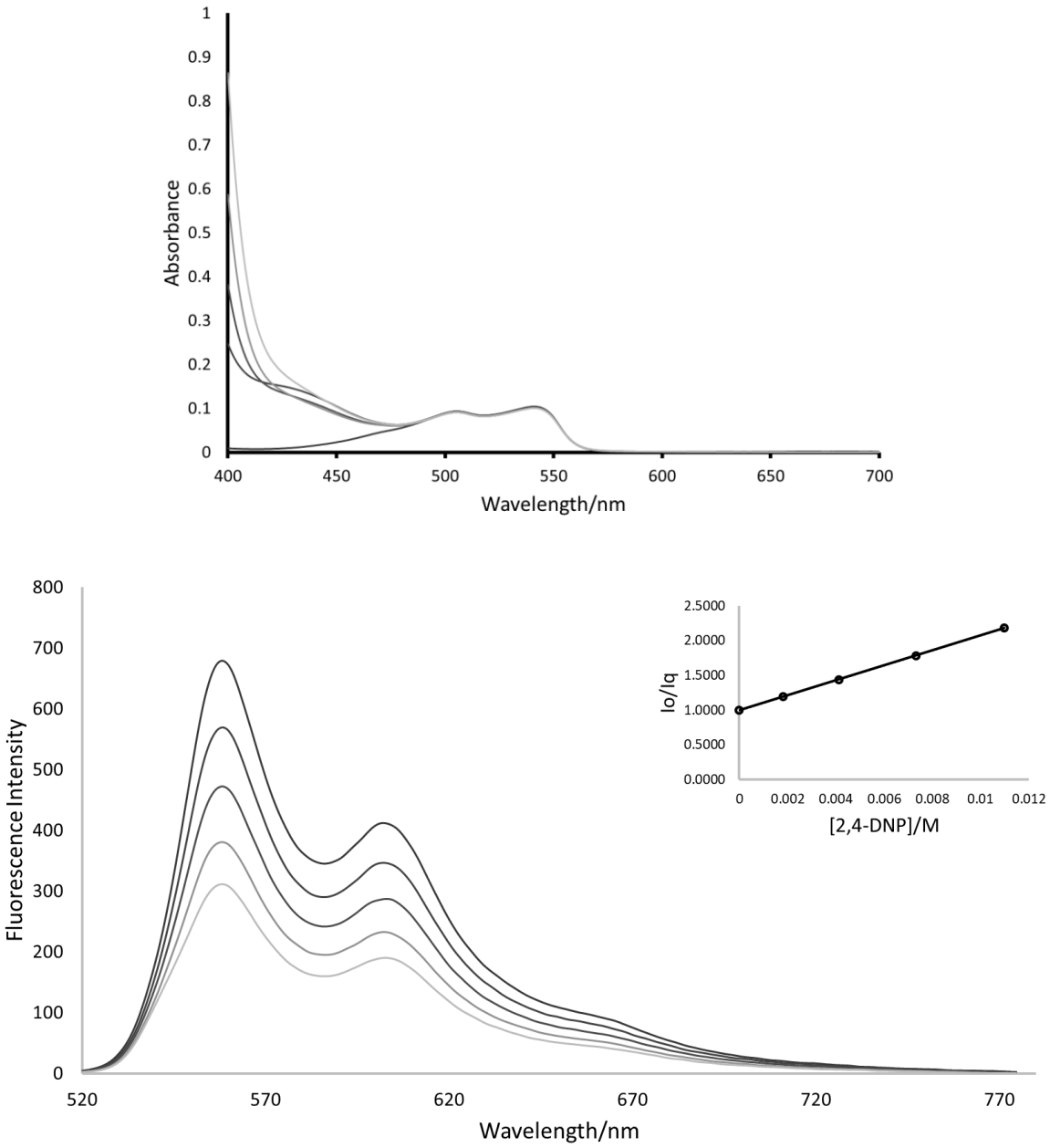


Figure B4.7: Top: Absorption spectra of TBDPP in acetonitrile with 2,4-dinitrophenol. Bottom: Fluorescence emission spectra of TBDPP in acetonitrile with increasing concentration of 2,4-dinitrophenol.